MAX PLANCK INSTITUTE
FOR DYNAMICS OF COMPLEX
TECHNICAL SYSTEMS
MAGDEBURG

Otto-von-Guericke-University Magdeburg
Faculty of Process & Systems Engineering
Department of Process Systems Engineering

Optimization-based Operation Strategy and Storage Design for Coupled Processes

Andreas Himmel

Dissertation presented in partial fulfillment of the requirements for the degree of Doctor in Engineering (Dr.-Ing)

February 12, 2021

Optimization-based Operation Strategy and Storage Design for Coupled Processes

Der Fakultät für Verfahrens- und Systemtechnik
der Otto-von-Guericke-Universität Magdeburg
zur Erlangung des akademischen Grades

Doktoringenieur
(Dr. - Ing.)

am 02. März 2021 vorgelegte Dissertation

von M.Sc. Andreas Himmel

Abstract

Modern model-based control strategies are fundamental components when dealing with process engineering systems. They ensure stable, safe, and economically profitable operations. Especially when considering changing feed qualities, electric energy availability, or prices, these control strategies are needed to adapt the process operation. Among these hierarchically structured control strategies, real-time optimization is responsible for a frequent recalculation of the operating points according to an economic assessment. Since production systems consist of strongly interlinked units, storage elements are used to buffer fluctuations in the supply of materials and energy of particular processes. These fluctuations occur, among other things, when the operating points of the production system are changed within defined load ranges or are shut down completely. For a given storage capacity, the control system architecture must ensure that the storage is used optimally, providing sufficient reserve for future operational adaptation. At the same time, it is essential to avoid oversizing of storage capacity.

This thesis treats the two tasks of developing an optimization-based operational strategy as part of the control architecture and designing storage elements based on this strategy. In particular, the operational strategy addresses the real-time optimization (RTO) layer, which has to consider the unsteady production system operation due to frequent charging and discharging storage elements when determining the economically optimal operating points.

We propose an RTO scheme where information from the closed-loop control of the production system is used to predict the dynamic behavior of the storage levels. This RTO formulation is a bilevel problem. To solve this problem efficiently, we present techniques to reformulate it into a static RTO and an optimal control problem (OCP). The task of the OCP is to guarantee a fast transition between two operating points, where the RTO determines the economically optimal operating point exploiting the results of the OCP. To solve the OCP, we introduce a coordinate transformation of the system states and propose a novel setup function for the output trajectory. This function guarantees

a smooth transition between two stationary operating production levels and allows adapting the output trajectory by a finite number of parameters. In this way, the OCP is transformed into a parameter estimation problem that can be solved in the presence of additional system-related constraints. Thus, the proposed RTO scheme provides a time-dependent trajectory for the input and output in addition to the operating points.
Based on this operational strategy, we investigate its relation to storage levels. For this purpose, we analyze the effect of changes in economic factors on the RTO result. It allows us to assess the storage behavior of the production system. Furthermore, we show how this information is employed to estimate the minimum storage size. By utilizing stochastic scenarios for the economic factors, we propose a method to expand the storage capacity beyond the minimum size, achieving the best economic operation without storage-based restrictions. A chemical process example will exemplify the theoretical derived techniques and algorithms of the operational strategy and storage size estimation.
The main intention of this work is twofold: Firstly, we demonstrate that the classic concept of a static RTO can be extended by closed-loop information without using a complete dynamic model. This way, economical optimal production system operation, including time-optimal transition, is achieved while considering the storage level evolution predictions. Secondly, we link the evolution of storage levels with the economic uncertainties affecting the RTO. It allows estimating storage capacities decoupled from the economic assessment of the investment costs of the storage elements. Hence, a combined design of storage tanks and optimal operation of the production system using these storage elements is achieved.

Deutsche Kurzfassung

Der Einsatz moderner modellbasierter Regelungsstrategien spielt für den Betrieb verfahrenstechnischer Produktionssysteme oder Anlagen eine wesentliche Rolle. Sie gewährleisten sowohl einen sicheren und stabilen als auch einen wirtschaftlich rentablen Betrieb. Insbesondere bei schwankenden Qualitäten der Eingangsströme, der Verfügbarkeit der elektrischen Energie oder den Einkaufspreisen werden diese Regelungsstrategien benötigt, um den Prozessbetrieb anzupassen. Innerhalb dieser hierarchisch aufgebauten Regelstrategien sorgt die Echtzeitoptimierung für eine stete Neuberechnung der Betriebspunkte gemäß einer wirtschaftlichen Bewertung. Da verfahrenstechnische Anlagen häufig aus miteinander verketteten Prozessen oder Prozesselementen bestehen, werden Speicherelemente zur Pufferung von Fluktuationen in der Material- und Energieversorgung der einzelnen Prozesse eingesetzt. Diese Schwankungen treten u.a. auf, wenn die Betriebspunkte der Anlage innerhalb definierter Lastbereiche verändert werden oder Teilprozesse vollständig abgeschaltet werden. Bei einer gegebenen Speicherkapazität muss die Regelungsarchitektur sicherstellen, dass der Speicher optimal genutzt wird und genügend Reserve für zukünftige Anpassungen des Anlagenbetriebs bietet. Gleichzeitig ist es wichtig, eine Überdimensionierung der Speicherkapazität zu vermeiden.

Die vorliegende Arbeit beschäftigt sich mit zwei Aufgaben, nämlich eine optimierungsbasierte Betriebsstrategie als Teil der Regelungsarchitektur zu entwickeln und die Speicherelemente auf Basis dieser Strategie zu entwerfen. Die Betriebsstrategie adressiert insbesondere die Ebene der Echtzeitoptimierung (engl. Real Time Optimization, RTO), die bei der Ermittlung der wirtschaftlich optimalen Betriebspunkte den instationären Anlagenbetrieb aufgrund der häufigen Be- und Entladung von Speicherelementen berücksichtigen muss.

Wir schlagen ein RTO-Verfahren vor, bei dem Informationen aus der Regelung der Anlage verwendet werden, um das dynamische Verhalten der Speicherstände vorherzusagen. Bei dieser Formulierung der RTO handelt es sich um ein Bilevel-Optimierungsproblem. Um das Problem effizient zu lösen, werden Techniken vorgestellt, um es in eine statische RTO und

ein Optimalsteuerungsproblem (engl. Optimal Control Problem, OCP) umzuformulieren. Die Aufgabe des OCP besteht darin, einen schnellen Übergang zwischen zwei Betriebspunkten zu gewährleisten, wobei die RTO den wirtschaftlich optimalen Betriebspunkt unter Ausnutzung der Ergebnisse des OCP ermittelt. Um das OCP zu lösen, wird eine Koordinatentransformation der Systemzustände eingeführt und eine neuartige Setup-Funktion für die Trajektorie der Produktionsniveaus vorgeschlagen. Diese Funktion garantiert einen glatten Übergang zwischen zwei stationären Produktionsniveaus und ermöglicht außerdem die Anpassung der Trajektorie durch eine endliche Anzahl von Parametern. Das OCP wird so in ein Parameterschätzproblem umgewandelt, das unter Berücksichtigung zusätzlicher anlagenspezifischer Nebenbedingungen gelöst werden kann. Das vorgeschlagene RTO-Verfahren erzeugt somit zusätzlich zu den Arbeitspunkten eine zeitabhängige Trajektorie für den Systemeingang und die Produktionsniveaus.

Basierend auf dieser Betriebsstrategie wird in dieser Arbeit auch die Beziehung zu den Speicherständen näher untersucht. Hierzu wird der Einfluss von Änderungen der wirtschaftlichen Faktoren auf das Ergebnis der RTO betrachtet. Dies ermöglicht es, das Speicherverhalten der Anlage zu bewerten. In diesem Zusammenhang wird gezeigt, wie die Informationen genutzt werden können, um die erforderliche minimale Speichergröße abzuschätzen. Durch die Einführung stochastischer Szenarien für die wirtschaftlichen Faktoren schlagen wir eine Methode zur Erweiterung der Speicherkapazität über die Mindestgröße hinaus vor, um einen wirtschaftlich optimalen Betrieb ohne speicherbedingte Restriktionen zu gewährleisten. Anhand eines chemischen Prozessbeispiels werden die theoretisch abgeleiteten Techniken und Algorithmen der Betriebsstrategie und der Speichergrößenabschätzung erprobt.

Die Ziele dieser Arbeit können in zwei Punkten zusammengefasst werden: Zum einen wird dargestellt, dass das klassische Konzept einer statischen RTO um Informationen des geschlossenen Regelkreises erweitert werden kann, ohne das vollständige dynamische Modell zu verwenden. Hierdurch wird ein wirtschaftlich optimaler Anlagenbetrieb einschließlich der zeitoptimalen Übergänge unter Berücksichtigung der Entwicklung der Speicherstände erreicht. Zum anderen werden die ökonomischen Unsicherheiten, die die RTO beeinflussen, mit der Entwicklung der Speicherniveaus verknüpft. Dies entkoppelt die Auslegung der Speicherkapazitäten von der ökonomischen Bewertung der Investitionskosten der Speicherelemente. Auf diese Weise wird die Auslegung der Speicher mit dem Design einer optimalen Betriebsstrategie der Anlage verknüpft.

Symbols

Abbreviations and Acronyms

AD	anaerobic digestion
cl	closed-loop
LQR	linear quadratic regulator
MPC	model predictive control
NLP	nonlinear programming problem
OCP	optimal control problem
ODE	ordinary differential equation
pdf	probability density function
PI	proportional–integral
RSR	reactor-separation-recycle
RTO	real-time optimization
D/S-RTO	dynamic/static real-time optimization
w.l.o.g.	without loss of generality

Mathematical Notation

Production system components.

$\mathcal{B}_i{}^{\alpha}$	storage element (α-th element of the i-th process)
$\mathcal{D}_{\mathrm{p}}$	downstream process constraints
$\mathcal{P}$	production system (or system)
$\mathcal{S}_i$	process

Sets and Spaces.

$\mathcal{A}_{\mathfrak{F}}$	subset of $\mathcal{D}$ denoting the attractive region of the storage level
$\mathcal{C}_i/\mathcal{C}$	product space of the i-th process/production system
$\mathcal{C}_\mathrm{e}$	extension of $\mathcal{C}_\mathrm{o}$ by Δ_c
$\mathcal{C}_\mathrm{o}$	operating area of the product space
$\mathcal{D}$	space of the storage level
${\mathcal{H}_j}^\alpha$	terminal constraints for the storage level of ${\mathcal{B}_i}^\alpha$
$\mathcal{IH}/\mathcal{SH}/\mathcal{TH}$	initial/seasonal/total hypercube
Q	set of the product quality functions
${\mathcal{R}_{[\Delta_\mathrm{p} t,\ell]}}_j^{\ \alpha}$	space of feasible storage rates of ${\mathcal{B}_i}^\alpha$
${\mathcal{T}_\theta^\mathrm{n}}_k$	season for a constant mean value of the feed parameter θ
$\mathcal{T}_{\theta k}, {\mathcal{T}_\theta^\mathrm{r}}_{kl}$	time interval for constant feed parameter θ
$\mathcal{U}_i/\mathcal{U}$	input space of the i-th process/production system
$\mathcal{X}_i/\mathcal{X}$	state space of the i-th process/production system
$\mathcal{X}_\mathrm{e}$	extension of $\mathcal{X}$ by Δ_c
$\mathcal{X}_\mathrm{e}^\mathrm{s}$	extension of $\mathcal{X}_\mathrm{o}^\mathrm{s}$ by Δ_c
$\mathcal{X}_\mathrm{o}$	operating area within the state space
$\mathcal{X}_\mathrm{o}^\mathrm{s}$	subset of $\mathcal{X}_\mathrm{o}$ containing steady states
$\mathcal{X}_{\mathrm{o},\delta c}^\mathrm{s}$	subset of $\mathcal{X}_\mathrm{o}^\mathrm{s}$ with feasible production levels due to δc
$\mathcal{X}_\mathrm{q}$	subset of $\mathcal{X}$ with no reduction in product quality
$\mathcal{X}_\omega$	subset of $\mathcal{X}$ feasible for downstream process constraints
Δ_c	set of admissible production level changes from c
Θ	space of the feed parameter
$\mathit{\Theta}$	set of possible scenarios of the feed parameter

Variables.

c_i/c^α	product/production level of the i-th process/production system
c_n	nominal product/production level of the production system
${D_j}^\alpha$	storage size of ${\mathcal{B}_i}^\alpha$
${\underline{D}_j}^\alpha$	minimum storage size of ${\mathcal{B}_i}^\alpha$
${\hat{D}_j}^\alpha$	additional storage size of ${\mathcal{B}_i}^\alpha$
${\ell_i}^\alpha$	storage level (α-th element of the i-th storage system)
u_i/u^α	input or feed coordinate of the i-th process/production system
${x_i}^\alpha/x^\alpha$	state coordinate of the i-th process/production system
δc	change of the production level
$\underline{\Delta}_\theta t$	lower bound for the time until the feed parameter changes
$\Delta_\theta t$	time until the feed parameter changes

$\overline{\Delta}_\theta t$	upper bound for the time until the feed parameter changes
Δ_d	length of the design horizon for the storage size
$\Delta_\mathrm{p} t$	maximum production phase
$\underline{\Delta}_\mathrm{s}$	minimum time for the production phase
$\Delta_\mathrm{s} t$	production phase
${\zeta_j}^\alpha$	safety boundary of ${\mathcal{B}_i}^\alpha$
θ/θ_n	feed parameter/nominal feed parameter
$\hat{\theta}_k, {\hat{\theta}^\mathrm{n}}_k, {\hat{\theta}^\mathrm{r}}_{kl}$	feed parameter value defining a scenario
${\varrho_\mathrm{s}}_j^\alpha$	storage rate of ${\mathcal{B}_i}^\alpha$

Maps and Functions.

$\mathfrak{c}$	trajectory of the production level
f	vectorfield for the process dynamics
F	economic objective function
$\mathfrak{F}$	deviation of the optimal profit
h	map for the primary product
$id_\mathcal{X}$	identity map on $\mathcal{X}$
$\boldsymbol{k}, K, K_\mathrm{ex}$	control law
l	length of a time interval
$\mathfrak{l}$	trajectory of the storage level
$\mathfrak{P}_\mathrm{c}^\mathrm{e}$	map for the optimal stationary production level
$\mathfrak{P}_\mathrm{f}^\mathrm{e}$	map for the optimal profit value
${\mathfrak{P}_\mathrm{r}}_j^\alpha$	map for the optimal storage rates of ${\mathcal{B}_i}^\alpha$
$\mathfrak{P}_\mathrm{u}^\mathrm{e}$	map for the optimal stationary feed level
q	map for the secondary feed
q_s	product quality
r	map for the primary product and byproduct
s	map for input and state constraints of the production system
$\mathfrak{T}_\mathrm{t}$	reduced transition-time map
$\tilde{\mathfrak{T}}_{\mathrm{t},c}$	surrogate model of the transition-time map
$\mathfrak{T}_\mathrm{t}^\mathrm{e}$	transition-time map
$\mathfrak{T}_\mathrm{x}^\mathrm{e}$	transition-state map
$\mathfrak{T}_{\mathrm{x},\delta c}^\mathrm{e}$	parametric form of the transition-state map
$\mathfrak{x}$	trajectory of the state variable
$\boldsymbol{\theta}$	scenario of the feed parameter
Λ_T	setup function for the production level
${\rho_j}^\alpha$	storage rate of ${\mathcal{B}_i}^\alpha$
ω	map for downstream process constraints

Contents

Chapter 1

Introduction

The optimal and safe operation of chemical production networks is a pervasive goal related to the maximization of economic benefits while considering system limitations. Optimal control schemes can address this task. To design such control strategies, a deep understanding of the underlying process structures and inherent connections is necessary.

Chemical production networks are characterized by a hierarchical and complex structure consisting of many interconnected processes and process elements. Thus a production system is a combination of several processes, where each process converts a finite number of educts into a finite number of products. The educts are either provided from external suppliers or delivered within the production system from other processes, where the products are distributed to downstream processes or sold to other customers. The exchange of material and energy flows between the processes is usually supported by storage devices, which perform several tasks [53, 54]:

(i) ***Attenuation of disturbances:*** The propagation of disturbances between the two connected elements is damped. Here, one can distinguish between disturbances regarding the quality (e.g., composition, temperature, or pH) or the rate (i.e., amount per time) of the flow.

(ii) ***Decoupling of process operations:*** The downstream process element can temporarily be operated independently of the upstream element. This allows for coupling batch and continuous processes or partially shutting down production system parts.

Storages perform essential tasks and need to be carefully selected concerning their location, capacity, and dynamic properties. The processes themselves are composed of a large number of elements that are necessary to convert the educts. In particular, there are elements for mixing, reacting, and separating the individual chemical components. Heat exchangers, compressors, and others are used to change the temperature or pressure level.

Mathematical models to describe the processes stem from balance equations for material and energy flows and constitutive equations, i.e., thermodynamic relationships and kinetic information, of the individual elements. However, the focus of this thesis is not on the modeling of processes because we assume that such a nonlinear dynamic model already exists.

In general, the structure of production systems, consisting of processes and process elements, and thus the modeling is performed hierarchically. This structure is also reflected in the control levels, which are responsible for stable, feasible, and safe operation and economically optimal production levels [68, 244]. The decisions made at different levels are embedded in different time horizons. At the planning and scheduling layer, decisions are made about the sources of raw materials or the manufactured products and their schedules and quantities. This layer includes actions that extend over several days or weeks. Production specifications based on hours or days refer to low-frequency economic criteria and are implemented in the real-time optimization layer. Below that layer is the supervisory level, which determines the control policy to implement the load changes. At the bottom level, the regulatory layer (e.g., consisting of PI-controllers) is responsible for the compensation of high-frequency disturbances. The load changes determined by the real-time optimization layer occur around a nominal operating point for which the production system is designed. However, frequently changing economic conditions, e.g., raw material and product prices, quantity, and quality of raw materials or demand, require that the process outputs have to be adjusted. For instance, frequent load changes occur in processes fed with renewable energies, as these are subject to short- or medium frequency fluctuations. Especially the storage of short-term surplus of energy has received much attention in the literature [208].

A challenging issue arises when these fluctuations are process-specific, and the processes are connected via storages. In such cases, the interaction of the operating strategy with the restrictions set by the storages is a decisive factor. It determines both the control performance and thus the realization of production changes, and the economic quality of the production system. In terms of the design of the control strategies and the production system, there are two different types of approaches [157, 48, 230].

(i) ***Sequential approach for design and control:*** The classical approach designs the control system after the processes are fixed. This includes the selection of the control structure in combination with the controlled and manipulated variables, type of control law, and its tuning. Once the process structure is defined, the degrees of freedom of the controller are limited, which might narrow its performance. Another drawback is that a sequential approach can lead to conflicts between the original objectives of the process and the desired control objective. In general, methods for a sequential approach consider only parts of the design process and neglect the interaction between them.

(ii) ***Integrated approach for design and control:*** Here, design and control tasks are performed simultaneously in an iterative fashion, which increases both economic efficiency and control performance. This allows integration of the interaction between process and control structure but also increases the complexity of the problems. In many cases, this is accompanied by the evaluation of controllability, flexibility, or operability, and multi-objective optimization problems. Some methods use steady-state models or model reduction techniques to reduce the numerical complexity. Moreover, the number or type of controllers used is often limited, so that the resulting mathematical formulation of the problems can be solved numerically or analytically.

In this thesis, we consider generic production system topologies that consist of two processes that exchange material and energy via storages. Thereby the storages ensure a temporary decoupling of the processes so that the identification of new operating points for both processes can be performed independently. In this way, each process operates at an economic optimum. Besides, we assume that the two processes are already designed, and their raw material requirements and production outputs are of the same order of magnitude. Designing the processes, including the regulatory layer, can be done either by an integrated or sequential approach, which is not the focus of this thesis. However, we address the design of the operational strategy and the design of the storage capacity according to this strategy. Specifically, we focus on the real-time optimization layer considering the behavior of the storage levels when identifying economically optimal operating points. The next section gives some examples of the production systems, which are covered in this thesis.

1.1 Examples of Process Networks

As mentioned in the previous section, this work focuses on production systems consisting of two processes connected via storages. More precisely, each process converts a primary feed into its primary product, while exchanging additional byproducts, which can be both chemicals and energy. These system structures result either from sub-networks within larger production systems or they can be formed from individual, mutually supporting processes.
In the following, we present five process examples to illustrate that the considered process topology is widespread among chemical production systems.

1. Methane production. The production system consists of two methane-producing processes, as shown in Figure 1.1. The first process is biological methanation, which takes place inside a biogas plant by anaerobic decomposition of organic waste. After several conversion steps, biogas is formed, which contains the main product methane as well as the byproduct carbon dioxide. Once the biogas has been purified, the carbon dioxide is stored in an intermediate storage element before it is fed into the second process as secondary feed.
In the second process, electrical energy is used to produce hydrogen first via water electrolysis. Subsequently, hydrogen is converted to methane utilizing the carbon dioxide of the storage element. The heat generated by the exothermic reaction is transferred to the biogas plant via a second storage element in order to ensure the optimal temperature level for the microorganisms.
This procedure is also known as biogas upgrading as the yield of methane will increase by additional hydrogen, see [120, 264]. An alternative approach to raise the amount of methane and thus to reduce carbon dioxide emissions is discussed by Bensmann et al. [16]. Thereby, hydrogen is fed directly into the fermenter of the biogas plant in order to raise the methane output.

According to the quality of the organic substrates, the amount of methane and carbon dioxide can vary, which can influence the operational costs of the plant. This, in turn, should result in an adaptation of the system operation. The same applies to the catalytic methanation process, which depends on hydrogen as raw material and on the electricity price.

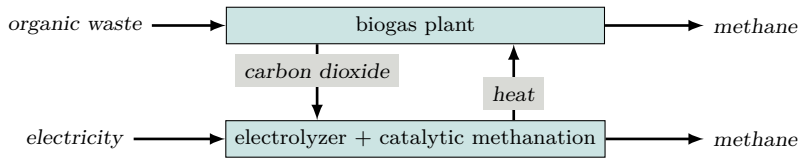

Figure 1.1: Production system consisting of a biological and a catalytic methanation process for upgrading biogas.

2. Syngas and hydrogen production. The production system consists of two processes, where the first one forms primarily syngas (mixture of carbon monoxide and hydrogen) and the second one hydrogen, as illustrated in Figure 1.2. The syngas is formed from methane employing a partial oxidation process (POX) through under-stoichiometric combustion with oxygen. This highly exothermic reaction produces sufficient heat, which can be supplied to high-temperature water electrolysis via a storage element. Based on the higher temperature level at which the electrolysis operates, less voltage and thus less power are required for the decomposition of water. The raw material for this second process is again electricity, and the byproduct is oxygen, which is conducted to a storage element and finally to the POX.
In this example, fluctuations of the electricity or methane price could cause a change in the optimal production output and, thus, the storage level dynamics.

A combined approach, where the conversion of both processes occurs in one electrolysis process, is discussed in [261, 155, 143]. Thereby, partial oxidation takes place on the anode side and hydrogen production on the cathode side.

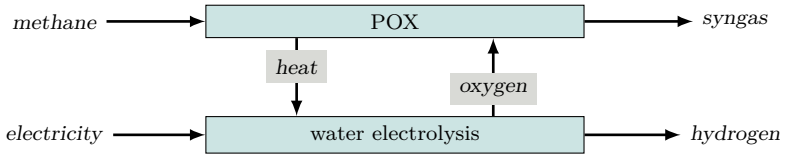

Figure 1.2: Production system consisting of a POX and water electrolysis coupled by two storage elements.

3. Hydrogen cyanide and methane production. An essential raw material in the industry for many other processes is hydrogen cyanide (HCN), as its derivatives, such as cyanogen chloride, cyanogen fluoride, or cyanogen halide, etc., are used for the production of pesticides, dyes, plastics, and pharmaceuticals [75]. A standard process is the BMA process, in which ammonia as the primary feed material is converted into HCN utilizing methane at high temperatures and in an endothermic reaction [149, 150]. Methane, as well as part of the required heat energy, can be obtained from catalytic methanation that consumes syngas as primary feed. If the process is sufficiently dimensioned, the produced methane can support the production of hydrogen cyanide and forms the main product of the second process. Figure 1.3 illustrates the entire production system, whose economic characteristics are sensitive to the price of ammonia and syngas. It is also feasible for syngas that the gas composition, i.e., the ratio of hydrogen and carbon monoxide, influences the process operation. Compared to the two previous examples, the processes are only coupled in a mono-directional way.

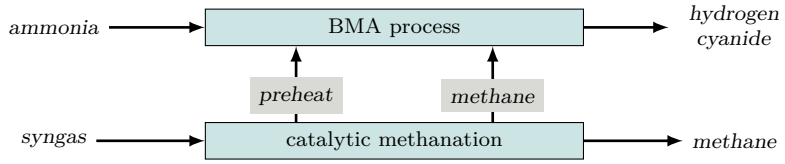

Figure 1.3: Production system consisting of a BMA and a catalytic methanation process coupled by two storage elements.

4. Solvay process. This classic process is an example of how the structure described previously can be identified even in a traditional production system. The Solvay process is primarily used for the production of sodium carbonate [49, 22]. However, the resulting waste product calcium chloride can also be considered as the main product in this framework, as it has several industrial uses. For example, it is used for deicing in road traffic, for the production of cooling baths, or dust control, see [124].
The feed for this process is brine ($NaCl + H_2O$) and calcium carbonate. Figure 1.4 shows a simplified process scheme, in which the individual process elements are combined so that two sub-processes are formed. The first process involves the reaction of brine with carbon dioxide and ammonia to form sodium hydrogen carbonate, which is then further converted to sodium carbonate by calcination. The byproduct ammonium chloride is fed via a storage element to the second process, where it reacts with calcium oxide from the lime burning to recycle the ammonia and produce calcium chloride as the main product. Besides ammonia, carbon dioxide, produced by converting calcium carbonate into calcium oxide, is transported via storages to the first process. For a detailed description of the individual parts, see [111].

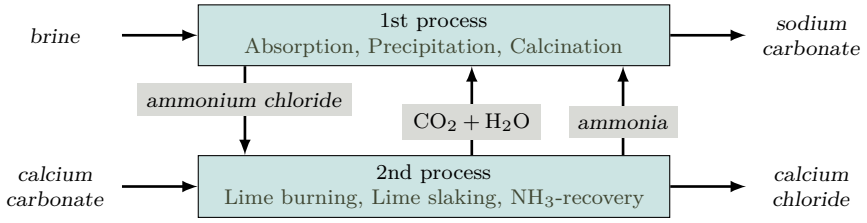

Figure 1.4: Solvay process devided into two sub-processes.

5. Hydrodesulfurization (HDS) and Claus process. In our last example, we consider a production system whose first process is often used in refineries to remove organosulfur from petroleum products and natural gas. This is the HDS process, where hydrogen is applied to purify crude oil at higher temperatures and pressures by catalytic reaction. For more details about the reaction steps

and process conditions see [10, 12, 111]. The byproduct of this process is hydrogen sulfide, which is supplied to the Claus process by a storage element [198]. In this second process, oxygen is used as a feed to purify the hydrogen sulfide to pure sulfur. The entire process has a mono-directional process flow, as can be seen in the scheme shown in Figure 1.5.
The factors determining the economic efficiency and, thus, possibly the process operation are either the raw material price or the proportion of sulfur compounds in the crude oil. This means that the oxygen may have to be produced beforehand by air separation with high energy consumption. Considering the HDS process, the sulfur fraction of the feed to be desulphurized might vary over time, which is indicated by fluctuating raw material qualities, as mentioned in the first example.

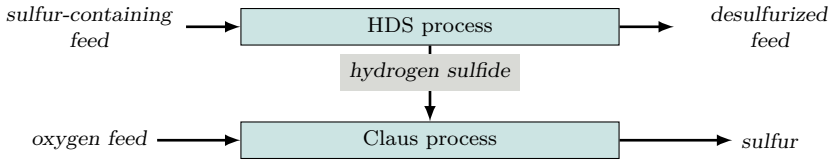

Figure 1.5: Production system consisting of a HDS and a Claus process coupled by one storage elements.

This thesis considers a generalized and mathematically abstract description, covering all the previously mentioned production system examples.

1.2 Contributions

This thesis presents several contributions in three fields: The first field concerns a generic description of the production system, including the dynamic processes and the economic model. The second topic refers to designing an operational strategy for a production system consisting of two processes connected by storages. In the third field, the design of the storages in the presence of this operational strategy is addressed. In order to illustrate the contributions in detail, this thesis introduces an example process through which the results of each chapter are discussed. The contributions presented in Chapters 2-5 are structured as follows.

Part I – Description of the Production System

We develop a systematic mathematical description for a generic production system composed of two processes connected by storages. For this purpose, we define the production system as a tuple of the dynamic process and storage systems, the constraints due to downstream processes, and economic criteria for evaluation. Thus, the system description is generally valid and independent of a concrete example process. Based on these production system components, we state properties to characterize the system structure. To assess the production system profit, we introduce the notion of the feed parameter and propose feed-parameter-dependent economic objective functions in the form of a hybrid approach. The benefits of this approach are twofold:

(i) According to their meaning, the individual terms of the function are economically interpretable: sales, revenue, and operating costs.

(ii) The training of the function is based on uncertain data from rigorous economic models or the experience of the operators.

Finally, we discuss the dynamic properties of the production system and their relation to time-dependent scenarios of the feed parameter. This allows us to evaluate which operational strategy can be employed, and thus, which approach for the storage design must be chosen in the following chapters.

Part II – Design of the Operational Strategy

We propose the closed-loop static real-time optimization (RTO) with integrated trajectory generation as an operational strategy for the production system. In this way, the control law acting on the production system can be considered during the optimization of the operational points. This approach follows a similar idea as used by Jamaludin and Swartz [106] for the closed-loop dynamic RTO. In contrast, here, a static optimization is applied for determining the operating points. Generally, the concept relies on two assumptions:

(i) ***static RTO:*** The economic conditions change with a lower frequency than the system would need for a load change. Hence one distinguishes between the transition phase and the stationary production phase in the processes operation.

(ii) ***closed-loop behavior:*** The storages never operate in stationary mode, which implies constant charging or discharging. Therefore, it is essential to predict their behavior during load changes.

The operational strategy follows a two-layer architecture, which is common for process systems [52, 41]. Contrary to many other approaches [270, 246, 122], we do not use a model predictive controller to steer the system to the new operating point or to generate the control signal for it. Instead, we focus on an inversion-based approach, where the trajectory of the production level is parameterized, similar to [81].

In its original form, closed-loop static RTO is a bilevel optimization, since the control system driving the processes has to be integrated during solving. We show how this optimization can be decoupled into a static RTO and a dynamic optimal control problem (OCP). This step allows reducing the computational complexity of the problem and the related calculation times. The decoupling is based on two aspects.
Firstly, two types of storage constraints are introduced. In the static RTO, the regulation of the storage rates ensures a restriction on the slope of the storage level dynamics within the production phase. In the dynamic OCP, the terminal storage level is constrained to ensure the feasibility of the static RTO solution. Secondly, the generation of a transition-time map allows transferring information from the OCP to the static RTO. In this way, the static RTO can determine the possible length of the transition phase in advance.

The dynamic OCP steers the system to the new operating point in minimum time by generating a manipulating trajectory. This allows an economically optimal operation while considering constraints. Since the production phase requires a stationary production level, we apply a coordinate change of the process states to formulate the dynamic OCP based on a partially inversed process model. The generation of an inversed model is often used in control engineering, see, e.g. [1,2,3], and is related to the concept of differential flatness [104]. Similar to work [82], we propose a novel setup function to parameterize the trajectory of the production level. The benefit of this setup function results from the use of two parameter-dependent terms. Here, each of the individual terms has a different task, which is given as follows:

(i) ***1st term:*** it guarantees a smooth transition between the two production levels, whereby the parameters are determined by the relative degree

(ii) ***2nd term:*** it allows adapting the trajectory between these two points, where the parameters are a degree of freedom for the dynamic OCP

The setup function acts directly on the control law. Thus, the free parameters must be chosen to satisfy process constraints, e.g., for the inputs and states, and system constraints, e.g., for economic aspects and downstream processes. A general advantage of this approach is that the degree of freedom of the setup function is independent of the discretization accuracy.

The main contribution in this part is developing a novel static RTO formulation considering the closed-loop behavior of the production system and unsteady operating storages.

Part III – Design of the Storage Elements

A common approach in dealing with storages is to control their levels via an averaging level controller directly, see [99, 168, 209]. Even if this might reduce the required storage size, it leads to strongly coupled processes. The RTO needs to consider that coupling, which restricts the choice of operating points and thus the economic efficiency. Therefore, our approach does not further restrict the RTO by additional equality constraints requiring a particular level. Instead, we focus on identifying the required capacities to obtain the best possible results. For this, we extend the existing concepts of the operational strategy and the description of the feed parameter by a

(i) ***relaxed problem*** of the static RTO as a reference, which neglects the storage constraints as they are never active if the storages are large enough,

(ii) ***stochastical-based feed parameter*** scenarios to describe the change of economic conditions.

Finally, we propose an approach that uses the relaxed problem to analyze the feed parameter space and design the storage capacities. The works of [185, 186, 187] consider a similar case, where two processes are connected by intermediate storage. Depending on the probability distribution for the input flow, the probability of an overflow or underflow of the strorages is deduced. Similarly, we present a method to analyze the evolution of storage levels based on probability densities for the storage rates. In contrast, here, the densities of the rates result from the probability density of the feed parameter scenarios. These are described by piecewise valid Gaussian distributions, which are transferred via the unscented transformation and the RTO. The storage size is defined as the confidence interval that contains the storage levels for a given probability and over a design horizon. The proposed storage design allows us to find suitable minimum storage sizes to obtain economically optimal dynamic production with coupled systems.
The main contribution of this part is developing a design strategy for estimating the average storage capacities for dynamically operated storages.

1.3 Outline and Structure

This thesis is divided into three parts. Part I Chapter 2 introduces the production system structure and some notations needed for Part II and III. In Section 2.1, the system topology is composed of two processes, each forming its main product while exchanging material and energy flows via storage systems. A general mathematical framework to define the production system in an abstract way is introduced in Section 2.2. In this context, we introduce the feed parameter that characterizes the economic properties of the production system. Furthermore, we show how the evolution of the storage levels can be derived from the process variables by calculating the storage rates. One essential component of the production system is the economic objective function, which depends on the feed parameter. We provide a method to formulate this function, which is needed for the operational control strategy and the estimation of the storage capacities. The time behavior of the feed parameter and the time structure of the production system, in general, is illustrated in Section 2.3.

Part II Chapters 3 and 4 deal with the proposed operational strategy to determine the optimal economic production level and generate a trajectory that steers the system to this level in minimum time. Based on the hierarchical structure of the system control, this operational strategy addresses the real-time optimization layer, which is evaluated when feed parameters or selling prices change. In Section 3.1, we start with a brief overview of the overall production-system control structure focusing on the real-time optimization approaches. Since the storage system is directly included in the control policy of the production system, we introduce in Section 3.2 storage constraints utilizing the storage rates. We present an optimization problem to determine the operating point by production levels for each process in Section 3.3. Here, the transition time, which results for the corresponding level, must be taken into account. A brief overview of appropriate control strategies is presented in Section 4.1 to identify a suitable approach for reaching the new operating point. In Section 4.2, we consider a dynamic optimization problem to parameterize the control law that steers the system to the new level. A surrogate map provides the transition time required to optimize the operating point. This map is generated by an algorithm shown in Section 4.3, which calculates the transition time for specific changes in the production level and creates a Gaussian process based on this. Moreover, we discuss the concept of a globally and locally valid map depending on the production levels and additionally on the system states.

Finally, Part III Chapter 5 focuses on the analysis of storage capacity concerning the feed parameter. We begin again with a brief review of storages in general and some design concepts in Section 5.1. Since the design method is based on real-time optimization for identifying new operating points, in Section 5.2, we

reformulate this optimization to a relaxed problem, which does not consider storage rates. Based on the relaxed problem, we show in Section 5.3 how to estimate the minimum storage capacities. Employing a stochastic description of the feed parameter scenarios, we present in Section 5.4 a method for estimating the average storage capacities in addition to the minimum size.

Mathematical Notation

In this thesis we use concepts from differential geometry to describe the mathematical structure of the system and the control strategy. This includes, in particular, the terminology of manifolds and bundles and their coordinate-free representation or their local coordinates. Moreover, we use tensor notation and the Einstein summation convention throughout this thesis. More precisely, one writes simplified $\omega_\alpha X^\alpha = \sum_{\alpha=1}^{n} \omega_\alpha X^\alpha$. Appendix A.1 gives a detailed introduction into this topic.
Let $\mathcal{B}$, $\dim(\mathcal{B}) = n_\mathrm{b}$ a manifold with local coordinates $\left(x^1, \dots, x^{n_\mathrm{b}}\right)$ or shortly x^α. In general, we assume that $\mathcal{B}$ is a bounded subset of $\mathbb{R}^{n_\mathrm{b}}$, which allows the simplified formulation $x = x(p) \in \mathcal{B}$ for a point $p \in \mathcal{B}$. A bundle $\mathcal{M} \xrightarrow{\pi} \mathcal{B}$ is given by a total manifold $\mathcal{M}$, a base manifold $\mathcal{B}$, and surjective projection π. The map $f : \mathcal{B} \to \mathcal{M}$ is called section if $\pi \circ f = id_\mathcal{B}$, where $id_\mathcal{B}$ is the identify on $\mathcal{B}$. The set of all sections into $\mathcal{M}$ is denoted by $\Gamma(\mathcal{M})$.
To describe dynamic systems and control techniques, the tangent bundle $\mathcal{TB} \xrightarrow{\pi} \mathcal{B}$ and the cotangent bundle $\mathcal{T}^*\mathcal{B} \xrightarrow{\pi} \mathcal{B}$ are useful concepts, which are the disjoint unions of tangent spaces $\mathcal{T}_x\mathcal{B}$ and the cotangent spaces $\mathcal{T}_x^*\mathcal{B}$ over all $x \in \mathcal{B}$. The local coordinates of $\mathcal{TB}$ and $\mathcal{T}^*\mathcal{B}$ are $\left(x^1, \dots, x^{n_\mathrm{b}}, \dot{x}^1, \dots, \dot{x}^{n_\mathrm{b}}\right)$ and $\left(x^1, \dots, x^{n_\mathrm{b}}, \dot{x}_1, \dots, \dot{x}_{n_\mathrm{b}}\right)$ respectively. A section $f \in \Gamma(\mathcal{TB})$ is called vector field. Given a vector field $f \in \Gamma(\mathcal{TB})$, the local representation of a vector $X \in \mathcal{T}_x\mathcal{B}$ is given by $X = f^\alpha(x)\frac{\partial}{\partial x^\alpha}$, where $f^\alpha(x)$ are the vector components and $\frac{\partial}{\partial x^\alpha}$ are the basis vectors. Similary, for a covector field $g \in \Gamma(\mathcal{T}^*\mathcal{B})$, the local representation of a covector $\omega \in \mathcal{T}_x^*\mathcal{B}$ is given by $\omega = g_\alpha(x)\mathrm{d}x^\alpha$, where $g_\alpha(x)$ are the covector components and $\mathrm{d}x^\alpha$ are the basis vectors.

Remark 1.1. *To simplify and reduce the number of variables, we denote the coordinate function and the point obtained by evaluating the function synonomously. The meaning should be evident in terms of the application of the expression. Thus the variable denotes a tuple of real numbers if a function has to be evaluated at a certain point (e.g. t, x). In the case of a composition with other functions, the coordinate function is implied (e.g. t, x). This is illustrated in the diagram in Figure 1.6.*

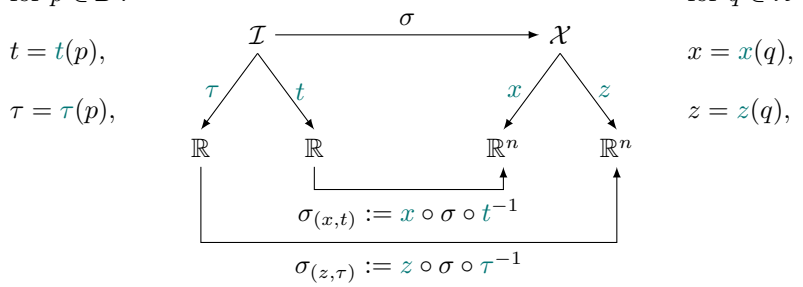

Figure 1.6: Scheme of coordinate functions and coordinate changes.

Furthermore, we will omit the explicit notation of the underlying coordinates, used to represent a function, if these are the standard coordinates. For instance, we write simply σ for $\sigma_{(x,t)}$ such that

$$\sigma(t) := \sigma_{(x,t)}(t) := \left(x \circ \sigma \circ t^{-1}\right)\left(t(p)\right)$$

The explicit notation of the underlying coordinates are important, when we consider coordinate changes in Chapter 4.

Part I

Description of the Production System

Chapter 2

Production System: Topology, Model and Objective

2.1 Topology of the Production System

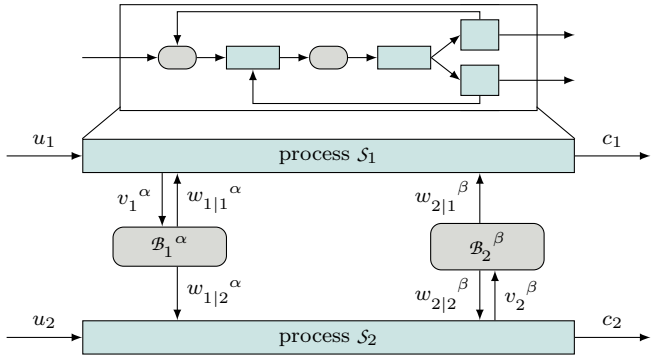

Figure 2.1: General topology of the production system.

In general, we consider an entire production system with a structure, as shown in Figure 2.1. This system consists of two different processes $\{\mathcal{S}_i\}_{i=1,2}$ in which specific primary feeds $u_i \in \mathbb{R}^+$ are converted into the products $c_i \in \mathbb{R}^+$, $i = 1, 2$. The two products of the system serve as a raw material in the downstream process. The process itself can be composed of different process elements, which are coupled sequentially or also by recycles. In addition to the products c_i, each

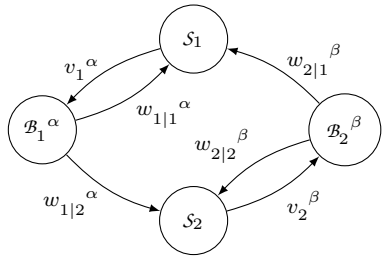

Figure 2.2: General graph representation of the production system topology.

process may also generate byproducts $v_i{}^{\alpha} \in \mathbb{R}^+,\ i = 1, 2,\ \alpha = 1, \ldots, n_i$. The subscript describes the process the byproduct comes from and the superscript denotes the number of the byproduct. These byproducts are stored in the storage systems $\{\mathcal{B}_i\}_{i=1,2}$ and can be recycled via secondary feeds $w_{i|j}{}^{\alpha} \in \mathbb{R}^+$, $i = 1, 2,\ j = 1, 2,\ \alpha = 1, \ldots, n_i$ to the individual processes. Here, the subscripts i and j denotes the process the byproduct comes from and the process where the stored byproduct is transferred to. The number of storages filled by $\mathcal{S}_1$ is n_1 and the number of storages filled by $\mathcal{S}_2$ is n_2. For a more compact representation of the process topology, we use a graph as represented in Figure 2.2 [161, 113, 241].

We can summarize the structure of the production system by the adjacency matrix

$$A = \overbrace{\begin{bmatrix} 0 & 0 & v_1{}^1 & \ldots & v_1{}^{n_1} & 0 & \ldots & 0 \\ 0 & 0 & 0 & \ldots & 0 & v_2{}^1 & \ldots & v_2{}^{n_2} \\ w_{1|1}{}^1 & w_{1|2}{}^1 & 0 & \ldots & 0 & 0 & \ldots & 0 \\ \vdots & \vdots & 0 & \ldots & 0 & 0 & \ldots & 0 \\ w_{1|1}{}^{n_1} & w_{1|2}{}^{n_1} & 0 & \ldots & 0 & 0 & \ldots & 0 \\ w_{2|1}{}^1 & w_{2|2}{}^1 & 0 & \ldots & 0 & 0 & \ldots & 0 \\ \vdots & \vdots & 0 & \ldots & 0 & 0 & \ldots & 0 \\ w_{2|1}{}^{n_2} & w_{2|2}{}^{n_2} & 0 & \ldots & 0 & 0 & \ldots & 0 \end{bmatrix}}^{\substack{A_{1,1} \quad\quad A_{1,2} \\ A_{2,1} \quad\quad A_{2,2}}} . \tag{2.1}$$

Example 2.1 (Adjacency matrix for two coupled reactors)**.** *We consider two reactor models linked by three storage elements see Figure 2.3. The structure is given by the adjecency matrix*

$$A = \begin{bmatrix} 0 & 0 & {v_1}^1 & {v_1}^2 & 0 \\ 0 & 0 & 0 & 0 & {v_2}^1 \\ 0 & {w_{1|2}}^1 & 0 & 0 & 0 \\ {w_{1|1}}^2 & {w_{1|2}}^2 & 0 & 0 & 0 \\ {w_{2|1}}^1 & 0 & 0 & 0 & 0 \end{bmatrix}$$

Storage element ${\mathcal{B}_1}^1$ *is charged via a molar flow of process* $\mathcal{S}_1$ *and only discharged by process* $\mathcal{S}_2$*. Storage element* ${\mathcal{B}_1}^2$ *is charged via a heat flow from process* $\mathcal{S}_1$*, which is supplied to both processes. A molar flow from process* $\mathcal{S}_2$ *charges storage element* ${\mathcal{B}_2}^1$ *and is fed to process* $\mathcal{S}_1$*.*

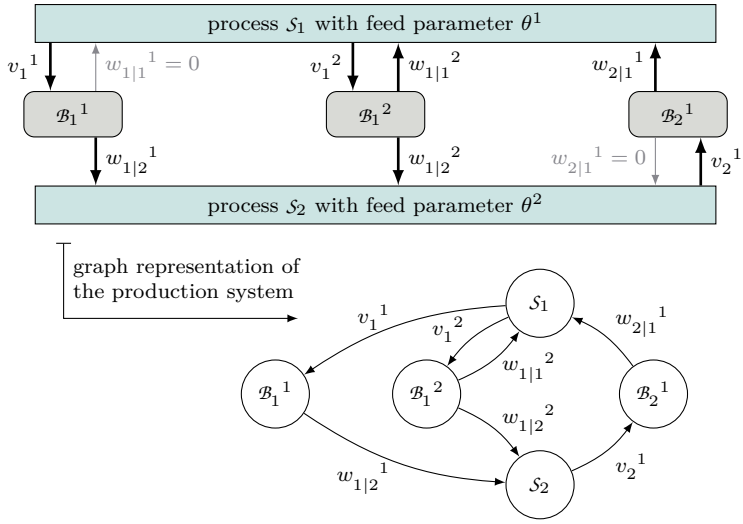

Figure 2.3: Two reactors coupled via three storage elements.

This system topology occurs when two processes complement each other to increase overall efficiency or yield. However, an important question that arises is how changes within one process affect the other. This concerns the operating points of the system and hence the production level and economic efficiency determined by its profit. In general, two different types of effects on the system profit can be distinguished. Firstly, the available feed quantity can differ, so that the corresponding process has to produce less or more product. Secondly, the price or the quality of the feed may vary so that the corresponding process

generates the same amount of product, but at higher or lower operational costs. The following assumption states that we will restrict to the latter case.

Assumption 2.1. *The size of the feed reservoir is sufficiently large so that the required feed quantity can always be guaranteed.*

The profit of the system or more precisely its operational costs are subject to time-dependent fluctuations described by the feed parameter $\theta \in \Theta \subset \mathbb{R}^2$. We assume that θ^1 is related to the first process and θ^2 to the second process, respectively.

It is required that the entire system always operates at the economic optimum. This means when θ^α changes, the operating condition of $\mathcal{S}_\alpha$ change, and thus, the product level c_α needs to be adapted. However, since the two processes are connected via the storage systems $\mathcal{B}_1$ and $\mathcal{B}_2$, the process operation cannot be modified independently of each other. Any process modification leads to variations of the byproducts or the secondary feeds so that the accumulation within the storage tanks changes. One way to avoid extensive modifications can be achieved by using intermediate storage tanks before or within the processes that are used for buffering. At times when the feed parameter has beneficial properties, the storage tanks are charged or discharged when this results in higher operating costs. In this way, the quantity of the secondary feed, primary product and byproduct can be kept bounded.
Another strategy relates to the specific system topology. It is assumed that each process can be operated in a defined load range, where c_i can be set so that $\mathcal{S}_i$ operates in the economic optimum according to its feed parameter. In this context, any change of the storage rate describing the accumulation within the storage element has to be considered. Since the sizes of ${\mathcal{B}_i}^\alpha$ are limited due to investment costs, accurate planning of the new production level by predicting the future storage level is crucial. This way, we want to ensure that $\{\mathcal{B}_i\}_{i=1,2}$ does not impose an additional dynamic on the system apart from changing θ.

2.2 Model of the Production System

So far, we discussed the topology of the system as a combination of the processes and storage elements. This section deals with the internal mathematical structure of the production system and thus with the process and storage models. We rely on a differential geometric representation of the dynamic system model, similar to the works [223, 224, 222, 133] or [76]. A more general introduction to this topic can be found in Frankel [72] or Lee [141].
First, we start with the process model, which describes the processing, separation

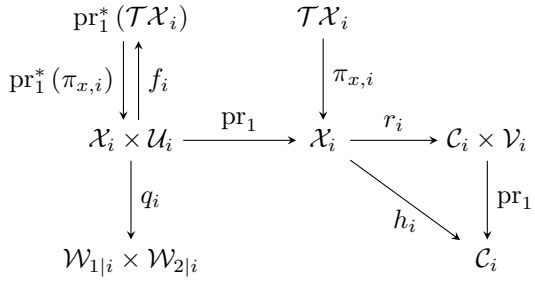

Figure 2.4: Commutative diagram of the mathematical structure of $\mathcal{S}_i$.

and the variation of temperature and pressure levels for certain substances. Next, we discuss the storage model that allows for the intermediate exchange of the byproducts. The third part deals with the entire system model that combines the two process and the storage models and the constraints resulting from downstream processes. Finally, the economic system objective is presented to describe the economic framework and to derive an integrated operating strategy.

2.2.1 Process Model

Each process is considered as a dynamic process on a smooth state manifold $\mathcal{X}_i \subset \mathbb{R}^{n_{\mathrm{x},i}}$, with coordinates ${x_i}^\alpha$, together with the input manifold $\mathcal{U}_i \subset \mathbb{R}$, with coordinate u_i called manipulating variable. The vector field $f_i : \mathcal{X}_i \times \mathcal{U}_i \to \mathrm{pr}_1^*(\mathcal{T}\mathcal{X}_i)$ is defined as a map into the pullback bundle $\mathrm{pr}_1^*(\mathcal{T}\mathcal{X}_i) \xrightarrow{\mathrm{pr}_1^*(\pi_{x,i})} \mathcal{X}_i \times \mathcal{U}_i$ induced by the projection $\mathrm{pr}_1 : \mathcal{X}_i \times \mathcal{U}_i \to \mathcal{X}_i$. Figure 2.4 illustrates the individual spaces by a commutative diagram. The general form of a process models is given by

$$
\mathcal{S}_i : \begin{cases}
{\dot{x}_i}^\alpha = {f_i}^\alpha(x_i, u_i), \;\; x_i(0) = x_{i0} & \text{(2.2a)} \\
(c_i, v_i) = r_i(x_i), & \text{(2.2b)} \\
(w_{1|i}, w_{2|i}) = q_i(x_i, u_i), & \text{(2.2c)} \\
0 \geq s_i(x_i, u_i), & \text{(2.2d)} \\
c_{\mathrm{n},i} \in \mathcal{C}_{\mathrm{o},i}. & \text{(2.2e)}
\end{cases}
$$

By f_i the process dynamics are described in (2.2a) and we denote the set of all possible functions f_i by $\Gamma\big(\mathrm{pr}_1^*\left(\mathcal{TX}_i\right)\big)$. In (2.2b) the relation between the state coordinate x_i and the primary product c_i and the byproduct v_i is described by a map $r_i : \mathcal{X}_i \to \mathcal{C}_i \times \mathcal{V}_i$. It maps into the total product space $\mathcal{C}_i \times \mathcal{V}_i$ of the bundle $\mathcal{C}_i \times \mathcal{V}_i \xrightarrow{\mathrm{pr}_1} \mathcal{C}_i$. The spaces $\mathcal{C}_i \subset \mathbb{R}$ and $\mathcal{V}_i \subset \mathbb{R}^{n_i}$ denote the set of all possible production levels of the primary product and byproducts. In addition, we can define a map $h_i : \mathcal{X}_i \to \mathcal{C}_i$ by $h_i := \mathrm{pr}_1 \circ r_i$ describing the production level.
The relation between (x_i, u_i) and the secondary feeds $\big(w_{1|i}, w_{2|i}\big)$ is given by a map $q_i : \mathcal{X}_i \times \mathcal{U}_i \to \mathcal{W}_{1|i} \times \mathcal{W}_{2|i} \subset \mathbb{R}^{n_1} \times \mathbb{R}^{n_2}$ as presented in (2.2c). The space $\mathcal{W}_{1|i} \times \mathcal{W}_{2|i}$ of secondary feeds is of the dimension $n_1 + n_2$. From (2.2c) it follows that the secondary feeds cannot be chosen arbitrarily because they result from defined production standards. Besides, we consider the map $s_i : \mathcal{X}_i \times \mathcal{U}_i \to \mathbb{R}^{n_{\mathrm{s},i}}$ in the inequality condition (2.2d), such that we restrict $\mathcal{X}_i \times \mathcal{U}_i$ by a feasible region. Finally, the condition in (2.2e) requires that there is a nominal production level $c_{\mathrm{n},i} \in \mathcal{C}_{\mathrm{o},i}$ of the primary product encoded by the constraints. The set $\mathcal{C}_{\mathrm{o},i}$ is the operating area.

Definition 2.1 (Operating Area)**.** *Let $\mathcal{S}_i$ be a process with product manifold $\mathcal{C}_i$. The submanifold*

$$\mathcal{C}_{\mathrm{o},i} := \{\xi \in \mathcal{C}_i \mid \underline{c}_i \leq \xi \leq \overline{c}_i\} \subset \mathcal{C}_i, \tag{2.3}$$

is called operating area and $\underline{c}_i \in \mathbb{R}$ and $\overline{c}_i \in \mathbb{R}$ are the lower and upper production level.

Furthermore, we introduce a subset of the state manifold $\mathcal{X}_i$ that yields operable production levels by the following definition.

Definition 2.2 (Operating State Area)**.** *Let $\mathcal{S}_i$ be a process with manifolds $\mathcal{X}_i$ and $\mathcal{C}_i$ of state variables and the primary product. Moreover, let $h_i : \mathcal{X}_i \to \mathcal{C}_i$ be a map and $\mathcal{C}_{\mathrm{o},i}$ be the operating area. The submanifold*

$$\mathcal{X}_{\mathrm{o},i} := \operatorname*{preim}_{h_i}\left(\mathcal{C}_{\mathrm{o},i}\right), \tag{2.4}$$

is called operating state area.

Remark 2.1. *To make working with indices easier, we use Latin letters (i, j, etc.) to indicate the process element and Greek letters (α, β, etc.) to indicate the component of a variable. For instance, ${x_i}^{\alpha}$ describes the coordinate α of the process i.*

2.2.2 Storage Model

The storage elements are used for the intermediate storage of a certain byproduct and the supply of a secondary feed stream. For modelling, we do not focus on specific storage technologies, but instead use a general approach see e.g. [216, 209]. In order to describe the storage element, we consider the system

$$\mathcal{B}_j{}^{\alpha} : \begin{cases} \dot{\ell}_j{}^{\alpha} = v_j{}^{\alpha} - w_{j|1}{}^{\alpha} - w_{j|2}{}^{\alpha}, & \text{(2.5a)} \\ \ell_j{}^{\alpha} \in \left[\zeta_j{}^{\alpha},\, D_j{}^{\alpha} - \zeta_j{}^{\alpha}\right], & \text{(2.5b)} \end{cases}$$

where $\ell_j{}^{\alpha}$ is called the storage level. The maximum capacity of the storage $\mathcal{B}_j{}^{\alpha}$ is given by $D_j{}^{\alpha} \in \mathbb{R}_0^+$ and a lower safety boundary by $\zeta_j{}^{\alpha} \in \mathbb{R}_0^+$, $\zeta_j{}^{\alpha} < D_j{}^{\alpha}$. While the first index $j = 1, 2$ describes whether the process $\mathcal{S}_1$ or $\mathcal{S}_2$ fills the storage, the second index $\alpha = 1, \ldots, n_j$ specifies the number of the storage element.

Remark 2.2. *For the sake of simplicity, it is assumed that the minimum storage level $\zeta_j{}^{\alpha}$ is equal to the minimum distance from the maximum capacity, as stated in* (2.5b)*.*

Considering the storage capacity, we can classify the connection of these processes by the following definition.

Definition 2.3 (Topological Process Connection)**.** *Consider the processes $\{\mathcal{S}_i\}_{i=1,2}$ and the storage systems $\{\mathcal{B}_j\}_{j=1,2}$. The processes are called topologically*

- *(i) disconnected, if $D_j{}^{\alpha} \to \infty$ and $\ell_j{}^{\alpha} \gg \zeta_j{}^{\alpha}$,*
- *(ii) weakly connected, if $D_j{}^{\alpha} > \zeta_j{}^{\alpha}$ and $\ell_j{}^{\alpha} \in \left[\zeta_j{}^{\alpha},\, D_j{}^{\alpha} - \zeta_j{}^{\alpha}\right]$ or*
- *(iii) strongly connected, if $D_j{}^{\alpha} = \zeta_j{}^{\alpha} = 0$,*

for all elements $\mathcal{B}_j{}^{\alpha}$.

If the storages are infinitely large and sufficiently filled, changes that occur in one process do not affect the other, cf. Definition 2.3 (i). The contrary case is if the storage capacity is zero, i.e., no storage is available, cf. Definition 2.3 (iii). Any change of the process operation of $\mathcal{S}_i$ is immediately transferred to the other process. This is undesirable in many processes, as it causes additional fluctuations and inefficient operation. Therefore we will not consider the case

(iii) in this thesis. From Definition 2.3 follows that the storage level should not be controlled at a constant level since the effect of a constant level is similar to the case (iii).

2.2.3 Coupling the Models to form the Production System

For a description of the entire system, we have to combine the single processes $\mathcal{S}_1$ and $\mathcal{S}_2$ and storage systems $\mathcal{B}_1$ and $\mathcal{B}_2$. In addition to the individual models, we need further structures in order to describe the system from an economic point of view in a production network. For notational simplicity, we introduce $\mathcal{U} := \mathcal{U}_1 \times \mathcal{U}_2$, $\dim \mathcal{U} = 2$, $\mathcal{X} := \mathcal{X}_1 \times \mathcal{X}_2$, $\dim \mathcal{X} = n_{\mathrm{x},1} + n_{\mathrm{x},2}$ and $\mathcal{C} := \mathcal{C}_1 \times \mathcal{C}_2$, $\dim \mathcal{C} = 2$ as smooth input, state and primary product manifold of the system. It is clear from the definition, that the first $n_{\mathrm{x},1}$ coordinates of $\mathcal{X}$ correspond to the states of $\mathcal{S}_1$, where the last $n_{\mathrm{x},2}$ coordinates belong to $\mathcal{S}_2$. The same applies to the coordinates of $\mathcal{U}$ and $\mathcal{C}$. The operating area in (2.3) and the operating state area in (2.4) can also be extended to $\mathcal{C}$ and $\mathcal{X}$ by $\mathcal{C}_\mathrm{o} := \mathcal{C}_{\mathrm{o},1} \times \mathcal{C}_{\mathrm{o},2}$ and $\mathcal{X}_\mathrm{o} := \underset{h}{\mathrm{preim}}\,(\mathcal{C}_\mathrm{o})$ where $h : \mathcal{X} \to \mathcal{C}$, $(x) \mapsto h(x) := \big(h_1(x_1), h_2(x_2)\big)$. For the nominal production level, it applies that $c_\mathrm{n} := (c_{\mathrm{n},1}, c_{\mathrm{n},2}) \in \mathcal{C}_\mathrm{o}$. In the same way, the vector fields for describing the system dynamics can be summarized by $f\,(x,u) := \big(f_1\,(x_1,u_1)\,, f_2\,(x_2,u_2)\big)$. To describe the feasible region of bothe processes, we define $s\,(x,u) := \big(s_1\,(x_1,u_1)\,, s_2\,(x_2,u_2)\big)$. For the sake of simplicity, we will use u, x and c for the coordinates of $\mathcal{U}$, $\mathcal{X}$ and $\mathcal{C}$, respectively.

Considering the primary product c of the system, which is transferred to downstream processes, the question of its quality arises. This product quality plays a crucial role in the economic evaluation of the system, as the proceeds from the sale can be better quantified.

Definition 2.4 (Product Quality)**.** *Let $\mathcal{X}$ be a state manifold. A map $q_\mathrm{s} : \mathcal{X}_\mathrm{o} \to (0,\,1]$ is called product quality, if there exist $\xi \in \mathcal{X}_\mathrm{o}$ such that $q_\mathrm{s}(\xi) = 1$, i.e., no quality reduction occurs at this point.*

For a given $x_0 \in \mathcal{X}$ with the production level $c_0 = h(x_0)$, $q_\mathrm{s}(x_0)$ describes how the sales price has changed compared to other production levels $c_1 = h(x_1) \in \mathcal{C}_\mathrm{o}$ with $c_0 \neq c_1$.
In general, two different products are generated by the system, so that the product quality is usually related to the product of one of the processes $\{\mathcal{S}_i\}_{i=1,2}$. Furthermore, it is possible to define more than one function q_s for a process to describe the quality of c completely. It should be noted that it is not excluded that the system can produce a joint product. From this follows that a downstream process gets $c^1 + c^2$ and q_s is determined by both processes.
We will denote $Q := \big\{q_{\mathrm{s},1}, \ldots q_{\mathrm{s},n_\mathrm{q}}\big\}$ as the set of all quality functions that are

used to describe the system. Later on, the economic objective for the evaluation of the system is determined using Q.

In addition to the evaluation of the product quality, it is important to satisfy constraints resulting from downstream processes. For this purpose we introduce a function $\omega : \mathcal{X} \to \mathbb{R}^{n_\omega}$ such that the set

$$\mathcal{D}_\mathrm{p} : \Big\{ \qquad \mathcal{X}_\omega := \big\{ \xi \in \mathcal{X} \;\mid\; 0 \geq \omega\left(\xi\right) \big\}, \tag{2.6}$$

is a submanifold of $\mathcal{X}$ containing all feasible states that yield a primary product that is admissible for downstream processes. Typical specifications could be restrictions on the total quantity or composition of the product and the requirement that the products have to be provided at specific pressures and temperatures level. In particular, compliance with particular quality standards prevents excessive fluctuations in the sales price. Contrary to the map s, which concerns the individual processes, ω describes additional conditions, which result from the combination of the processes to a production system. Finally, we can combine the individual parts into one production-system model.

Definition 2.5 (Production System)**.** *A production-system model (or short system) is defined by a 6-tuple* $\mathcal{P} := (\mathcal{S}_1, \mathcal{S}_2, \mathcal{B}_1, \mathcal{B}_2, Q, \mathcal{D}_\mathrm{p})$ *that contains the process models* (2.2)*, the storage models* (2.5)*, the set* Q *and the downstream process constraints* (2.6)*. The augmented system is given by*

$$\mathcal{P} : \begin{cases} \dot{x}^\alpha = f^\alpha\left(x, u\right), & \text{(2.7a)} \\ \dot{\ell}_j{}^\alpha = \rho_j{}^\alpha\left(x, u\right), & \text{(2.7b)} \\ c = h\left(x\right), & \text{(2.7c)} \\ 0 \geq s\left(x, u\right), & \text{(2.7d)} \\ 0 \geq \omega\left(x\right), & \text{(2.7e)} \\ u \in \mathcal{U},\, x \in \mathcal{X},\, \ell \in \mathcal{D}, & \text{(2.7f)} \\ c \in \mathcal{C},\, c_\mathrm{n} \in \mathcal{C}_\mathrm{o} & \text{(2.7g)} \end{cases}$$

where the storage rates from (2.5a) *are*

$$\begin{aligned} \rho_j{}^\alpha\left(x, u\right) = &\big(\mathrm{pr}_2 \circ r_j\left(x_j\right)\big)^\alpha \\ &- \big(\mathrm{pr}_j \circ q_1\left(x_1, u_1\right)\big)^\alpha - \big(\mathrm{pr}_j \circ q_2\left(x_2, u_2\right)\big)^\alpha \end{aligned} \tag{2.8}$$

and describe how the storage levels ${\ell_j}^{\alpha}$ change over time. The set

$$\mathcal{D} := \prod_{\alpha=1}^{n_1} \left[{\zeta_1}^{\alpha},\, {D_1}^{\alpha} - {\zeta_1}^{\alpha}\right] \times \prod_{\alpha=1}^{n_2} \left[{\zeta_2}^{\alpha},\, {D_2}^{\alpha} - {\zeta_2}^{\alpha}\right]. \tag{2.9}$$

denote the feasible space of the storage levels. Furthermore, we denote the state and the storage level trajectory by $\chi : \mathbb{R} \to \mathcal{X}$ and $\ell : \mathbb{R} \to \mathcal{D}$. Similarly $c : \mathbb{R} \to \mathcal{C}$ denotes the trajectory of the production level.

Based on the nominal production level $c_{\mathrm{n}} \in \mathcal{C}_{\mathrm{o}}$ of the production system, we specify the systems addressed in this thesis by the following definition.

Definition 2.6 (Well Designed Production System)**.** *A production system $\mathcal{P}$ with nominal production level $c_{\mathrm{n}} \in \mathcal{C}_{\mathrm{o}}$ is well designed if there exists a $\xi \in \underset{h}{\mathrm{preim}}\,(c_{\mathrm{n}}) \cap \mathcal{X}_{\omega}$ with $q_{\mathrm{s}}(\xi) = 1$ for all $q_{\mathrm{s}} \in Q$.*

To ensure that in the following, we only consider systems that do not show a reduction of the sales price in nominal operation, we pose the following assumption.

Assumption 2.2. *The system $\mathcal{P}$ is well designed according to Definition 2.6.*

It should be emphasized that the secondary feeds ${w_{i|j}}^{\alpha}$ and the byproducts ${v_i}^{\alpha}$ are not explicitly listed anymore, as they act indirectly on the storage dynamics. The set $\mathcal{D}$ depends on the safety boundary and the capacity of the storage elements that can be individually defined or estimated, as shown later. In the following, we can assume w.l.o.g. that ${\zeta_i}^{\alpha} = 0$, as the corresponding safety margin, is added as an offset to the designed storage capacity.
After defining the system model, we can introduce and discuss some properties of $\mathcal{P}$ that are necessary to assess whether $\mathcal{P}$ is suitable for dynamic operation. By using Definition 2.4, we can analyze the state space in terms of its economic properties for the system.

Definition 2.7 (Economically Attractive Area)**.** *Let $\mathcal{P}$ be a production system with state space $\mathcal{X}$ and a set Q of quality functions. The level set $\mathcal{X}_{\mathrm{q}} := \{\xi \in \mathcal{X} \mid q_{\mathrm{s}}(\xi) = 1,\ \forall q_{\mathrm{s}} \in Q\}$, $\dim \mathcal{X}_{\mathrm{q}} = n_{\mathrm{x}} - n_{\mathrm{q}}$ is denoted as economically attractive area.*

Definition 2.8 (Economically Operable)**.** *Let $\mathcal{P}$ be a production system with state space $\mathcal{X}$, operating area $\mathcal{C}_{\mathrm{o}}$ and a set Q of quality functions. The production system is called*

(i) locally economically operable (lEO), if $c_{\mathrm{n}} \in h\,(\mathcal{X}_{\mathrm{q}} \cap \mathcal{X}_{\mathrm{o}})$.

(ii) globally economically operable (gEO), if $\mathcal{C}_{\mathrm{o}} = h\,(\mathcal{X}_{\mathrm{q}} \cap \mathcal{X}_{\mathrm{o}})$.

Definition 2.9 (Economic Process Connection)**.** *Let $\mathcal{P}$ be a production system with the two processes $\{\mathcal{S}_i\}_{i=1,2}$ and a set Q of quality functions. The two processes are called economically disconnected if*

$$\frac{\partial h^{\alpha}}{\partial x^{\beta}} \neq 0 \quad \Rightarrow \quad \frac{\partial q_{\mathrm{s}}}{\partial x^{\beta}} = 0, \ \forall q_{\mathrm{s}} \in Q,$$

i.e., product quality and production level, have no joint states, on which they depend. Conversely, the processes are called economically connected if this is not the case.

By means of the downstream process constraints $\mathcal{D}_{\mathrm{p}}$ in (2.6), we can introduce further terms.

Definition 2.10 (Compatibility with Downstream Processes)**.** *Let $\mathcal{P}$ be a production system with the operating area $\mathcal{C}_{\mathrm{o}}$ and the set $\mathcal{X}_{\omega}$ admissible for downstream process constraints. The production system is called locally compatible with downstream processes, if $\mathcal{X}_{\mathrm{o}} \cap \mathcal{X}_{\omega} \neq \emptyset$ and globally compatible with downstream processes, if $h\left(\mathcal{X}_{\mathrm{o}} \cap \mathcal{X}_{\omega}\right) = \mathcal{C}_{\mathrm{o}}$.*

Definition 2.11 (Economically Compatible)**.** *Let $\mathcal{P}$ be a production system with operating area $\mathcal{C}_{\mathrm{o}}$, a set $\mathcal{X}_{\omega}$ and a set Q of quality functions such that the system is compatible with downstream processes. The production system is called*

(i) locally economically compatible (lEC), if $c_{\mathrm{n}} \in h\left(\mathcal{X}_{\mathrm{q}} \cap \mathcal{X}_{\mathrm{o}} \cap \mathcal{X}_{\omega}\right)$.

(ii) globally economically compatible (gEC), if $\mathcal{C}_{\mathrm{o}} = h\left(\mathcal{X}_{\mathrm{q}} \cap \mathcal{X}_{\mathrm{o}} \cap \mathcal{X}_{\omega}\right)$.

From Assumption 2.2, it can be concluded that we only consider production systems that are at least lEC and thus lEO. Figure 2.5 shows various Venn diagrams to illustrate the concepts of the above definitions. The difference between the ideas in Definition 2.9 and 2.11 is the consideration of possible restrictions resulting from downstream processes. This separation results from the fact that the system can operate as an independent unit or as part of a more extensive network. However, it should be mentioned that these properties only apply to the state and product spaces and exclude the input space. Also, the dynamical properties of $\mathcal{P}$ are not addressed. This may result in two consequences for a change between two production levels where its states lie in $\mathcal{X}_{\mathrm{q}} \cap \mathcal{X}_{\mathrm{o}} \cap \mathcal{X}_{\omega}$. On the one hand, the transition might not be realizable due to the dynamic system model or the manipulated variables. On the other hand, the corresponding subset of $\mathcal{X}$ is not invariant to the system dynamics. The previous definitions are purely static properties and neglect dynamic aspects, so they primarily characterize the phases where the production levels are stationary. The following example will help us to understand the concept introduced above.

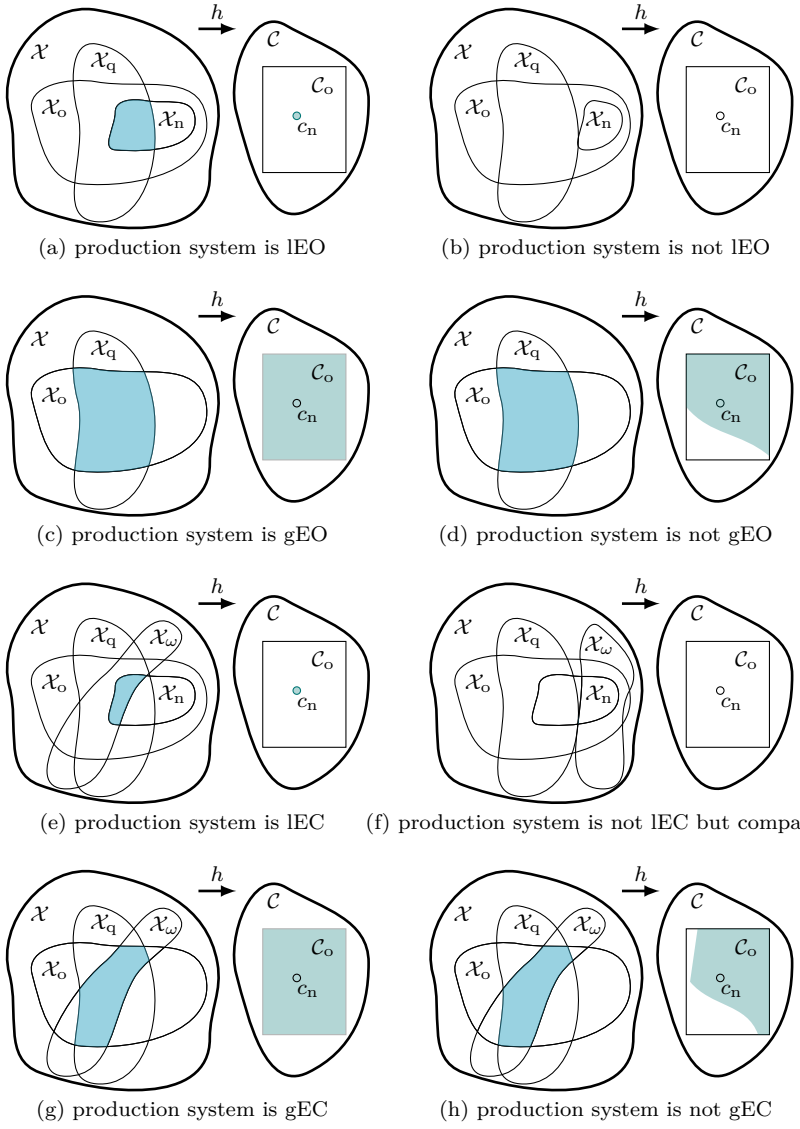

(a) production system is lEO

(b) production system is not lEO

(c) production system is gEO

(d) production system is not gEO

(e) production system is lEC

(f) production system is not lEC but compatible

(g) production system is gEC

(h) production system is not gEC

Figure 2.5: Illustration of the system properties using Venn diagrams, whereby $\mathcal{X}_\mathrm{n} := \underset{h}{\mathrm{preim}}\,(c_\mathrm{n})$.

Example 2.2 (Simple Process)**.** *Consider two processes with one storage element. Within the first process a feed stream is converted to* D *and* E *using* C *as secondary feed. The primary product of* $\mathcal{S}_1$ *is given by a mixture of* D *and* E*. In a second process, a feedstream is decomposed into* F *and* C*, where* F *is the primary product of* $\mathcal{S}_2$ *and* C *is the byproduct that is sent to* $\mathcal{S}_1$ *via a storage element. The coordinates of the state space* $\mathcal{X}$ *are given by* $x = \big(p, G^{\mathrm{D}}, G^{\mathrm{E}}, T, G^{\mathrm{F}}, G^{\mathrm{C}}\big)$*, where the first three coordinates belong to* $\mathcal{S}_1$ *and denote the pressure* p *and the molar flow* G^{D} *and* G^{E} *of* D *and* E*. The last three coordinates belong to* $\mathcal{S}_2$ *and specify the temperature* T *and molar flow* G^{F} *and* G^{C} *of* F *and* C*.*
Figure 2.6 illustrates the state and the product space. For better representation, $\mathcal{X}$ *has been divided into two parts given by the state spaces of the individual processes, cf. Figure 2.6 bottom left and right. We start with an operating area* $\mathcal{C}_{\mathrm{o}}$ *defined by the box constraints* $[\underline{c}, \overline{c}]$ *and a nominal production level* $c_{\mathrm{n}} \in \mathcal{C}_{\mathrm{o}}$*, see Figure 2.6 top. From that we can determine* $\mathcal{X}_{\mathrm{o}}$ *and the preimage of* c_{n} *presented by the blue area and the black line(s), see Figure 2.6 bottom.*
In addition, three different product quality functions are formulated. For $\mathcal{S}_1$ *it is preferred that the composition* $S(x) := \big(G^{\mathrm{D}} - G^{\mathrm{E}}\big)\big(G^{\mathrm{D}}\big)^{-1}$ *as well as a pressure level* p *are set to a certain value so that no reduction of the selling price occurs. The product qualities can be defined by*

$$q_{\mathrm{s},1}(x) := -a_1\big(S(x) - S_{\mathrm{d}}\big)^2 + 1 \quad \textit{and} \quad q_{\mathrm{s},2}(x) := -a_2\big(p - p_2\big)^2 + 1.$$

Here, $a_1, a_2 \in \mathbb{R}^+$ *describes the decline in quality/price and* S_{d} *is the composition number that should be kept constant. In the bottom left part of Figure 2.6, the subsets with* $q_{\mathrm{s},1}(x) = 1$ *and* $q_{\mathrm{s},2}(x) = 1$ *are represented by the red vertical plane and the horizontal plane at* p_2*.*
The primary product of $\mathcal{S}_2$ *has the maximum selling price at the temperature level* T_3*, such that* $q_{\mathrm{s},3}(x) := -a_3\big(T - T_2\big)^2 + 1$*,* $a_3 \in \mathbb{R}^+$*. The subset* $q_{\mathrm{s},3}(x) = 1$ *is shown by the red plane in the bottom right part of Figure 2.6. The space* $\mathcal{X}_{\mathrm{q}}$ *is obtained from the intersection* $\bigcap_{i=1}^{3} \operatorname*{preim}_{q_{\mathrm{s},i}}(1)$*.*
Since the $\mathcal{P}$ *is part of a larger production network, downstream processes impose additional requirements on the primary product* c*. For instance, the mixture supplied by* $\mathcal{S}_1$ *should not contain too much* D*. Processes, which subsequently use* F*, further reduce the operating range of* $\mathcal{S}_2$ *by allowing less variation in production quantity. The yellow area illustrates this subset* $\mathcal{X}_\omega$ *in the left and right part in the bottom of Figure 2.6.*
The states in $\mathcal{X}_{\mathrm{q}} \cap \mathcal{X}_\omega \cap \mathcal{X}_{\mathrm{o}}$ *do not cover the entire operating area* $\mathcal{C}_{\mathrm{o}}$ *under the map* h *so that the system is not gEC. Nevertheless, the nominal production level is included in* $\mathcal{X}_{\mathrm{q}} \cap \mathcal{X}_\omega \cap \mathcal{X}_{\mathrm{o}}$ *so that the system is at least lEC. However, that only the local property applies results from* $\mathcal{X}_\omega$*, so* $\mathcal{P}$ *is gEO.*
The three product qualities are determined by the states $\big(p, G^{\mathrm{D}}, G^{\mathrm{E}}, T\big)$*. The map* h *that yields the primary product depends on* $\big(G^{\mathrm{D}}, G^{\mathrm{E}}, G^{\mathrm{F}}\big)$*. Using*

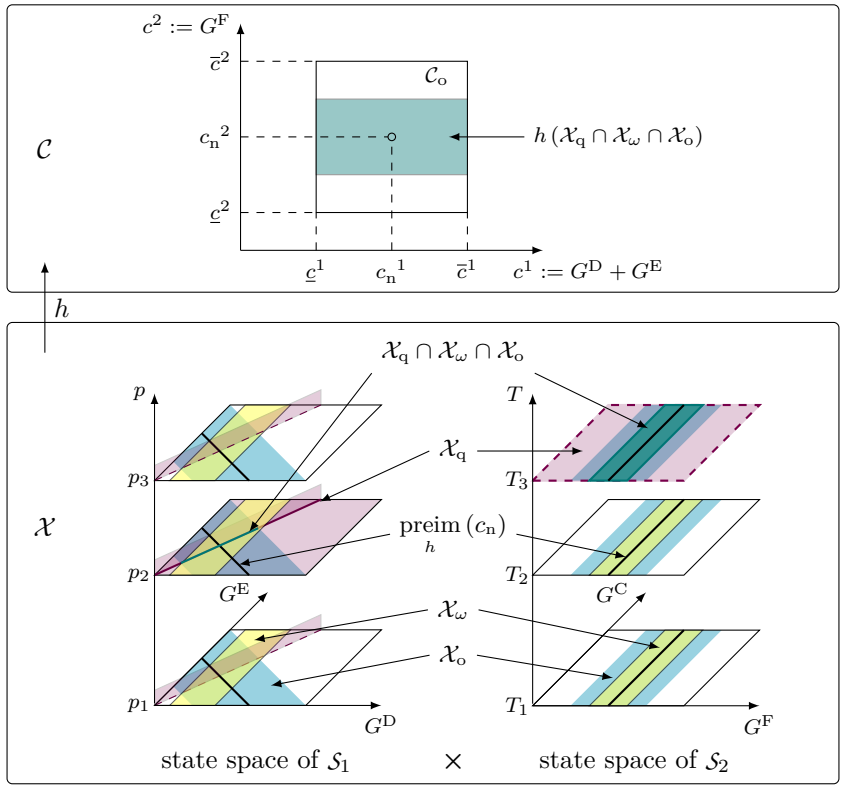

Figure 2.6: Illustration of the state and product space of Example 2.2.

Definition 2.9, we can conclude that the two processes are economically connected. Responsible for this is the composition of the product c^1. In case there is no specification regarding the product composition of $\mathcal{S}_1$, the processes are economically disconnected, which implies a higher degree of freedom when changing the production levels.

Example 2.3 (Production System Formed by an AD- and RSR-Process)**.** *We consider a production system consisting of two processes to form the substance* M. *Within the process* $\mathcal{S}_1$*, an anaerobic digestion reaction takes place, resulting in the decomposition of an organic substrate* S_1 *to* C *and* M. *The process* $\mathcal{S}_2$ *illustrates a classical reactor-separator-recycle (RSR) process using* H *from an upstream process element and* C *from* $\mathcal{S}_1$ *to form* M*, too. The* C *is temporarily stored in the storage element* ${\mathcal{B}_1}^1$*. The energy generated by the exothermic reaction is intermediately stored in a second storage element* ${\mathcal{B}_2}^1$ *to ensure that the decomposition in* $\mathcal{S}_1$ *can always proceed in the optimal temperature range. The feed parameter of* $\mathcal{S}_1$ *describes the quality of the organic substrate and relates with the production of* M*. In general, a higher quality causes a higher production of* M *while using the same amount of feed. For the RSR-process, we use the electricity price to parametrize the operating costs, since* H *is produced via an upstream process element, the electricity price correlates directly with the price of input stream of* H*. A detailed description of the model equations can be found in Appendix B.1.*

Before discussing the dynamic behavior of the production system, we will analyze some properties of the system where the dynamics and the input are not necessary. It only concerns the relationship between the states and the production levels, the product quality and the requirements by downstream processes. These properties are therefore independent of the specific dynamic model of the system.
First, we analyze the system with respect to its local or global economically operable, cf. Definition 2.8. In other words, we analyze whether there exists a state value for all production levels, that makes the product quality equal to one (gEO) or if this only applies to the nominal level (lEO). We discretized $\mathcal{C}_\mathrm{o}$ *by an equidistant grid with 100 times 100 points, and for each point, we determined a state employing a feasibility analysis. In this way, the result can only be approximated, but it can be verified that the system is gEO. Considering the production level and quality, it is obvious that the processes are economically connected, see Definition 2.9. This can be seen from the fact that the functions for the production level and quality have common states on which they depend. By adding the downstream process constraints in our analysis, it shows that the system is locally compatible according to Definition 2.10 since the total production amount is restricted. It follows that the system is only lEC as described in Definition 2.11 .*

Below, we examine how the system behaves during changes in operation resulting from changing feed parameters. However, no precise operational strategy was used. Of course, this affects the entire system, both the temporarily intended stationary operation and the transition between the production levels. In Part II, we will propose an operational strategy and examine how it performs for the given scenario.

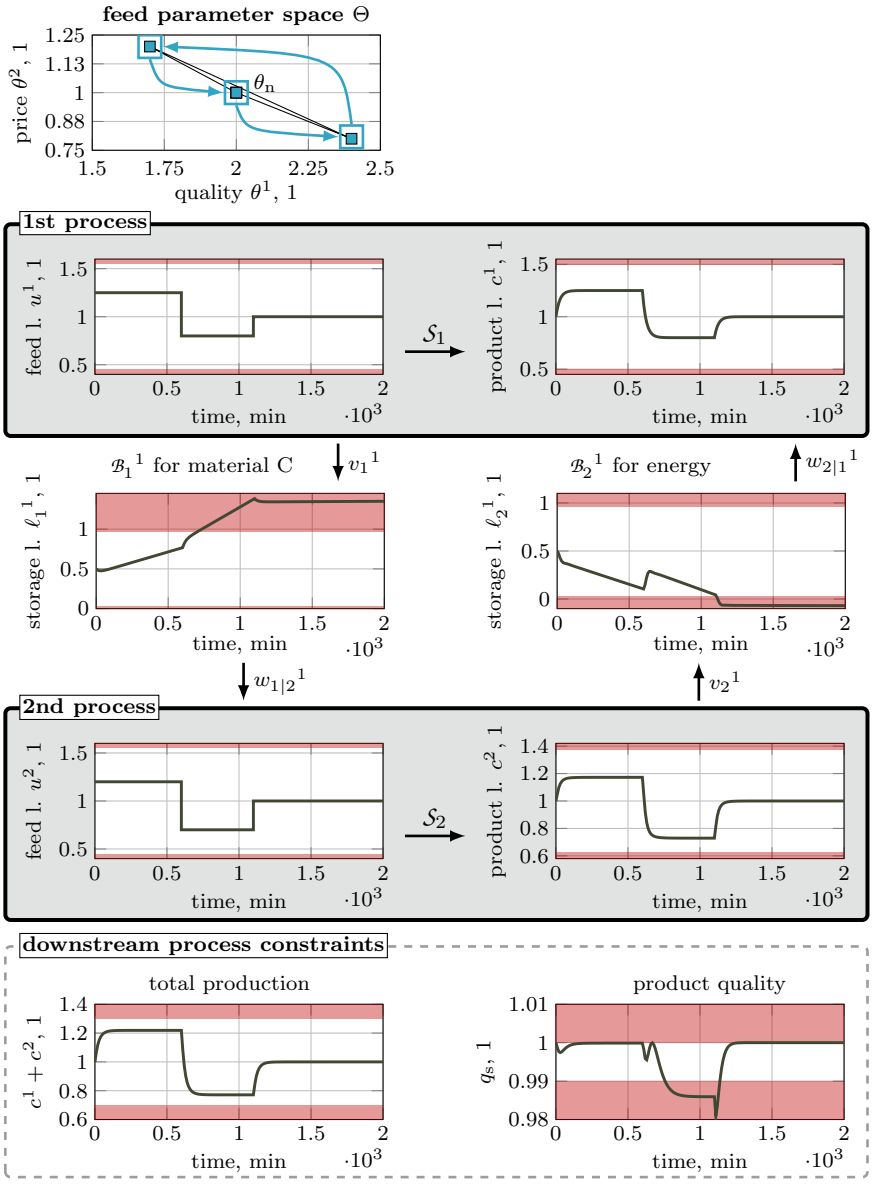

Figure 2.7: Illustration of the input-output behavior of the two processes.

Figure 2.7 shows the input-output behavior of the system, based on the feed parameter change depicted in the first row left column. Thereby, the feed and production levels are normalized to the nominal operating point. In general, the red shaded area in Figure 2.7 indicate the constraints of the system. The change of the quality factors is displayed in Figure 2.7 first row left column. Starting from θ_{n}, the H *price decreases to 80% of its nominal value and the feed quality increase by 20% due to reduced raw material prices. Before the nominal point is reached again, the price of* H *increase to 20% of its nominal value, while the quality decreases by 15%.*
Based on this scenario, the feed signal is modified according to the principle that higher feed prices (or lower feed qualities) lead to a reduction in process operation or vice versa. For $\mathcal{S}_1$, the feed signal and the corresponding production level is depicted in Figure 2.7 second row left and right column . The input-output behavior of $\mathcal{S}_2$ is shown in Figure 2.7 fourth row left and right column. The total production of the coupled process is displayed in Figure 2.7 fifth row left column, which changes according to the production levels. In the fifth row right column of Figure 2.7, the evolution of the production quality q_{s} is illustrated. It is evident that this was not considered for both the production and the transition phase, as they are violated for certain time spans. For instance, after the second transition, the stationary product quality violates the constraints (indicated by the red shaded area).
The processes are connected via the storage system, whose storage level is displayed in Figure 2.7 third row. This coupling of processes and storages is illustrated via the black vertical arrows showing byproducts and secondary feeds. Considering the evolution of storage levels, it can be concluded that the storage capacity of ${\mathcal{B}_1}^1$ and ${\mathcal{B}_2}^1$ are too small, and a minor increase in capacity achieve an improvement in only one cycle. The storage levels are related to the selected storage size $D_0 = (3\,\mathrm{kmol}, 3\,\mathrm{kJ})$, assuming that the initial level is given by half of the storage size. In this way, we dispense with modelling the start-up of the system and consider only the regular operation.

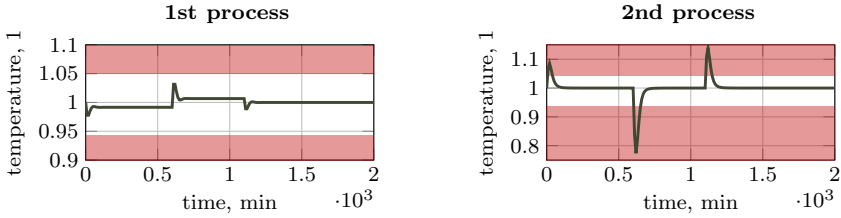

Figure 2.8: Illustration of the temperature behavior of the two processes.

Besides the input-output behavior, the process states are also important. In particular, we look at the reactor temperatures here, since their feasible region is relatively small compared to the other states, as the red shaded areas in Figure 2.8 show. Due to underlying regulatory systems, which were indirectly included in the modelling, the reactor temperatures are kept constant during steady-state operation. During the production transition, temperature changes can occur if the transitions are implemented too quickly, as can be seen in Figure 2.8 during all process transitions. To avoid these violations, an operational strategy is required that has to consider the entire system model (process and storage properties) with its dynamic characteristics. Another essential aspect is the design of the storage system based on this strategy, as the behavior of the storage levels is directly influenced from the decisions of a control instance.

2.2.4 Economic Model of the Production System

The need for an economic model of the production system is based on the central requirement that the system $\mathcal{P}$ should always be operated in the economic optimum, i.e., at maximum profit. For this purpose, we introduce in this section the profit function F and describe how it can be derived from a data set. We use the profit as economic criteria for two reasons. Firstly, it connects the system input, resulting in costs, with the system output resulting in income. The costs are described by the feed parameter and the income by the production level and their price. Secondly, it represents a time-varying factor when the feed parameter and the price are fluctuating over time. Specifically, the profit F of $\mathcal{P}$ is defined as the difference between the proceeds from selling the products c and the operational costs. Moreover, it depends on the state $x \in \mathcal{X}$ of the two processes, the selling price $p \in \mathbb{R}^2$ and the feed parameter $\theta \in \Theta$ describing the operational costs.

A standard method to describe the economical objective function, e.g. the profit, is via a parametric function, see [229, 47, 156, 267]. Depending on the application and task, different aspects such as yield, sales revenue, energy and material costs, total annual cost or a combination of these aspects are taken into account. Pintarič and Kravanja [196] address the problem of which economic optimization criteria are suitable. As mentioned above, we focus on the profit of the production system, using the most generic formulation. Even though revenues are easy to model, operational costs cover various aspects that are more challenging to represent because they are highly process-specific. A detailed modelling of operational costs requires a high level of specific knowledge of the process, cf. [79, 164, 232]. Thus, we will abstain from a purely parametric approach, since a generic formulation might be too restricted by the choice of

setup functions. This is especially true if these setup function shall only depend on the feed parameter θ.

For this reason, we propose a hybrid approach for the objective function consisting of a parametric and a non-parametric part. The parametric part describes the proceeds by the selling price, product quality and production level. The operational costs are modelled by a non-parametric function utilizing a set $\mathscr{F}$ of training data. Thus, the part of the objective function to be learned can be defined on a smaller subspace (i.e., lower dimension) of the domain and requires less training points. Specifically, we assume that the operational cost functions depend only on the production level c and the feed parameter θ. Instead, the parametric model allows us to extend the domain of F, which yields a clear benefit.

Various techniques are available for a learning-based approach to operational costs. For instance, artificial neural networks are a well established technique to build surrogate models, see [86, 18, 249, 142]. An alternative approach is the description of the cost by a Gaussian process, see [203]. Both techniques are based on training data consisting of input values and their corresponding output values.

Generally, the use of learning-based approaches in the context of optimization problems mostly concerns the system modeling [131, 151, 129, 160, 189]. Either the whole model is trained, or a simple first principle model is combined with an additional term that is trained by learning-based techniques. The resulting model structure of the latter one is similar to the hybrid approach for the economic objective function considered in the following. Nevertheless, there are also works in which the objective function or parts of it are learned directly, although those do not deal with economic issues. So, in [243], the stage costs are repeatedly updated with data from another MPC using a more detailed model and a longer planning horizon to ensure better control performance. In [14], the stage costs are defined via machine learning techniques. In [210, 25] the terminal cost are updated in each iteration.
Contrary to the approaches mentioned above, we will use the derived economic objective function within a static optimization. Besides, it is only trained before the system is commissioned and then updated at varying times (i.e., when new data is available). Since we are considering two processes and thus, two different operational costs, an additional condition will be required besides the set $\mathscr{F}$ of profit data to guarantee a unique economic function. Here, we will exploit the nominal operating point and clarify how the data needs to be provided. Before we take a closer look at the training part, the profit function is introduced by the following definition.

Definition 2.12 (Profit Function)**.** *Let $\mathcal{P}$ be a production system with the set Q of quality functions. Furthermore, let $\mathcal{F}$ be a training set. From Q, the subset Q_α is derived, which elements are those quality functions that describe the product c^α of $\mathcal{S}_\alpha$. If there is no quality function related to c^α, the subset contains only the function $q_\mathrm{s}(x) := 1$, for all $x \in \mathcal{X}$. Let $\Theta := \left\{\xi \in \mathbb{R}^2 \mid \underline{\theta} \leq \xi \leq \overline{\theta}\right\}$ be a set of all possible feed parameters of the system. The profit function is defined by*

$$F : \mathbb{R}^2 \times \mathcal{C}_\mathrm{o} \times \Theta \times \mathcal{X} \to \mathbb{R},\ (p, c, \theta, x) \mapsto F\left(p, c, \theta, x\right),$$

where

$$F\left(p, c, \theta, x\right) := \sum_{\alpha=1}^{2} \Big(P_\alpha\left(p^\alpha, c^\alpha, x\right) - O_\alpha\left(\theta^\alpha, c^\alpha\right) \Big). \tag{2.10}$$

Here, P_α denotes the proceeds from the sale of the product c^α, given by the parametric approach

$$P_\alpha\left(p^\alpha, c^\alpha, x\right) := p^\alpha c^\alpha \prod_{q_{\mathrm{s},i} \in Q_\alpha} q_{\mathrm{s},i}(x).$$

The operational costs $O_\alpha : \mathcal{C}_\mathrm{o} \times \Theta \to \mathbb{R}^+$, $\alpha = 1, 2$ will be expressed by an nonparametric approach specified by $\mathcal{F}$.

The system $\mathcal{P}$ is considered as one element in a larger network, so we assume that the profit information is provided for the entire production system and not for each process. From Definition 2.12, it can be deduced that only the operational costs have to be determined from $\mathcal{F}$. These are dependent on the particular production level c and the feed parameter θ, so that $\mathcal{F}$ has to contain this information as training inputs. The training outputs are given by the corresponding profit values to be provided at the corresponding inputs (c, θ). However, it is recommended to choose only those training inputs whose states x obtain a product quality value of one, as it simplifies. The reason for this is that we need to derive training points for operating costs O_α from F, whereby the value of the product quality must be known. If $\mathcal{P}$ is gEO according to Definition 2.8 there is at least one $x \in \mathcal{X}$ for each $c \in \mathcal{C}_\mathrm{o}$, which simplifies the selection of the training inputs and thus the economic analysis. For the design of F in the sense of Definition 2.12, we rely on the following assumption.

Assumption 2.3. *The system $\mathcal{P}$ is gEO according to Definition 2.8.*

To determine the operational costs of a non-parametric approach using $\mathcal{P}$, we propose Gaussian processes (GPs) for O_α that are trained separately.

Appendix A.2 gives a brief introduction to this topic and describes besides the application also some properties.
A cruical aspect is to show how the training outputs, i.e., the function values of F at different points in $\mathcal{C}_\mathrm{o} \times \Theta$, can be used to obtain $\{O_\alpha\}_{\alpha=1,2}$. For this purpose, we assume that there exists a unique point in $\mathcal{C}_\mathrm{o} \times \Theta$ where accurate economic information is available. This leads to the following assumption.

Assumption 2.4. *For the system $\mathcal{P}$, with the nominal production level $c_\mathrm{n} \in \mathcal{C}_\mathrm{o}$, the nominal profit value $\boldsymbol{F}_\mathrm{n} \in \mathbb{R}^+$ is known for a nominal selling price $p_\mathrm{n} \in \mathbb{R}^+$. Furthermore, for $\mathcal{P}$ a ratio*

$$r_\mathrm{n} := \frac{O_1\left({\theta_\mathrm{n}}^1, {c_\mathrm{n}}^1\right)}{O_2\left({\theta_\mathrm{n}}^2, {c_\mathrm{n}}^2\right)} \in \mathbb{R}^+,$$

is given, where $\theta_\mathrm{n} \in \Theta$ is called nominal feed parameter.

Besides the nominal point, as indicated in Assumption 2.4, we also need a series of training inputs $\boldsymbol{u} := \{\boldsymbol{u}_1, \ldots\}$ and its corresponding profit values as training outputs $\boldsymbol{F} := \{\boldsymbol{F}_1, \ldots\}$ from the economic analysis. Since such an analysis may be subject to uncertainties, this should be considered in $\mathscr{F}$ and thus for the determination of $\{O_\alpha\}_{\alpha=1,2}$.
Before describing the structure of the training set, we briefly review the profit function F. Considering Assumption 2.3 and 2.4, for a given nominal selling price p_n and $x_\mathrm{q} \in \mathcal{X}_\mathrm{o} \cap \mathcal{X}_\mathrm{q}$, we define a reduced profit function

$$F_\mathrm{r} : \mathcal{C}_\mathrm{o} \times \Theta \to \mathbb{R},\ (c, \theta) \mapsto F_\mathrm{r}(c, \theta) := F(p_\mathrm{n}, c, \theta, x_\mathrm{q}), \tag{2.11}$$

which is evaluated for the fixed nominal price p_n and state $x_\mathrm{q} \in \mathcal{X}_\mathrm{q}$.

Remark 2.3. *From Assumption 2.3 it is clear that there exists an $x \in \mathcal{X}_\mathrm{o} \cap \mathcal{X}_\mathrm{q}$ for all $c \in \mathcal{C}_\mathrm{o}$. However, it should be noted that the set $\mathcal{X}_\mathrm{o} \cap \mathcal{X}_\mathrm{q}$ does not have to be invariant with respect to system dynamics.*

In order to use F as an economic objective, which allows to achieve an optimal operational management, the following assumption is made.

Assumption 2.5. *Any reduced profit function $F_\mathrm{r}(\cdot, \theta)$ is concave over $\mathcal{C}_\mathrm{o}$ for all $\theta \in \Theta$.*

Finally, the set $\mathscr{F}$ is defined by specifying its elements.

Definition 2.13 (A Suitable Training Set $\mathscr{F}$)**.** *Let $\mathbb{I}_1 := \{1, \ldots, n_{\theta,1}\}$ and $\mathbb{I}_2 := \{n_{\theta,1}+1, \ldots, n_{\theta,1}+n_{\theta,2}\}$ denote two index sets. The set*

$$\begin{aligned}\mathscr{F} := \big\{ &(\boldsymbol{u}_1, \boldsymbol{F}_1), \ldots, \left(\boldsymbol{u}_{3n_{\theta,1}}, \boldsymbol{F}_{3n_{\theta,1}}\right), \\ &\left(\boldsymbol{u}_{3n_{\theta,1}+1}, \boldsymbol{F}_{3n_{\theta,1}+1}\right), \ldots, \left(\boldsymbol{u}_{3(n_{\theta,1}+n_{\theta,2})}, \boldsymbol{F}_{3(n_{\theta,1}+n_{\theta,2})}\right) \big\},\end{aligned}$$

of training points for the operational costs $\{O_\alpha\}_{\alpha=1,2}$ *is said to be suitable if it satisfies the input and output consistency properties. The input consistency specifies the structure of the training points and is defined by the following properties:*

(i) The training inputs $\boldsymbol{u}_i \in \mathcal{C}_\mathrm{o} \times \Theta \times \mathbb{R}_0^+$ *are given by*

$$\boldsymbol{u}_{3(i-1)+1} := \left(\underline{c}^1, {c_\mathrm{n}}^2, {\theta_i}^1, {\theta_\mathrm{n}}^2, 0\right), \quad i \in \mathbb{I}_1, \tag{2.12a}$$

$$\boldsymbol{u}_{3(i-1)+2} := \left({c_i}^1, {c_\mathrm{n}}^2, {\theta_i}^1, {\theta_\mathrm{n}}^2, \varepsilon_i\right), \quad i \in \mathbb{I}_1, \tag{2.12b}$$

$$\boldsymbol{u}_{3(i-1)+3} := \left(\overline{c}^1, {c_\mathrm{n}}^2, {\theta_i}^1, {\theta_\mathrm{n}}^2, 0\right), \quad i \in \mathbb{I}_1, \tag{2.12c}$$

for the first $3n_{\theta,1}$ *input points that are related to* $\mathcal{S}_1$ *and*

$$\boldsymbol{u}_{3(i-1)+1} := \left({c_\mathrm{n}}^1, \underline{c}^2, {\theta_\mathrm{n}}^1, {\theta_i}^2, 0\right), \quad i \in \mathbb{I}_2, \tag{2.13a}$$

$$\boldsymbol{u}_{3(i-1)+2} := \left({c_\mathrm{n}}^1, {c_i}^2, {\theta_\mathrm{n}}^2, {\theta_i}^1, \varepsilon_i\right), \quad i \in \mathbb{I}_2, \tag{2.13b}$$

$$\boldsymbol{u}_{3(i-1)+3} := \left({c_\mathrm{n}}^1, \overline{c}^2, {\theta_\mathrm{n}}^1, {\theta_i}^2, 0\right), \quad i \in \mathbb{I}_2, \tag{2.13c}$$

for the last $3n_{\theta,2}$ *input points that are related to* $\mathcal{S}_2$*.*

(ii) The training outputs $\boldsymbol{F}_i \in \mathbb{R}^+ \times \mathbb{R}_0^+$ *are given by*

$$\boldsymbol{F}_{3(i-1)+1} := \left(\hat{\boldsymbol{F}}_{3(i-1)+1}, \delta_{3(i-1)+1}\right), \quad i \in \mathbb{I}_1 \cup \mathbb{I}_2,$$

$$\boldsymbol{F}_{3(i-1)+2} := \left(\hat{\boldsymbol{F}}_{3(i-1)+2}, \delta_{3(i-1)+2}\right), \quad i \in \mathbb{I}_1 \cup \mathbb{I}_2,$$

$$\boldsymbol{F}_{3(i-1)+3} := \left(\hat{\boldsymbol{F}}_{3(i-1)+3}, \delta_{3(i-1)+3}\right), \quad i \in \mathbb{I}_1 \cup \mathbb{I}_2.$$

Here, $\varepsilon_i \in \mathbb{R}_0^+$ *and* $\delta_i \in \mathbb{R}_0^+$ *describe the uncertainties of the optimal production level and the measurements of the profit values* $\hat{\boldsymbol{F}} \in \mathbb{R}^+$ *at the corresponding production level. Let* $\mathrm{pr}_c : \mathcal{C}_\mathrm{o} \times \Theta \times \mathbb{R}_0^+ \to \mathcal{C}_\mathrm{o},\ (\boldsymbol{u}_i) \mapsto \mathrm{pr}_\mathrm{c}(\boldsymbol{u}_i) := \left({\boldsymbol{u}_i}^1, {\boldsymbol{u}_i}^2\right)$ *be a projection on the production level. Moreover, let* $\mathrm{pr}_\theta : \mathcal{C}_\mathrm{o} \times \Theta \times \mathbb{R}_0^+ \to \Theta,\ (\boldsymbol{u}_i) \mapsto \mathrm{pr}_\theta(\boldsymbol{u}_i) := \left({\boldsymbol{u}_i}^3, {\boldsymbol{u}_i}^4\right)$ *be a projection on the feed parameter. The output consistency characterize the properties of the objective function at the training points and is defined by*

(i) For $c_l := \mathrm{pr}_c(\boldsymbol{u}_l)$ *and* $\theta_l := \mathrm{pr}_\theta(\boldsymbol{u}_l)$*, the function* F_r *has to satisfy*

$$-{\boldsymbol{F}_l}^2 \leq F_\mathrm{r}\left(c_l, \theta_l\right) - {\boldsymbol{F}_l}^1 \leq {\boldsymbol{F}_l}^2, \quad l = 3(i-1)+j, i \in \mathbb{I}_1 \cup \mathbb{I}_2,\ j = 1,3 \tag{2.14}$$

(ii) For $\theta_l := \mathrm{pr}_\theta(\boldsymbol{u}_l)$, the function F_r has to satisfy

$$-\left(\boldsymbol{u}_l{}^5, 0\right) \leq \arg\max_{c\in\mathcal{C}_0} F_\mathrm{r}\left(c, \theta_l\right) - \boldsymbol{u}_l{}^1 \leq \left(\boldsymbol{u}_l{}^5, 0\right), \; l = 3i-1, \, i \in \mathbb{I}_1 \tag{2.15a}$$

$$-\left(0, \boldsymbol{u}_l{}^5\right) \leq \arg\max_{c\in\mathcal{C}_0} F_\mathrm{r}\left(c, \theta_l\right) - \boldsymbol{u}_l{}^2 \leq \left(0, \boldsymbol{u}_l{}^5\right), \; l = 3i-1, \, i \in \mathbb{I}_2. \tag{2.15b}$$

(iii) For $\theta_l := \mathrm{pr}_\theta(\boldsymbol{u}_l)$, the function F_r has to satisfy

$$-\boldsymbol{F}_l{}^2 \leq \underset{c\in\mathcal{C}_0}{\text{maximize}} \; F_\mathrm{r}\left(c, \theta_l\right) - \boldsymbol{F}_l{}^1 \leq \boldsymbol{F}_l{}^2, \; l = 3i-1, \, i \in \mathbb{I}_1 \cup \mathbb{I}_2. \tag{2.16}$$

Remark 2.4. *The training set $\mathscr{F}$ includes the nominal points introduced in Assumption 2.4.*

In the following we will discuss the individual aspects of Definition 2.13 to clarify their importance. The conceptual idea concerns three points:

(i) The two operational costs are independent of from each other, as they belong to different processes.

(ii) The training outputs refer to the reduced profit function in (2.11) and thus to the profit values. Hence, the process-specific operational costs need to be extracted from the overall profit values.

(iii) We assume that the economic analysis be uncertain, so that the profit values and the optimal production level can only be indicated by safety ranges.

Figure 2.9 illustrates the different domains, such as Θ and $\mathcal{C}_\mathrm{o}$ and is helpful to understand the requirements from Definition 2.13. The operating costs of the individual processes only depend on their production level c^α and feed paramter θ^α, so the corresponding functions $\{O_\alpha\}_{\alpha=1,2}$ can also be trained individually. To this end we have to choose a fixed and suitable point (i.e., c and θ coordinates) for one of the processes to train the other. For this purpose, the nominal operating point is used, as described in Assumption 2.4. Figure 2.9 a) shows the set Θ and the positions of the different training points for the feed parameter by the green dots. In Figure 2.9 b) the level sets of $F_\mathrm{r}\left(\cdot, \theta_\mathrm{n}\right)$ are presented by thin black lines, where the optimal production level agrees with c_n. If a change in the feed parameter θ^α occurs for one of the processes, the optimal production level shifts due to changing operational costs. This can be achieved in two ways. Either θ^α only influences the optimal production level of S_α, as shown by the green arrow in Figure 2.9 b). Or the optimal production

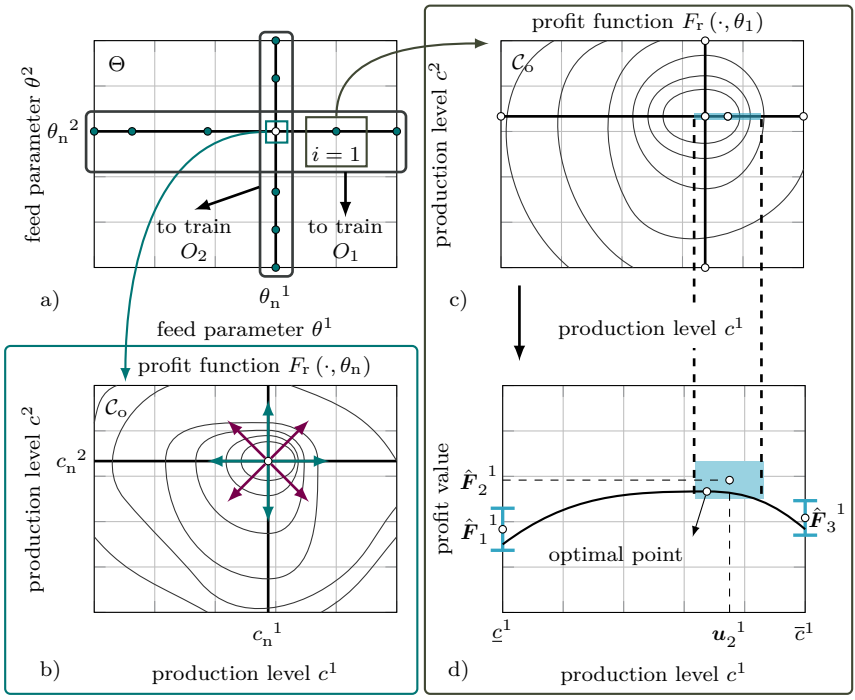

Figure 2.9: Principal of the training set $\mathscr{F}$ for the profit function.

levels of both processes might be changed, as the red arrow indicates. The latter situation occurs when the storage levels reach their boundaries or a common product is produced and the processes are economically connected.
According to (2.12) and (2.13), the three training inputs $\left\{\boldsymbol{u}_{3(i-1)+j}\right\}_{j=1,2,3}$, $i \in \mathbb{I}_1 \cup \mathbb{I}_2$, describe one point in Θ. For one representative point $\theta_1 = \left(\theta_1{}^1, \theta_n{}^2\right) \in \Theta$, Figure 2.9 c) and d) illustrate the idea of three training points $\left\{\boldsymbol{u}_j\right\}_{j=1,2,3}$. Furthermore, Figure 2.9 c) shows the possible level sets of $F_r(\cdot, \theta_1)$. However, these are uncertain, as shown in Figure 2.9 d) by the profit curve over the production level. The uncertainties are expressed by box constraints at boundaries $\underline{c}^1$ and $\bar{c}^1$ as well as for the possible position of the optimum.

To train $\{O_\alpha\}_{\alpha=1,2}$, the profit values have to be converted into values for the operational costs, whereby the defined structure of $\mathscr{F}$ is well suited, as we will show next. In addition, the information about the uncertainties also has to be included to the operational costs. However, we start with deriving an initial set for the training process to obtain primary functions $\left\{O_\alpha^0\right\}_{\alpha=1,2}$. Subsequently,

we will modify $\left\{O_\alpha^0\right\}_{\alpha=1,2}$ by iteratively solving an optimization problem to meet the specifications of the profit function F_r, considering the uncertainties.

The initial training sets $\left\{\mathscr{O}_\alpha^0\right\}_{\alpha=1,2}$ for the operational costs are generated from $\mathscr{F}$ using Assumption 2.4. Algorithm 2.1 describes the procedure to obtain both sets and also describes the structure of the training inputs and outputs.

Algorithm 2.1: Initial sets to train the Operational Costs

Input: the ratio r_n, the nominal selling price p_n,
the nominal profit value $\boldsymbol{F}_\mathrm{n}$ and the set $\mathscr{F}$
initialize the sets $\{\boldsymbol{v}_i\}_{i=1,2} = \emptyset$, $\{\boldsymbol{O}_i\}_{i=1,2} = \emptyset$; compute for both processes
the nominal costs $K_1 := r_\mathrm{n} K_2$ and $K_2 := \left(\sum_{\alpha=1}^{2} {p_\mathrm{n}}^\alpha {c_\mathrm{n}}^\alpha - \boldsymbol{F}_\mathrm{n}\right)(1 + r_\mathrm{n})^{-1}$
for $i \in \mathbb{I}_1$ **do**
  for $j = 1, 2, 3$ **do**
    determine the index $l \leftarrow 3(i-1) + j$
    set up the training inputs $\boldsymbol{v}_1 \leftarrow \left\{\boldsymbol{v}_1, \left({\boldsymbol{u}_l}^1, {\boldsymbol{u}_l}^3\right)\right\}$
    and the training outputs $\boldsymbol{O}_1 \leftarrow \left\{\boldsymbol{O}_1, {p_\mathrm{n}}^1 {\boldsymbol{u}_l}^1 + {p_\mathrm{n}}^2 {c_\mathrm{n}}^2 - {\boldsymbol{F}_l}^1 - K_2\right\}$
  end
end
for $i \in \mathbb{I}_2$ **do**
  for $j = 1, 2, 3$ **do**
    determine the index $l \leftarrow 3(i-1) + j$
    set up the training inputs $\boldsymbol{v}_2 \leftarrow \left\{\boldsymbol{v}_2, \left({\boldsymbol{u}_l}^2, {\boldsymbol{u}_l}^4\right)\right\}$
    and the training outputs $\boldsymbol{O}_2 \leftarrow \left\{\boldsymbol{O}_2, {p_\mathrm{n}}^2 {\boldsymbol{u}_l}^2 + {p_\mathrm{n}}^1 {c_\mathrm{n}}^1 - {\boldsymbol{F}_l}^1 - K_1\right\}$
  end
end
Result: training sets $\mathscr{O}_1^0 := \left\{\left(\boldsymbol{v}_{1,1}, \boldsymbol{O}_{1,1}\right), \ldots, \left(\boldsymbol{v}_{1,3n_{\theta,1}}, \boldsymbol{O}_{1,3n_{\theta,1}}\right)\right\}$
and $\mathscr{O}_2^0 := \left\{\left(\boldsymbol{v}_{2,1}, \boldsymbol{O}_{2,1}\right), \ldots, \left(\boldsymbol{v}_{2,3n_{\theta,2}}, \boldsymbol{O}_{2,3n_{\theta,2}}\right)\right\}$

As mentioned before, the operational costs are obtained by two GPs, where no prior knowledge about the costs are assumed so that the prior mean function is set to be zero. A more detailed introduction about GPs is given in Appendix A.2. Using the training set $\left\{\mathscr{O}_\alpha^k\right\}_{\alpha=1,2}$ and the hyperparameter $\mathfrak{h}_\alpha^k := (l_\alpha, \sigma_{\mathrm{f},\alpha}, \sigma_{\mathrm{y},\alpha})$, $\alpha = 1, 2$ we can define the k-th operational cost function

$$O_\alpha^k : \mathcal{C}_\mathrm{o} \times \Theta \to \mathbb{R}^+,\ (c, \theta) \mapsto O_\alpha^k(c, \theta) := (a_\alpha)^\beta \left(\eta_\alpha^{\boldsymbol{v}}\right)_\beta \left(c^\alpha, \theta^\alpha\right), \tag{2.17}$$

of the process $\mathcal{S}_\alpha$, where the terms $(a_\alpha)^\beta := (L_\alpha)^{\beta\iota} (\boldsymbol{O}_\alpha)_\iota$ and $(\eta_\alpha^{\boldsymbol{v}})_\beta$ are specified in more detail in Appendix A.2. It should be emphazised that the index k denotes that O_α^k are obtained by the training set $\mathscr{O}_\alpha^k$ and the hyperparameter $\mathfrak{h}_\alpha^k$. In general, the profit function generated from O_α^0 and $\mathfrak{h}_\alpha^0$ does not satisfies the output consistency formulated in Definition 2.13. In particular, the optimal production levels are not necessarily within the predefined box constraints for a fixed feed parameter $\mathrm{pr}_\theta(\boldsymbol{u}_l)$. Hence, it is important to modify $\mathscr{O}_\alpha^0$ and $\mathfrak{h}_\alpha^0$ iteratively for both processes. In this context, the reduced k-th profit function

$$F_\mathrm{r}^k : \mathcal{C}_\mathrm{o} \times \Theta \to \mathbb{R},$$

$$(c, \theta) \mapsto F_\mathrm{r}^k (c, \theta) := {p_\mathrm{n}}^1 c^1 + {p_\mathrm{n}}^2 c^2 - O_1^k \left(c^1, \theta^1\right) - O_2^k \left(c^2, \theta^2\right),$$

formed with $\mathscr{O}_\alpha^k$ and $\mathfrak{h}_\alpha^k$ is used to check whether the output consistency is met after a finite number of iterations. Considering (2.17), it is easy to see that there are three ways to adapt the operational costs and thus the profit function. First, the hyperparameter can be changed, which effects the entire GP and thus also those areas that already fulfill the output consistency. Second, it is possible to add virtual training points to the set $\mathscr{O}_\alpha^k$. This additional training data will cause a local deformation of the cost function. The third option combines the two ways mentioned before and is proposed here.
To add new virtual training points, it is crucial to know at which feed parameters they should be located. Therefore, we define the ordered set

$$\Theta_\mathrm{f}^k := \{\theta \in \mathrm{pr}_\theta(\boldsymbol{u}) \subset \Theta \mid \text{(2.15) and (2.16) are not satified using } F_\mathrm{r}^k \text{ and without repetition}\},$$

of all feed parameters for which the output consistency is violated. In the same way, the index sets $\left\{\mathbb{I}_{\mathrm{f},\alpha}^k \subseteq \mathbb{I}_\alpha\right\}_{\alpha=1,2}$ can be generated containing those indices of the feed parameters, which are elements of Θ_f^k, related to the individual process. If $\Theta_\mathrm{f}^k = \emptyset$, the operating costs are consistent with the requirements of the profit function. The update of the training set is given by

$$\mathscr{O}_\alpha^k := \mathscr{O}_\alpha^{k-1} \cup \hat{\mathscr{O}}_\alpha^k, \tag{2.18}$$

where

$$\hat{\mathscr{O}}_\alpha^k := \bigcup_{\substack{\boldsymbol{\theta}_l \in \Theta_\mathrm{f}^k, \\ {\boldsymbol{\theta}_l}^{\beta\neq\alpha} = {\theta_\mathrm{n}}^{\beta\neq\alpha}}} \left(\hat{\boldsymbol{c}}_{\alpha\, l}^k, {\boldsymbol{\theta}_l}^\alpha, \hat{\boldsymbol{O}}_{\alpha\, l}^k\right).$$

This means that the training set for deriving O_α^k consists of points that are already known and new virtual points summarized in $\hat{\mathscr{O}}_\alpha^k$. Based on $\hat{\mathscr{O}}_\alpha^k$, the sets

of the virtual training inputs $\hat{\boldsymbol{c}}_\alpha^k := \left\{\hat{\boldsymbol{c}}_{\alpha\,1}^k, \hat{\boldsymbol{c}}_{\alpha\,2}^k, \ldots\right\}$ and the corresponding virtual training outputs $\hat{\boldsymbol{O}}_\alpha^k := \left\{\hat{\boldsymbol{O}}_{\alpha\,1}^k, \hat{\boldsymbol{O}}_{\alpha\,2}^k, \ldots\right\}$ can be derived. The identification of these points in combination with suitable hyperparameter $\mathfrak{h}_\alpha^k$ can be done by solving a feasibility problem. However, before we address this problem, it is useful to discuss some basic aspects.
The conditions (2.15) and (2.16) imply the solving of an optimization problem. To reduce the complexity of the feasibility problem, this optimization problem can be reformulated by its first-order optimality conditions. As both processes are separated, the operational costs and thus the update of $\mathscr{O}_\alpha^k$ and $\mathfrak{h}_\alpha^k$ will be done individually, which reduces the complexity of the calculation. In order to write the feasibility problem in a more compact form, we introduce a further reduced form of profit function for each process as follows:

1. For a given feed parameter $\vartheta \in \left[\underline{\theta}^1, \overline{\theta}^1\right]$ of $\mathcal{S}_1$, let

$$F_{\mathrm{r},1,\vartheta}^k : \left[\underline{c}^1, \overline{c}^1\right] \to \mathbb{R},\ (c) \mapsto F_{\mathrm{r},1,\vartheta}^k\,(c) := F_{\mathrm{r}}^k\Big(\left(c, {c_{\mathrm{n}}}^2\right), \left(\vartheta, {\theta_{\mathrm{n}}}^2\right)\Big).$$

2. For a given feed parameter $\vartheta \in \left[\underline{\theta}^2, \overline{\theta}^2\right]$ of $\mathcal{S}_2$, let

$$F_{\mathrm{r},2,\vartheta}^k : \left[\underline{c}^2, \overline{c}^2\right] \to \mathbb{R},\ (c) \mapsto F_{\mathrm{r},2,\vartheta}^k\,(c) := F_{\mathrm{r}}^k\Big(\left({c_{\mathrm{n}}}^1, c\right), \left({\theta_{\mathrm{n}}}^1, \vartheta\right)\Big).$$

These functions describe the profit depending on the production level c^α of $\mathcal{S}_\alpha$ trained by $\mathscr{O}_\alpha^k$ and $\mathfrak{h}_\alpha^k$. In addition, we define for both processes the ordered sets

$$\mathrm{C}_{\alpha,<}^i := \left\{\underline{c}^\alpha, \left(c_{\alpha,<}^i\right)_1, \left(c_{\alpha,<}^i\right)_2, \ldots, \tilde{c}_{\alpha\,i}\right\}, \quad i = 1, \ldots, n_{\theta,\alpha},$$

with $\underline{c}^\alpha < \left(c_{\alpha,<}^i\right)_1 < \ldots < \tilde{c}_{\alpha\,i}$ to characterize the ascending branch and

$$\mathrm{C}_{\alpha,>}^i := \left\{\tilde{c}_{\alpha\,i}, \left(c_{\alpha,>}^i\right)_1, \left(c_{\alpha,>}^i\right)_2, \ldots, \overline{c}^\alpha\right\}, \quad i = 1, \ldots, n_{\theta,\alpha},$$

with $\tilde{c}_{\alpha\,i} < \left(c_{\alpha,>}^i\right)_1 < \ldots < \overline{c}^\alpha$ to characterize the descending branch of the profit function, cf. Figure 2.9 d). These sets describe a discretization of the operating area depending on the feed parameter of $\mathcal{S}_\alpha$. Here, $\tilde{c}_{\alpha\,i}$ denotes the optimal production level of $\mathcal{S}_\alpha$ for a given feed parameter ϑ_i based on $F_{\mathrm{r},\alpha,\vartheta_i}^k$. Definition 2.13 states a number of criteria for those optimal production levels that have to be fulfilled by the final profit function. The set of all optimal production levels for $\mathcal{S}_\alpha$ is denoted by $\tilde{c}_\alpha := \left\{\tilde{c}_{\alpha\,1}, \ldots, \tilde{c}_{\alpha\,n_{\theta,\alpha}}\right\}$. Finally, the feasibility problem for each process in the k-th iteration reads as

$$\text{find} \qquad \hat{\boldsymbol{c}}_\alpha^k,\ \hat{\boldsymbol{O}}_\alpha^k,\ \mathfrak{h}_\alpha^k,\ \tilde{c}_\alpha \tag{2.19a}$$

subject to

$$\underline{\mathfrak{h}}_\alpha^k \leq \mathfrak{h}_\alpha^k \leq \overline{\mathfrak{h}}_\alpha^k \tag{2.19b}$$

$$0 = \vartheta_i - \mathrm{pr}_\alpha \circ \mathrm{pr}_\theta \left(\boldsymbol{u}_{3i}\right), \qquad \forall i \in \mathbb{I}_\alpha^k, \tag{2.19c}$$

$$-\boldsymbol{F}_{3i-2}{}^2 \leq F_{\mathrm{r},\alpha,\vartheta_i}^k \left(\boldsymbol{u}_{3i-2}{}^\alpha\right) - \boldsymbol{F}_{3i-2}{}^1 \leq \boldsymbol{F}_{3i-2}{}^2, \quad \forall i \in \mathbb{I}_\alpha^k, \tag{2.19d}$$

$$-\boldsymbol{F}_{3i}{}^2 \leq F_{\mathrm{r},\alpha,\vartheta_i}^k \left(\boldsymbol{u}_{3i}{}^\alpha\right) - \boldsymbol{F}_{3i}{}^1 \leq \boldsymbol{F}_{3i}{}^2, \qquad \forall i \in \mathbb{I}_\alpha^k, \tag{2.19e}$$

$$-\boldsymbol{F}_{3i-1}{}^2 \leq F_{\mathrm{r},\alpha,\vartheta_i}^k \left(\tilde{c}_{\alpha\, i}\right) - \boldsymbol{F}_{3i-1}{}^1 \leq \boldsymbol{F}_{3i-1}{}^2, \qquad \forall i \in \mathbb{I}_\alpha^k \tag{2.19f}$$

$$-\boldsymbol{u}_{3i-1}{}^5 \leq \tilde{c}_{\alpha\, i} - \boldsymbol{u}_{3i-1}{}^\alpha \leq \boldsymbol{u}_{3i-1}{}^5, \qquad \forall i \in \mathbb{I}_\alpha^k, \tag{2.19g}$$

$$0 = \partial_1 F_{\mathrm{r},\alpha,\vartheta_i}^k \left(\tilde{c}_{\alpha\, i}\right), \qquad \forall i \in \mathbb{I}_\alpha^k, \tag{2.19h}$$

$$0 \leq F_{\mathrm{r},\alpha,\vartheta_i}^k \left(c_{j+1}\right) - F_{\mathrm{r},\alpha,\vartheta_i}^k \left(c_j\right), \qquad \forall i \in \mathbb{I}_\alpha^k, \ \forall c_j, c_{j+1} \in \mathrm{C}_{\alpha,<}^i, \tag{2.19i}$$

$$0 \leq F_{\mathrm{r},\alpha,\vartheta_i}^k \left(c_j\right) - F_{\mathrm{r},\alpha,\vartheta_i}^k \left(c_{j+1}\right), \qquad \forall i \in \mathbb{I}_\alpha^k, \ \forall c_j, c_{j+1} \in \mathrm{C}_{\alpha,>}^i, \tag{2.19j}$$

where $\mathbb{I}_\alpha^k \subseteq \mathbb{I}_\alpha$ is an index set of those feed parameters used for the update. The objective (2.19a) of this problem is to identify feasible virtual training points and hyperparameter, so that the profit function satisfies the output consistency. In this context, suitable optimal production levels have also to be determined. The constraint (2.19b) is used to keep the hyperparameter in a predefined area given by a lower and upper bound. Using (2.19c), the corresponding feed parameter ϑ_i is extracted, which describes the cross-sectional plane of the profit function, which is further specified by the additional constraints. The constraints (2.19d) and (2.19e) describe the output consistency (2.14) at the lower and the upper bound of the operating area of $\mathcal{S}_\alpha$. To ensure that the optimal production level and its profit value lies within the predefined area, we use (2.19f) and (2.19g). Moreover, the derivative at the optimal production level has to be zero, which is guaranteed by (2.19h). Finally, the monotony of $F_{\mathrm{r},\alpha,\cdot}^k$ is included by (2.19i) and (2.19j).

The feasibility problem (2.19) for updating the cost function has to be solved iteratively. For this it is necessary to determine which subset $\mathbb{I}_\alpha^k$ is used and

hence which feed parameters are considered in each iteration step. If the entire index set $\mathbb{I}_\alpha$ is used and the problem is feasible, the algorithm terminates after one step. However, if the problem is not feasible, we propose to restrict $\mathbb{I}_\alpha^k$ only to those feed parameters that violate the output consistency. This means in particular $\mathbb{I}_\alpha^k := \mathbb{I}_{\mathrm{f},\alpha}^k$. In this way, the problem usually has to be solved several times, but improves the feasibility of the solution. A suitable termination criteria results from the set Θ_f^k and the requirement that this has to be empty. The following algorithm summarizes the individual points and allows to determine the final profit function.

Algorithm 2.2: Final profit function

Input: the initial hyperparameter $\mathfrak{h}_\alpha^0$ and training set $\left\{\mathscr{O}_\alpha^k\right\}_{\alpha=1,2}$

for $\alpha = 1, 2$ **do**
  set index $k := 1$ and generate the sets Θ_f^k and $\mathbb{I}_{\mathrm{f},\alpha}^k$
  while $\mathbb{I}_{\mathrm{f},\alpha}^k \neq \emptyset$ **do**
    update the set $\mathscr{O}_\alpha^k$ according to (2.18) and build F_r^k using $\mathfrak{h}_\alpha^k$
    initialize $s := 1$
    while $\mathbb{I}_{\mathrm{f},\alpha}^k \neq \emptyset$ **and** $s < 10$ **do**
      determine boundaries $\underline{\mathfrak{h}}_\alpha^k \leftarrow \mathfrak{h}_\alpha^0 - 0.1s\,\mathfrak{h}_\alpha^0$; $\overline{\mathfrak{h}}_\alpha^k \leftarrow \mathfrak{h}_\alpha^0 + 0.1s\,\mathfrak{h}_\alpha^0$
      solve feasibility Problem (2.19) and generate Θ_f^k and $\mathbb{I}_{\mathrm{f},\alpha}^k$
      update $s \leftarrow s + 1$
    end
    set the index $k \leftarrow k + 1$
  end
end

Result: the final training set $\mathscr{O}_\alpha^\infty := \mathscr{O}_\alpha^k$ and hyperparameter $\mathfrak{h}_\alpha^\infty := \mathfrak{h}_\alpha^k$ for both processes

The result of Algorithm 2.2 are the final training set and hyperparameter that are used to generate the final operational cost functions $\{O_\alpha\}_{\alpha=1,2}$ and the final profit function F. It should be noted that in the Algorithm 2.2 we first propose a stepwise increase of the hyperparameter range before adding new virtual training points. This avoids redundant local deformations of the GPs.

Example 2.4 (Economy of a Coupled AD- and RSR-Process (2.3 continued))**.** *After we have discussed the production system and their dynamic behavior, we introduce the economic objective function, which combines the feed parameters with the economic aspects of the system. As described in Appendix B.1, the two feed parameters represent the raw material prices, where for $\mathcal{S}_1$, we express this by the substrate quality. In general, the modelling of the profit function of the system follows the principle that a higher feed price (or lower feed quality)*

causes an increase in operating costs. This means that the maximum possible profit can only be achieved at a lower production level or vice versa for lower feed prices.
Based on a given economic analysis of the production system, areas for each process are identified through which the profit function passes for five different feed parameter values.
In Figure 2.10 these areas are represented by the green rectangle for optimal

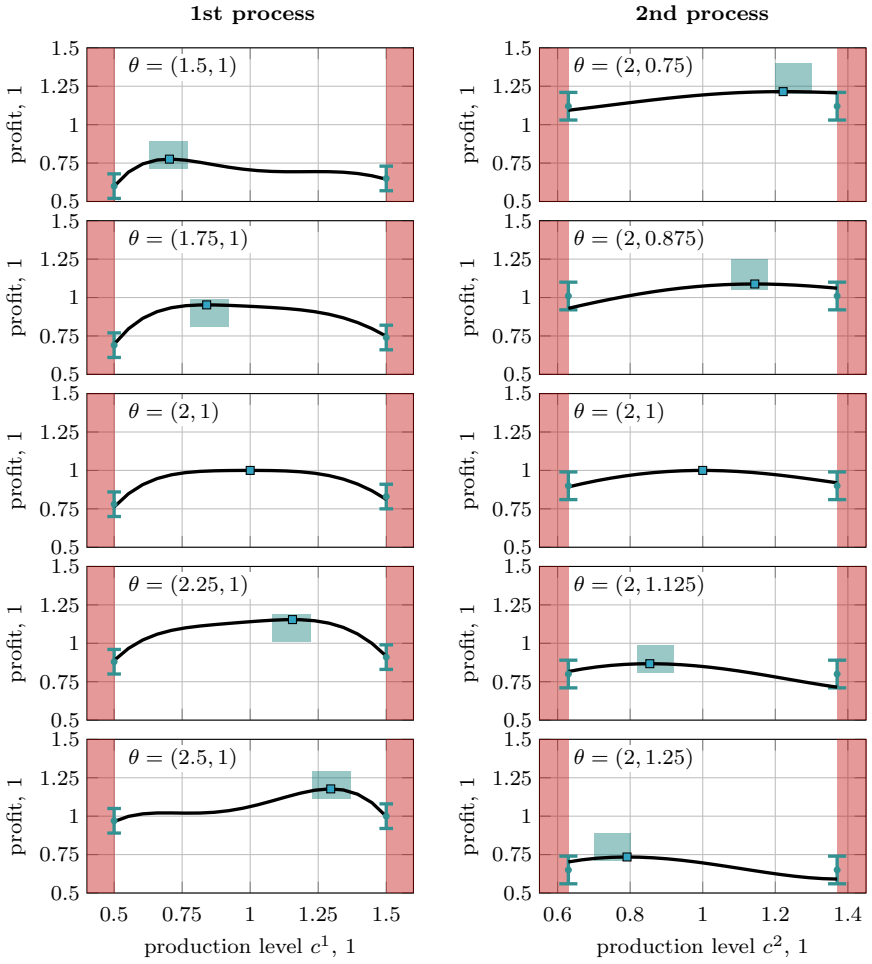

Figure 2.10: Illustration of the cutting planes for that we have economic information.

profit and at the boundaries by the green intervals. These areas indicate that the information on the profit function is described by uncertain data. However, the nominal feed parameter value is an exception to this rule, since the maximum profit value and the corresponding production level are known precisely. It should be noted that the data shown are normalized to the nominal profit value, which allows a better initial guess of the hyperparameter values for the training of the function. Due to the specifications of the feed parameters used for training, the domain of the economic objective around the nominal operating point is also defined. For process $\mathcal{S}_1$*, the admissible feed parameters (substrate quality) are given by* $\theta^1 \in [1.5,\, 2.5]$*, see Figure 2.10 left side. Based on the data on the right side in Figure 2.10, the admissible feed parameters (price for* H*) for* $\mathcal{S}_2$ *are given by* $\theta^2 \in [0.75,\, 1.25]$*. Hence, the space of the feed parameters is defined by* $\Theta := \left\{\xi \in \mathbb{R}^2 \;\middle|\; (1.5,\, 0.75) \leq \xi \leq (2.5,\, 1.25)\right\}$*.*

It is easy to see that with increasing quality, the profit rises and also the aspired production level. Conversely, a lower price for H *causes a higher production level and a higher profit value. The data is given in a way that if one parameter value is changed, the other one will remain at the nominal point. This procedure is admissible since, for the corresponding data points, states can be identified, which would not reduce the product quality to less than 1.*
Figure 2.10 also shows the curve of the trained profit function within these cutting-planes. It can be seen that the optimal production levels (blue rectangles) are always within the specified admissible regions. Furthermore, the individual curves are increasing from the lower production bound to the optimum and decreasing up to the upper production bound. For the final objective function, we additionally include the weighting of the sales price by the product quality q_s *introduced in Appendix B.1.*

2.3 Time Horizon and Time-Dependent Feed Parameter

In the last section we discussed in detail the model structure and the interaction of the process and storage elements from an economic point of view. From the fact that the feed parameter θ and thus the operational costs can change arbitrarily and the system should be operated constantly in an economic optimum, it can be concluded that the production level c needs to be adapted as well. This adaptation is caused by a variation of the primary feed u realized by an integrated operational strategy. In this context, the system $\mathcal{P}$ and the profit function F play an important role. Moreover, it is important to ensure that the unsteady operated storage systems are not charged or discharged beyond their boundaries. In order to derive such an operational strategy and also to use this

strategy to estimate the storage size, it is essential to structure the time horizon more precisely.

As mentioned above, a trigger for modifying the production level is a change of θ due to its effect on operational costs as introduced in Section 2.2.4. For this reason, we characterize the time dependency of the feed parameter by the following definition.

Definition 2.14 (Scenarios and Time-Dependent Feed Parameter)**.** *Let Θ be the space of all feed parameter. For a finite $n_\theta \in \mathbb{N}$, we introduce a feed-parameter scenrio as a piecewise constant function*

$$\boldsymbol{\theta} : \mathbb{R}_0^+ \to \Theta,\ (t) \mapsto \boldsymbol{\theta}(t) := \sum_{k=0}^{n_\theta} \hat{\theta}_k \, \mathbb{1}_{\mathcal{T}_{\theta k}}(t). \tag{2.20}$$

Here, $\hat{\theta}_k \in \Theta$ denotes a realization of the feed parameter and

$$\mathbb{1}_{\mathcal{T}_{\theta k}}(t) := \begin{cases} 1 & \text{if } t \in \mathcal{T}_{\theta k} \\ 0 & \text{if } t \notin \mathcal{T}_{\theta k} \end{cases}$$

is the indicator function, where the time horizon $\mathcal{T}_{\theta k} := [t_k,\, t_{k+1})$ describes a time period in which the feed parameter is constant. The set of all scenarios is denoted with $\boldsymbol{\Theta}$.

It follows from the definition that a scenario is uniquely defined by the tuples $\hat{\theta}$ and $\mathcal{T}_\theta$ of the feed parameter values and its corresponding time horizons. For the components of $\mathcal{T}_\theta$ it applies that they are pairwise disjoint $\mathcal{T}_{\theta k} \cap \mathcal{T}_{\theta l} = \emptyset$, for $k \neq l$. Furthermore, we introduce the function $l : (\mathcal{T}_{\theta k}) \mapsto l\,(\mathcal{T}_{\theta k}) := t_{k+1} - t_k =: \Delta_\theta t_k$ to measure the length of the time horizons $\mathcal{T}_{\theta k}$, which motivates for definition of the following operators

$$\min_{\mathrm{t}}(\boldsymbol{\theta}) := \min\, l\,(\mathcal{T}_{\theta k}) \quad \text{and} \quad \max_{\mathrm{t}}(\boldsymbol{\theta}) := \max\, l\,(\mathcal{T}_{\theta k})\,,$$

to determine the lower and upper bound of the time length. Of particular importance for our further studies are those scenarios which are restricted by a lower and an upper time length $\underline{\Delta}_\theta t \in \mathbb{R}^+$ and $\overline{\Delta}_\theta t \in \mathbb{R}^+$. This means we only consider those $\boldsymbol{\theta} \in \boldsymbol{\Theta}$ where the following holds:

$$\min_{\mathrm{t}}(\boldsymbol{\theta}) \geq \underline{\Delta}_\theta t \quad \text{and} \quad \max_{\mathrm{t}}(\boldsymbol{\theta}) \leq \overline{\Delta}_\theta t. \tag{2.21}$$

The aim is to identify $\underline{\Delta}_\theta t$ and $\overline{\Delta}_\theta t$ based on the operational strategy and the storage size estimation that are yet to be developed.

Using the definition of the scenario $\boldsymbol{\theta}$ and the dynamic properties of the system $\mathcal{P}$, the time horizons $\mathcal{T}_{\theta k}$ can be more structured. To illustrate the following

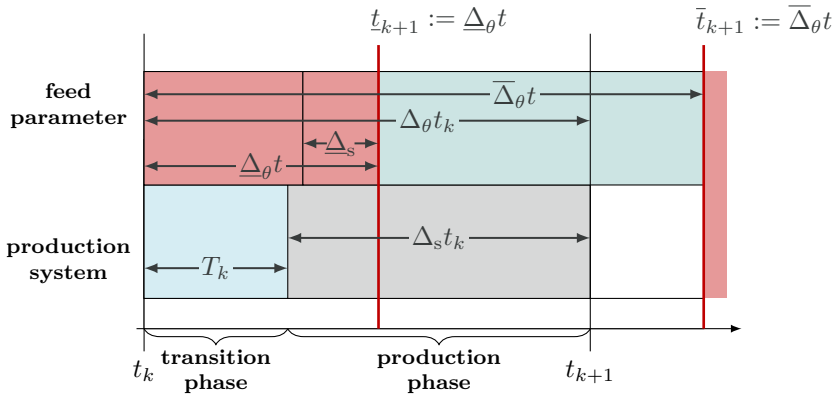

Figure 2.11: Structure of the time horizon and connection between time-related parameters.

statements about the structure of the time horizon, Figure 2.11 is used. The time horizons $\mathcal{T}_{\theta k}$ can be split into the

$$\begin{aligned} \text{transition phase:} \quad & [t_k, t_k + T_k)\,, \\ \text{and the production phase:} \quad & [t_k + T_k, t_{k+1})\,, \end{aligned}$$

where T_k denote the length of the time span that is required to realize the transition of the production level as illustrated by the blue area in Figure 2.11. The duration of the production phase results naturally from $\Delta_\mathrm{s} t_k := \Delta_\theta t_k - T_k$, cf. the grey area in Figure 2.11. This structure is based on the following idea. If we assume that the feed parameter θ changes at any time during the production phase, a new production level has to be determined first by an operation strategy. Subsequently, a suitable control signal needs to be implemented to achieve the production change.
The length T_k of the transition phase depends directly on the production level change δc of the system $\mathcal{P}$ and thus on the transition times of the individual processes $\mathcal{S}_i$. The following definitions introduce the concept of the transition time for an admissible change of the production level.

Definition 2.15 (Admissible Change of the Production Level)**.** *Given is the operating area $\mathcal{C}_\mathrm{o}$. A production level change $\delta c \in \Delta_c$ is called admissible, if for a given $c \in \mathcal{C}_\mathrm{o}$ it holds that $c + \delta c \in \mathcal{C}_\mathrm{o}$. The set of all admissible changes is denoted by $\Delta_c := \left\{\xi \in \mathbb{R}^2 \mid c + \xi \in \mathcal{C}_\mathrm{o}\right\}$.*

Definition 2.16 (Transition Time)**.** *Let $\mathcal{P}$ be a production system and $\delta c \in \Delta_{h(x_0)}$ an admissible change of the production level from an initial state $x_0 \in \mathcal{X}_\mathrm{o}$. The transition time T^* for a given $(x_0, \delta c)$ defined by*

$$T^* := \underset{t_\mathrm{f},\, \boldsymbol{k}}{\arg\min} \quad t_\mathrm{f} \tag{2.22a}$$

$$\text{subject to} \quad \dot{\varkappa}^\alpha(t) = f^\alpha\Big(\varkappa(t), \boldsymbol{k}\big(\varkappa(t), t\big)\Big), \tag{2.22b}$$

$$0 = \varkappa(0) - x_0, \tag{2.22c}$$

$$0 = f^\alpha\Big(\varkappa(t_\mathrm{f}), \boldsymbol{k}\big(\varkappa(t_\mathrm{f}), t_\mathrm{f}\big)\Big), \tag{2.22d}$$

$$0 = h\left(x_0\right) + \delta c - h\big(\varkappa(t_\mathrm{f})\big), \tag{2.22e}$$

$$0 \geq s\Big(\varkappa(t), \boldsymbol{k}\big(\varkappa(t), t\big)\Big), \tag{2.22f}$$

$$0 \geq \omega\big(\varkappa(t)\big), \tag{2.22g}$$

where $\varkappa$ is the state trajectory achieved by the control law $\boldsymbol{k} : [0, t_\mathrm{f}] \times \mathcal{X} \to \mathcal{U}$.

The motivation of Definition 2.16 results from the fact that $\mathcal{P}$ works in an economic optimum only in the production phase, where the production level correlates with the feed parameter. Hence, the new production level $h\left(x_0\right) + \delta c$ has to be reached as fast as possible and then remain constant, which is specified by (2.22d) and (2.22e). In addition, a stationary operation is also preferred for safety reasons, and in fact, any transition is an expensive intervention in the production system operation and should be carefully examined. This leads to the proposition that a transition should only occur if the production phase is maintained for at least the time $\underline{\Delta}_\mathrm{s}$, see also Figure 2.11. Using Definition 2.16, we can define a map that yields the transition time for a given configuration of the system state. Definition 2.16 allows a more precise description of the restriction of the scenario space Θ by a lower bound $\underline{\Delta}_\theta t$. For this purpose we introduce the concept of the transition-time map by

$$\mathfrak{T}_\mathrm{t}^\mathrm{e} : \mathcal{X}_\mathrm{e} \to \mathbb{R}^+, \ (\mathfrak{x}) \mapsto \mathfrak{T}_\mathrm{t}^\mathrm{e}(\mathfrak{x}) := T^*, \tag{2.23}$$

where T^* is given by the solution of Problem (2.22) and

$$\mathcal{X}_\mathrm{e} := \big\{(\xi, \varsigma) \in \mathcal{X}_\mathrm{o} \times \Delta_{h(\xi)}\big\}.$$

It should be noted that the components of $\mathcal{X}_\mathrm{e}$ are not independent as the planned change δc of the production level has to be valid for the particular state x, from which a change in production occurs.

Assumption 2.6. *For all* $\mathfrak{x} \in \mathcal{X}_\mathrm{e}$ *there exists a unique solution of Problem* (2.22)*, which guarantees the well-definedness of* $\mathfrak{T}_\mathrm{t}^\mathrm{e}$.

Considering the definition of $\mathfrak{T}_\mathrm{t}^\mathrm{e}$, it is clear that a dynamic optimization problem has to be solved, where the state coordinates at the beginning of the transition have to be priori known. This might be a drawback if the transition time is applied within a static optimization. Furthermore, in Section 3.3 we will use a local surrogate model of $\mathfrak{T}_\mathrm{t}^\mathrm{e}$, since the change in production is based on a fixed initial production level from which the transition occurs. Consequently, only admissible changes are considered, so that we introduce for a given $x_0 \in \mathcal{X}_\mathrm{o}$ the local surrogate transition-time map

$$\tilde{\mathfrak{T}}_{\mathrm{t},h(x_0)} : \Delta_{h(x_0)} \to \mathbb{R}^+, \tag{2.24}$$

which is derived from (2.23) and yields the transition time. Section 4.3 describes in more detail how $\mathfrak{T}_\mathrm{t}^\mathrm{e}$ and thus $\tilde{\mathfrak{T}}_{\mathrm{t},\cdot}$ are generated using a certain control law. Moreover, we discuss a condition which allows to formulate the transition-time map for the whole operating area, whereby the states are only used as parameters.
The map $\mathfrak{T}_\mathrm{t}^\mathrm{e}$ can be used for an explicit description of the lower bound $\underline{\Delta}_\theta t$ and thus a restriction of the scenario space $\boldsymbol{\Theta}$. In this way, the set $\boldsymbol{\Theta}$ of admissible scenarios for the economic description of $\mathcal{P}$ is related to the underlying control concept.

The upper bound $\overline{\Delta}_\theta t$ (see Figure 2.11) is related to the storage size and will be analyzed in more detail in Section 5.4. The reason for this connection is the unsteady behavior of the storage elements caused by frequent charging and discharging. For instance, if θ does not change in the time span Δt_k, it follows that the storage elements will be either empty or full at a certain time point. If this time is reached before θ has changed, the process conditions have to be reevaluated so that a less optimal production level has to be set.

Assumption 2.7. *A change of the production level is only triggered by a change of the feed parameter* θ.

To satisfy Assumption 2.7, we have to predict the storage level ℓ for the transition and production phase, while determining the new production level. Here, the upper bound $\overline{\Delta}_\theta t$ has to be considered as well as the storage size D. Therefore, it would be useful to relate both variables.

Example 2.5 (Scenario for a coupled AD- and RSR-process (2.4 continued))**.** *For a detailed analysis of the operational strategy to be developed, we consider a random scenario. From the economic analysis, we have already specified* Θ*. Besides, we state that the length of the time horizons has to lie within the*

interval $[500,\ 1800]\,\mathrm{min}$. *That means, if a change of* θ *occurs, it is necessary to ensure that the corresponding value is maintained for at least* $500\,\mathrm{min}$ *and not longer than* $1800\,\mathrm{min}$. *The minimum length guarantees that the transition phase will be completed, and the subsequent production phase will continue for a specific time period. To determine the lower bound, the dynamic properties of the system need to be analyzed using a concrete control law.*

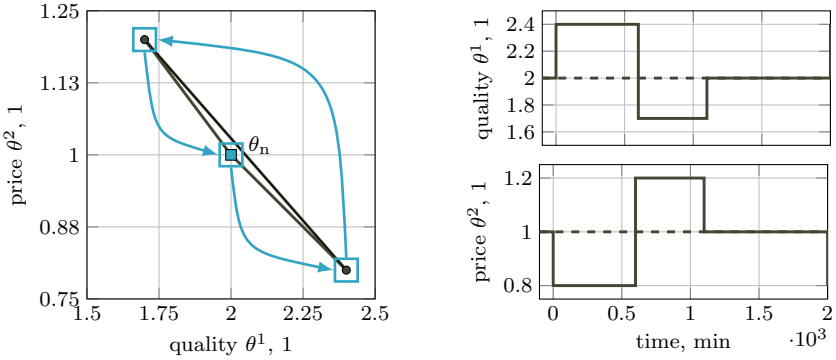

Figure 2.12: Scenario for the production system.

Figure 2.12 shows a concrete scenario based on the one used in Example 2.3. The tuple of the feed parameter values to be realized and the corresponding time horizons are defined as follows

$$\hat{\theta} = \big((2.4,\ 0.8)\,,(1.7,\ 1.2)\,,(2.0,\ 1.0)\big), \tag{2.25a}$$

$$\mathcal{T}_\theta = \big([0,\ 600)\,,[600,\ 1100)\,,[1100,\ 2000)\big). \tag{2.25b}$$

The scenario is closed, i.e., the individual feed parameters are repeated after particular time intervals. It should be noted that this is only a snapshot of the scenario and that the feed parameters may change further beyond the considered time horizon. The scenario presented here is revisited and extended in Section 5.4.

2.4 Summary of Part I and Motivation for an Operational Strategy

In this chapter, we discussed the topology, model, and structure of the time horizon of the considered production system. Accordingly, we consider two processes that produce different primary products from different raw materials.

These processes are weakly connected according to Definition 2.3 via storage systems, which allows an exchange of material and energy flows. The storage elements are always operated unsteadily over the entire time. This gives us certain flexibility in modifying the production levels, but at the same time, the change in the storage levels has to be considered as part of an integrated operational strategy. In addition to the system model, we also discussed the economic model to describe the system's profit based on changing operational costs due to a time-dependent feed parameter.

Using this information, we can tackle the objective of developing an integrated operational strategy from Chapter 1. This strategy aims to control production levels based on economic aspects. In this context, the operational strategy follows a twofold objective. Firstly, if the feed parameter changes, the production level needs to be changed to ensure that the system operates at the economic optimum. Here, a variety of constraints have to be considered, e.g. the unsteady operation of the storage elements and their size. The result of this part directly influences the production phase. Secondly, a control signal needs to be derived that allows the system to move to the new production level as fast as possible. Here it is essential to know precisely where the new production levels are located. This part of the operational strategy relates to the transition phase.

Problem 2.1 (Integrated Operational Strategy)**.** *Let $\mathcal{P}$ be a production system and F be a profit function that describes the economics of the system. An integrated operational strategy is divided into two sections:*

(i) ***Production Level Optimization:*** *Design a map*

$$\mathfrak{P}_{\mathrm{c}}^{\mathrm{e}} : \mathcal{X}_{\mathrm{o}} \times \Theta \times \mathcal{D} \to \mathcal{C}_{\mathrm{o}}$$

that determines the new setpoint c_{s} for the production level for the next production phase, such that the profit F is maximized.

(ii) ***Production Level Transition:*** *Design a control law*

$$K_{\mathrm{ex}} : \mathbb{R} \times \mathcal{X} \to \mathcal{U}$$

that steers the production level of the system $\mathcal{P}$ to the new setpoint c_{s}.

Remark 2.5. *From Problem 2.1, the production phase can be defined as the time horizon where the setpoint c_{s} is constant. The transition phase is characterized by a time-dependent reference to c_{s}.*

Part II

Design of the Operational Strategy

Chapter 3

Production Level Optimization

In the previous chapter, we introduced the structure of the production system and all crucial components. Furthermore, the problem of the operation strategy was introduced formally. This chapter addresses the problem of identification of new production levels defined in Problem 2.1 (i). Section 3.1 gives a brief overview about the hierarchical structure of the production system control. In Section 3.2, we introduce the storage constraints that allow us to predict and evaluate the unsteady behavior during the production phase. We describe the S-RTO problem in Section 3.3 and define some maps used in Chapter 5 to address the storage design.

Remark 3.1. *The problem of determining an optimal production level discussed in this chapter must be valid for all time horizons* $[t_k, t_{k+1})$*. Therefore, w.l.o.g., it is assumed in this section that* $t_k = 0$*. In addition, we also omit the explicit notation of the* k*-th time horizon.*

3.1 Brief Review of Hierarchical Production System Control

Modern chemical production systems and process networks are characterized by a hierarchical structure of their operational and control management, which is made up of different layers, cf. [68, 202, 235, 41]. These individual layers address different tasks on different time horizons. Figure 3.1 shows a typical layout

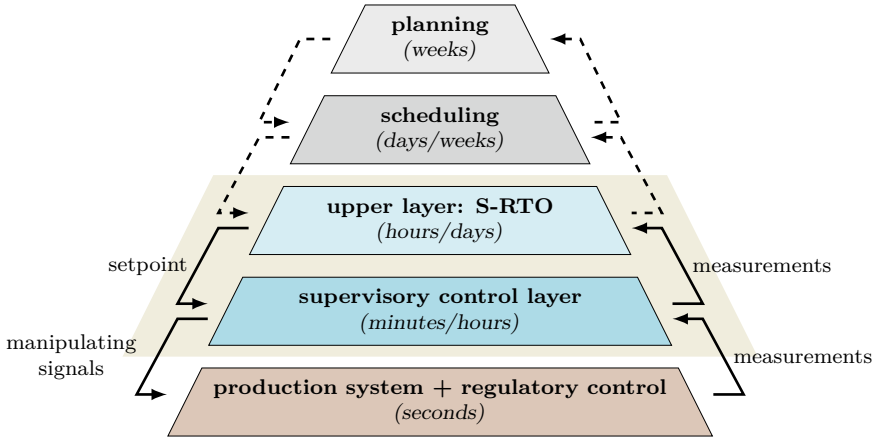

Figure 3.1: Schematic sketch of the hierarchical control structure of a production system.

for such an operational management system. On the planning layer, long-term decisions are made regarding the questions of what should be produced and how. These human-based considerations include economic forecasts regarding future trends in the development of feedstocks and the markets for products. The scheduling layer takes into account optimal times at which particular products are to be produced. It considers logistical aspects regarding the distribution of raw materials and intermediate products, including storage capacities and changes in operation mode over extended periods, see [41]. In the following, we assume that the feedstock, the production system, and the target products are specified and that the system has to operate continuously.

This thesis focuses on the real-time optimization (RTO) layer, which provides economic decisions about setpoints of current production levels over hours or a few days. An underlying supervisory control layer executes these setpoints, typically employing a model predictive control (MPC). The main idea of an MPC is that for a given objective, an optimal control problem is repeatedly solved on a moving horizon. Thereby the input of the system is continuously updated by comparing current measurements with the predicted system behavior to ensure different kinds of constraints. For general information regarding MPC, we refer to [174, 87, 171].

The production system itself has another regulatory layer (such as PI-controllers), which directly implements decisions of the supervisory layer on the process elements within seconds. Moreover, this layer provides stability and the rejection of high-frequency disturbances. However, communication is not only directed from top to bottom layers. Using measurements and their evaluation, the layers

above also receive information about the current states and parameters, allowing them to update the individual models (e.g., system model, secondary conditions, or economic objectives). For reviews on the hierarchical control structure of process system, we recommend Tatjewski [245] and Scattolini [217].

From the previous chapter, we can deduce that the RTO regularly receives updated information on the parameters θ that influence the system economy. Thus, it is necessary to set new production levels that lead to maximum profit continuously. Furthermore, we consider an unsteadily operating system, where the processes are steady-state from a specific point in time, but the storage systems are not.

A common standard in industry practice is the utilization, as mentioned above, of an RTO and a supervisory control layer, also known as the two-layer approach, cf. [42, 52]. The RTO is a nonlinear programming problem (NLP) with an economic objective function (system profit or operational costs), subject to a nonlinear steady-state system model and other constraints. The decision variables are the setpoints for the production levels and their corresponding states and input variables. In this way, the RTO provides an optimal operating point for the production system, which needs to be attained by the supervisory controller. Since production level optimization is a regularly executed static problem, we will call it Static-RTO (S-RTO) in the following. Engell [52] stated that a clear advantage of this two-layer structure is separating the two tasks of identifying the optimal operating point and control towards this point. This gives reliability and also safety, especially when dealing with large-scale systems, see [265]. Nevertheless, there are some disadvantages to this approach. For instance, different system models are valid for the two layers, which can lead to inconsistencies and, thus, to feasibility and stability problems [265]. In other words, the nonlinear steady-state model of the S-RTO might conflict with the dynamic model of the MPC of the supervisory layer, which is often linear [271, 202, 40]. A further disadvantage in the context of S-RTO is the requirement that a new operating point can only be determined if the system has reached the steady-state of the previous point. This might lead to dead times, in which economically beneficial points cannot be addressed.

In order to solve these challenges, Helbig et al. [97] and Backx et al. [11] proposed to combine the two optimization problems (S-RTO and MPC) in a single layer architecture. The control problem is characterized by an economic objective that has to be solved repeatedly with respect to the nonlinear dynamic system model and other constraints. In literature, these integrated control structures are also referred to as economic MPC. These controllers have been investigated in numerous theoretical studies on performance and stability properties, cf. [95, 2]. In particular, the effects of various constraints, e.g., terminal constraints, are addressed, and it is examined how they can be modified to obtain specific

convergence properties, such as in the Lyapunov-based economic MPC. An overview of economic MPC can be found in Ellis et al. [51] or Faulwasser et al. [60]. Several applications on process systems have been achieved in recent years by [218, 148, 80]. Typical applications for economic MPC are processes for which no optimal steady-state exists that must be maintained for a certain time after achieving it. Among others, these are batch processes or cyclic processes (e.g. pressure swing adsorption). The ratio between sampling times has a significant influence on computational complexity and real-time-feasibility. The former should be as short as possible for fast disturbance rejection, while the latter should be as long as possible in order to assess the economic effects, cf. [106, 52]. Since fast sampling and long horizons result in extensive online calculations, a tradeoff must be found to allow for online implementation. Moreover, Findeisen and Allgöwer [67] pointed out that for large-scale nonlinear systems with fast dynamics, the loss of control performance and possibly instability can appear due to delays caused by long calculation times.

An alternative way to address the drawbacks of S-RTO is the Dynamic RTO (D-RTO). The main idea here is to reformulate the S-RTO into an economic MPC but to retain the two-layer architecture. The D-RTO outcome is a reference trajectory for the production levels and eventually, the manipulating variables. A tracking MPC subsequently follows these reference trajectories, cf. [246, 122, 121]. The D-RTO operates at a lower sampling rate than the controller on the supervisory layer, ensuring a clear separation of tasks on different time scales, see [270]. Therefore, the D-RTO can follow dynamic fluctuations over longer time horizons while the tracking MPC can react to high-frequency disturbances.

Remark 3.2. *The two-layer D-RTO structure can be interpreted as a cascade of an economic MPC and a tracking MPC, see [106]. In the literature, the exact distinction between D-RTO and economic MPC is not always clear and is sometimes used synonymously, cf. [59, 204, 60]. In our perspective, the term D-RTO is valid instead of economic MPC if the following conditions hold:*

(i) an economic objective is evaluated,

(ii) a dynamic system model is used for the constraints,

(iii) a reference trajectory is generated for controlled and/or manipulating variables and

(iv) the reference is applied to the system using a supervisory control layer (two-layer architecture).

For the implementation of the D-RTO, Jamaludin and Swartz [106] distinguish between two more cases. Typically, the D-RTO model has no information about the control law utilized in the lower supervisory layer. Thus the trajectory generated in the D-RTO represents an open-loop prediction of the system, see [270, 182]. In contrast, the approach proposed in Jamaludin and Swartz [106] considers this controller during the economic optimization process, which means that the closed-loop behavior is included. More precisely, it is an MPC with a different prediction horizon than the D-RTO, and as usual with MPC, the input of the first time step is applied to the production system. In this way, for each time step of the prediction horizon of the D-RTO, a separate optimization problem of the MPC has to be solved, which leads to a multilevel dynamic optimization problem. This problem is reformulated to a single-level MPC using the KKT optimality conditions. Jamaludin and Swartz [107] continue this approach and discuss different techniques of reformulation to reduce complexity. Among other things, a bilevel approach is presented that uses only a single MPC optimization. Further applications for closed-loop D-RTO are given by Li and Swartz [145] for distributed MPC systems and by Remigio and Swartz [206], where it is included in production scheduling decisions.
Using the closed-loop behavior of the system to achieve other goals in terms of optimization-based problems is quite common, especially for robust control, see [147]. However, there are also approaches for integrated planning and control tasks, for example, in Zhuge and Ierapetritou [278], where a multi-parametric MPC is used.

For a suitable choice of the operational strategy, it is essential to know the time scales of the disturbances affecting the economy and the transitions of the system, cf. [97]. We assume that the frequency of the feed parameter change is lower than the frequeny of transitions between production levels within $\mathcal{C}_\mathrm{o}$. Besides, the behavior of the production system at the end of the transition is necessary to determine the new operating points. This is due to the unsteady operation of the storage systems, whose behavior needs to be predicted and taken into account when changing production levels.

Based on these aspects, we propose the closed-loop S-RTO (cl S-RTO) with integrated trajectory generation. Figure 3.2 illustrates the general setup of this problem and the decomposition strategy to solve it efficiently. This approach is a two-layer architecture where the upper layer identifies the optimal operating point and generates a time-optimal reference trajectories u and c towards the new production level, cf. Figure 3.2. Thus, the cl S-RTO meets conditions (i), (iii) and (iv) of Remark 3.2.
Decisive for choosing a new stationary production level by the steady-state optimization of the S-RTO is the endpoint of the trajectory. It contains information about the transition time and the position of the storage levels. To

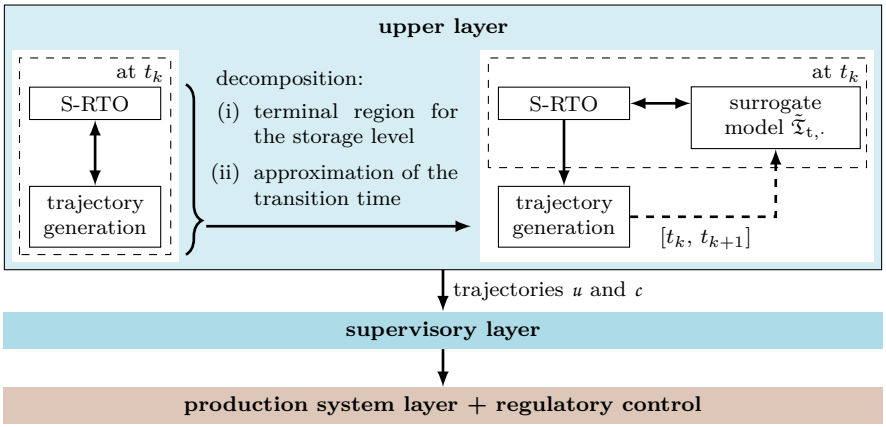

Figure 3.2: Concept of the closed-loop S-RTO with integrated trajectory generation.

solve the cl S-RTO, it is necessary to design the controller as an underlying problem, which requires the integration of the dynamic system model. Hence the cl S-RTO is a bilevel optimization problem, where the upper-level optimization is an NLP and the lower-level optimization an OCP, see the left side in the light blue area of Figure 3.2. This bilevel problem can be decomposed into a static S-RTO and a dynamic problem for trajectory generation assuming the following conditions:

(i) The terminal region for the storage levels at the end of the transition is located around the initial storage levels $\ell_i{}^{\alpha}(t_k)$,

(ii) The transition time needed for the S-RTO is approximated using a surrogate model $\tilde{\mathfrak{T}}_{t,\cdot}$ of the transition-time map $\mathfrak{T}_t^e$.

The right-hand side of Figure 3.2 shows this in the light blue area. We discuss the trajectory generation in more detail in Chapter 4 so that in the following, we assume that a surrogate model $\tilde{\mathfrak{T}}_{t,\cdot}$ is available. In the introduction to Chapter 4, we will also examine the supervisory control layer that implements the generated trajectory.

Regardless of the specific method used to determine economic operating points, the RTO layer operates in a two-step approach. This means that in addition to optimizing the production system, the underlying models are updated using measurements for accounting for system-model mismatch and process disturbances, cf. [31, 169]. Chachuat et al. [29] provides an overview of

adaptation strategies for RTO by discussing and comparing them. We want to mention only two of these strategies briefly. The first one is the model-parameter adaptation, where the parameters of the models are usually determined by the least-squares estimation considering the error between measurements and predicted outputs, cf. [31, 272, 41]. The second is the modifier adaptation, where additional terms are used to adjust the constraints and possibly the objective function. In literature, several examples are presented for such applications, see [77, 64] or [167].

However, it is a common standard in model adaptation for the S-RTO that the measurement data must be obtained in steady-state operation to be valid for stationary models. For this reason, additional mathematical tools are used to verify if the system is in a steady-state with a specific tolerance utilizing the measurement data. Many of these are based on statistical methods or the application of filters, cf. [28, 19]. The approach proposed by [207] is based on the estimation of rate signals, and the assumption of a certain model structure consists of states with slow and fast dynamics.
In recent years, an increasing research effort has been made to use also dynamic data, allowing to minimize delay times while reacting faster to economic changes. These approaches are usually based on the implementation of observers as in [170, 135], or on linear ARX system models as presented in [77]. In this context, Krishnamoorthy et al. [135] propose a hybrid RTO concept, while using an extended Kalman filter.
In general, observers provide an excellent way to estimate states and parameters based on noisy and dynamic measurement data. For an excellent overview of different observer techniques and their properties, see Simon [233]. Without going into further detail, we suggest an extended or an unscented Kalman filter [117] for the estimation step of the cl S-RTO, to implement a time-optimal trajectory.

3.2 Storage Constraints

Following, we derive the storage constraints that are used to separate the two subproblems of production level optimization and transition in Problem 2.1. Figure 3.3 shows the evolution of the storage levels ${\ell_i}^{\alpha}$ in the transition and production phase by a thick black solid line. During the transition phase, the inlet streams ${v_i}^{\alpha}$ and the two outlet streams ${w_{i|1}}^{\alpha}$ and ${w_{i|2}}^{\alpha}$ may vary over time due to the changing feed u. We assume that the storage level at the end of the transition satisfies the condition

$$ {\ell_i}^{\alpha}(T^*) \in {\mathcal{H}_j}^{\alpha} := [{\ell_i}^{\alpha}(0) - {\delta_i}^{\alpha},\, {\ell_i}^{\alpha}(0) + {\delta_i}^{\alpha}] \,. \tag{3.1} $$

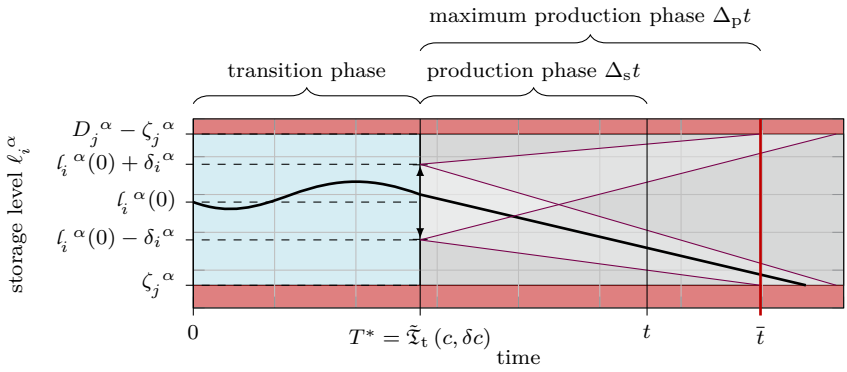

Figure 3.3: Illustration of the storage constraints.

These constraints are illustrated in Figure 3.3 via a double headed black arrow at time T^*. The storage reserve $\delta_i{}^\alpha$ of the transition phase indicates the degree of freedom that the solver of the transition problem has. We will call $\mathcal{H}$ the terminal region of the later discussed transition problem. The length T^* of the transition is obtained from the surrogate model $\tilde{\mathfrak{T}}_{t,\cdot}$ of the transition-time map $\mathfrak{T}_t^e$ defined in (2.24). Furthermore, we rely on the following assumption.

Assumption 3.1. *For given storage elements $\mathcal{B}_j{}^\alpha$, the byproduct streams $v_j{}^\alpha$, and the secondary feed streams $w_{j|1}{}^\alpha$ and $w_{j|2}{}^\alpha$ are constant within the production phase.*

For a given setpoint $c_s \in \mathcal{C}_o$, we can determine the steady state rates $\varrho_{sj}{}^\alpha \in \mathbb{R}$ of $\mathcal{B}_j{}^\alpha$ during the production phase by solving

$$0 = f^\alpha(x_s, u_s), \tag{3.2a}$$

$$0 = h(x_s) - c_s, \tag{3.2b}$$

$$\varrho_{sj}{}^\alpha = \rho_j{}^\alpha(x_s, u_s), \tag{3.2c}$$

using (2.7b-c) and the steady-state condition of (2.7a). Here, x_s denotes the steady-state achieved by the feed u_s.

Remark 3.3. *It should be noted that* (3.2) *might have multiple solutions. However, we consider only a solution that is reachable from the initial production level by a control law K_{ex}.*

Based on Assumption 3.1, we can derive an analytical solution to the storage level for the production phase using the storage model (2.5). The trajectories

of the storage levels at time $t \in [T^*, t_1)$ are given by

$$\ell_j{}^{\alpha}(t) = \ell_j{}^{\alpha}(T^*) + \varrho_{\mathrm{s}j}{}^{\alpha}(t - T^*), \tag{3.3}$$

where at time $t_1 \in \mathbb{R}$ the feed parameter changes. The evolution of the storage level is based on constant rates $\varrho_{\mathrm{s}j}{}^{\alpha}$, as shown in Figure 3.3 from time T^*. We can easily determine the time t until the storage levels would reach their boundaries (red area in Figure 3.3) by using $D_j{}^{\alpha} - \zeta_j{}^{\alpha}$ or $\zeta_j{}^{\alpha}$ for left hand-side of (3.3). This time has to be greater than the maximal length $\overline{\Delta}_\theta t$ of a constant feed parameter to prevent the storage system from causing a change in the production level, which leads to an economically suboptimal operating point. This results in a further constraint for optimizing the new production level, which needs to be satisfied. The main disadvantage here is that a case distinction has to be made to calculate the time. Depending on whether $\varrho_{\mathrm{s}j}{}^{\alpha}$ is less or greater than zero, the lower or upper bound has to be used. For this reason, we will avoid a time-based formulation of the storage constraints.

An alternative way to describe this type of constraints is to analyze the storage rates directly. For this purpose, we consider the rates $\varrho_j{}^{\alpha} \in \mathbb{R}$ of the elements $\mathcal{B}_j{}^{\alpha}$ as real numbers. The stationary rates $\varrho_j{}^{\alpha}$ for the production phase depend on the level ℓ at the end of the transition and the length

$$\Delta_{\mathrm{p}} t := \overline{\Delta}_\theta t - T^* = \overline{\Delta}_\theta t - \tilde{\mathfrak{T}}_{\mathrm{t},c(0)}\left(\delta c\right),$$

of the maximum production phase. They need to be in a closed interval $\mathcal{R}_{[\Delta_{\mathrm{p}} t, \ell]_j{}^{\alpha}} \subset \mathbb{R}$. For a given storage sizes $D_j{}^{\alpha} \in \mathbb{R}^+$ and level boundaries $\zeta_j{}^{\alpha} \in \mathbb{R}^+$ of $\mathcal{B}_j{}^{\alpha}$, we define the set of all admissible storage rates by

$$\mathcal{R}_{[\Delta_{\mathrm{p}} t, \ell]_j{}^{\alpha}} := \left\{ \xi \in \mathbb{R} \;\middle|\; \underline{\varrho}_j{}^{\alpha} \le \xi \le \overline{\varrho}_j{}^{\alpha} \right\}. \tag{3.4}$$

Here, the lower and upper bounds are defined by

$$\underline{\varrho}_j{}^{\alpha} := \frac{\zeta_j{}^{\alpha} - \ell_j{}^{\alpha}}{\Delta_{\mathrm{p}} t}, \quad \text{and} \quad \overline{\varrho}_j{}^{\alpha} := \frac{D_j{}^{\alpha} - \zeta_j{}^{\alpha} - \ell_j{}^{\alpha}}{\Delta_{\mathrm{p}} t}. \tag{3.5}$$

At the end of the transition phase, the storage levels have to be within specified intervals $\mathcal{H}_j{}^{\alpha}$ according to (3.1). For the set of the rates, it applies that $\varrho_j{}^{\alpha} \in \mathcal{R}_{[\Delta_{\mathrm{p}} t, \mathcal{H}]_j{}^{\alpha}}$ where

$$\mathcal{R}_{[\Delta_{\mathrm{p}} t, \mathcal{H}]_j{}^{\alpha}} := \mathcal{R}_{\left[\Delta_{\mathrm{p}} t, \ell_j{}^{\alpha}(0) + \delta_j{}^{\alpha}\right]_j{}^{\alpha}} \cap \mathcal{R}_{\left[\Delta_{\mathrm{p}} t, \ell_j{}^{\alpha}(0) - \delta_j{}^{\alpha}\right]_j{}^{\alpha}}.$$

It is easy to see that this set can be rewritten utilizing (3.4) to

$$\mathcal{R}_{[\Delta_{\mathrm{p}} t, \mathcal{H}]_j{}^{\alpha}} = \left\{ \xi \in \mathbb{R} \;\middle|\; \underline{\varrho}_j{}^{\alpha} \le \xi \le \underline{\varrho}_j{}^{\alpha} \right\}, \tag{3.6}$$

where $\underline{\varrho}_j{}^{\alpha} := \frac{\zeta_j{}^{\alpha} - \ell_j{}^{\alpha}(0) + \delta_j{}^{\alpha}}{\Delta_\mathrm{p} t}$ and $\overline{\varrho}_j{}^{\alpha} := \frac{D_j{}^{\alpha} - \zeta_j{}^{\alpha} - \ell_j{}^{\alpha}(0) - \delta_j{}^{\alpha}}{\Delta_\mathrm{p} t}$. In this way, the storage constraints can be expressed by the rates given by

$$\rho_j{}^{\alpha}(x, u) \in \mathcal{R}_{[\Delta_\mathrm{p} t, \mathcal{H}]_j}{}^{\alpha}, \tag{3.7}$$

The concept of storage constraints is motivated by the specification of how the storage levels will behave during the production phase, where the prediction horizon determines by the properties of the scenario set Θ. Storage rates or maximum charging and discharging times can be used to describe the production level evolution. However, the formulation employing storage rates allows using the constraints in an RTO framework because the time-based formulation is not continuously differentiable through the required case distinction. Hence, we prefer the formulation of the storage constraints by using $\mathcal{R}_{[\Delta_\mathrm{p} t, \ell]_j}{}^{\alpha}$ in the following.

3.3 Static Real-Time Optimization

In the last sections, we discussed the storage constraints utilizing the storage rates resulting from unsteady operation. For this, we assumed that the map $\tilde{\mathfrak{T}}_{\mathrm{t}, h(x_0)}$ is given for the current state $x_0 \in \mathcal{X}_\mathrm{o}$ that provides the transition time for the production system $\mathcal{P}$ as stated in Definition 2.16. The storage constraints allow to predict the behavior of the storage system. Responsible for the storage level change is the secondary feed and byproduct streams, which are directly related to the production level. The production levels have to be chosen so that the economic objective function (2.10) is maximized and the system $\mathcal{P}$ always yields the maximum profit.
In the following, we present the production level optimization as an S-RTO formulated via a parametric NLP. This NLP has to be solved, whenever the feed parameter θ causes an economic change.

As mentioned above, the objective F should be at maximum during the production phase. Throughout the production phase, the two processes operate in a steady-state, and the storage rates are constant, so the optimization problem of the production levels is static. For a given state $x_0 \in \mathcal{X}_\mathrm{o}$, feed parameter $\theta \in \Theta$ and storage level $\ell \in \mathcal{D}$, the optimization problem to determine the new

production level reads

$$\mathcal{S}_{\text{opl}} := \underset{c,\,u,\,x}{\arg\max} \quad F(p,c,\theta,x) \tag{3.8a}$$

$$\text{subject to} \qquad 0 = f\left(x,u\right), \tag{3.8b}$$

$$0 = c - h(x), \tag{3.8c}$$

$$0 \geq s\left(x,u\right), \tag{3.8d}$$

$$0 \geq \omega\left(x\right), \tag{3.8e}$$

$$x \in \mathcal{X},\, c \in \mathcal{C}_{\text{o}},\, u \in \mathcal{U}, \tag{3.8f}$$

$$\rho_j{}^{\alpha}\left(x,u\right) \in \mathcal{R}_{\left[\Delta_{\text{p}}t,\mathcal{H}\right]_j{}^{\alpha}}, \tag{3.8g}$$

$$\Delta_{\text{p}}t = \overline{\Delta}_{\theta}t - \tilde{\mathfrak{T}}_{\text{t},h(x_0)}\big(c - h(x_0)\big), \tag{3.8h}$$

and we call this the S-RTO. In addition to maximizing the profit, it is also crucial that the solution is stationary since the S-RTO (3.8) determines the production phase. For this reason, the steady condition (3.8b) is included. Moreover, we have to ensure the feasibility of the processes by (3.8d) as well as the downstream process constraints through (3.8e). In (3.8g), $\mathcal{H}$ indicates that the rates also depend on the initial storage level as given in (3.6).
The solution of the S-RTO (3.8) determines the set $\mathcal{S}_{\text{opl}} := \big\{(c_{\text{s}}, u_{\text{s}}, x_{\text{s}}) \in \mathcal{C}_{\text{o}} \times \mathcal{U} \times \mathcal{X}_{\text{o}}\big\}$ of operating points. For further discussions, the following assumption is posed.

Assumption 3.2. *For all $(x_0, \theta, \ell) \in \mathcal{X}_{\text{o}} \times \Theta \times \mathcal{D}$, the solution set $\mathcal{S}_{\text{opl}}$ is not empty, which means there always exists a solution of the S-RTO* (3.8).

In general, however, the uniqueness of the solution is not guaranteed, as the system may have several stationary operating points, which might maximize the profit. To identify a specific operating point $\mathfrak{o} \in \mathcal{S}_{\text{opl}}$ and thus a production level, one has to pick one solution. This choice also depends on the control law governing the transition. A detailed discussion is provided in Section 4.2, where the transition time for each feasible solution point is used as a criterion for the choice.

Figure 3.4 illustrates the result of (3.8) on the operating area $\mathcal{X}_{\text{o}}$ within the state space. Assume that the system is in the state $x_0 \in \mathcal{X}_{\text{o}}$ (see Figure 3.4 middle green branch) during a production phase with the production level $c_0 \in \mathcal{C}_{\text{o}}$. Solving (3.8) yields the set $\mathcal{S}_{\text{opl}}$, where red circles in Figure 3.4 represent the states of the operating points contained in $\mathcal{S}_{\text{opl}}$. At these states

$\mathrm{pr}_3(\mathcal{S}_{\mathrm{opl}})$, the profit is maximal. The steady states for three production levels are depicted as white circles in Figure 3.4. The set of all steady states is denoted by $\mathcal{X}_{\mathrm{o}}^{\mathrm{s}} := \{\xi \in \mathcal{X}_{\mathrm{o}} \mid \exists u \in \mathcal{U},\ 0 = f^{\alpha}(\xi, u)\} \subset \mathcal{X}_{\mathrm{o}}$ and illustrated by the red and green curves on $\mathcal{X}_{\mathrm{o}}$, where the color represents the different stability properties. Due to (3.8b) it is clear that for all operating points $\mathfrak{o} \in \mathcal{S}_{\mathrm{opl}}$ follows that $\mathrm{pr}_3(\mathfrak{o}) \in \mathcal{X}_{\mathrm{o}}^{\mathrm{s}}$.

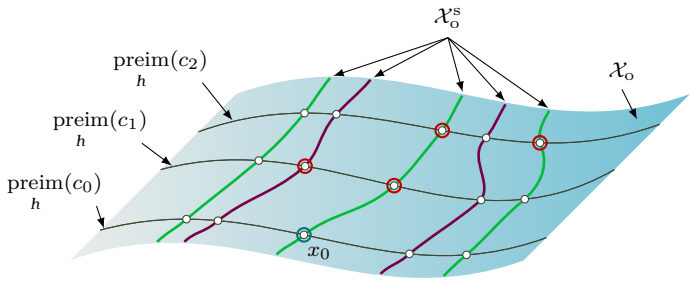

- ... states of $\mathcal{S}_{\mathrm{opl}}$ of Problem (3.8)
- ... initial state $x_0 \in \mathcal{X}_{\mathrm{o}}$
- ... steady state for a given production level $c \in \mathcal{C}_{\mathrm{o}}$

Figure 3.4: Operating area $\mathcal{X}_{\mathrm{o}}$ of the state space and the solution set $\mathcal{S}_{\mathrm{opl}}$.

It is possible to interpret the S-RTO (3.8) as a parametric NLP, where $(x_0, \theta, \ell) \in \mathcal{X}_{\mathrm{o}} \times \Theta \times \mathcal{D}$ is a parameter for which the optimization problem has to be solved, see [13]. After an operating point $\mathfrak{o} \in \mathcal{S}_{\mathrm{opl}}$ is chosen, we can define two maps. The first one is given by

$$\mathfrak{P}_{\mathrm{c}}^{\mathrm{e}} : \mathcal{X}_{\mathrm{o}} \times \Theta \times \mathcal{D} \to \mathcal{C}_{\mathrm{o}},\ (x_0, \theta, \ell) \mapsto \mathfrak{P}_{\mathrm{c}}^{\mathrm{e}}(x_0, \theta, \ell) := c_{\mathrm{s}} \tag{3.9}$$

and yields the new setpoint of the production level that has to be used for the next production phase. The second map

$$\mathfrak{P}_{\mathrm{u}}^{\mathrm{e}} : \mathcal{X}_{\mathrm{o}} \times \Theta \times \mathcal{D} \to \mathcal{U},\ (x_0, \theta, \ell) \mapsto \mathfrak{P}_{\mathrm{u}}^{\mathrm{e}}(x_0, \theta, \ell) := u_{\mathrm{s}} \tag{3.10}$$

allows determining the feed input to this new production value. In addition to the production level, and the corresponding feed input, the economic profit of the system is also essential. Therefore we define the additional function

$$\mathfrak{P}_{\mathrm{f}}^{\mathrm{e}} : \mathcal{X}_{\mathrm{o}} \times \Theta \times \mathcal{D} \to \mathbb{R},\ (x_0, \theta, \ell) \mapsto \mathfrak{P}_{\mathrm{f}}^{\mathrm{e}}(x_0, \theta, \ell) := F(p, c_{\mathrm{s}}, \theta, x_{\mathrm{s}}).$$

Based on Assumption 3.2, it can be concluded that the optimal profit value is also unique. Utilizing the fact whether the storage constraints are active or not, the loss of profit can be evaluated with $\mathfrak{P}_{\mathrm{f}}^{\mathrm{e}}$, which is used in Chapter 5 for dimensioning the storage.

Example 3.1 (S-RTO of a Coupled AD- and RSR-Process (2.5 continued))**.** *In the following, we will analyze the S-RTO based on the scenario introduced in Example 2.5 and the economic objective derived in Example 2.4. Compared to Example 2.3, the S-RTO now ensures that the production levels satisfy the economic specifications and that all constraints are fulfilled during the stationary case. We maintain the capacity of the two storage elements from Example 2.3, as we want to analyze how the same system behaves under an operational strategy adapted to their conditions. However, to compare if an increase of the capacity can achieve even better results, we consider a second case. In this relaxed case, we assume that the storage systems are infinitely large and sufficiently well filled, as stated in Definition 2.3 (i). In summary, we analyze the cases:*

$$\textit{(i)} \quad \textit{bounded storage capcity:} \qquad D_1 := (3\,\mathrm{kmol},\, 3\,\mathrm{kJ})\,,$$

$$\textit{(ii)} \quad \textit{unbounded storage capcity:} \quad D^{\infty} \gg D_1.$$

It should be noted that the transition-time map used for this simulation is trained using the control law in Section 4.2 and introduced in Section 4.3. However, as we have not yet discussed a concrete control law to realize these transitions, we hide the areas with nonconstant states, inputs, and outputs, in Figures 3.5 and 3.6. We also abstain from illustrating the temperature evolution, as this is kept constant at the stationary setpoint during the production phases by underlying regulatory systems. The transitions of the temperature are not considered here, as they are only crucial during the transition. We will discuss these states in Section 4.2.

Figure 3.5 illustrates the input-output behavior of the production system, based on the scenario of Example 2.5. The feed parameter trajectory in the Θ space is shown in Figure 3.5 first row left column and the time evolution of the profit influenced by θ in the first row right column. Additionally, Figure 3.5 shows the inputs u^1 and u^2 and production levels c^1 and c^2 of the two processes in the second and fourth row. The storage levels ℓ for the storages connecting the processes are presented in the third row. In the fifth row of Figure 3.5, the downstream process constraints (total production and production quality) are depicted.
As the operating conditions differ in the time span $[0,\, 600]$ min for the cases (i) and (ii), this section is analyzed separately in Figure 3.6. The blue area in Figure 3.5 indicates this. In the diagrams, case (i) is represented by solid grey lines and case (ii) green dashed lines.

Until $t = 0$ min, the system is at the nominal operating point. At time $t = 0$ min, the feed parameter changes from θ_{n} to $\hat{\theta}_1$ specified in (2.25a). Subsequently, the profit value increases due to better conditions, see economic objective in Figure 3.5 first row right column. However, as there can a better production

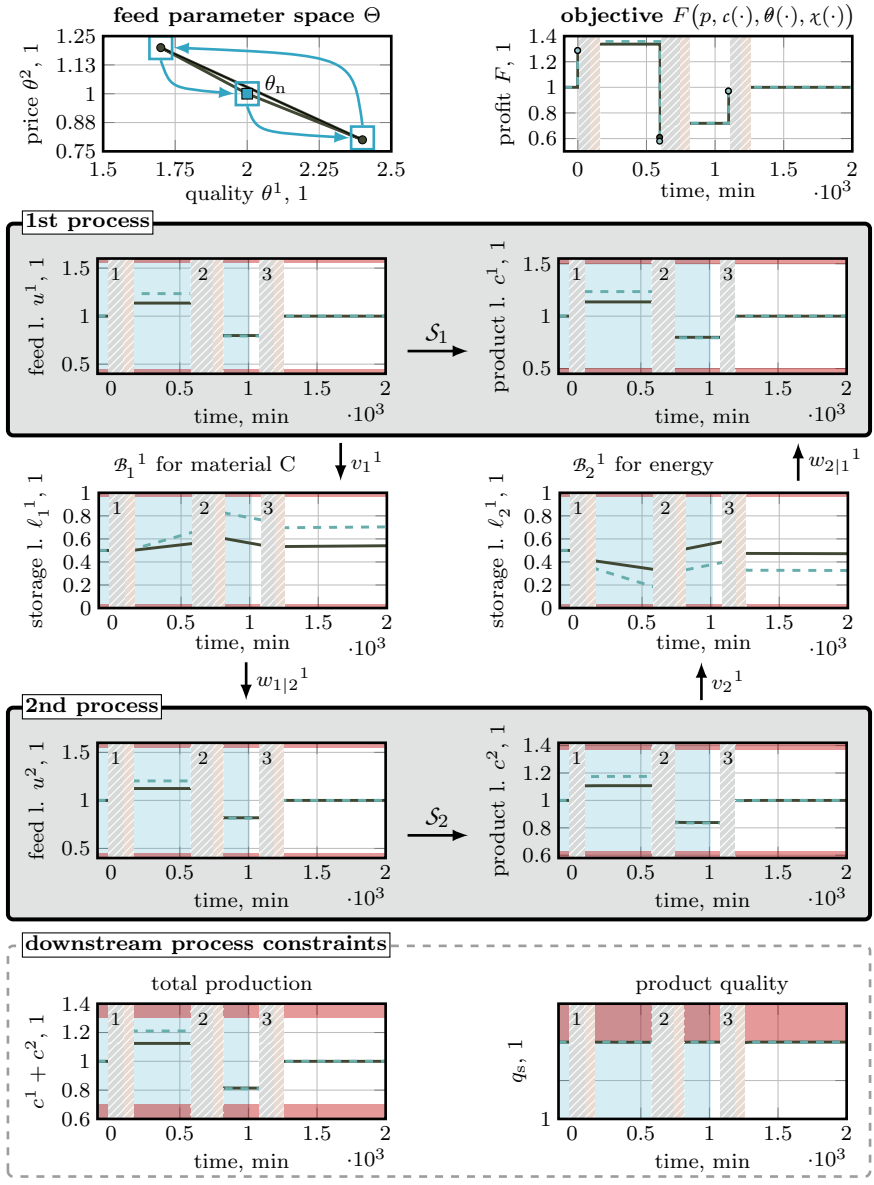

Figure 3.5: Illustration of the input-output behavior of the two processes (grey solid line for D_1) (green dashed line for D^∞).

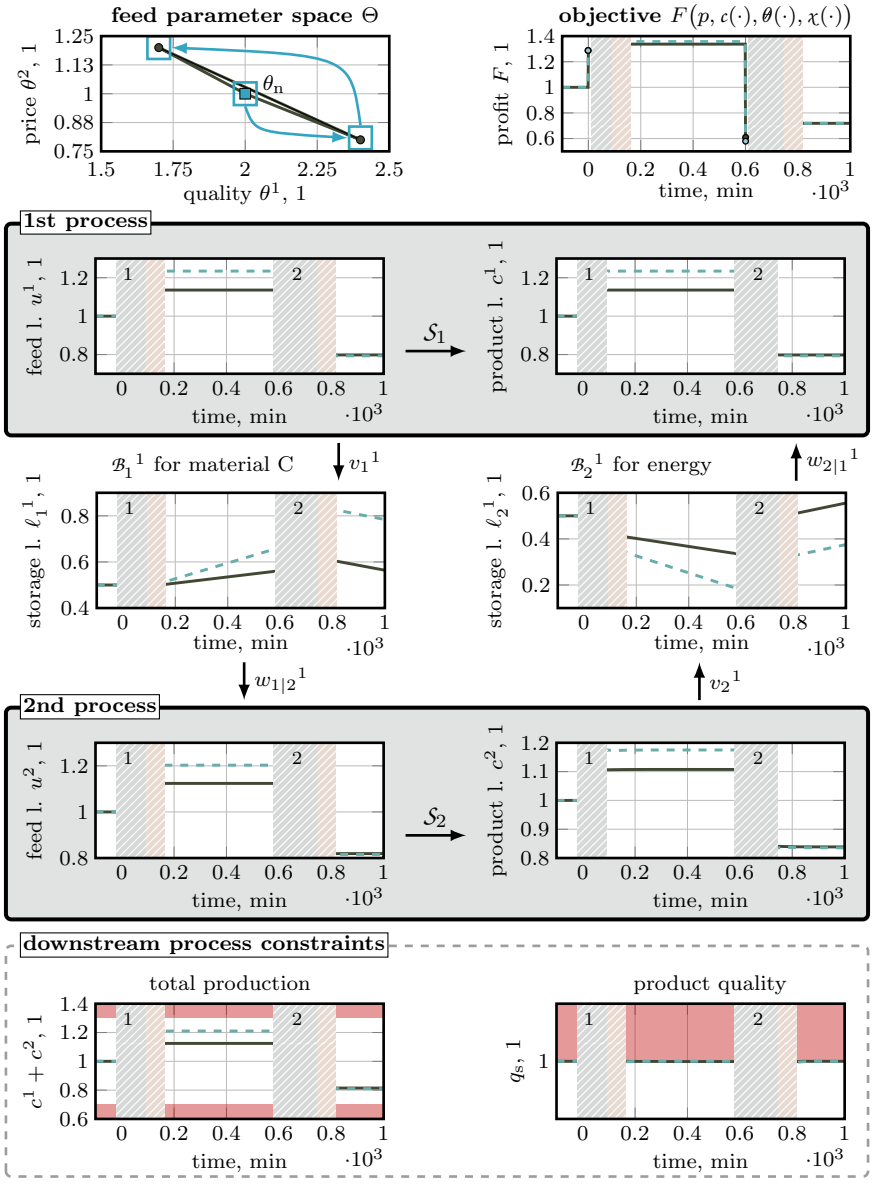

Figure 3.6: Transition and production phase of a segment of the two processes (grey solid line for D_1) (green dashed line for D^∞).

level at this θ value, the S-RTO needs to redetermine the operating point. This new point has a profit value close to the previous one, as shown in Figure 3.6 first row right column. Nevertheless, 5 to 7 % of economic improvement can be achieved. Considering Figure 3.6, one can see a difference between the cases (i) and (ii) indicated by the solid black and dashed green lines, respectively. The reason for this is described in more detail using Figure 3.7.

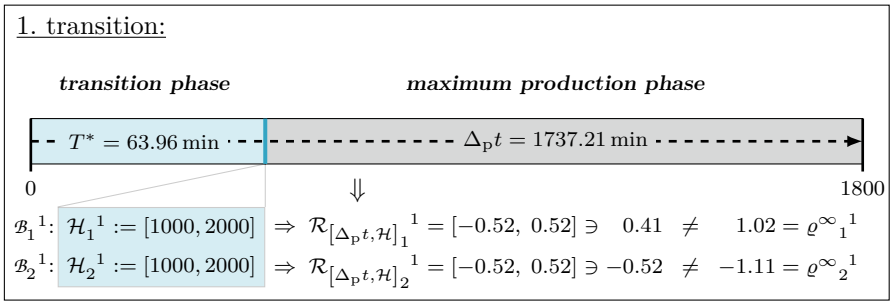

Figure 3.7: Storage constraints during the first transition of the production system.

We start at a storage level that corresponds to half of its capacity. At the end of the transition phase, the storage levels have to be within $\mathcal{H}_1{}^1$ and $\mathcal{H}_2{}^1$, so the admissible reserve during the production phase is given by ± 900 mol *or* kJ *due to the safety boundaries $\zeta_j{}^\alpha$ of 100* mol *or* kJ.
If the storage system is infinitely large (case (ii)), the desired production level yields the rates $\varrho^\infty{}_j{}^\alpha$ as stated in Figure 3.7. The transition time necessary to reach the new operation point can be calculated using the transition-time map and is $T^* = 95.34\,\text{min}$. From this, the time for the maximum production phase is determined. It follows that the rates for both elements have to be within $[-0.528, 0.528]$. *However, since the storage capacities are essential in a real application (case (i)), this production level cannot be achieved. The operating point, which is finally approached after the first transition, has the rates $\varrho_1{}^1 = 0.41$ and $\varrho_2{}^1 = -0.52$ as indicated in Figure 3.7. Thus, the storage constraints specified by $\mathcal{R}_{[\Delta_\text{p}t,\mathcal{H}]_j{}^\alpha}$ in Figure 3.7, and which are imposed by the corresponding transition time $T^* = 95.91\,\text{min}$, are fulfilled.*
The higher absolute value of the rates for case (ii) can be seen in Figure 3.6 third row by the slope of the storage level (green dashed lines). In general, the result of the S-RTO behaves as one might expect. Thus a better feed quality $\left(\theta^1 > 2\right)$ and a lower price $\left(\theta^2 < 1\right)$ yield a higher production level for the first and the second process.

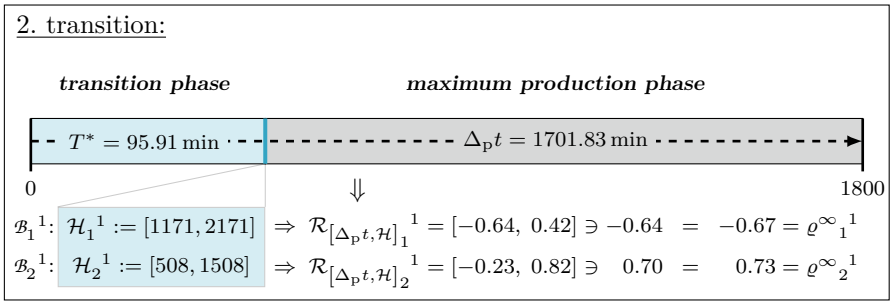

Figure 3.8: Storage constraints during the second transition of the production system.

At time $t = 600\,\text{min}$ *the economic circumstances change because of the feed quality for* $\mathcal{S}_1$ *decreases, and the price for* $\mathcal{S}_2$ *increases. In both cases, this change goes beyond the nominal feed parameter value. The profit value of the system falls significantly, as can be seen in Figures 3.5 and 3.6 first row right column. However, it falls to a different value for cases (i) and (ii) as the production levels are different at* $t = 600\,\text{min}$*. The S-RTO evaluation shows that profit can be increased again to a certain extent by modifying the production levels. This new operating point of the production system leads to a reduced production output in both processes, as otherwise, the operational costs would be too high. In Figure 3.8 the details of the second transition are presented. Based on the evolution of the storage level, the terminal region for this level is also different at the end of the second transition. For instance, the level of the first element at* $t = 600\,\text{min}$ *is* $\ell_1{}^1 = 1671\,\text{mol}$*. The requirement that the level at the end of the second transition has to be within* $\mathcal{H}_1{}^1 := [1171,\ 2171]$ *yields again restrictions for the steady-state rate related to the necessary transition time. However, the operating points for the real and relaxed case deviate only minimal from each other.*

Figure 3.6 illustrates that the storage levels between 800 and 1000 min *move in the opposite direction than before. The first storage element, which was previously charged, is now discharged, cf. Figure 3.6 third row left column. The same applies to the second storage element, which was discharged and is now filled. It is easy to see that the initial storage levels for cases (i) and (ii) are different at the beginning of the second production phase. There are two different reasons for this. Firstly, the different rates in the first production phase are responsible for this effect. Secondly, the different operating points, i.e., the production levels, lead to a different transition behavior concerning transition time and storage dynamics. We will discuss the latter in more detail in the next chapter.*

Finally, at time $t = 1100$ min*, the feed parameter changes again back to the nominal value. This directly results in a profit benefit illustrated by the vertical line at* $t = 1100$ min *in the objective function shown in Figure 3.6. However, this benefit can be further improved by the S-RTO. The new production levels* c^1 *and* c^2 *(Figure 3.6 second and fourth row, right column) are the nominal ones, where the storage rates are close to zero. By examining all state coordinates* x^α *of the system, we can conclude that these have also returned to their initial values. If it is generally true that reaching the same production level means that the system moves to the same point in the state space* $\mathcal{X}$*, the surrogate transition-time maps, generated at the individual operating points, can be reused. We will discuss this aspect in more detail in Section 4.3.*

It should be noted that after the first transition phase (indicated by the striped area enumerated with 1 in Figures 3.5 and 3.6), the operational points for cases (i) and (ii) are different, but their optimal profit values are close to each other. For the second and third transition (indicated by the striped area enumerated with 2 and 3), the operational points for cases (i) and (ii) are almost identical. This allows the conclusion that the selected scenario storage capacity is already well-chosen and might need to be increased only marginally. The classification of the two considered cases motivates an approach to the storage size estimation discussed in Chapter 5.

So far, we have focused on which level to produce after the feed parameters change. It is not yet clear whether such a change should also occur. Considering the first and the third transition, the benefit of a change is only small. The higher profit might not recoup the transition costs to the new operating point. To analyze this, we need to know whether the economic objective function is also valid for the transition.
A further aspect is the unsteady operated storage system. However, if the transition is not profitable, the storage levels need to be monitored, and it has to be ensured that they can be operated at current rates.

Chapter 4

Production Level Transition

In the last chapter we introduced the cl S-RTO, which is a bilevel optimization problem. To solve the problem efficiently, we separated it into a static S-RTO and a dynamic transition problem. The S-RTO provides a new production level to which the production system must be steered.
This chapter addresses the problem of the transition to these production levels, which was defined in Problem 2.1 (ii). Section 4.1 presents a brief overview about control strategies to steer a system from one operating point to a final one. In Section 4.2, we derive the trajectory generation based on an inverted system model using optimization techniques and a particular setup function to ensure stationarity of the production level. We conclude this section by discussing the framework of the supervisory control layer. Further, we describe in Section 4.3 an algorithm to generate the transition-time map that the cl S-RTO needs in Section 3.3.

Remark 4.1. *The transition problem to steer the system to a new production level discussed in this chapter must be valid for all time horizons* $[t_k, t_{k+1})$*. Therefore, w.l.o.g., it is assumed in this section that* $t_k = 0$*. In addition, we also omit the explicit notation of the* k*-th time horizon.*

4.1 Brief Review of Setpoint Transition

Following our discussion of the new production level identification in the last chapter, we will focus on implementing the transition between the old and the new production level. Specifically, this refers to Problem 2.1 (ii) and to the trajectory generation part within the cl S-RTO. In Section 3.2 we specified

that the storage levels have to be within ${\mathcal{H}_j}^{\alpha}$ at the end of the transition, as given by (3.1). It was one of the conditions to decompose the original bilevel problem of cl S-RTO into two separate problems. This requirement occurs as an additional constraint, given by a terminal region for the storage level, for the optimal control problem (OCP) within the trajectory generation. Afterward, the resulting trajectory can be utilized as a reference for a setpoint tracking problem, cf. [205].
As mentioned before, the OCP objective is equal to the transition time, which refers to the classical time-optimal setpoint transition problem, see [8, 188]. The trajectory generation obtains a new setpoint $\hat{c} \in \mathcal{C}_\mathrm{o}$ for the production level given by the map $\mathfrak{P}_\mathrm{c}^\mathrm{e}$ in (3.9) which must be reached in minimal time. Besides this, we also have information about the feed $\hat{u} \in \mathcal{U}$ and the state $\hat{x} \in \mathcal{X}_\mathrm{o}$ at this point.

The transition problem is a typical task in control engineering, as it occurs in many applications, such as robotics, aerospace, or process systems engineering, as presented by Devasia [43]. For instance, Santos et al. [215] use an offline planned reference and an MPC framework to track a pilot plant reactor towards steady state setpoints. In general, we can separate between optimal state and output transition, see [191, 43, 44]. In the former, the state coordinate is moved from an initial value $x_0 \in \mathcal{X}_\mathrm{o}$ to a final value $\chi(T) \in \mathcal{X}_\mathrm{o}$, where $T \in \mathbb{R}^+$ is the transition time. The latter refers to the transition of the output from the initial value $c_0 \in \mathcal{C}_\mathrm{o}$ to the final value $c(t_\mathrm{f}) \in \mathcal{C}_\mathrm{o}$. The two problems are connected since state transition approaches can be used to achieve output transition. Devasia [43] stated that if only the output and not the complete state of the system is considered, the transition time can be reduced.
A particular focus is often on integrating different types of constraints during the transition process to meet safety regulations or to ensure proper operating conditions. This is particularly important when minimum transition times are required, as it can lead to bang-bang solutions, cf. [138, 226]. The associated abrupt changes in the input signal can lead to higher wear of certain process elements [276].

In the following, we want to give a brief overview of strategies that can be exploited to address the trajectory generation in the sense of Problem 2.1 (ii). We primarily refer to the generation of a trajectory for the production level and a corresponding signal for the manipulating variable, which provides this output behavior. In this context, the optimization-based trajectory generation can be categorized into two different fields. For the first case, the manipulation variables are the decision variables of an OCP. While solving the OCP, these variables are modified to meet production-level requirements and other input and state constraints. The second case considers the time-dependent curve of the production level as a decision variable, which allows determining the system

input. To achieve this, we need an inversion of the system model and a suitable control law.

Path following Before we discuss the individual approaches in more detail, an alternative method is briefly described. Besides specifying the transition by a time-dependent curve in $\mathcal{C}_\mathrm{o}$, it can also be defined by a geometric path, cf. [231, 94, 56]. This path can be planned under various aspects, such as low operational costs, low energy consumption, or high energy integration of individual elements during the production transition. The timing is not necessarily optimal, determined online by the controller, and independent of the planning phase. The supervisory layer controller has to ensure that the path is traversed accurately and as fast as possible, with speed itself being a degree of freedom. Because no further specifications are made for the transition, time optimality cannot be guaranteed in general if a path is chosen arbitrarily. A different path may be traversed faster than another. Hence, we exclude path planning and following as a method for describing the transition for two reasons. Firstly, it requires an additional planning step, where a state-dependent criterion, e.g., the economic objective of the S-RTO, is needed to assess the transition. Secondly, the path has no information about the transition time required by the S-RTO, since the minimum transition time specification can only be considered online by the controller. Typical applications for path following can be found in robotics, see [256, 252], or for the motion of vehicles, see [154]. Faulwasser et al. [57] discusses this concept also for a fast setpoint change of a van de Vusse continuous stirred tank reactor (CSTR) in the field of process engineering.

Without coordinate transformation Let us return to the trajectory generation, where the information of the transition time is directly included. First of all, the basic idea is to discretize the continuous system model and parameterize the manipulating signal, e.g., by a piecewise constant function. The objective function is the transition time, and the setpoint to be reached is considered by a constraint for the terminal region for the production level. Consequently, we consider a fixed time horizon to describe the evolution of the dynamic process. One classical technique to address this aspect is time scaling, where the unknown interval $[0, T]$ is transformed to $[0, 1]$, and the transition time T becomes a parameter of the system, cf. [173].
Two alternative approaches arise if $[0, T]$ becomes the time horizon during discretization, consisting of $N \in \mathbb{N}$ subintervals with an interval length of $\Delta t_\mathrm{l} \in \mathbb{R}^+$. In this way, the transition time $T = N\Delta t_\mathrm{l}$ can be adjusted either by the number or the length of the intervals.
Considering a fixed length Δt_l the number N is typically reduced by a bisection

algorithm, see Van den Broeck [250], Janssens et al. [109]. For this purpose, a two-layer framework is used, whereby the horizon length described by N is reduced in the upper layer, while an NLP is solved in the lower layer. The algorithm reaches a minimal time if the NLP can not guarantee a feasible solution. Van den Broeck [250] proposes this approach as an online application where the settling time N is to be minimized from a given current state $x_{\text{now}} \in \mathcal{X}_{\text{o}}$ to a reference $(\hat{x}, \hat{u})$. The minimization of the number N of time steps to reach the steady-state of a time-discrete linear time-invariant system with linear constraints is also discussed in Janssens et al. [110], using a Newton-Raphson instead of a bisection method.
Another strategy is not to reduce the number N but to minimize the interval length Δt_{l} and thus the time to reach the states or production levels at the intermediate stages. Rösmann et al. [212] uses an approach where the nonlinear dynamic equation of the system is discretized by an explicit Euler method. The objective is to minimize Δt_{l} by modifying the state and input variables describing the trajectory from the initial to the final value. Using the step size as a further decision variable allows for contraction and expansion of the control and state sequence. Rösmann et al. [213] presents an extension of this approach. Therein, among other things, the lengths of the time intervals between the discrete points of the trajectory can differ. Verschueren et al. [257] discusses two different approaches focusing on both the minimization of N and Δt_{l}. The first one uses a time-scaled system model, which is discretized using different length parameters $\Delta t_{\text{l},k}$ for each subinterval, and its sum must be minimized. The second problem considers the minimization of N for time-discrete system models. It is shown how this mixed-integer optimization can be approximated by another problem with a fixed horizon N. The objective function of this new problem considers the weighted sum of the absolute values of the errors between the final state and the state at the intermediate stages.
A characteristic of these methods is that the original state coordinates of the system are used resulting from the modeling. Further examples for generating the trajectory of the manipulating variable while maintaining the coordinates can be found in [165, 103].

With coordinate transformation An alternative way is to use the inversion of the system model for trajectory generation. By a specific type of coordinate transformation, the states are reformulated considering the output and its time derivatives. A vital system property that we have to account for is differential flatness. For a general introduction to this topic, we refer to Fliess et al. [70] or Lévine [144]. In a differentially flat system model, the evolution of the states and manipulating variables are determined algebraically through the trajectory of output and their time derivatives. This allows converting the differential equations of the OCP into a finite-dimensional NLP with an

appropriate parameterization of $\tilde{c}$ [58]. Moreover, it offers a natural way to introduce stationarity for the final output value.
Early works where flatness is directly employed are [254, 55, 90]. Flatness in trajectory generation can be exploited when describing the trajectory of the production level with setup functions whose parameters are determined by optimization. For this, the system model and the constraints need to be expressed by the new coordinates, i.e., by the flat output and its derivatives, cf. [102]. Several setup functions are proposed in the literature. Van Loock et al. [253] uses B-Spline to ensure constraint satisfaction not only at the grid points, where the optimization is performed. Examples for polynomial functions to describe the flat output are given in [98, 176].

In literature, there are numerous approaches on how such flat outputs can be determined or constructed. For instance, a possible way to distinguish between the approaches relates to the duality of input and output variables. Waldherr and Zeitz [258] determine a new input for a given output, where in [221] or [225] an algorithm is presented to construct a flat output. For a semi-batch reactor, Oldenburg and Marquardt [184] has converted the non-flat model to a differentially flat by manipulating the input structure.

Nevertheless, a large class of process models is either not flat, or a flat output cannot be identified. In particular, for chemical industrial processes where large-scale models, with many states and few inputs, are used, flatness is usually not guaranteed, cf. [184]. Consequently, some state evolution cannot be derived directly from the evolutions of the output and its time derivatives. This means that the so-called internal states have to be determined additionally by solving their differential equations, as discussed in detail in Graichen [81].

Hence, in the following, we assume that the system is not differentially flat. According to the stability property of their zero dynamics, one can distinguish between two different classes of systems, see [104, 242, 105]. If these zero dynamics are unstable at the final steady-state $\hat{x} \in \mathcal{X}_\mathrm{o}$ during the production phase, we have to consider this for the controller design.

Remark 4.2. *A common term used in this context in the control engineering literature is minimum-phase or nonminimum-phase systems. However, Zeitz [275] pointed out that one has to be careful with this distinction, so we will refrain from using this term.*

One of the first approaches for a system inversion with unstable zero dynamics is presented by Devasia et al. [45] utilizing the input–output normal form and a predefined reference $\tilde{c}$. However, the disadvantage of this approach is that it causes a non-causal feedforward control signal because it is defined on $[-\infty, \infty]$ while $\tilde{c}$ is defined on $[0, T]$, $T < \infty$. Non-causality is caused by splitting the

internal dynamics into its stable and unstable parts, which are iteratively solved forward and backward in time. For linear time-invariant systems, Benosman and Le Vey [15] proposes to plan the reference $\tilde{c}$, which guarantees a causal signal by the additional degree of freedom. More precisely, no pre-actuation on $[-\infty, 0]$ is required for the control signal.
The planning of the trajectory $\tilde{c}$ also offers the possibility to consider input and output constraints. A minimal-time transition problem is addressed in [194, 195], where single input single output linear systems with stable and unstable internal dynamics are considered. Here the time required for the transition is iteratively reduced until the input and/or output constraints become active for a predefined $\tilde{c}$. Further works on inversion-based control, especially in the field of linear systems with unstable internal dynamics, can be found, e.g., in [193, 36, 279, 259, 260, 112, 37]. For nonlinear systems, Graichen and Zeitz [82] proposed a method to satisfy input and output constraints during the feedforward design. For this purpose, a system in input–output normal form is transformed utilizing saturation functions to account for constraints of the output $\tilde{c}$ and their time derivatives. The transition problem becomes a two-point boundary value problem where the dimension of the state space determines the number of parameters of $\tilde{c}$. In this way, the output trajectory is planned at the same time when designing the feedforward signal. An application of this strategy to multiple inputs and multiple output systems is discussed in [81]. This strategy is also successfully implemented on a discretized model of a tubular reactor with input constraints, see [263]. Furthermore, Käpernick and Graichen [123] apply the coordinate transformation from [82] to obtain an unconstrained optimal control problem for a class of nonlinear systems. In general, the application of a suitable coordinate transformation is a common technique to solve transition problems, cf. [66] and the reference therein.

Regardless of the coordinate transformation rule to achieve an inversion-based control design, the setup function is used for the output trajectory. In literature, several types of functions are listed, which are parameterized by a finite number of parameters and are determined considering system constraints. While in [82] or [195] polynomial or cosine-series are used as reference, in [71] Gevrey functions and in [247] splines are applied to avoid oscillations during setpoint changes.
The next section will introduce the most important notions to define and solve the transition problem formally. We focus mainly on coordination change and provide a control law to determine the feed signal. In particular, we introduce a new setup function for $\tilde{c}$, which ensures a smooth transition and allows adjusting the trajectory to the system constraints.

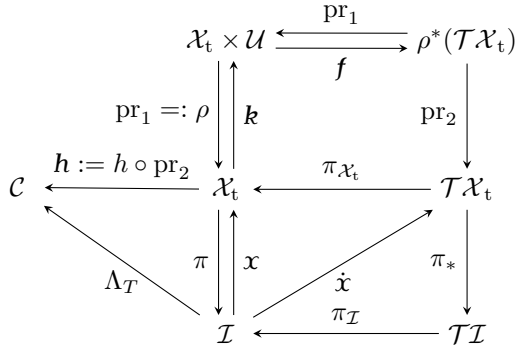

Figure 4.1: Commutative diagram of the process model.

4.2 Transition Problem for the Production Level

In this section, we address the transition of production levels. In this context, we use differential geometry to formulate this task mathematically. Furthermore, the problem of finding a controller to steer the system from an initial production level to a level desired by the S-RTO is specified. For this, several properties, including stability, reachability and stationarity, are introduced in a differential geometric context.

4.2.1 Mathematical Formulation of Transition

Subsequently, we consider the dynamic system (2.7a) and the output equation (2.7c). For the sake of simplicity, we temporarily ignore all additional equations in (2.7) and conditions that define the system. This also includes the dynamical system (2.7b) of the storage system. For the production level transition, we generate a trajectory by designing a control law that implements the transition. The following description refers to a differential geometric representation of the dynamic system model, similar to [223, 224, 222, 133] or [76]. General information about this topic can be found in the work of Frankel [72] and Lee [141].

To describe the transition problem and the associated concepts, we use the geometric structure of the process model shown by the commutative diagram in Figure 4.1. First, we consider an open subset $\mathcal{I} \subset \mathbb{R}$ of the real numbers and denote this as time manifold with local coordinate (t). In combination with the extended state space $\mathcal{X}_\mathrm{t} := \mathcal{I} \times \mathcal{X}$, $\mathcal{I}$ forms the bundle $(\mathcal{X}_\mathrm{t}, \pi, \mathcal{I})$. Note that the local coordinates of $\mathcal{X}_\mathrm{t}$ are given by $x_\mathrm{t} := (t, x)$ where (t) comes from

the time manifold and (x) is the standard chart introduced in Section 2.2. A section $\boldsymbol{x} \in \Gamma(\mathcal{X}_\mathrm{t})$ is called extended state trajectory. In addition, the tangential bundle $(\mathcal{T}\mathcal{X}_\mathrm{t}, \pi_{\mathcal{X}_\mathrm{t}}, \mathcal{X}_\mathrm{t})$ can be constructed for the extended state space $\mathcal{X}_\mathrm{t}$. Since the system is not autonomous, the input manifold $\mathcal{U}$ has to be included for a complete description. For this purpose we introduce the bundles $(\mathcal{X}_\mathrm{t} \times \mathcal{U}, \rho, \mathcal{X}_\mathrm{t})$ and the pullback bundle $\big(\rho^*(\mathcal{T}\mathcal{X}_\mathrm{t}), \mathrm{pr}_1, \mathcal{X}_\mathrm{t} \times \mathcal{U}\big)$ constructed from it. Similar as before, the local coordinates of $\mathcal{X}_\mathrm{t} \times \mathcal{U}$ are given by $u_\mathrm{t} := (t, x, u)$. By definition of a pullback bundle, the total space $\rho^*(\mathcal{T}\mathcal{X}_\mathrm{t})$ can be expressed as tangent spaces of $\mathcal{X}_\mathrm{t}$ attached on $\mathcal{X}_\mathrm{t} \times \mathcal{U}$. Finally, we will denote the sections $\boldsymbol{k} \in \Gamma(\mathcal{X}_\mathrm{t} \times \mathcal{U})$ and $\boldsymbol{f} \in \Gamma\big(\rho^*(\mathcal{T}\mathcal{X}_\mathrm{t})\big)$ as state controller and vector field of a system. Indeed, a map $\boldsymbol{k}$ yields for a given (t, x) an input value $u = \boldsymbol{k}(t, x)$. The vector field is given by a first-principle model of our system.
Because the considered manifolds $\mathcal{I}$, $\mathcal{X}$ and $\mathcal{U}$ are equivalent to $\mathbb{R}$, $\mathbb{R}^{n_\mathrm{x}}$ and $\mathbb{R}^2$ the identity map determines coordinate functions. We call these coordinates the original coordinates to distinguish them from the output coordinates that are introduced later.

Remark 4.3. *To distinguish the chart representation of the trajectory and controller, we use corresponding indices. For instance, if the original coordinates are used, we write $\boldsymbol{x}_{(x_\mathrm{t},t)}$ or $\boldsymbol{f}_{(u_\mathrm{t})}$. However, to simplify the notation, we omit an explicit representation when using the original coordinates for the corresponding functions. Only the expression in the new coordinates is displayed.*

Remark 4.4. *To simplify the notation of the indices, we agree that $t = {x_\mathrm{t}}^0$ and $x^\alpha = {x_\mathrm{t}}^\alpha$, $\alpha = 1, \ldots, n_\mathrm{x}$ or $t = {u_\mathrm{t}}^0$, $x^\alpha = {u_\mathrm{t}}^\alpha$, $\alpha = 1, \ldots, n_\mathrm{x}$ and $u^\beta = {u_\mathrm{t}}^{n_\mathrm{x}+\beta}$, $\beta = 1, 2$ respectively. In this way, the state trajectory introduced in Section 2.2 can be denoted by $\chi^\alpha := \boldsymbol{x}^\alpha$, $\alpha = 1, \ldots, n_\mathrm{x}$.*

However, it has to be ensured that the introduced objects $\boldsymbol{x}$, $\boldsymbol{k}$ and $\boldsymbol{f}$ are compatible, so that the diagram in Figure 4.1 commutes. Thus it has to be ensured that a vector field $\boldsymbol{f} \in \Gamma\big(\rho^*(\mathcal{T}\mathcal{X}_\mathrm{t})\big)$ is projectable, which means that $\pi_* \circ \mathrm{pr}_2(\boldsymbol{f}) \in \Gamma(\mathcal{T}\mathcal{I})$. In the following, we consider only vector fields that, in adapted coordinates (u_e), have the form

$$\boldsymbol{f} = \partial_t + f^\alpha(x, u)\, \partial_{x^\alpha},$$

where f^α are given by the dynamical system (2.7a) of the system $\mathcal{P}$. It is easy to see that $\boldsymbol{f}$ is projectable, as the component of ∂_t is one and thus independent of the state coordinates. Furthermore, a trajectory is valid if its velocity coincides with the vector field $\boldsymbol{f}$, where the components of the velocity at time t are given by $\dot{x}^\alpha(t) := \partial_t x^\alpha(t)$. The dynamical system of $\mathcal{P}$ is obtained in local coordinates by

$$\dot{x}^\alpha(t) = (\boldsymbol{f}^\alpha \circ \boldsymbol{k} \circ \boldsymbol{x})(t) \tag{4.1}$$

Remark 4.5. *A trajectory $\boldsymbol{x}$ is also called integral curve, cf. [104].*

Remark 4.6. *Note that the dynamical system* (4.1) *on $\mathcal{X}_\mathrm{t} \times \mathcal{U}$ is a reformulation of the System* (2.7) *of $\mathcal{P}$. This is true as the expanded space $\mathcal{X}_\mathrm{t} \times \mathcal{U}$ is constructed from the original spaces $\mathcal{X}$ and $\mathcal{U}$ of the system. Also $\boldsymbol{f}$ is generated by using the vector field in* (2.7a). *The description given here is only an alternative formulation.*

Before presenting the control concept and the associated transformation rules used to solve the transition problem, some terminology is introduced, following Isidori [104] and Sontag [238]. In the following, the concept of reachability is defined for $\mathcal{P}$.

Definition 4.1 (Reachability)**.** *Let $\mathcal{P}$ be a production system and let $\mathcal{I}$ be a time interval on which a dynamical system* (4.1) *is formulated. The equations are expressed, w.l.o.g., in original coordinates. A state $(t_0 + T, x_2) \in \mathcal{X}_\mathrm{t}$, $T \in \mathbb{R}^+$, is called reachable on $\mathcal{I}$ from the state $(t_0, x_1) \in \mathcal{X}_\mathrm{t}$, if there exist a control law $\boldsymbol{k} \in \Gamma\left(\mathcal{X}_\mathrm{t} \times \mathcal{U}\right)$ that solves*

$$\dot{x}^\alpha(t) = \left(\boldsymbol{f}^\alpha \circ \boldsymbol{k} \circ \boldsymbol{x}\right)(t), \tag{4.2a}$$

$$\dot{\iota}_j{}^\alpha(t) = \left(\rho_j{}^\alpha \circ \boldsymbol{k} \circ \boldsymbol{x}\right)(t), \tag{4.2b}$$

$$(t_0, x_1) = \boldsymbol{x}(t_0), \tag{4.2c}$$

$$(t_0 + T, x_2) = \boldsymbol{x}(t_0 + T), \tag{4.2d}$$

$$0 = \iota_j{}^\alpha(t_0), \tag{4.2e}$$

$$\iota_j{}^\alpha(t_0 + T) \in \left[-\delta_j{}^\alpha,\, \delta_j{}^\alpha\right], \tag{4.2f}$$

$$0 \geq \left(s \circ \boldsymbol{k} \circ \boldsymbol{x}\right)(t), \tag{4.2g}$$

$$0 \geq \left(\omega \circ \boldsymbol{x}\right)(t). \tag{4.2h}$$

This gives rise to a further definition, where the reachability is extended to the operating area.

Definition 4.2 (Dynamically Operable)**.** *Let $\mathcal{P}$ be a production system. The system is called*

(i) locally dynamically operable, if for all $c \in \tilde{\mathcal{C}} \subset \mathcal{C}_\mathrm{o}$ there exists a state $x_\mathrm{t} \in \underset{h}{\mathrm{preim}}\,(c) \subseteq \mathcal{X}_\mathrm{t}$, that is reachable from all states within $\mathcal{X}_\mathrm{o}$ and $c_\mathrm{n} \in \tilde{\mathcal{C}}$.

(ii) globally dynamically operable, if for all $c \in \mathcal{C}_\mathrm{o}$ there exists a state $x_\mathrm{t} \in \underset{h}{\mathrm{preim}}\,(c) \subseteq \mathcal{X}_\mathrm{t}$, that is reachable from all states within $\mathcal{X}_\mathrm{o}$.

Assumption 4.1. *The system $\mathcal{P}$ is at least local dynamically operable.*

Assumption 4.1 guarantees that the result of the S-RTO by (3.9) can be achieved by a suitable control law. The subset $\tilde{\mathcal{C}}$ from Definition 4.2 represents the feasible production levels of (3.9).
It should be emphasized that Definition 4.1 was formulated for the extended state space $\mathcal{X}_\mathrm{t}$, where time is an explicit state coordinate. In this way, the time until reaching the new state can be directly included in the definition. For instance, if $x_2 \in \mathcal{X}$ remains constant, but T is changed, the new state may not be reachable even if the same point in $\mathcal{X}$ should be set.
An additional important concept is asymptotic stability, which is defined below.

Definition 4.3 (Asymptotic Stability)**.** *Let $\mathcal{P}$ be a production system with vector field $\boldsymbol{f}$. For a given control law $\boldsymbol{k} \in \Gamma\left(\mathcal{X}_\mathrm{t} \times \mathcal{U}\right)$ let $x_\mathrm{s} \in \mathcal{X}$ be a steady-state that solves $0 = \left(\boldsymbol{f}^\alpha \circ \boldsymbol{k}\right)(t, x_\mathrm{s}), \quad \alpha = 1, \ldots, n_\mathrm{x}, \ \forall t \in \mathcal{I}$. The system is called asymptotically stable at $x_\mathrm{s} \in \mathcal{X}$ if for the trajectory χ obtained by solving* (4.1) *it holds that*

(i) for all $\varepsilon \in \mathbb{R}^+$ there exists a $\delta \in \mathbb{R}^+$ such that $\chi(t_0) \in \mathcal{B}_\delta\left(x_\mathrm{s}\right)$ implies $\chi(t) \in \mathcal{B}_\varepsilon\left(x_\mathrm{s}\right)$ for all $t \geq t_0$,

(ii) there exists a $\zeta \in \mathbb{R}^+$ such that for $\chi(t_0) \in \mathcal{B}_\zeta\left(x_\mathrm{s}\right)$ follows $\lim\limits_{t \to \infty} \chi(t) = x_\mathrm{s}$.

Assumption 4.2. *Let $\mathcal{P}$ be a production system. For each production level $c \in \mathcal{C}_\mathrm{o}$, there exist a state $x \in \mathcal{X}$ that is asymptotically stable.*

Assumption 4.2 is valid, as it can be assumed that there exist stabilizing regulatory controllers at the production system layer, cf. [41] and Figure 3.2 in Section 3.1.

Remark 4.7. *It should be noted that Definition 4.1 and 4.3 are formulated in original coordinates, but it can be shown that this property is invariant under a coordinate transformation, see [1]. However, both stability and reachability depend on the choice of the control law $\boldsymbol{k} \in \Gamma\left(\mathcal{X}_\mathrm{t} \times \mathcal{U}\right)$.*

As the system operates at its economic optimum during the production phase, the production level should be constant at the end of the transition phase. We will call this a stationary production level, which is introduced in the following definition.

Definition 4.4 (Stationary Production Level)**.** *Let $\boldsymbol{x} \in \Gamma(\mathcal{X}_\mathrm{t})$ be a state trajectory and $\boldsymbol{h} \in C^\infty(\mathcal{X}_\mathrm{t} \times \mathcal{U})$. A production level $c_\mathrm{s} \in \mathcal{C}$ is called stationary at time $T \in \mathbb{R}^+$, if it holds that*

$$\dot{\boldsymbol{x}}_{x(t)}(\boldsymbol{h}) = 0, \quad \text{for } t \geq T, \tag{4.3a}$$

$$(\boldsymbol{h} \circ \boldsymbol{x})(t) = c_\mathrm{s}, \quad \text{for } t \geq T. \tag{4.3b}$$

where $\dot{\boldsymbol{x}}_{x(t)} \in \rho^*(\mathcal{T}\mathcal{X}_\mathrm{t})$ is the velocity vector of the trajectory $\boldsymbol{x}$ at time t.

A stationary production level is characterized by a constant system output, even if the states of the system may vary. This stationarity is formulated by (4.3a), which describes the time-dependent change of the production level along the state trajectory as a solution of (4.1).
To conclude this section, we intend to address the transition of production level the following problem.

Problem 4.1 (Transition problem)**.** *Given is a production system $\mathcal{P}$ and two setpoints $c_{\mathrm{s},1}, c_{\mathrm{s},2} \in \mathcal{C}_\mathrm{o}$ within the operating area. Design a control law $\boldsymbol{k} \in \Gamma(\mathcal{X}_\mathrm{t} \times \mathcal{U})$ that achieves:*

(i) The production levels are connected through a smooth curve $\boldsymbol{h} \circ \boldsymbol{x}$ such that $c_{\mathrm{s},1} = (\boldsymbol{h} \circ \boldsymbol{x})(0)$ and $c_{\mathrm{s},2} = (\boldsymbol{h} \circ \boldsymbol{x})(T)$.

(ii) The state $\boldsymbol{x}(T)$ has to be reachable according to Definition 4.1 from $\boldsymbol{x}(0)$.

(iii) The production level $c_{\mathrm{s},2}$ has to be stationary according to Definition 4.4 at time T.

(iv) The transition time $T^* \in \mathbb{R}^+$ has to be minimal.

4.2.2 Principle of Coordinate Transformation

Next, we discuss the coordinate change and its effect on the process dynamics. This allows deriving a method to solve Problem 4.1 efficiently. First, we deal with the coordinate change in general, before we discuss a specific transformation

law. For this purpose consider a coordinate transformation of the form

$$\begin{aligned}
\text{on } \mathcal{I}\colon \qquad & \tau = \varphi(t), \\
\text{on } \mathcal{X}_\mathrm{t}\colon \qquad & z_\mathrm{t} := (\tau, z) = \chi(t, x) = \big(\varphi(t), \varphi_1(t, x)\big), \\
\text{on } \mathcal{X}_\mathrm{t} \times \mathcal{U}\colon \qquad & v_\mathrm{t} := (\tau, z, v) = \psi(t, x, u) = \big(\varphi(t), \varphi_1(t, x), \varphi_2(t, x, u)\big).
\end{aligned}$$

In order to express the velocity components in terms of the new coordinates (τ) and (z_t), one can derive the following transformation rule

$$\begin{aligned}
\dot{\boldsymbol{x}}_{(z_\mathrm{t},\tau)}{}^{\alpha} &= \partial_1 \left({z_\mathrm{t}}^{\alpha} \circ \boldsymbol{x} \circ \tau^{-1}\right) = \partial_1 \left({z_\mathrm{t}}^{\alpha} \circ {x_\mathrm{t}}^{-1} \circ x_\mathrm{t} \circ \boldsymbol{x} \circ t^{-1} \circ t \circ \tau^{-1}\right) \\
&= \partial_\beta \left({z_\mathrm{t}}^{\alpha} \circ {x_\mathrm{t}}^{-1}\right) \partial_1 \left({x_\mathrm{t}}^{\beta} \circ \boldsymbol{x} \circ t^{-1}\right) \partial_1 \left(t \circ \tau^{-1}\right) \\
&= \partial_{{x_\mathrm{t}}^{\beta}} \chi^{\alpha}\, \dot{\boldsymbol{x}}^{\beta}\, \partial_\tau \varphi^{-1} = \partial_{{x_\mathrm{t}}^{\beta}} \chi^{\alpha}\, \partial_\tau \varphi^{-1}\, \dot{\boldsymbol{x}}^{\beta}
\end{aligned}$$

Remark 4.8. *It is important to note that the coordinate function is used in the equation above and not the coordinate (point within the considered space) as indicated in Remark 1.1.*

The factor $\partial_{{x_\mathrm{t}}^{\beta}} \chi^{\alpha}$ corresponds to the standard transformation rule of vector components within the tangent space. Whereas, $\partial_\tau \varphi^{-1}$ results from a reparametrization of the time manifold and determines the speed at which $\boldsymbol{x}$ is passed through.

Assumption 4.3. *The transformation maps φ_1 and φ_2 of the state and input coordinates are time-independent. Moreover, φ_2 is also independent of the state variables.*

The motivation of Assumption 4.3 is twofold. First, it ensures that the new input variables have no dynamical component. Second, one can use $\partial_{{x_\mathrm{t}}^{\beta}} \chi^{\alpha}$ to transform the components of the vector field in the same way as for the velocity. Finally, we can express (4.1) in new coordinates by multiplying $\partial_{{x_\mathrm{t}}^{\beta}} \chi^{\alpha}$ and $\partial_\tau \varphi^{-1}$ on both sides of the equation, which yields

$$\dot{\boldsymbol{x}}_{(z_\mathrm{t},\tau)}{}^{\alpha}(\tau) = \Big(\underbrace{\partial_{{x_\mathrm{t}}^{\beta}} \chi^{\alpha}}_{\text{(I)}}\, \underbrace{\partial_\tau \varphi^{-1}}_{\text{(II)}}\, \underbrace{\boldsymbol{f}^{\beta}}_{\text{(III)}} \circ \underbrace{\psi^{-1}}_{\text{(IV)}} \circ \underbrace{\boldsymbol{k}_{(v_\mathrm{t},z_\mathrm{t})}}_{\text{(V)}} \circ \underbrace{\boldsymbol{x}_{(z_\mathrm{t},\tau)}}_{\text{(VI)}}\Big)(\tau). \tag{4.4}$$

Let us discuss the individual parts of (4.4) in more detail. The expression (I) results from the fact that the original system model will be expressed in different coordinates. By choosing a suitable transformation χ, the transition problem becomes much easier to solve. We will discuss in the next section a transformation law with which this can be achieved. The term (II) is obtained

from a reparametrization of the time domain, which is also called time scaling. This allows us to consider a fixed time horizon for integrating (4.4). Part (III) is given by (2.7a) of the original system model introduced in Section 2.2. The transformation ψ has to be inverted as the vector field of the system is formulated in the original coordinates. This leads to additional algebraic equations which must be considered when solving the transition problem. A key element for the implementation of the transition is the control law in (V). Here we will present an approach based on a specific class of setup functions. In this way, the structure of the controller is predefined and only a parameterization has to be determined. The trajectory in (VI) will be obtained by integrating (4.4) by state-of-the-art solvers.

Finally, we will introduce the concept of the relative degree, cf. [104, 125], as it allows the introduction of the output coordinates in the next section. Therefore, it should be noted that the vector field $\boldsymbol{f}$ can also be interpreted as a map $\boldsymbol{f} : C^\infty(\mathcal{X}_\mathrm{t} \times \mathcal{U}) \to C^\infty(\mathcal{X}_\mathrm{t} \times \mathcal{U})$.

Definition 4.5 (Relative Degree)**.** *Let $\mathcal{P}$ be a production system with vector field $\boldsymbol{f} \in \Gamma\big(\rho^*(\mathcal{TX}_\mathrm{t})\big)$. For a function $\boldsymbol{h} \in C^\infty(\mathcal{X}_\mathrm{t} \times \mathcal{U})$ it holds that $\mathrm{d}\boldsymbol{h} \in \mathcal{T}^*(\mathcal{X}_\mathrm{t} \times \mathcal{U}) = \mathcal{T}^*(\mathcal{X}_\mathrm{t}) \oplus \mathcal{T}^*(\mathcal{U})$, where $\oplus$ means the direct sum of two vector spaces. Let*

$$(\boldsymbol{f})^0(\boldsymbol{h}) := \boldsymbol{h}, \quad \textit{and} \quad (\boldsymbol{f})^{i+1}(\boldsymbol{h}) := \boldsymbol{f}\big((\boldsymbol{f})^i(\boldsymbol{h})\big),$$

be the repeated action of $\boldsymbol{f}$ on a function $\boldsymbol{h}$. We call r the relative degree of the system if it holds that

$$\mathrm{d}\big((\boldsymbol{f})^i(\boldsymbol{h})\big) \in \mathcal{T}^*(\mathcal{X}_\mathrm{t}), \quad i = 0, \dots, r-1, \quad \textit{and}$$

$$\mathrm{d}\big((\boldsymbol{f})^r(\boldsymbol{h})\big) \in \mathcal{T}^*(\mathcal{X}_\mathrm{t}) \oplus \mathcal{T}^*(\mathcal{U}).$$

4.2.3 Inversion-Based Control Law

Once we have introduced the key concepts and formally described the transition problem, we will now focus on its solution. For this purpose, the applied coordinate transformations and its effects on the system will be discussed in detail. First, we consider the time interval. In order to fix the time horizon for the transition phase, φ is chosen as

$$\tau = \varphi(t) := \frac{1}{T}t \quad \Rightarrow \quad t = \varphi^{-1}(\tau) = T\tau$$

It follows that part (II) in (4.4) is given by $\partial_\tau \varphi^{-1} = T$. In this way, the length T of the transition phase becomes a parameter that scales the velocity of the trajectory.

The coordinate transformation φ_1 for the system states is motivated by property (iii) in Problem 4.1. For a more precise and compact description, we introduce the index sets $\mathbb{I}^{\mathcal{X}}{}_i := \{1, \dots, n_{\mathrm{x},i}\}$, $\mathbb{I}^{\mathrm{in}}{}_i := \{1, \dots, n_{\mathrm{x},i} - r_i\}$ and $\mathbb{I}^{\mathrm{ex}}{}_i := \{1, \dots, r_i\}$. Based on the fact that the system is composed of the model equations of two individual processes, we define

$$z^{(i-1)n_{\mathrm{x},1}+\alpha} = \varphi_1{}^{(i-1)n_{\mathrm{x},1}+\alpha}(x) := (T\boldsymbol{f})^{\alpha-1}\left(h^i\right)(x), \quad \alpha \in \mathbb{I}^{\mathrm{ex}}{}_i, \tag{4.5a}$$

$$z^{(i-1)n_{\mathrm{x},1}+r_i+\beta} = \varphi_1{}^{(i-1)n_{\mathrm{x},1}+r_i+\beta}(x), \qquad \beta \in \mathbb{I}^{\mathrm{in}}{}_i. \tag{4.5b}$$

Remark 4.9. *Here we have directly used the fact that $\partial_\tau \varphi^{-1} = T$. In other words, the coordinate change is defined by the repeated actions of the scaled vector field on the corresponding output function.*

In this way, $r_1 + r_2$ coordinates are uniquely defined. The first and $(n_{\mathrm{x},1}+1)$-th state coincides with the production level of the corresponding processes. The other states represent the time derivatives of the two production levels. It follows that the requirement of a stationary production level can be transferred to the new state coordinates by defining suitable boundary conditions. We will call the coordinates in (4.5a) external states.
However, there is still the question of how to select the remaining $n_{\mathrm{x}} - r_1 - r_2$ coordinates. A necessary condition for this choice is that φ_1 is a diffeomorphism. Besides, it is useful that the coordinate transformation does not cause any additional coupling of the individual processes. Therefore, the functions $\varphi_1{}^{\alpha}$, $\alpha = r_1, \dots, n_{\mathrm{x},1}$ should only depend on the states of $\mathcal{S}_1$, where the functions $\varphi_1{}^{\beta}$, $\beta = n_{\mathrm{x},1} + r_2 + 1, \dots, n_{\mathrm{x}}$ should only depend on the states of $\mathcal{S}_2$. It is suitable to choose the remaining states identical to a subset of the original states. Considering (4.5b), the transformations are given by

$$z^{(i-1)n_{\mathrm{x},1}+r_i+\beta} = x^{m_{i,\beta}} \quad \beta \in \mathbb{I}^{\mathrm{in}}{}_i, \tag{4.6}$$

where $m_{i,\beta} \in \mathbb{I}^{\mathrm{id}}{}_i := \left\{(i-1)n_{\mathrm{x},1} + \xi \mid \xi \in \mathbb{I}^{\mathcal{X}}{}_i\right\}$ are a selection of indices of the original states for the two processes $i = 1, 2$. The coordinates $z^{(i-1)n_{\mathrm{x},1}+r_i+\beta}$, $\beta \in \mathbb{I}^{\mathrm{in}}{}_i$, are called internal states.

Example 4.1. *The process $\mathcal{S}_1$ is described through five state coordinates, such that $\mathbb{I}^{\mathcal{X}}{}_1 := \{1, 2, 3, 4, 5\}$. The relative degree is $r_1 = 2$, that yields $\mathbb{I}^{\mathrm{in}}{}_i := \{1, 2, 3\}$. It follows that the first two states are uniquely defined by* (4.5a)*, and three states have to chosen to make φ_1 to be a diffeomorphism. For this purpose, we choose the first, the third and the fourth state so that $\mathbb{I}^{\mathrm{id}}{}_1 := \{1, 3, 4\}$. The new states are given by $z^{2+1} = x^{m_{1,1}} = x^1$, $z^{2+2} = x^{m_{1,2}} = x^3$ and $z^{2+3} = x^{m_{1,3}} = x^4$.*

To complete the transformation ψ, the transformation rule for the input coordinate has to be defined. Here, the identity map is choosen such that $v = \varphi_2(u) = u$.

Next, we will determine the vector field concerning the new coordinates. Due to the choice of φ, φ_1 and φ_2, the transformation

$$\boldsymbol{f}_{(v_\mathrm{t})}{}^{\alpha} = \partial_{x_\mathrm{t}{}^{\beta}} \chi^{\alpha}\, \partial_{\tau} \varphi^{-1}\, \boldsymbol{f}^{\beta} \circ \psi^{-1},$$

in (4.4) with vector components $\boldsymbol{f}^{\beta}$ in original coordinates, is now discussed in detail. The first component of the vector field in new coordinates refers to the dynamic equation of the time component and is obtained via

$$\boldsymbol{f}_{(v_\mathrm{t})}{}^{0} = \partial_t \chi^0\, T\, 1 + \partial_{x^\alpha} \chi^0\, T\, \boldsymbol{f}^{\alpha} = \partial_t \varphi\, T\, 1 + \partial_{x^\alpha} \varphi\, T\, \boldsymbol{f}^{\alpha} = \partial_t \varphi\, T\, 1 = 1.$$

To derive the dynamic equations of the states, we will distinguish the individual components in a similar way as in (4.5). In general, the new vector components can be determined from

$$\boldsymbol{f}_{(v_\mathrm{t})}{}^{\alpha} = \partial_t \chi^{\alpha}\, T\, 1 + \partial_{x^\alpha} \chi^{\alpha}\, T\, \boldsymbol{f}^{\alpha} = T\, \boldsymbol{f}^{\alpha}\; \partial_{x^\alpha} {\varphi_1}^{\alpha}.$$

From this, we derive the individual components of both processes by

$$\boldsymbol{f}_{(v_\mathrm{t})}{}^{(i-1)n_{\mathrm{x},1}+\alpha} = T\, \boldsymbol{f}^{\alpha}\, \partial_{x^\alpha} \left(T\boldsymbol{f}\right)^{\alpha-1} \left(h^i\right) = \left(T\boldsymbol{f}\right)^{\alpha} \left(h^i\right), \quad \alpha \in \mathbb{I}^{\mathrm{ex}}{}_i,$$

$$\boldsymbol{f}_{(v_\mathrm{t})}{}^{(i-1)n_{\mathrm{x},1}+r_i+\beta} = T\, \boldsymbol{f}^{\alpha}\, \partial_{x^\alpha} x^{m_{i,\beta}} = T\, \boldsymbol{f}^{m_{i,\beta}}, \qquad \beta \in \mathbb{I}^{\mathrm{in}}{}_i.$$

By definition of the coordinate change in (4.5a), it follows that

$$\boldsymbol{f}_{(v_\mathrm{t})}{}^{(i-1)n_{\mathrm{x},1}+\alpha} = z^{(i-1)n_{\mathrm{x},1}+\alpha+1}, \quad \alpha \in \mathbb{I}^{\mathrm{ex}}{}_i \setminus \{r_i\},$$

which means that the dynamics of the states $\left(z^1, \ldots, z^{r_1-1}\right)$ and $\left(z^{n_{\mathrm{x},1}+1}, \ldots, z^{n_{\mathrm{x},1}+r_2-1}\right)$ are expressed by two integrator chains. In addition, the approach in (4.6) and Definition 4.5 tells us that $\boldsymbol{f}_{(v_\mathrm{t})}{}^{r_1} = \left(T\boldsymbol{f}\right)^{r_1} \left(h^1\right)$ depends on the input u^1 of $\mathcal{S}_1$ and $\boldsymbol{f}_{(v_\mathrm{t})}{}^{n_{\mathrm{x},1}+r_1} = \left(T\boldsymbol{f}\right)^{r_2} \left(h^2\right)$ on the input u^2 of $\mathcal{S}_2$. This fact defines implicitly a control law $\boldsymbol{k}$. Note that $\boldsymbol{f}_{(v_\mathrm{t})}{}^{r_1}$ and $\boldsymbol{f}_{(v_\mathrm{t})}{}^{r_2}$ is equal with the r_1- and r_2-th time derivative of the production levels c^1 and c^2. For instance, if a suitable function gives the left-hand side of the differential equation for the time derivative of the production level, the input signal can be determined. Such a time and parameter-dependent function is called a setup function, and we define it by

$$\Lambda_T : \mathcal{I} \times \mathbb{R}^{r_1+r_2+2} \times \mathbb{R}^{n_{\mathrm{q},1}+n_{\mathrm{q},2}} \to \mathcal{C}_{\mathrm{o}}.$$

Here, two types of parameters are involved. While the relative degree of the two processes determines the dimension and value of the first parameter $p \in \mathbb{R}^{r_1+r_2+2}$, the dimension and value of the second parameter $q \in \mathbb{R}^{n_{\mathrm{q},1}+n_{\mathrm{q},2}}$ can be chosen arbitrarily. It should be emphasized that the number of components of q results from the degree of freedom $n_{\mathrm{q},i}$, $i = 1, 2$, of the two individual processes. As we will see later, the parameters q and T have to be determined to achieve the production level transition and thus to define the control law. Considering property (i) and (iii) in Problem 4.1, it can be concluded that Λ_T connect the two setpoints $c_{\mathrm{s},1}, c_{\mathrm{s},2} \in \mathcal{C}_{\mathrm{o}}$ and thus the states $\left(\boldsymbol{x}_{(z_{\mathrm{t}},\tau)}{}^{1}(0),\ \boldsymbol{x}_{(z_{\mathrm{t}},\tau)}{}^{n_{\mathrm{x},1}+1}(0)\right) = c_{\mathrm{s},1}$, at the beginning and $\left(\boldsymbol{x}_{(z_{\mathrm{t}},\tau)}{}^{1}(1),\ \boldsymbol{x}_{(z_{\mathrm{t}},\tau)}{}^{n_{\mathrm{x},1}+1}(1)\right) = c_{\mathrm{s},2}$, at the end of the transition. Furthermore, the requirement of a stationary production level motivates the following definition.

Definition 4.6 (Admissible Setup Function)**.** *Let $c_{\mathrm{s},1}, c_{\mathrm{s},2} \in \mathcal{C}_{\mathrm{o}}$ two setpoints within the operating area. For a given change of the production level $\delta c := c_{\mathrm{s},2} - c_{\mathrm{s},1} \in \Delta_{c_{\mathrm{s},1}}$, the setup function Λ_T of the form*

$$(t, p, q) \mapsto \Lambda_T(t, p, q) := c_{\mathrm{s},1} + \delta c\, \lambda_T(t, p, q), \tag{4.7}$$

is called admissible, if λ_T satisfies component-wise the following properties:

(i) at time $t = 0$, λ_T and all time derivatives up to the relative degree r_α vanish: $0 = \left({\lambda_T}^{\alpha}\right)^{(k)}(0, p, q)$, $k = 0, \ldots, r_\alpha$,

(ii) at time $t = T$, λ_T has to be one: $1 = {\lambda_T}^{\alpha}(T, p, q)$,

(iii) at time $t = T$, all time derivatives up to the relative degree r_α of λ_T vanish: $0 = \left({\lambda_T}^{\alpha}\right)^{(k)}(T, p, q)$, $k = 1, \ldots, r_\alpha$.

The properties in Definition 4.6 guarantee the stationarity. Additionally, condition (ii) ensures that the new setpoint is reached. For the structure of λ_T, we propose the form

$$\lambda_T(t, p, q) := A_T(t, p) + B_T(t, q).$$

where A_T is denoted as basic and B_T as variation term. The basic term satisfies component-wise all properties of Definition 4.6. The individual components ${A_T}^{\alpha}$ depend only on the relative degree r_α of the corresponding process $\mathcal{S}_\alpha$. This means that $p \in \mathbb{R}^{r_1+r_2+2}$ is fixed. A_T ensures that there exists a smooth curve between the two production levels $c_{\mathrm{s},1}$ and $c_{\mathrm{s},2}$.
In contrast, the variation term B_T adapts the curve between the two setpoints. For this, we will choose B_T satisfying $\left({B_T}^{\alpha}\right)^{(k)}(0, p, q) = \left({B_T}^{\alpha}\right)^{(k)}(T, p, q) = 0$, $k = 0, \ldots, r_\alpha$. The parameter $q \in \mathbb{R}^{n_{\mathrm{q},1}+n_{\mathrm{q},2}}$ can be chosen arbitrarily. Table 4.1

lists two different approaches for the basic and the variation term, see [100]. Appendix A.5 describes how to determine the parameters p based on the relative degree. Subsequently, we use the r_α-th derivative of ${\Lambda_T}^\alpha$ to determine the input signal, which allows defining the control law $\boldsymbol{k}$ implicitly by

$$0 = \left((T\boldsymbol{f})^{r_\alpha}\left(h^\alpha\right)\right)(x,u) - \left({\Lambda_1}^\alpha\right)^{(r_\alpha)}(t,p,q). \tag{4.8}$$

Using the implicit function theorem, for a given (t,x), it is possible to formulate $\boldsymbol{k}$ locally and to compute the input u.

Example 4.2. *In this example, we consider the process $\mathcal{S}_1$, which means that we only focus on the first component of the control law. The process is an input affine system of the form $\boldsymbol{f}^\alpha(x,u) = f^\alpha(x) + g^\alpha(x)u$, where the production level is described by $h \in C^\infty(\mathcal{X}\times\mathcal{U})$. The dimension of $\mathcal{S}_1$ is $n_{\mathrm{x},1} = 5$, and the relative degree is $r_1 = 2$. From the given structure of the system, it is easy to see that $\boldsymbol{f}$ is a sum of two vector fields and one can write $\boldsymbol{f} = \boldsymbol{f}_\mathrm{s} + \boldsymbol{g}_\mathrm{s}$, where $\boldsymbol{f}_\mathrm{s} = f^\alpha(x)\partial_{x^\alpha}$ and $\boldsymbol{g}_\mathrm{s} = u\, g^\alpha(x)\partial_{x^\alpha}$. Furthermore, for an input-affine system, the control law can be explicitly represented by*

$$u = \boldsymbol{k}(t,x) := \frac{\left({\Lambda_T}^\alpha\right)^{(r_\alpha)}(t) - \left(\left(\boldsymbol{f}_\mathrm{s}\right)^2(h)\right)(x)}{\Big(\boldsymbol{g}_\mathrm{s}\big(\boldsymbol{f}_\mathrm{s}(h)\big)\Big)(x)}.$$

We conclude this section by presenting the optimization problem to solve Problem 4.1. For this purpose, we use property (ii) and formulate the reachability of a state coordinate of the system as a minimization problem. Considering (4.4), it is clear that the inverse of the transformation ψ has to be used to represent the new system dynamics. Similar to the implicitly given control law (4.8), the coordinate change ψ is added to (4.2) in order to avoid the explicit inversion.

Since the time evolution of the states $\boldsymbol{x}_{(z_\mathrm{t},\tau)}^{(i-1)n_{\mathrm{x},1}+\alpha}$, $\alpha \in \mathbb{I}^{\mathrm{ex}}{}_i$ is directly defined by the setup function, the number of dynamical equations is reduced. In addition, the internal states are equivalent to a subset of the original states, which allows using the original dynamical equations. However, it should be

Table 4.1: Ansatz functions for λ_T.

	Polynomial	**Trigonometric**
${A_T}^\alpha(t,p)$	$\sum_{i=1}^{r_\alpha+1} p_i \left(\frac{t}{T}\right)^{r_\alpha+i}$	$\sum_{i=1}^{r_\alpha+1} p_i \cos\left((i-1)\pi\left(\frac{t}{T}\right)\right)$
${B_T}^\alpha(t,q)$	$\sum_{i=1}^{n_{\mathrm{q},\alpha}} q_i \left(\frac{t}{T}\right)^i \left(\left(\frac{t}{T}\right)^2 - \left(\frac{t}{T}\right)\right)^{r_\alpha+2}$	$\sum_{i=1}^{n_{\mathrm{q},\alpha}} q_i \sin^{r_\alpha+2}\left(i\pi\left(\frac{t}{T}\right)\right)$

emphasized that ψ needs to be used to determine states that are not determined by solving the dynamic equations but via the setup function.
For a given initial value $x_{\mathrm{t},0} = (0, x_0) \in \mathbb{R}_0^+ \times \mathcal{X}_\mathrm{o}$ with $\boldsymbol{h}(x_{\mathrm{t},0}) = c_{\mathrm{s},1}$ and an admissible production change $\delta c \in \Delta_{c_{\mathrm{s},1}}$, the transition problem can be reformulated by

$$(T^*, q^*) := \underset{T,\, q}{\arg\min} \quad T \tag{4.9a}$$

subject to

$$\dot{\boldsymbol{x}}_{(\tau)}{}^{(i-1)n_{\mathrm{x},1}+\alpha}(\tau) = T\, \boldsymbol{f}^{m_{i,\alpha}}(x, u) \qquad \alpha \in \mathbb{I}^{\mathrm{in}}{}_i, \tag{4.9b}$$

$$\left(\Lambda_1{}^i\right)^{(\alpha-1)}(\tau, p, q) = \varphi_1{}^{(i-1)n_{\mathrm{x},1}+\alpha}(x) \qquad \alpha \in \mathbb{I}^{\mathrm{ex}}{}_i, \tag{4.9c}$$

$$\boldsymbol{x}_{(\tau)}{}^{(i-1)n_{\mathrm{x},1}+\alpha}(\tau) = \varphi_1{}^{(i-1)n_{\mathrm{x},1}+r_i+\alpha}(x) \qquad \alpha \in \mathbb{I}^{\mathrm{in}}{}_i, \tag{4.9d}$$

$$\left(\Lambda_1{}^i\right)^{(r_i)}(\tau, p, q) = \left((T\boldsymbol{f})^{r_i}\left(h^i\right)\right)(x, u), \tag{4.9e}$$

$$\dot{\ell}_{(\tau)j}{}^{\beta}(\tau) = T\, \rho_j{}^{\beta}(x, u), \tag{4.9f}$$

$$0 = \boldsymbol{x}(0) - (0, x_0), \tag{4.9g}$$

$$0 = \ell_{(\tau)j}{}^{\beta}(0), \tag{4.9h}$$

$$\ell_{(\tau)j}{}^{\beta}(1) \in \left[-\delta_j{}^{\alpha},\, \delta_j{}^{\alpha}\right], \tag{4.9i}$$

$$0 \geq s(x, u), \tag{4.9j}$$

$$0 \geq \omega(x) \tag{4.9k}$$

Property (iv) in Problem 4.1 states that the objective function is defined by the parameter $T \in \mathbb{R}^+$. The equality constraints (4.9b-d) represent the model equations and the coordinate transformation of both processes. Given the relative degrees of the two processes, the implicit given control law (4.9e) is determined by the time derivative of the setup function up to this value. The time evolution of the storage levels during the transformation is included via (4.9f), where the initial value is zero, see (4.9h). For the process dynamics, the initial value in (4.9g) needs to coincide with the initial production level. Using (4.9i), it is guaranteed that the result of the transition problem is not in contradiction with the determined production level c_s using (3.9). Since other processes or downstream processes constraints should not be violated during the transition, (4.9j) and (4.9k) have to be included. The new production level

c_s is not explicitly considered in transition Problem (4.9) since it is used to define the setup function Λ_T.

Assumption 4.4. *For all* $(x_0, \delta c) \in \mathcal{X}_\mathrm{o} \times \Delta_{h(x_0)}$*, there exist a solution of Problem* (4.9)*.*

Remark 4.10. *From Assumption 4.4 follows that the minimal transition time* T^* *is unique due to the objective function. In contrast, the uniqueness of the solution* $q^* \in \mathbb{R}^{n_{\mathrm{q},1}+n_{\mathrm{q},2}}$ *is not guaranteed. In the case of several solutions for* q^**, one can choose an arbitrary value, as no further specifications are made to the control law.*

For solving Problem (4.9), we propose a direct approach that transforms the transition problem into an NLP, following the principle first-discretize-then-optimize, see [5, 73, 205]. This approach is preferable to an indirect approach, such as Pontryagin's maximum principle [199], since the input trajectory u is already parameterized. In other words, the optimal trajectory does not have to be identified within a function space and then determined as precisely as required by solving an ODE system.
In general, the direct approaches can be classified into sequential or simultaneous approaches, whereby the general idea is always to parameterize the occurring trajectories. For instance, the single shooting method can be assigned to the sequential approach, where state-of-the-art solvers for integration are employed to discretize the state trajectory of the ODE. The NLP solver only determines the parameters T and q that are constant over the entire time span. For the simultaneous approach, the state trajectory is approximated by a finite sum of special basis functions, thus avoiding numerical integration routines. In addition to the original decision variables, the NLP solver determines the coefficients of these trajectories. The collocation method has been used for several decades, especially for the simulation of ODEs and for optimization, cf. [158, 159, 20, 108, 39]. Multiple shooting, which was first proposed by Bock and Plitt [21], represents a hybrid of sequential and simultaneous approaches. The idea is to divide the time horizon into smaller parts with their initial conditions and then to integrate the dynamical system over each of these parts. Finally, the NLP has to consider additional constraints, called matching conditions, to ensure a continuous trajectory, whereby the initial conditions of the individual parts become decision variables of the NLP.

The advantage of Problem (4.9) is that we only consider a transition to a stationary production level, which gives a shorter transition time than the transition to a stationary state, see [100]. The result of (4.9) is beside the transition time T^* also the corresponding parameterization q^* for the control law (4.8). In this way, we have parameterized the setup function and the controller that implements the nominal case transition, i.e., without disturbance

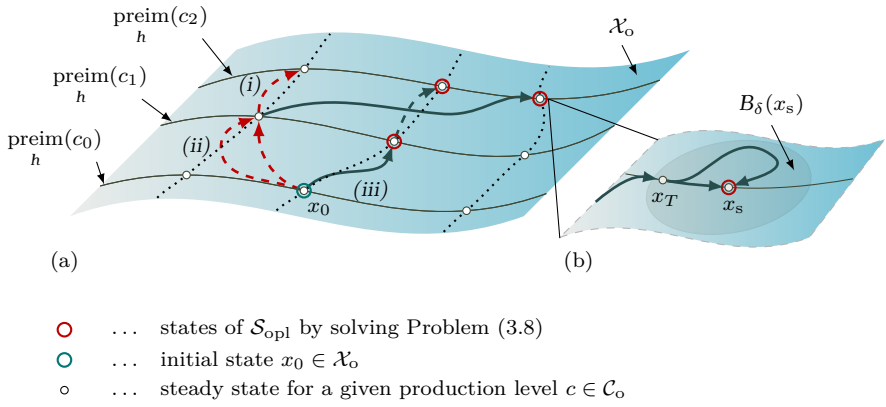

Figure 4.2: Scheme of the state trajectory during the transition phase.

rejection. Utilizing q^*, the setup function now directly defines the trajectory $c^* := \Lambda_{T^*}$ of the production levels. Contrary, the trajectory u^* for the feed is generated by integrating the system model (2.7) up to time T^* while including (4.8). Therefore, the trajectory generation consists of two phases. First, the transition problem is solved, and then the system is integrated using the solution.

As mentioned in Section 3.3, the solution set $\mathcal{S}_{opl}$ of the S-RTO is used to define the functions $\mathfrak{P}_c^e$ and $\mathfrak{P}_u^e$. To make these functions well-defined, we have to pick up a solution point. Thus, we finally discuss the result of the trajectory generation focusing on selecting one point of the set $\mathcal{S}_{opl}$. Figure 4.2 (a) shows an illustration of the state space, which serves as a basis for discussion here. For different production levels $c_i \in \mathcal{C}_o$, the preimage as a subset of $\mathcal{X}_o$ is presented by the black lines. Moreover, we assume several steady states that are asymptotically stable for each production level, illustrated as white circles. Note that there have to be unstable steady states between the stable points, as shown in Figure 3.4. Based on Assumption 3.2, one obtains for a given $(x_0, \theta, \ell) \in \mathcal{X}_o \times \Theta \times \mathcal{D}$ a nonempty set $\mathcal{S}_{opl}$ of steady-state operating points $(c_s, u_s, x_s) \in \mathcal{C}_o \times \mathcal{U} \times \mathcal{X}_o$ by solving Problem (3.8). These solutions are a subset of the steady states (their production level and input value) and indicated by the red circles. By solving Problem (4.9) for various production changes $\delta c_i \in \Delta_{h(x_0)}$ resulting from $\mathcal{S}_{opl}$, we obtain the optimal transition times ${T^*}_i$ and parameters ${q^*}_i$. Afterward, these are used to determine the potential steady states $x_{s,i}$ by integrating the system model. By comparing these results with that within $\mathcal{S}_{opl}$, we can distinguish three cases as indicated Figure 4.2 (a).

(i) *No δc_i yields a feasible operating point.* No production level change specified by the S-RTO, will result in a state that meets the economic requirements. Thus, the reachable states are not part of the solution set $\mathcal{S}_{\text{opl}}$. Assumption 4.1 implies that there is a controller so that the state given by the S-RTO can be reached after a particular time, but by choosing (4.8) a precise controller is defined. Hence, Assumption 4.1 must be extended by this specific control law to exclude such a situation.

(ii) *Only one δc_i yields a feasible operating point.* There is only one feasible production level, so the choice of the operating point is uniquely defined.

(iii) *More than one δc_i yields a feasible operating point.* If the system can be steered to more than one production level, the point that can be reached as fast as possible is selected.

To ensure that the operating points of the S-RTO can be implemented, we pose the following assumption. Moreover, the separation of the original bilevel problem of the cl S-RTO leads to two incompatible subproblems.

Assumption 4.5. *The production system $\mathcal{P}$ is at least local dynamically operable using the control law* (4.8).

4.2.4 Supervisory Control Layer

So far, we have shown how to generate the trajectory for the production level and the manipulating feed to achieve the transition. These signals are implemented by the control law of the supervisory layer. Two different control strategies can be pursued, as illustrated in Figure 4.3. The first is a pure feedback approach, where the controller, typically an MPC, uses the trajectories as reference signals, see Figure 4.3 left. For the second strategy, the feed trajectory is directly applied to the system as a feedforward signal. An additional feedback controller ensures disturbance reaction. This two-degree-of-freedom control is shown in Figure 4.3 right. In both strategies, an observer is used to estimate the system state x by measurements.

Pure feedback control This type of implementation refers to an online trajectory tracking problem, as described in [8, 56]. The objective of the MPC is to minimize the squared error between the current position and the reference u^* and c^* at discrete time points $t_k + i\Delta t_\text{s}$. In this way, the precalculated nominal trajectory is adapted to react on high-frequency disturbances with sampling time $\Delta t_\text{s} \in \mathbb{R}^+$. Finally, the feed $\hat{u}_{ki}$ is applied on the system.
In certain cases, an upstream steady state target optimization (SSTO) ensures

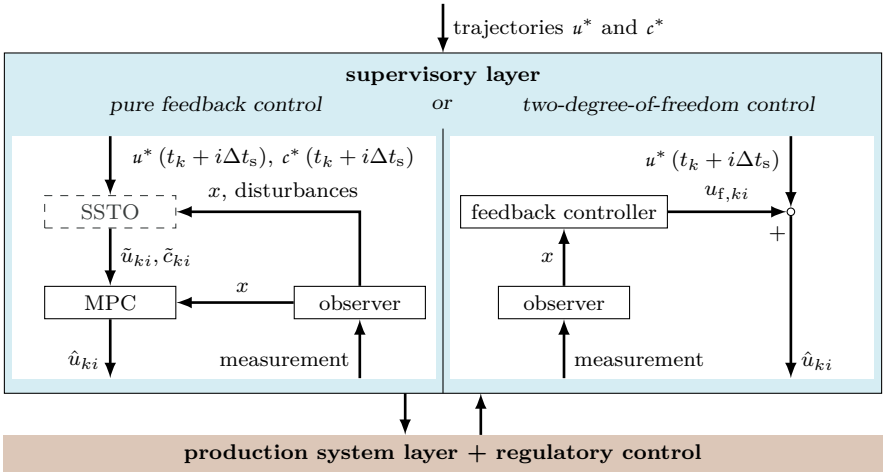

Figure 4.3: Control architecture within the supervisory layer.

the feasibility of the setpoint in some applications if different models are used on different layers, cf. [271, 166, 200]. This strategy is called the two-stage approach and represents a cascade of two MPC problems.
Typical applications of tracking MPC are generally associated with the use of D-RTO, see for example [122, 106]. Gadkar et al. [74] presents a nonlinear MPC for tracking a time-discrete reference signal on a continuous bioreactor. For a batch polymerization reactor, Nagy et al. [180] uses an MPC to compute setpoints for the subordinate PI controller.
More theoretical works about trajectory tracking are presented in Ferramosca et al. [62] and Ferramosca et al. [63]. In particular, this involves ensuring feasibility and convergence to a target steady state. Limon et al. [152] presents an MPC strategy for tracking piecewise constant references, as they might occur when discretizing formerly generated trajectories.

Two-degree-of-freedom control A classical strategy to perform the transition is a two-degree-of-freedom controller, where a feedforward signal guarantees the success of the transition, while an additional feedback controller ensures disturbance reaction by adding $u_{f,ki}$ to the feed value reference $u^*(t_k + i\Delta t_s)$, see [4, 254, 83]. Several approaches exist regarding the type of feedback controllers that can be applied. Hagenmeyer and Delaleau [90] uses a standard PID controller, where Graichen [81] employs a PI and an LQ controller for a transition of a CSTR and a double pendulum. The feedback term in [45] is defined by the weighted error between the current and the reference state.

A further type of control law that can be assigned to this category is the neighboring extremal controller [268, 270]. For a theoretical background to this approach, which was initially introduced for indirect methods in optimal control, see [192, 85]. The update coming from the feedback control is determined by solving an optimization problem based on a parameter update by measurements. This optimization problem is derived from the problem that has generated the nominal reference using the nominal parameters. In this way, the update exploits sensitivity information regarding particular parameters.

Control law used for trajectory generation Besides the two strategies mentioned above, we propose another technique combining both in a certain way. For this, not the generated trajectory is applied to the system. Instead, the control law (4.8) with the optimal parameters T^* and q^* is taken to define the controller K for the supervisory layer. This is motivated by the stationarity Definition 4.4. At the end of the transition, the system has reached a stationary production level. At the same time, the internal states are in a neighbourhood of their new steady state. However, the control law is designed to compensate for the evolution of these internal states, if $\left({\Lambda_{T^*}}^{i}\right)^{(r_i)}(t,p,q^*) := 0$, for $t \geq T^*$. A crucial aspect is the stability of $\mathcal{P}$ at the steady-state to be achieved when using (4.8). Even if $\mathcal{P}$ is asymptotically stable, the control law can cause an unstable system, see [242]. It is essential to consider this when we derive a control law valid for the transition and production phase. Using (4.8) and the optimal parameters T^* and q^*, we define the implicit controller

$$\boldsymbol{k}_{\mathrm{im}}^{\mathrm{tp}}(t,x,u_{\mathrm{t}}) := \left(\left(\boldsymbol{f}\right)^{r_\alpha}(h^\alpha)\right)(x,u_{\mathrm{t}}) - \left({\Lambda_{T^*}}^{\alpha}\right)^{(r_\alpha)}(t,p,q^*), \tag{4.10}$$

to steer the system to the new production level. For the production phase with the steady-state input $u_{\mathrm{s}} = \mathfrak{P}_{\mathrm{u}}^{\mathrm{e}}(x,\theta,\ell)$, we define

$$\boldsymbol{k}_{\mathrm{im}}^{\mathrm{pp}}(x,u_{\mathrm{t}}) := \begin{cases} \left(\left(\boldsymbol{f}\right)^{r_\alpha}(h^\alpha)\right)(x,u_{\mathrm{t}}), & \text{stable internal dynamics,} \quad (4.11a) \\ u_{\mathrm{s}} - u_{\mathrm{t}}, & \text{unstable internal dynamics.} \quad (4.11b) \end{cases}$$

whereby the two stability cases are distinguished. If the internal dynamics are stable, the setup function is set to zero, since the production level for $t > T^*$ has to be stationary. The remaining part (4.11a) ensures that the production level does not change along the trajectory until all states have reached the new steady state. However, if the internal dynamics are unstable, the control law is substituted by the feed value u_{s}. Based on Assumption 4.2, the system is asymptotically stable without using (4.11a). Those states that are not yet in a

steady state are converging towards it.
The controller for both phase has the form

$$K_{\mathrm{im}}(t,x,u_{\mathrm{t}}) := \begin{cases} \boldsymbol{k}_{\mathrm{im}}^{\mathrm{tp}}(t,x,u_{\mathrm{t}}), & t \in [0,\, T^*]\,, \quad (4.12a) \\ \boldsymbol{k}_{\mathrm{im}}^{\mathrm{pp}}(x,u_{\mathrm{t}}), & t > T^*, \quad (4.12b) \end{cases}$$

The feed signal obtained by (4.12) ensures the transition and maintaining the new steady-state. To guarantee disturbance rejection and noise compensation, we additionally consider a feedback law $\boldsymbol{k}_{\mathrm{fb}} : \mathcal{X} \times \mathcal{C} \to \mathcal{U}$ similar to the two-degree-of-freedom approach. For instance, a PI or an LQ controller is possible. Finally, the total control law for the supervisory layer has the form

$$K : \begin{cases} u = u_{\mathrm{t}} + \boldsymbol{k}_{\mathrm{fb}}(x,c), & (4.13a) \\ 0 = K_{\mathrm{im}}(t,x,u_{\mathrm{t}}). & (4.13b) \end{cases}$$

Remark 4.11. *It is possible to formulate the controller K at least locally by the map K_{ex}, as introduced in Problem 2.1.*

The case distinction in (4.11) allows two interpretations of control law (4.13). For an unstable internal dynamic, the controller becomes a two-degree-of-freedom control, as discusses above. The only difference is that here we use the current states of the system and not those determined by an offline simulation. Therefore, it is essential to ensure that the model describes the system well.
The advantage of (4.13) over a classical two-degree-of-freedom approach appears for a stable internal dynamic. In this context, (4.11a) ensures that the evolution of the states is precisely compensated and will not affect the production level. Figure 4.2 (b) illustrates the case distinction for a chosen steady-state from the S-RTO. First, the controller steers $\mathcal{P}$ to $x_T \in \mathcal{X}_{\mathrm{o}}$ during the transition phase. For a stable steady-state $x_{\mathrm{s}} \in \mathcal{X}_{\mathrm{o}}^{\mathrm{s}} \subset \mathcal{X}_{\mathrm{o}}$, the time evolution of the internal states while moving to x_{s} is compensated. Conversely, for an unstable x_{s}, the stationary input u_{s} is applied, while a well-tuned feedback controller ensures that the production level does not deviate too far from the setpoint. Furthermore, we assume that x_T is within the region of attraction $B_\delta(x_{\mathrm{s}})$ of x_{s}, see [274].

Example 4.3 (Transition of a Coupled AD- and RSR-Process (3.1 continued))**.** *We continue with the scenario-based analysis of the operational strategy introduced in Example 3.1 and take a closer look at the transition phases. However, we will focus only on the first and second transition, as already discussed in more detail in Example 3.1. Furthermore, we will first consider*

only the real case, i.e., limited storage capacity (case (i)). To finish this example, we briefly review the second transition and compare the trajectories in the output space $\mathcal{C}$ for the real (i) and the relaxed (ii) case.

Before we discuss the effect of the controller on the system, we will address its specifications and the numerical method for its solution. It should be remarked that the manipulating signal is directly applied to the system as a feedforward controller, following the two-degree-of-freedom control approach.
For the implemented control strategy, we use a polynomial setup function for both processes and the parts A_T and B_T, as given in Table 4.1. The properties of the controller are summarized in Table 4.2. Two factors can explain the reason why a polynomial function with six parameters each was chosen. Firstly, the more parameters are used, the more the trajectory of production levels can be modified (high degree of flexibility). In other words, the more variation parameters and the broader their acceptable range, the better signals can be described that have "kinks", allowing a rapid change of the signal direction. Secondly, the input trajectory is determined by the derivatives of the output, and the solution of Problem (4.9)*, which is numerically challenging. So, for numerical solvers, a high degree of flexibility in the design of the signals could mean that the stability and convergence of the solutions cannot be guaranteed. Hence we need to find a compromise between these two aspects in order to find a solution for any possible transition that might occur.*

Table 4.2: Properties of the controler.

	1st process	2nd process
relative degree	3	2
setup function	polynomial	polynomial
degree of freedom	$n_{\mathrm{q},1} = 6$	$n_{\mathrm{q},1} = 6$

To solve Problem (4.9)*, we use the direct collocation method since this yields an optimal solution for almost all transitions in a reasonable time. Alternative methods, such as direct single or multiple shooting, were also successfully implemented, but they were less efficient in the automated framework without readjusting solver options and initial values. Overall, we used five finite elements for the time interval* $[0, 1]$*, whereby five sampling points per element were applied, which corresponds to the polynomial degree. The solver used is CasADi/ipopt [6, 269] with front-end Matlab R2016b.*
Nevertheless, it turns out that a direct solution of Problem (4.9) *in the NLP formulation via direct collocation and the corresponding parameter and boundary requirements is hard to solve in general. For this reason, we use the following framework to identify the solution in several steps.*

1. *The system dynamics were simulated using the control law and a minor production change, whereby the parameters of the variation terms were set to zero. The calculated trajectories are used to generate initial conditions for the optimization.*

2a. *A repeated optimization, where the change in production levels is gradually increased to the desired value, is done on each step. The optimal solutions of the previous problem are used as warm start values for the new problem. The boundaries for the parameters of the variational term are set around* $\pm 10^4$*, and the boundaries for the terminal storage level are given by the reserve towards the upper and lower storage size. In this way, the transition problem will be determined first by modifying the transition time.*

2b. *The transition problem is optimized repeatedly with the required change of the production level, whereby the admissible parameter space of the variational terms is gradually increased. Thus the transition time can be further reduced by varying the trajectory of the production levels. The terminal storage levels still use the entire storage space.*

2c. *A final optimization sequence is used to reduce the terminal storage levels. This will continue until a required storage boundary is reached, or the transition time has increased by 20% of the original value.*

3. *The results of the optimization part are used for a subsequent simulation of the system to generate an offline trajectory.*

Using this algorithm, we obtain the following results of the transition problem for the first two transitions from Example 3.1 are obtained. We start with the first transition for which the input-output behavior is shown in Figure 4.4 and the temperature profile in Figure 4.5.

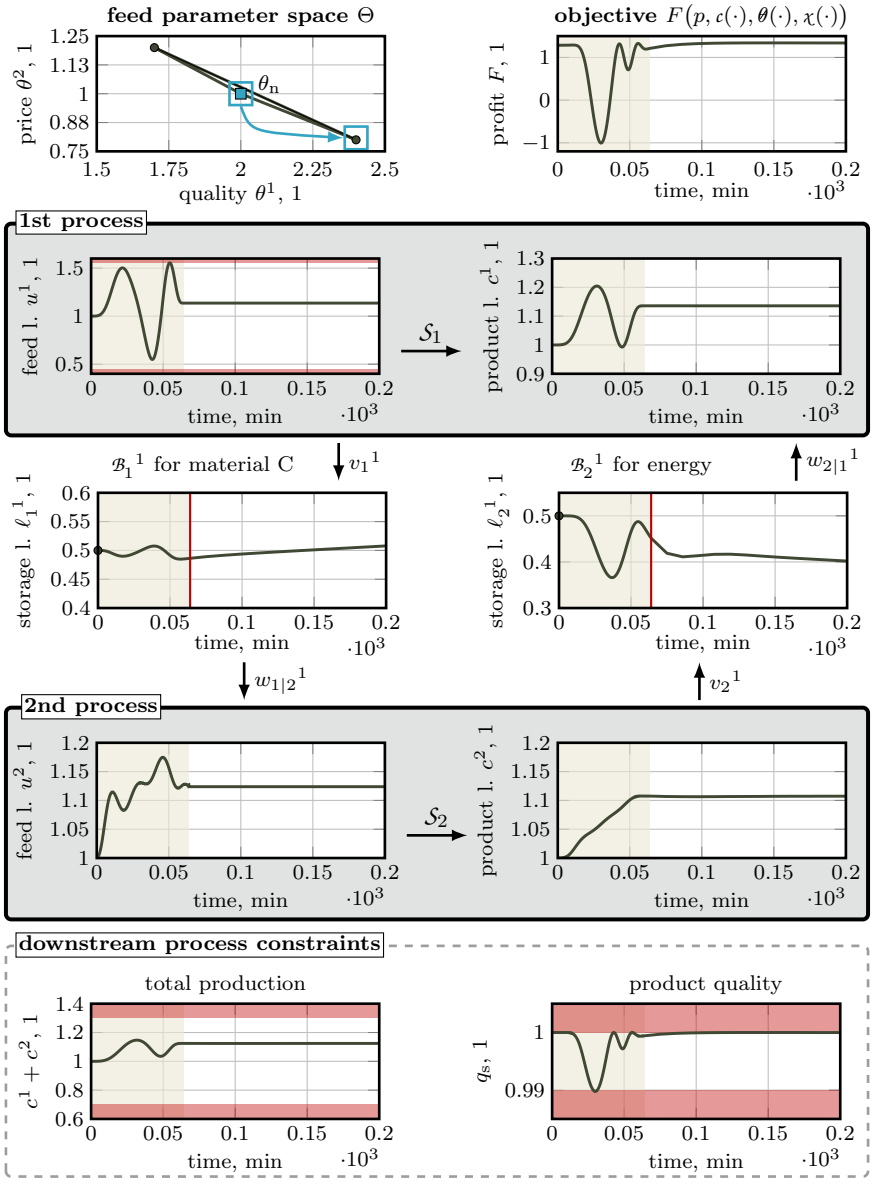

Figure 4.4: Illustration of the input-output behavior of the production system for the first transition.

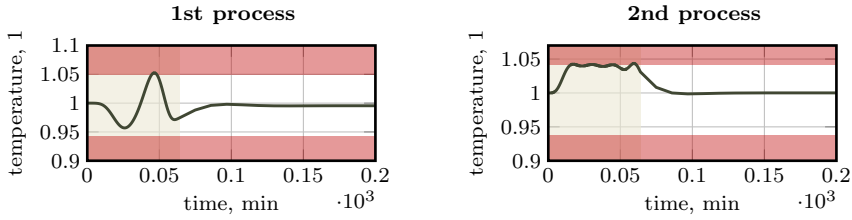

Figure 4.5: Illustration of the temperature behavior of the two processes for the first transition.

At time $t = 0$, the feed parameter changes as illustrated in the feed parameter space Θ in Figure 4.4 first row left column. In the following, we assume that the economic objective can also be applied to the transition phase. In this way, we can interpret the fluctuations in profits during the production change, which are even negative over time, as high transition costs occur, see Figure 4.4 first row right column. This allows assessing whether the transition is economically reasonable or not, as already mentioned in Example 3.1.
Another point that can be seen in the first row right column of Figure 4.4 is that the full economic potential is not yet reached at the end of the transition at $t = 63.96\,\mathrm{min}$. This is caused by the product quality q_s, as it depends on the state variables in general and these have not yet fully reached their steady state. For instance, the temperature of both processes, shown in Figure 4.5 is not constant after the transition phase (indicated by the gray area) but converges to its steady state. One way to achieve maximum product quality at the end of the transition is to add a terminal constraint either for the economic objective itself or the product quality to Problem (4.9). The latter way does not increase the complexity of the optimization, since the equation is already part of the problem.

Considering the trajectories of the process feed u and thus the production levels c, it is notable that the solver does not generate intuitive solutions, cf. Figure 4.4 second and fourth row. The input for the production phase is not attained directly, but goes through several changes of direction in between. This is mainly due to the constraints of the terminal storage level and the temperature profile, which we discuss below.
Terminal storage level. *In step 2c, we reduce the variation of the storage level around the initial point as much as possible. This minimizes the effects of a production change on the storage system in case of continuous operation and thus several cycles of the considered scenario. We will discuss this point again when estimating the storage capacity in Section 5.4.*
Until the end of the transition, the storage level can only vary by a certain factor around their initial value (black dot in Figure 4.4 third row) at the beginning of the transition. These terminal regions are implied in Figure 4.4 third row

by the red line at the end of the transition phase. Note that these regions are larger than finally achieved in step 2c. Furthermore, these regions are used for the S-RTO in Example 3.1 and are represented by ${\mathcal{H}_1}^1$ *and* ${\mathcal{H}_2}^1$.
A common strategy of the controller is first to move the levels of the storage elements in the opposite direction to obtain more flexibility. For instance, the production of $\mathcal{S}_2$ *is uniformly (almost constantly) increased, which means that the amount of supplied heat energy also increases in the same proportion, see Figure 4.4 fourth row. At the same time,* $\mathcal{S}_2$ *needs more of the component* C, *which can be concluded from the feed* u^2 *in Figure 4.4 fourth row left column. This effect is compensated by increasing the process performance of* $\mathcal{S}_1$ *in the first third of the transition drastically, see Figure 4.4 second row left column. By this, the production level* c^1 *is increased (see Figure 4.4 second row right column) and, at the same time, the production of* C. *However, it follows that* $\mathcal{S}_1$ *requires more energy, which results a drop in level* ${\ell_2}^1$ *of* ${\mathcal{B}_2}^1$ *as depicted in Figure 4.4 third row right column. However, this maneuver is only be pursued for a short time. By a sequence of increasing and decreasing the amount of feed* u^1, *followed by a final reduction of the feed value according to the production phase, the original storage level of* ${\mathcal{B}_2}^1$ *is almost reached again. At this time, all production levels are already close to the new setpoint, so the final reduction of* ${\ell_2}^1$ *is no longer as large as before. Essential for this procedure is that the transition time is not increased too much again. By step 2c, a trade-off between the effect of the transition on the storage levels and the time needed for the transition must to be found.*
Temperature profile. *A further interpretation of the control law strategy to change the amount of the feed for several times is given by a study of the temperature evolution in Figure 4.5. A change in system operation is also associated with a change in the temperature levels, as any cooling and heating elements have inertia. During the first transition, the reactor temperature in* $\mathcal{S}_2$ *rises because the process output is increased. Likewise, the temperature in* $\mathcal{S}_1$ *fluctuates strongly and is brought to the boundaries, as can also be seen for* $\mathcal{S}_2$ *in Figure 4.5, where the red areas illustrate the boundaries. To satisfy the process conditions, the temperature of* $\mathcal{S}_1$ *is first cooled down, creating more margin towards the upper boundary.*

Finally, we consider the product quality q_s *in Figure 4.4 fifth row right column, which are kept at 1 during the production phase (see Figure 3.5). Within the transition phase, the controller uses the entire range of feasible product qualities to achieve the fastest possible transition. This fluctuation is caused by the slower dynamics of the part of the* H *stream which forms the total product of* $\mathcal{S}_2$ *together with* M.

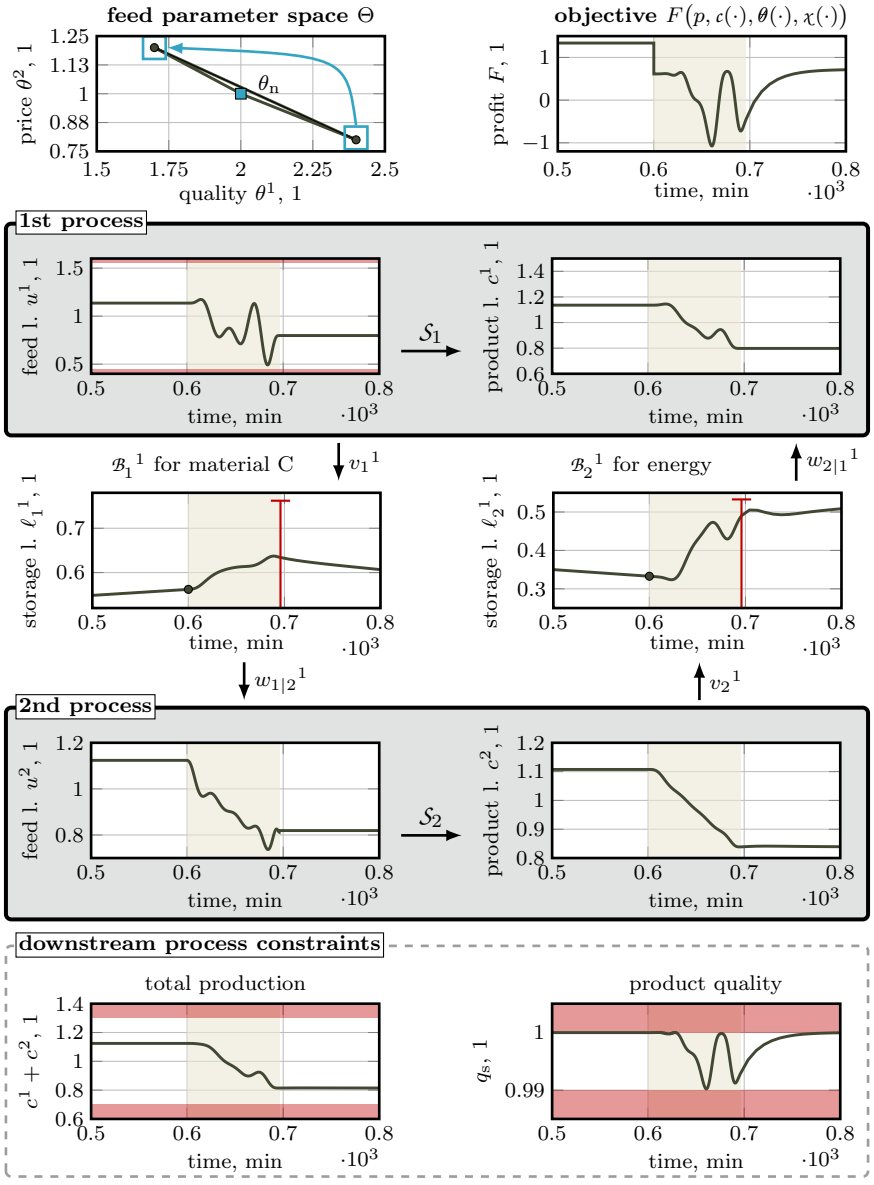

Figure 4.6: Illustration of the input-output behavior of the production system for the second transition.

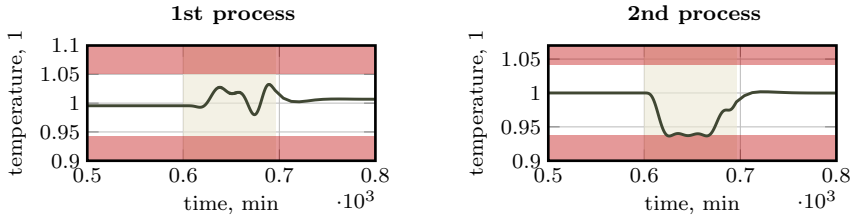

Figure 4.7: Illustration of the temperature behavior of the two processes for the second transition.

The second change of the production level starts at time $t = 600$ min *with a reduction and an increase in feed quality* θ^1 *or price* θ^2*, as shown in Figure 4.6 first row left column. Consequently, the production levels of both processes need to be reduced. The result is also a decrease of the heat energy supplied to the storage element* ${\mathcal{B}_2}^1$ *and the energy required by process* $\mathcal{S}_1$*. Similarly, less* C *is fed to the storage element* ${\mathcal{B}_1}^1$*, and less is taken from process* $\mathcal{S}_2$*. Considering the evolution of the storage level* ${\ell_2}^1$ *of* ${\mathcal{B}_2}^1$ *in Figure 4.6 third row right column, we see that after a short period in which the level changes only slightly, it then rises strongly for a certain time (*≈ 26.5 min*). However, before the transition phase ends, the storage element is briefly discharged before the level rises again. These terminal regions for* ${\ell_1}^1$ *and* ${\ell_2}^1$ *can be seen by the red lines in Figure 4.6 third row. So it is ensured that at the end of the transition, the S-RTO storage constraints are satisfied. The reason for this reaction of the controller is an adaptation in the trajectory of output* c^1 *for* $\mathcal{S}_1$ *during the last third of the transition, cf. Figure 4.6 second row right column. The result is a short-term increase in the heat demand provided by* ${\mathcal{B}_2}^1$*. Thus the initially increasing evolution of the storage level* ${\ell_2}^1$ *in the third row right column of Figure 4 temporarily drops before it reaches the final storage level within the terminal constraints.*

Figure 4.7 shows the temperature profiles for the second transition. While the temperature for the first process does not reach the boundaries, for $\mathcal{S}_2$ *the lower bound is active for a certain time period. To satisfy the lower bound, the slope of the trajectory of the production level* c^2 *is chosen by the optimizer so that the new setpoint can be reached quickly, but the derived feed signal is adapted to the inertia of the reactor cooling jacket.*

To conclude this example, we will look at the trajectory of the production levels for the second transition within the operating area $\mathcal{C}_\mathrm{o}$*, as shown in Figure 4.8. Within* $\mathcal{C}_\mathrm{o}$ *not all production levels are feasible for a steady state operation, as they have to meet the downstream process constraints. These constraints are the total amount of the product and the product quality. The green area in Figure 4.8*

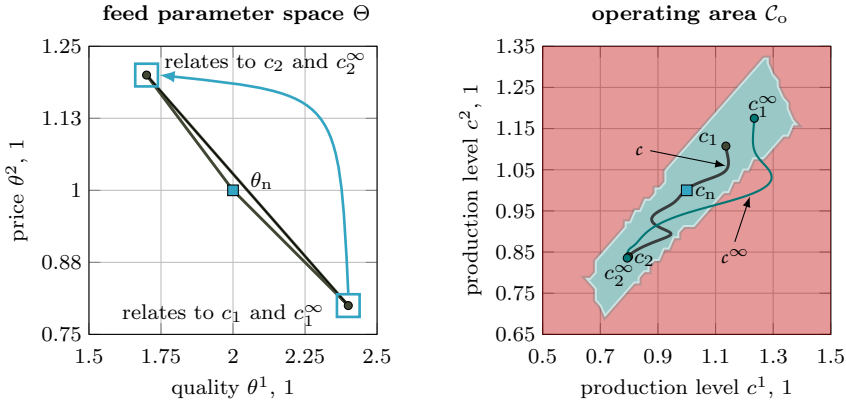

Figure 4.8: Illustration of the second transition (a) of the considered scenario within Θ and (b) for the trajectory of the production level within $\mathcal{C}_o$.

approximates the subset of feasible production levels achieved by the S-RTO without storage restrictions (i.e., case (ii)). On the left side in Figure 4.8, the trajectories c^∞ and c are presented. While c^∞ (green line) is determined by the S-RTO results for the relaxed case (ii) from Example 3.1, the trajectory c (gray line) belongs to the real case (i). In addition to the nominal production level c_n, the initial points c_1^∞ and c_1 at the beginning of the second transition, and the endpoints c_2^∞ and c_2 are shown.

For both trajectories c^∞ and c, we can conclude that the fastest path considering the dynamic properties and all other constraints is not a straight line. Indeed, the output follows small detours to the new setpoint, so that the derived input ensures the requirement to the storage system and the state variables (especially the temperature). Note that the trajectory for the relaxed case (green line) temporarily leaves the green area in Figure 4.8. During this time period, all constraints are satisfied nevertheless. The reason for this lies in the definition of the green area. It is identified as a feasible area for the stationary operation (during the production phase). This means that for dynamic operation, i.e., the feasible area can have a different shape and be larger during the transition phase. We will address this feasible area again when we discuss the time-transition map design in the next section.

It should also be noted that the description of this area has nothing to do with the properties of local economically compatible or local economically operable, as described in Example 2.3. For this classification of the system, the dynamics and the input did not matter at first. The focus was only on the relationship between subspaces of the state space $\mathcal{X}$ and the operating area $\mathcal{C}_o$.

A final remark on this example refers to the evolution of the storage level from the end of each transition. It can be concluded from Figures 4.4 or 4.6 that the storage rate at the end of the transitions is not yet constant, since the state has not reached the stationary value. However, the state at the end of the transition lies in a neighborhood of the new steady state and thus is within the attractive region. The small error resulting from not yet having a constant storage rate at the end of the transition can be regulated by choosing the safety range ξ and the terminal region for the storage level.

4.3 Transition-Time Map

In the previous section, we derived the control law to realize the transition of the production level. For this, we have to solve Problem (4.9) to obtain the minimal transition-time and an optimal parametrization of the setup function Λ_{T^*} and thus the control law (4.8). In this way, we can generate the trajectory transferred to the supervisory layer and receive the information for the duration of the transition phase required by the S-RTO.
To avoid repeatedly solving the transition problem during the S-RTO, we introduced the surrogate model $\tilde{\mathfrak{T}}_{\mathrm{t},-}$ in (2.24). In this way, the original bilevel problem of the cl S-RTO becomes a single level static optimization. Whereas in (2.23) the general transition Problem (2.22) was used to define the transition-time map $\mathfrak{T}_{\mathrm{t}}^{\mathrm{e}}$, Problem (4.9) is now employed. It follows that $\tilde{\mathfrak{T}}_{\mathrm{t},-}$ is trained on the results of the transition Problem (4.9). In general, the transition problem needs, besides the admissible change $\delta c \in \Delta_{h(x_{\mathrm{t},0})}$, also the initial value $x_{\mathrm{t},0} = (0, x_0) \in \mathbb{R}_0^+ \times \mathcal{X}_{\mathrm{o}}$. Hence, after each transition, the corresponding final state has to be computed, as they represent the initial value for a further change of the production level.

In the following, we address a strategy to derive transition-time map $\tilde{\mathfrak{T}}_{\mathrm{t},-}$ utilizing Problem (2.23). Thereby, the relationship between $\tilde{\mathfrak{T}}_{\mathrm{t},-}$ and the dependence on initial conditions will be discussed in more detail. More precisely, we will distinguish between a locally- and a globally-valid map for $\mathfrak{T}_{\mathrm{t}}^{\mathrm{e}}$ or $\tilde{\mathfrak{T}}_{\mathrm{t},-}$ and discuss under which circumstances the global ones can be generated. Here, the globally-valid version of $\mathfrak{T}_{\mathrm{t}}^{\mathrm{e}}$ is characterized by the fact that it only depends on a reference state and no longer on the current state of the production phase from which the next transition starts. This reduces the size of the domain of the transition-time map. So before we focus on a precise training strategy, the next section will first introduce this concept.

4.3.1 Reduced Transition-Time Map

In Section 4.2.3, we discussed that the states after the transition move towards $x_\mathrm{s} \in \mathcal{X}_\mathrm{o}^\mathrm{s}$ during the production phase. This allows to define the transition-state map

$$\mathfrak{T}_\mathrm{x}^\mathrm{e} : \mathcal{X}_\mathrm{e}^\mathrm{s} \to \mathcal{X}_\mathrm{o}^\mathrm{s},\ (\mathfrak{x}) \mapsto \mathfrak{T}_\mathrm{x}^\mathrm{e}(\mathfrak{x}) := x_\mathrm{s}, \tag{4.14}$$

that yields the state that will be reached after an admissible production change $\delta c \in \Delta_{h(x)}$ starting from stationary state $x \in \mathcal{X}_\mathrm{o}^\mathrm{s}$. Here, the set $\mathcal{X}_\mathrm{e}^\mathrm{s}$ is defined by

$$\mathcal{X}_\mathrm{e}^\mathrm{s} := \big\{(\xi, \varsigma) \in \mathcal{X}_\mathrm{o}^\mathrm{s} \times \Delta_{h(\xi)}\big\}.$$

Remark 4.12. *The map* (4.14) *is defined on* $\mathcal{X}_\mathrm{e}^\mathrm{s} \subset \mathcal{X}_\mathrm{e}$. *Since Problem* (2.23) *is not restricted to steady-state initial conditions, the domain of the transition-state map* $\mathfrak{T}_\mathrm{x}^\mathrm{e}$ *could also be extended to* $\mathcal{X}_\mathrm{e}$ *from* (2.23). *However, we will omit this, as a composition of* $\mathfrak{T}_\mathrm{x}^\mathrm{e}$ *would automatically lead to this restriction from* $\mathcal{X}_\mathrm{e}$ *to* $\mathcal{X}_\mathrm{e}^\mathrm{s}$.

For notational convenience, we introduce, for a given admissible δc, the parametric form of $\mathfrak{T}_\mathrm{x}^\mathrm{e}$ by the map

$$\mathfrak{T}_{\mathrm{x},\delta c}^\mathrm{e} : \mathcal{X}_{\mathrm{o},\delta c}^\mathrm{s} \to \mathcal{X}_\mathrm{o}^\mathrm{s},\ (x) \mapsto \mathfrak{T}_{\mathrm{x},\delta c}^\mathrm{e}(x) := \mathfrak{T}_\mathrm{x}^\mathrm{e}\big((x, \delta c)\big), \tag{4.15}$$

in the sense that one obtains an endomorphism on $\mathcal{X}_\mathrm{o}^\mathrm{s}$. The domain of this function is defined by $\mathcal{X}_{\mathrm{o},\delta c}^\mathrm{s} := \big\{\xi \in \mathcal{X}_\mathrm{o}^\mathrm{s} \mid h(\xi) + \delta c \in \mathcal{C}_\mathrm{o}\big\} \subset \mathcal{X}_\mathrm{o}^\mathrm{s}$ and consists of all stationary states that are valid for the production level change δc.

By the assumption that the initial state of $\mathcal{P}$ is known, the map $\mathfrak{T}_{\mathrm{x},\cdot}^\mathrm{e}$ allows determining a sequence of states that will occur in the respective production phases according to the sequence of production-level changes. In this way, one obtains the initial condition to solve Problem (4.9) for each transition. One might ask how this sequence of states of the production phase now depends on the sequence of production changes. The following definition is intended to specify the state dependency further to identify a suitable criterion for designing a globally-valid transition-time map.

Definition 4.7 (State Independency of a Minimal-Time Transition)**.** *Let* $\mathcal{P}$ *be a production system driven by the control law* (4.13), *that generates* $\mathfrak{T}_{\mathrm{x},\cdot}^\mathrm{e}$. *The system is called state-independent for a minimal-time transition, if for all* $x \in \mathcal{X}_\mathrm{o}^\mathrm{s}$ *it holds that*

(i) if the change δc *of the production level is zero, the state stays constant:* $\mathfrak{T}_{\mathrm{x},0}^\mathrm{e} = id_{\mathcal{X}}$,

(ii) the composition of multiple transitions is given by addition of their production level changes:
$\mathfrak{T}^{\mathrm{e}}_{\mathrm{x},(\delta c_0+\delta c_1)} = \mathfrak{T}^{\mathrm{e}}_{\mathrm{x},\delta c_0} \circ \mathfrak{T}^{\mathrm{e}}_{\mathrm{x},\delta c_1} = \mathfrak{T}^{\mathrm{e}}_{\mathrm{x},\delta c_1} \circ \mathfrak{T}^{\mathrm{e}}_{\mathrm{x},\delta c_0}$.

Otherwise, the system is called not state-independent for a minimal-time transition.

The concept of Definition 4.7 is illustrated in Figure 4.9. A system that is state-independent for a production level transition will always return to $x_0 \in \mathcal{X}_\mathrm{o}$ when the initial production level $c_0 \in \mathcal{C}_\mathrm{o}$ is set. Thus a transition can be achieved in several steps, as shown in Figure 4.9 (a). Here three production levels are shown, whereby a transition from c_0 is considered directly to $c_0 + \delta c_0 + \delta c_1$ and via the intermediate level $c_0 + \delta c_0$. The brown curve represents the image of $\mathfrak{T}^{\mathrm{e}}_{\mathrm{x}}$ on $\mathcal{X}^{\mathrm{s}}_{\mathrm{o}} \subset \mathcal{X}_\mathrm{o}$. It is characteristic of a system which is state-independent according to Definition 4.7 that it cannot be driven into two states with the same production level. Conversely, for a system that is not state-independent, there is no guarantee that the same state $x_0 \in \mathcal{X}_\mathrm{o}$ will be reached again for every closed production change sequence $\{\delta c_1, \ldots, \delta c_n\}$ with $\sum_{i=1}^{n} \delta c_i = 0$. Figure 4.9 (b) shows this for a transition starting from $x_0 \in \mathcal{X}_\mathrm{o}$ to $x_1 \in \mathcal{X}_\mathrm{o}$ back to the initial production level at $x_0{}' \in \mathcal{X}_\mathrm{o}$. Thus, the final state depends highly on the path that was passed over. The brown curve illustrates this in Figure 4.9 (b). Here, the controller acts on the vector field so that states on other branches (black dotted line) for steady states can be reached faster.

Using Definition 4.7, we now have the possibility to restrict the domain of $\mathfrak{T}^{\mathrm{e}}_{\mathrm{x}}$ to the operating area $\mathcal{C}_\mathrm{o}$ of the product. For this, let $x_\mathrm{r} \in \mathcal{X}_\mathrm{o}$ be a reference state, which allows defining the reduced transition-time map $\mathfrak{T}_\mathrm{t}$ by

$$\mathfrak{T}_\mathrm{t} : \mathcal{C}_\mathrm{e} \to \mathbb{R}^+,\ \big((c,\delta c)\big) \mapsto \mathfrak{T}_\mathrm{t}\big((c,\delta c)\big) := \mathfrak{T}^{\mathrm{e}}_{\mathrm{t}}\left(\left(\mathfrak{T}^{\mathrm{e}}_{\mathrm{x},\left(c-h(x_\mathrm{r})\right)}(x_\mathrm{r}), \delta c\right)\right), \quad (4.16)$$

where

$$\mathcal{C}_\mathrm{e} := \big\{(\xi,\varsigma) \in \mathcal{C}_\mathrm{o} \times \Delta_\xi\big\},$$

denotes the space of all production levels and their admissible production changes. The state becomes only a parameter which has to be predefined in advance. Finally, it must be shown that the reduced transition-time map $\mathfrak{T}_\mathrm{t}$ is uniquely defined by a reference $x_\mathrm{r} \in \mathcal{X}_\mathrm{o}$.
By definition of $\mathfrak{T}^{\mathrm{e}}_{\mathrm{x},\cdot}$ follows that for a given production level $c_0 \in \mathcal{C}_\mathrm{o}$ its associated state can be determined by

$$x_0 = \mathfrak{T}^{\mathrm{e}}_{\mathrm{x},\left(c_0-h(x_\mathrm{r})\right)}(x_\mathrm{r}).$$

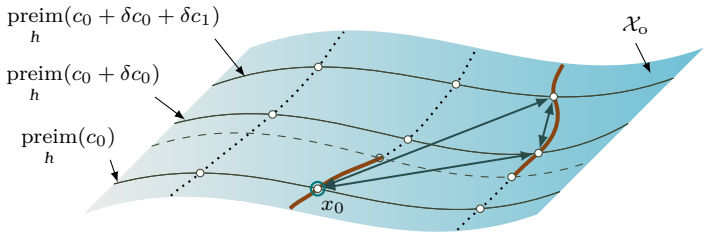

(a) State-independent system such that for each production level, only one state exists.

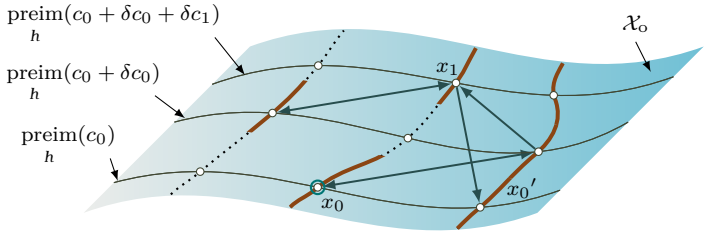

(b) Not state-independent system such that for each production level, several states exist.

- ○ ... initial state $x_0 \in \mathcal{X}_o$
- ∘ ... steady state for a given production level $c \in \mathcal{C}_o$

Figure 4.9: Illustration of the state independency of $\mathcal{P}$ with respect to a time minimal transition.

From this state and an admissible change δc_0, the transition-time can be calculated using $\mathfrak{T}^e_t$. In this way, the transition-time can be determined from $(c_0, \delta c_0) \in \mathcal{C}_e$. In order to show that this dependency is unique, we consider a finite number of arbitrary transition steps $\{\delta c_1, \ldots, \delta c_n\}$ from any point $c_1 \in \mathcal{C}_o$ to $c_0 \in \mathcal{C}_o$. The state after n transitions starting at c_1 is given by

$$x_n = \mathfrak{T}^e_{x,\delta c_n} \circ \ldots \circ \mathfrak{T}^e_{x,\delta c_1} \circ \mathfrak{T}^e_{x,\left(c_1 - h(x_r)\right)}(x_r).$$

For a state-independent system, and from the property (ii) in Definition 4.7 follows that

$$x_n = \mathfrak{T}^e_{x,\left(\sum_{i=1}^{n} \delta c_i + c_1 - h(x_r)\right)}(x_r).$$

Since we required for the sequence of transitions that $c_0 = c_1 + \sum_{i=1}^{n} \delta c_i$, one obtains

$$x_n = \mathfrak{T}^{\mathrm{e}}_{\mathrm{x},\left(c_0 - h(x_\mathrm{r})\right)}\left(x_\mathrm{r}\right) = x_0.$$

If c_1 and c_0 are identical, the property (i) in Definition 4.7 shows

$$x_0 = \mathfrak{T}^{\mathrm{e}}_{\mathrm{x},0} \circ \mathfrak{T}^{\mathrm{e}}_{\mathrm{x},\left(c_0 - h(x_\mathrm{r})\right)}\left(x_\mathrm{r}\right) = id_{\mathcal{X}} \circ \mathfrak{T}^{\mathrm{e}}_{\mathrm{x},\left(c_0 - h(x_\mathrm{r})\right)}\left(x_\mathrm{r}\right).$$

Thus the transition-time given by $\mathfrak{T}^{\mathrm{e}}_{\mathrm{t}}$ is independent of the previous transitions and the production level from which they begin. The uniqueness of $\mathfrak{T}_{\mathrm{t}}$ follows directly from the state-independency of the system.

Finally, we want briefly touch on the question of when a system is state-independent, for which the following lemma gives a sufficient condition.

Lemma 4.1 (Sufficient Condition for a State-Independent System)**.** *Let $\mathcal{P}$ be a production system driven by the control law* (4.13)*, that generates the state transition map $\mathfrak{T}^{\mathrm{e}}_{\mathrm{x}}$. Furthermore, for a given steady state $x \in \mathcal{X}^{\mathrm{s}}_{\mathrm{o}}$, a branch is defined by the set $B_x := \left\{\xi \in \mathcal{X}^{\mathrm{s}}_{\mathrm{o}} \mid \exists\, \mu \in C\big([0,1], \mathcal{X}_{\mathrm{o}}\big),\ \mathrm{imag}\,(\mu) \subset \mathcal{X}^{\mathrm{s}}_{\mathrm{o}},\ \mu(0) = x,\ \mu(1) = \xi\right\}$. The system at a steady state $x_\mathrm{r} \in \mathcal{X}^{\mathrm{s}}_{\mathrm{o}}$ is state-independent for a time minimal transition if it holds that:*

(i) no bifurcation point within $\mathcal{X}_{\mathrm{o}}$ for $\mathcal{P}$,

(ii) no multiple production levels: the restriction of h defined by $\tilde{h} : B_{x_\mathrm{r}} \to \tilde{\mathcal{C}}_{\mathrm{o}} \subset \mathcal{C}_{\mathrm{o}},\ x \mapsto \tilde{h}(x) := h(x)$, is bijective

(iii) no multiple states: $\forall\, x \in B_{x_\mathrm{r}},\ \forall\, \delta c \in \Delta_{h(x)} : \exists\, \gamma \in C\big([0,\,1], \mathcal{X}_{\mathrm{o}}\big)$ with $\mathrm{imag}\,(\gamma) \subset B_{x_\mathrm{r}}$, $\gamma(0) = x$ and $\gamma(1) = \mathfrak{T}^{\mathrm{e}}_{\mathrm{x},\delta c}(x)$.

The point $x_\mathrm{r} \in \mathcal{X}^{\mathrm{s}}_{\mathrm{o}}$ can be set as a reference state.

The first condition in Lemma 4.1 ensures that there is no state $x \in \mathcal{X}_{\mathrm{o}}$ from which one can move in two different directions. That means there is no particular point $x \in \mathcal{X}_{\mathrm{o}}$ where the number of solutions of the steady-state equation changes. More precisely, at such a bifurcation point x the manifold $\mathcal{X}^{\mathrm{s}}_{\mathrm{o}}$ is an intersection of at least two branches, see [228]. Considering Lemma 4.1 (ii), we can see the function $\tilde{h}$ as restriction of h to the branch B_{x_r}. In adapted coordinates, the function $\tilde{h}$ is a map from a subset of $\mathbb{R}^2$ (since $\dim \mathcal{X}^{\mathrm{s}}_{\mathrm{o}} = 2$) into a subset of $\mathbb{R}^2$. The second condition guarantees that no production level is hit twice when moving along a stationary branch B_{x_r}. In other words, the mapping between the states of a branch and the production levels is biunique. By the third condition of Lemma 4.1, it is ensured that no change between two branches occurs during a transition.

Proof. Let $x_1 \in \mathcal{X}_\mathrm{o}^\mathrm{s}$ and $\delta c_1 \in \Delta_{h(x_1)}$ be an arbitrary state and production level change. According to (iii), the new steady state $x_2 = \mathfrak{T}_{\mathrm{x},\delta c_1}^\mathrm{e}(x_1) \in \mathcal{X}_\mathrm{o}^\mathrm{s}$ lies on the same branch of $\mathcal{X}_\mathrm{o}^\mathrm{s}$ ($x_2 \in B_{x_1}$). Thus, there exists a $\gamma_1 \in C\big([0,\,1]\,,\mathcal{X}_\mathrm{o}\big)$ with $\gamma_1(0) = x_1$ and $\gamma_1(1) = x_2$. Figure 4.10 illustrates this curve γ_1 connecting

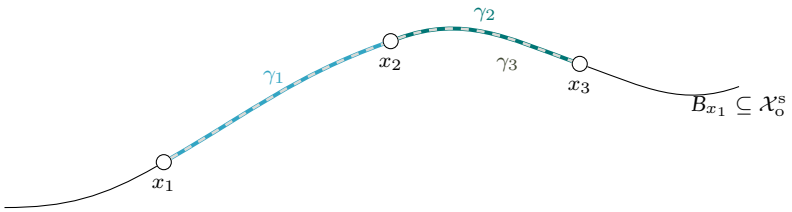

Figure 4.10: Schematic illustration of the curves connecting steady states on $\mathcal{X}_\mathrm{o}^\mathrm{s}$.

the two states. Furthermore, let $\delta c_2 \in \Delta_{h(x_2)}$ be an arbitrary production level change starting at x_2, such that the new steady state is

$$x_3 = \mathfrak{T}_{\mathrm{x},\delta c_2}^\mathrm{e}(x_2) = \mathfrak{T}_{\mathrm{x},\delta c_2}^\mathrm{e} \circ \mathfrak{T}_{\mathrm{x},\delta c_1}^\mathrm{e}(x_1) \in B_{x_1} \subseteq \mathcal{X}_\mathrm{o}^\mathrm{s}.$$

Again, according to Lemma 4.1 (iii), there must exist a curve $\gamma_2 \in C\big([0,\,1]\,,\mathcal{X}_\mathrm{o}\big)$ such that $\gamma_2(0) = x_2$ and $\gamma_2(1) = x_3$. Since the final point of γ_1 and the initial point of γ_2 are coincide, the curves belong to the same branch of $\mathcal{X}_\mathrm{o}^\mathrm{s}$.
If one applies the production level change $\delta c_1 + \delta c_2 \in \Delta_{h(x_1)}$ directly it follows that there exist a third curve $\gamma_3 \in C\big([0,\,1]\,,\mathcal{X}_\mathrm{o}\big)$ with $\gamma_3(0) = x_1$ and $\gamma_3(1) = \mathfrak{T}_{\mathrm{x},\delta c_1+\delta c_2}^\mathrm{e}(x_1)$. From the initial and final state and the continuous property of γ_3, it follows that γ_3 must lie on the same branch as γ_1 and γ_2. The second condition of Lemma 4.1 states that along γ_3 no production level occurs twice under h. Thus, we can construct γ_3 from γ_1 and γ_2 through

$$\gamma_3(\lambda) := \begin{cases} \gamma_1(2\lambda) & 0 \leq \lambda \leq 0.5, \\ \gamma_2(2\lambda - 1) & 0.5 < \lambda \leq 1 \end{cases}$$

Finally, we can conclude from $\gamma_2(1) = \gamma_3(1)$ that

$$\mathfrak{T}_{\mathrm{x},\delta c_2}^\mathrm{e} \circ \mathfrak{T}_{\mathrm{x},\delta c_1}^\mathrm{e}(x_1) = \mathfrak{T}_{\mathrm{x},\delta c_1+\delta c_2}^\mathrm{e}(x_1) = \mathfrak{T}_{\mathrm{x},\delta c_2+\delta c_1}^\mathrm{e}(x_1) = \mathfrak{T}_{\mathrm{x},\delta c_1}^\mathrm{e} \circ \mathfrak{T}_{\mathrm{x},\delta c_2}^\mathrm{e}(x_1).$$

In the case of $\delta c_2 = -\delta c_1$ it follows from $\gamma_1(0) = \gamma_2(1) = \gamma_3(1)$ that

$$\mathfrak{T}_{\mathrm{x},-\delta c_1}^\mathrm{e} \circ \mathfrak{T}_{\mathrm{x},\delta c_1}^\mathrm{e}(x_1) = \mathfrak{T}_{\mathrm{x},\delta c_1-\delta c_1}^\mathrm{e}(x_1) = \mathfrak{T}_{\mathrm{x},0}^\mathrm{e}(x_1) = id_\mathcal{X}(x_1). \qquad \square$$

4.3.2 Surrogate Model of the Transition-Time Map

Next, we want to design a surrogate model $\tilde{\mathfrak{T}}_{\mathrm{t},-}$ for the minimal transition time to avoid a bilevel optimization within the S-RTO. However, it is only necessary

that $\tilde{\mathfrak{T}}_{\mathrm{t},-}$ is locally available, i.e., at the current production level $c \in \mathcal{C}_{\mathrm{o}}$, when solving Problem (3.8). This is because $\delta c \in \Delta_c$ is considered as decision variable for the determination of the new production level. To obtain the locally valid surrogate model, we will use a GP. For a give state $x \in \mathcal{X}_{\mathrm{o}}$, it maps from the space $\Delta_{h(x)}$ of admissible production level changes to the transition time.

The training data are generated by solving the transition Problem (4.9), as discussed in the previous section. Considering (4.9), the production change δc is a parameter that appears in the setup function (4.7) within the control law (4.8). It follows that (4.9) is approximated by a parametric NLP where δc becomes a parameter [5]. This allows us to determine the sensitivities

$$S_\alpha := \partial_{\delta c^\alpha} \mathfrak{T}_{\mathrm{t}}^{\mathrm{e}}(x_0, \delta c)$$

for a given production change and $x_0 \in \mathcal{X}_{\mathrm{o}}$. The sensitivities can be calculated explicitly from the Lagrangian and the KKT conditions, see Appendix A.3. By adding the sensitivity information, we can improve the quality of the GP with the same number of training points, see [236, 201].

For a given initial state $x_0 \in \mathcal{X}_{\mathrm{o}}$, we will use a set $D_\delta := \{\delta c_1, \dots, \delta c_{n_{\mathrm{t}}}\}$, where $\delta c_i \in \Delta_{h(x_0)}$. From this set of training inputs, one can compute the initial set

$$\mathscr{T}^0 := \left\{ (\delta c_1, T_1, S_1), \dots, (\delta c_{n_{\mathrm{t}}}, T_{n_{\mathrm{t}}}, S_{n_{\mathrm{t}}}) \right\},$$

of training points to derive the surrogate model $\tilde{\mathfrak{T}}_{\mathrm{t},h(x_0)}$ iteratively, where $T_i = \mathfrak{T}_{\mathrm{t}}^{\mathrm{e}}(x_0, \delta c_i)$ and $(S_i)_\alpha = \partial_{\delta c^\alpha} \mathfrak{T}_{\mathrm{t}}^{\mathrm{e}}(x_0, \delta c_i)$. Based on this data, we obtain the surrogate model $\tilde{\mathfrak{T}}_{\mathrm{t},h(x_0)}$ by employing the mean function (A.3) assuming there is no prior knowledge of the transition time. Thus the initial transition-time map is given by employing the GP formula by

$$\tilde{\mathfrak{T}}_{\mathrm{t},h(x_0)}^0 (\delta c) := \left(a^\iota \eta^{\boldsymbol{x}}{}_\iota + b^{\iota\zeta} \rho^{\boldsymbol{x}}{}_{\iota\zeta} \right) (\delta c), \tag{4.17}$$

where

$$a^\alpha := L^{\alpha\iota} T_\iota + M^{\alpha\iota\zeta} S_{\iota\zeta} \quad \text{and} \quad b^{\alpha\beta} := M^{\iota\alpha\beta} T_\iota + R^{\alpha\iota\beta\zeta} S_{\iota\zeta},$$

are the initial weight factors, which describe the relationship between the individual transition times T_ι and their sensitivity values $S\iota$, $\iota = 1, \dots, n_{\mathrm{t}}$. The functions $\eta^{\boldsymbol{x}}$ and $\rho^{\boldsymbol{x}}$ evaluate the influence of the points in $\mathscr{T}^0$ on a new point $\delta c \in \Delta_{h(x_0)}$. For more details, see Appendix A.2.

Since the initial training points are chosen arbitrarily, map $\tilde{\mathfrak{T}}_{\mathrm{t},h(x_0)}^0$ might not describe the original map $\mathfrak{T}_{\mathrm{t}}^{\mathrm{e}}$ in sufficient detail. In such cases, additional training points have to be calculated to increase the quality of the surrogate model. To determine whether the function $\tilde{\mathfrak{T}}_{\mathrm{t},h(x_0)}^i$ is generally suitable, we

Algorithm 4.1: Locally-valid surrogate model of the transition-time map

Input: the initial model $\tilde{\mathfrak{T}}^0_{\mathrm{t},h(x_0)}$ generated from the initial hyperparameter $\mathfrak{h}^0$, a value $\bar{j} \in \mathbb{N}$ and the set $\mathscr{T}^0$

set index $j := 1$ and initialize the set $W_2 := \emptyset$ 1

while $W_2 \neq \emptyset$ *or* $j < \bar{j}$ **do** 2

  generate sets W_1 consisting of random points $\delta c \in \Delta_{h(x_0)}$ and $W_2 := \emptyset$ 3

  build $\hat{\kappa}$ using $\mathscr{T}^{j-1}$ and (A.5) 4

  for $i = 1, \ldots, |W_1|$ **do** 5

    determine $\delta c_i^* := \underset{\delta c \in \Delta_{h(x_0)}}{\arg\max}\, \hat{\kappa}\,(\delta c)$ with initial point $\delta c_i \in W_1$ 6

    if $\hat{\kappa}(\delta c_i^*) > tol_1$ **then** 7

      determine $T_i = \mathfrak{T}^{\mathrm{e}}_{\mathrm{t}}(x_0, \delta c_i^*)$ and $(S_i)_\alpha = \partial_{\delta c^\alpha}\, \mathfrak{T}^{\mathrm{e}}_{\mathrm{t}}(x_0, \delta c_i^*)$ 8

      update the set $W_2 \leftarrow W_2 \cup (\delta c_i^*, T_i, S_i)$ 9

    end 10

  end 11

  update the set $\mathscr{T}^j \leftarrow \mathscr{T}^{j-1} \cup W_2$ 12

  build $\tilde{\mathfrak{T}}^j_{\mathrm{t},h(x_0)}$ using $\mathscr{T}^j$ and (4.17) and by updating hyperparameter $\mathfrak{h}^j$ 13

  set the index $j \leftarrow j + 1$ 14

end 15

Result: the final surrogate model $\tilde{\mathfrak{T}}_{\mathrm{t},h(x_0)} := \tilde{\mathfrak{T}}^j_{\mathrm{t},h(x_0)}$ of the transition-time map and set $\mathscr{T} := \mathscr{T}^i$ of training data

analyze the posterior covariance function $\hat{\kappa}$ in (A.5) of the GP. This covariance allows evaluating the confidence of the GP at different δc, cf. [84, 237]. In [139] and [134], some theoretical approaches and assumptions are discussed for describing and calculating the error bounds using the covariance. In particular, the properties of the map to be approximated and the kernel function of the GPs are discussed.
Assuming that the covariance reflects the quality of $\tilde{\mathfrak{T}}^0_{\mathrm{t},h(x_0)}$, we propose to add further training points corresponding to a given tolerance of the covariance to improve the model. Algorithm 4.1 describes this procedure in more detail.

Remark 4.13. *It is possible that $\tilde{\mathfrak{T}}_{\mathrm{t},-}$ generated by Algorithm 4.1 still has areas where the error is greater than a specified tolerance. Thus, we suggest to use $\hat{\kappa}$ to evaluate the result of the S-RTO in Problem* (3.8).

Using Algorithm 4.1, we can generate a map that yields the transition time for different production level changes as required within the S-RTO.
Based on the local model, one can also consider designing a globally-valid surrogate model for the transition time, which approximates the reduced

Algorithm 4.2: Global surrogate model of the transition-time map

Input: a reference state $x_\mathrm{r} \in \mathcal{X}_\mathrm{o}$, the discretization $D_\mathrm{c} := \{c_1, \ldots, c_{n_\mathrm{c}}\}$ of the production area $\mathcal{C}_\mathrm{o}$

initialize the training set $\mathscr{T}_\mathrm{tot} := \emptyset$ 1

for $i = 1, \ldots, n_\mathrm{c}$ **do** 2

  generate the discretization $D_\delta := \{\delta c_1, \ldots, \delta c_{n_\delta}\}$, where $\delta c_j \in \Delta_{c_i}$ 3

  compute the inital state $x_i = \mathfrak{T}^\mathrm{e}_{\mathrm{x},(c_i - h(x_\mathrm{r}))}(x_\mathrm{r})$ and initialize $\mathscr{T}^0 := \emptyset$ 4

  for $j = 1, \ldots, n_\delta$ **do** 5

    compute $T_j = \mathfrak{T}^\mathrm{e}_\mathrm{t}(x_i, \delta c_j)$ and $(S_j)_\alpha = \partial_{\delta c^\alpha} \mathfrak{T}^\mathrm{e}_\mathrm{t}(x_i, \delta c_j)$ 6

    update the set $\mathscr{T}^0 \leftarrow \mathscr{T}^0 \cup (\delta c_j, T_j, S_j)$ 7

  end 8

  compute the final set $\mathscr{T}$ using Algorithm 4.1 and $\mathscr{T}^0$ 9

  update the set $\mathscr{T}_\mathrm{tot} \leftarrow \mathscr{T}_\mathrm{tot} \cup \mathscr{T}$ 10

end 11

build $\tilde{\mathfrak{T}}_\mathrm{t}$ using $\mathscr{T}_\mathrm{tot}$ and (4.17) 12

Result: the global surrogate model $\tilde{\mathfrak{T}}_\mathrm{t}$ of the transition-time map

transition-time map $\mathfrak{T}_\mathrm{t}$. The main idea is to interpret the production level $h(x_0)$ from which the transition starts as an additional independent variable. In this way, we can determine for each production level within $\mathcal{C}_\mathrm{o}$ a locally-valid model. It is important to note that a globally-valid surrogate model to describe $\mathfrak{T}_\mathrm{t}$ needs a state-independent system $\mathcal{P}$. The procedure is presented in Algorithm 4.2, using a reference state $x_\mathrm{r} \in \mathcal{X}_\mathrm{o}$ from that the initial states for each production level transition can be determined.

Example 4.4 (Transition Time Map of a Coupled AD- and RSR-Process (4.3 continued))**.** *We continue with the application of the operational strategy to the scenario from Example 2.5 for our system, which is described in detail in Appendix B.1. In Example 3.1, we have analyzed the S-RTO, which determines the new production level after a change of the feed parameter. For this purpose, we have assumed that we have information on the transition-times for the individual production levels in the form of a surrogate model of the transition-time map. In the following, we will describe how this local surrogate model is generated for at the production level $c_2 \in \mathcal{C}_\mathrm{o}$, where the system operates during the second production phase. The same procedure can be applied for all production level $c \in \mathcal{C}_\mathrm{o}$.*

First of all, we assume that the system is in a steady state of the current production phase. This state describes the initial point for the individual transition problems to be solved and ensures that the map is independent of the state coordinate. The map does not need to be trained on the entire operating

area $\mathcal{C}_o$ but only on a subset. This subset of $\mathcal{C}_o$ describes the feasible area where the S-RTO can find solutions, and it was already introduced in Example 4.3.
To train an initial map, we choose several production levels covering the area and solving the transition problem for these points. It is important to include several boundary points of this feasible area (cf. green area in Figure 4.8), as the surrogate model should be used for interpolation since no prior knowledge is assumed. Furthermore, the options and initial values used to solve the transition problem should be the same as those used online in the operational strategy. Hence, we need to proceed in the same way as described in the individual steps in Example 4.3. For the initial training set, we used 30 points, 20 points were on the boundary, and 10 were randomly distributed over the area.

After the training points are generated, the hyperparameters are optimized. For this, we use a maximum likelihood estimation, which is a standard approach to find the hyperparameter. However, we use additional inequality constraints on the posterior mean to ensure that the trained map only yields positive transition times. In [172], this strategy was used to identify reachable references. Obviously, this can only be done for a finite number of intermediate points.
Afterwards the map for the transition time and the standard deviation over the feasible area is calculated and evaluated. It is possible that there are subregions where the standard deviation is larger than a given tolerance. For these subregions, additional training points have to be generated and the map including the hyperparameter optimization has to be redesigned. This iterative procedure is repeated until a given quality of the transition-time map is obtained. In total, 8 iterations were performed, whereby different numbers of points were added in each iteration, as listed below:

1. iteration:	10 *points*	*2. iteration:*	2 *points*
3. iteration:	3 *points*	*4. iteration:*	5 *points*
5. iteration:	5 *points*	*6. iteration:*	5 *points*
7. iteration:	5 *points*	*8. iteration:*	5 *points*

Finally the map was trained with 70 training points.
Even though the posterior deviation of the GP surrogate model offers no guarantee that the original map, i.e., the transition Problem (4.9)*, is well approximated, it is often used as a measure. The standard deviation only allows us to assess the validity of the map based on the used training points. In the literature, one can find methods to assess this, if certain assumptions are true, see [139, 134]. Nevertheless, we assume that for sufficient training points, the standard deviation is initially a good measure.*

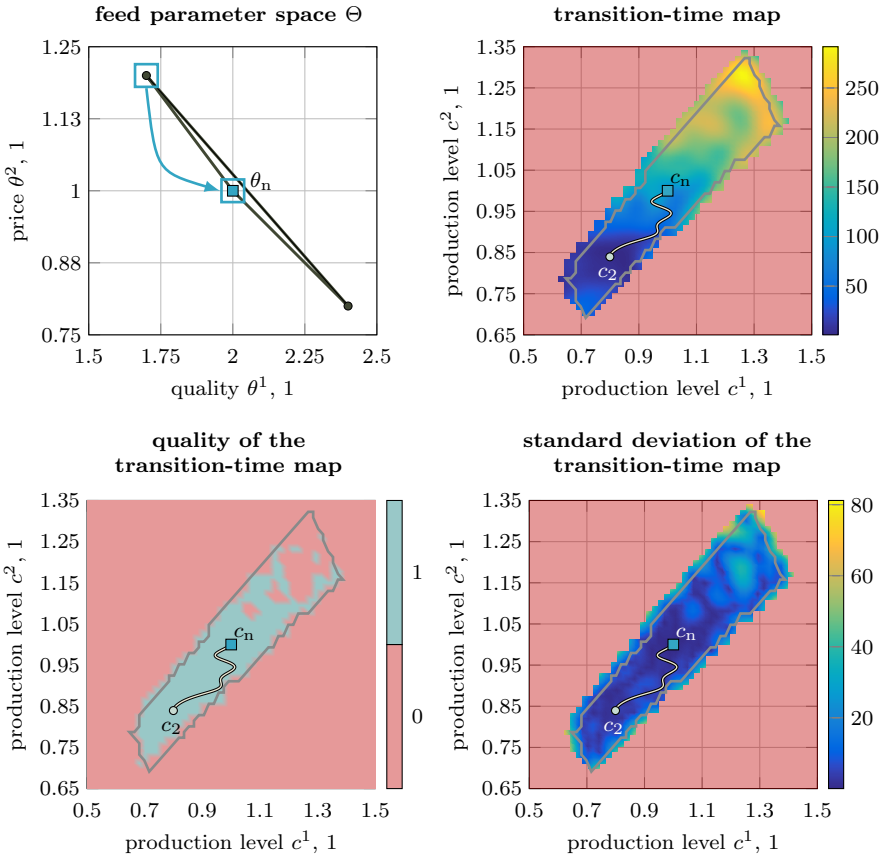

Figure 4.11: Transition-time map (top, right) and the quality of the surrogate model (bottom, left) derived from the standard deviation (bottom, right) over the feasible area of the S-RTO for the feed parameter change (top, left).

Figure 4.11 shows the evaluation of the transition-time map for the feasible area used to calculate the third transition. In addition, the standard deviation and the evaluation of the quality of the transition-time map are presented in Figure 4.11 bottom right. The tolerance to decide on the quality is fixed at 10 min. *The areas where this tolerance is met are depicted as green areas in Figure 4.11, bottom left. Additional points might need to be trained for those areas where the standard deviation is greater than 10. For instance, additional points for the upper right corner of the feasible area within $\mathcal{C}_o$ have to be determined. However, as we know that the next feed parameter will be the nominal value, it can be concluded where the S-RTO will roughly determine the production level. It is*

important that the map is most accurate between the current and the expected point or in a sufficiently large neighborhood around these points.

Similar to Figure 4.8, the heat maps show the trajectory between the production level immediately before the third transition (i.e., at c_2) and the nominal level c_n by a solid white line. Around these two points and along the trajectory, the map complies with the quality specifications that were previously defined. We can verify this because the trajectory runs through the green area (cf. Figure 4.11 bottom left), which means the standard deviation is less than 10 min.
Considering the heat map of the transition-time map in Figure 4.11 top right, we can see that in the direct neighborhood of the initial level, the time to reach the other points is a few minutes. With increasing change δc of the production, the transition time also grows significantly. The time to reach the final production level is $\tilde{T} = 85.51$ min *according to the surrogate model used for the S-RTO and the correct transition time as determined by the third transition $T = 87.57$* min.

4.4 Summary of Part II

In Part II, we discussed the operational strategy of a cl S-RTO. This strategy includes the identification of a production level for the production system according to an economic objective and considering the transition time determined by the underlying controller. The original cl S-RTO problem is a bilevel optimization, where the upper layer is a static, and the lower layer a dynamic optimization. Using certain assumptions, the cl S-RTO can be reformulated and separated into a static S-RTO and a dynamic transition problem. Figure 4.12 shows a roadmap of all terms and problems that are part of the operational strategy.

In Chapter 3, we addressed the S-RTO, which identifies a new stationary operating point whenever the economic characteristics change. We have introduced storage constraints that allow predicting the evolution of the storage level during the production phase and thus take it into account in the S-RTO. Furthermore, a locally valid transition-time map $\tilde{\mathfrak{T}}_{\mathrm{t},-}$ is used to estimate the maximum possible length of the production phase. This map is generated using the transition problem we developed and discussed in Chapter 4.

In Chapter 4, we focused on the transition to the production level determined by the S-RTO. First, we mathematically formulated the problem and then proposed a control law to achieve the transition. The optimal parameters for this controller can be calculated by an OCP, whose objective is to minimize the transition time. The result of the transition problem is used in two ways. Firstly, if the S-RTO provides multiple operating points, we can determine that point

within $\mathcal{S}_{\mathrm{opl}}$ that yields the minimum transition time. This allows defining two functions providing the new setpoint of the production level and the steady-state input depending on the current state $x \in \mathcal{X}_{\mathrm{o}}$, the storage level $\ell \in \mathcal{D}$, and the feed parameter $\theta \in \Theta$. Secondly, the optimal parameters specify the control law that steers the system to the new setpoint for the stationary production level. In this way, we can generate a reference trajectory implemented by the controller of the supervisory layer. Alternatively, under certain conditions, a controller K can be defined, which performs the transition and compensates the internal dynamics.

The transition problem defines the transition-time map $\mathfrak{T}_{\mathrm{t}}^{\mathrm{e}}$ that is used to design the local surrogate model $\tilde{\mathfrak{T}}_{\mathrm{t},-}$. Besides, we use K to define the transition-state map $\mathfrak{T}_{\mathrm{x}}^{\mathrm{e}}$ to determine the states $x \in \mathcal{X}_{\mathrm{o}}^{\mathrm{s}}$ for the production phase. Based on $\mathfrak{T}_{\mathrm{x}}^{\mathrm{e}}$, the concept of state independence is defined, which requires two properties for the composition of $\mathfrak{T}_{\mathrm{x}}^{\mathrm{e}}$. If one can show that the system is state-independent, it is sufficient to define a reference state $x_{\mathrm{r}} \in \mathcal{X}_{\mathrm{o}}$ from which the transitions can be observed. Hence, it is possible to define a reduced transition-time map $\mathfrak{T}_{\mathrm{t}}$ and, thus, a global surrogate model $\tilde{\mathfrak{T}}_{\mathrm{t}}$.

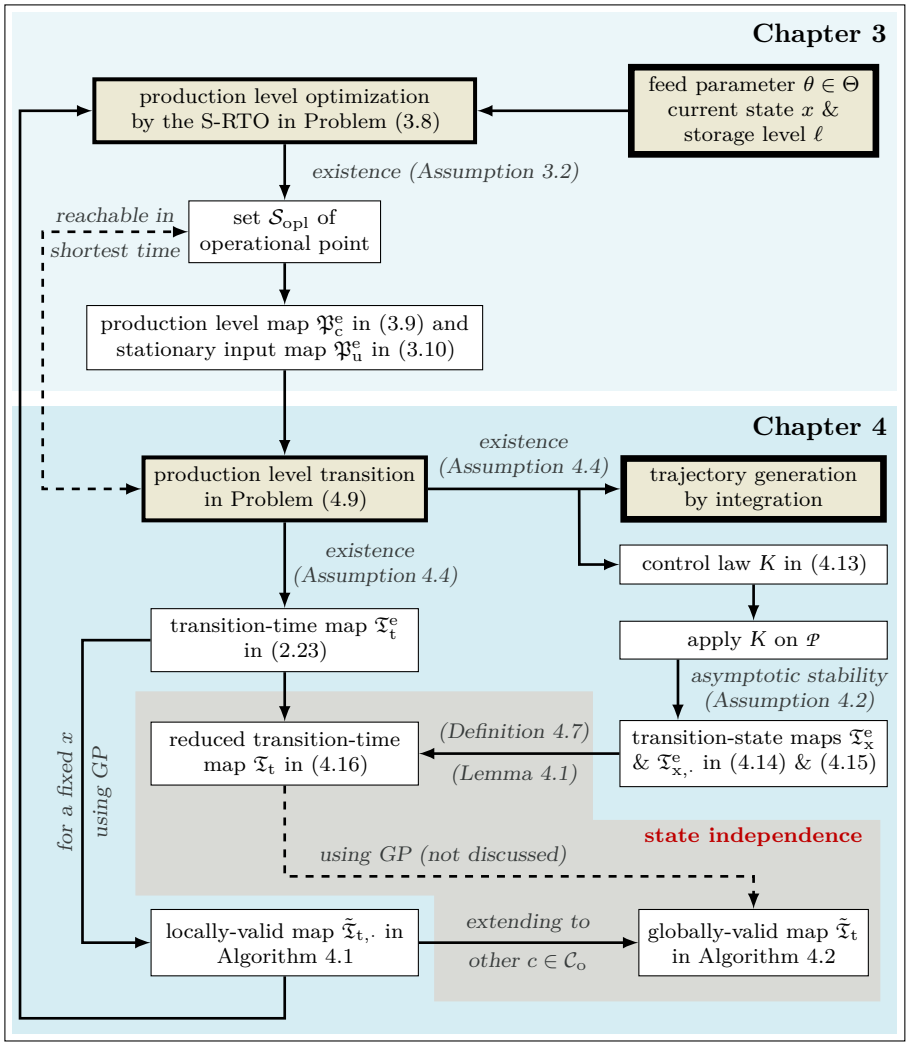

Figure 4.12: Roadmap of the concepts introduced for the transition.

Part III

Design of the Storage Elements

Chapter 5

Storage System Design

In the last two chapters, we discussed the operating strategy to ensure that the production system $\mathcal{P}$ operates at an economic optimum. For this purpose, we introduced the cl S-RTO and described how to efficiently solve this bilevel optimization by decoupling it into the static S-RTO and the dynamic transition problem. For the S-RTO, we have formulated storage constraints that become active when the storage level is close to the boundaries.
This chapter shows how to design the storage size, such that the storage constraints do not hinder optimal production. Employing the storage rates and a certain prediction horizon can determine when the storage elements are either full or empty. Section 5.1 gives a brief overview of storage sizing in general. In Section 5.2, we derive the relaxed S-RTO to calculate the optimal operating point when the storage system has no limiting effect because it is sufficiently large. By exploiting the relaxed S-RTO, we describe in Section 5.3 how the minimum storage size can be estimated. Finally, in Section 5.4, we propose a method to estimate the storage size depending on a given stochastic scenario.

5.1 Brief Review of Storage Design

In process engineering, the use of storage elements and their efficient design is an important issue, especially when the dynamic operation of processes and process elements is required. According to the field of application, various names for the storage elements are common [53, 54]. For compensation of quality properties within the flow, one uses mixing tanks and neutralization vessels. In contrast, if fluctuations in the flow rates are to be compensated, the elements are usually

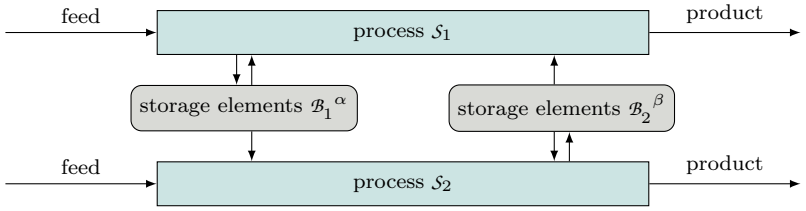

Figure 5.1: Illustriation of the structure of the production system.

referred to as surge, holdup or buffer tanks, or as intermediate storage vessels. In general, the storage elements can be classified into two different categories according to their tasks [54, 153].

(i) Attenuation of disturbances: The propagation of disturbances between two connected elements is damped.

(ii) Decoupling of process operations: The downstream process element can temporarily be operated independently from the upstream element.

Classical applications of the second category are processes with a partial shutdown of process elements [34, 35] or scheduling tasks [197, 266]. Typically, the storage sizes for such applications are predefined in advance, which means that the operational strategy needs to account for them as constraining elements. In this way, the operational strategy indirectly influences the levels of the storage elements. According to the precise target of the control strategy, it affects the required storage size.

In the present work, we consider a generic setup of two processes that exchange material and energy via one or more storage devices, see Figure 5.1. The flows supplying or discharging the storages are determined by the cl S-RTO with integrated trajectory generation. To guarantee optimal economic operation, we want to achieve a temporal decoupling of the two processes. The time span for this decoupling depends on the evolution of the economic influencing parameters, i.e., on the scenario, and the size of the storages. For this reason, we focus in this chapter on the relationship between the possible scenarios and storage capacity.

Faanes and Skogestad [54] state that conventional approaches for dimensioning the storage system are based on heuristics and rules of thumb for the residence time, i.e., the relation between volume and flow rate [38, 91]. Nevertheless, there are several publications that deal with the dimensioning and sizing of storage elements in specific applications, e.g. for water [227, 46, 26, 255, 214],

for hydrogen [126, 78, 50], for carbon dioxide [273], for chlorine [208], for thermal energy [3, 146], or for electrical energy [179, 89, 262, 219]. A characteristic feature, however, is that the procedures usually address the specific type and setup of the process system, specific storage technology is assumed, or particular scenarios (e.g., price developments, etc.) are used. The approaches used in the publications are often based on simulations. In this context, either a discrete set of storage sizes is tested and evaluated [273, 208, 219], or a decision is made according to different scenarios [179, 89] (e.g. using forecasts). In some cases, optimization-based approaches are also used, e.g., in [126].
However, there is no systematic technique and no general recipe for a strategy, as is the case with operational strategy from Chapters 3 and 4. Specifically, the relationship between the performance characteristics of a particular control strategy and the sizing of the storage elements leads to many interesting questions.

From a control engineering perspective, the averaging level control problem is used for managing the storage system for a given capacity, cf. [99, 168, 209]. The objective of an averaging level controller is to provide a smooth output flow for fluctuating input flows by utilizing the storage capacity. In order to achieve this, the controller can first change the storage level so that it deviates from its setpoint to adapt the output slowly and uniformly. Afterward, the controller returns the storage level to the setpoint to ensure sufficient reserve for further adaptations. Former work in this field can be found in [33], where P and PI controllers are used, or in [175, 27], where the focus is on predictive control techniques. To control interconnected storage elements, Sbarbaro and Ortega [216] focus on an energy-based description and make use of a passivity-based control approach. Rosander et al. [209] propose two linear control laws that imitate the behavior of a robust MPC. The averaging level control allows indirect minimization of the storage size by controlling the levels, considering the storage constraints directly. For a given controller, the storage size design is based on the analysis of particular disturbance models used for the input flow and on the specification of the maximum allowable variation in the output flow.
Another type of design technique for sizing storage elements for linear systems is proposed by Zheng and Mahajanam [277] and Mahajanam and Zheng [162]. The authors have defined a controllability index given by the additional storage capacity required to meet the control objective and constraints in the presence of the expected disturbances. In order to determine the optimal capacities, an economic objective function (e.g., annualized cost) is employed for evaluation.

Generally, two different design concepts can be distinguished. In integrated approaches, the controller tuning and the determination of the storage size are done simultaneously. Contrary, in sequential approaches, both steps are performed after each other. The optimization to determine the controllability

index in [162] considers both the storage capacity and the control system as decision variables, which leads to an integrated approach. An early work considering minimizing the storage capacity while determining the control parameters is presented in [9]. Different control laws and various types of disturbances for the inlet flow are addressed.

Faanes and Skogestad [54] solve the design problem by a two-step approach. In this way, a storage element is generally described by a linear system with a transfer function that modifies the inlet flow disturbance. The first step is to identify a suitable transfer function by determining its time constant and its order. Next, a physical realization of the function must be found together with suitable control parameters so that the controller can handle the modified disturbances. A slightly different approach is considered by Lee and Reklaitis [140] or Odi and Karimi [183], who determine the capacity of a intermediate storage that connects two processes. Here, no controller is used to regulate storage levels. A similar setup is exploited in Orbán-Mihálykó and Lakatos [185] and his further works [186, 187, 177]. The process that feeds the intermediate storage is a batch, followed by a continuous process receiving the material. While the output flow to the continuous process is assumed to be constant, the time intervals in which the batch feeds the storage is described by a stochastic process. Based on the integration of a stochastic ODE, the probability of reaching the upper and lower bounds can be determined on a finite and infinite time horizon.

Using this setup of intermediate storage between two processes, in the works [186, 187, 177], the storage size determination are further discussed. Thereby, the probability density functions that characterize different aspects (e.g., the finite shortage time or the overflow time) is described by an auxiliary function for which an integral equation can be given and solved analytically. Finally, the analytical solution allows determining the storage size. The authors also compute the initial amount to be stored to avoid emptying.

Based on the production system $\mathcal{P}$, we consider a similar structure where a system of storage elements connects two processes. However, in our setup, both processes are continuous and are described by deterministic models. Disturbances of the nominal operation and thus fluctuations of the input and output flows of the storages occur when considering specific scenarios $\theta \in \Theta$. To cover a larger class of scenarios, in Section 5.4 we extend the definition of Θ from Section 2.3 so that it describes a stochastic process. Employing the cl S-RTO, the storage rates, and thus the evolution of the storage levels, can be described by a stochastic process. Contrary to the approaches in [185, 186, 187], we propose the use of an unscented transformation [116] for describing the probability density of the storage level.

Besides, we do not use an averaging level control technique, as is common when dealing with storages, to ensure that both processes are weakly connected as

introduced in Definition 2.3. The cl S-RTO is designed to utilize the full storage capacity without being restricted by an additional level controller, which pushes the storage level back to a certain level at regular times and keeps it constant. The integration and control of the storage levels within the cl S-RTO is intended to fulfill only two tasks:

1. to restrict the variation around the initial value at the end of the transition,
2. to determine the slope during the production phase,

The technique proposed in this chapter contributes to estimating the storage size according to probabilistic scenarios for the feed parameter θ. Thus, the cl S-RTO yields economically optimal operating points to a given probability without being restricted by the storage elements. It should be emphasized that the approach described here does not include economic aspects of procuring the storage, such as investment costs. We show the relation between the economic parameters affecting the operational strategy and the storage level dynamics and, thus, the storage capacity.

5.2 Relaxed Static Real-Time Optimization

Before considering the storage size estimation, two further parametric NLPs for determining the production level are introduced. In this way, we obtain a tool to analyze the effect of the feed parameter on the storage level and the storage size. Here, the optimal storage rates are determined by a relaxed S-RTO resulting from the original S-RTO Problem (3.8) without considering the storage constraints (3.7).

The overview in Figure 5.2 is intended to illustrate the concepts described in this section. The blue field in the center summarizes the S-RTO introduced in Section 3.3. We already discussed the Problem (3.8) as part of the control strategy applied to the production system during online operation. Due to the transition time T required to reach a new production level, the maximum production phase $\Delta_\mathrm{p} t$ is obtained, and the admissible intervals $\mathcal{R}_{[\Delta_\mathrm{p} t, \mathcal{H}]_j}{}^{\alpha}$ for the storage rates.
Let us consider Problem (3.8) and assume that the transition time T is zero for all production level changes, i.e., the new level can be reached immediately and the transition-time map $\tilde{\mathfrak{T}}_{\mathrm{t},\cdot}$ is not necessary anymore. It follows that the length of the maximum production phase is given by $\overline{\Delta}_\theta t$, which is a parameter to characterize the scenario set Θ. The production level optimization with

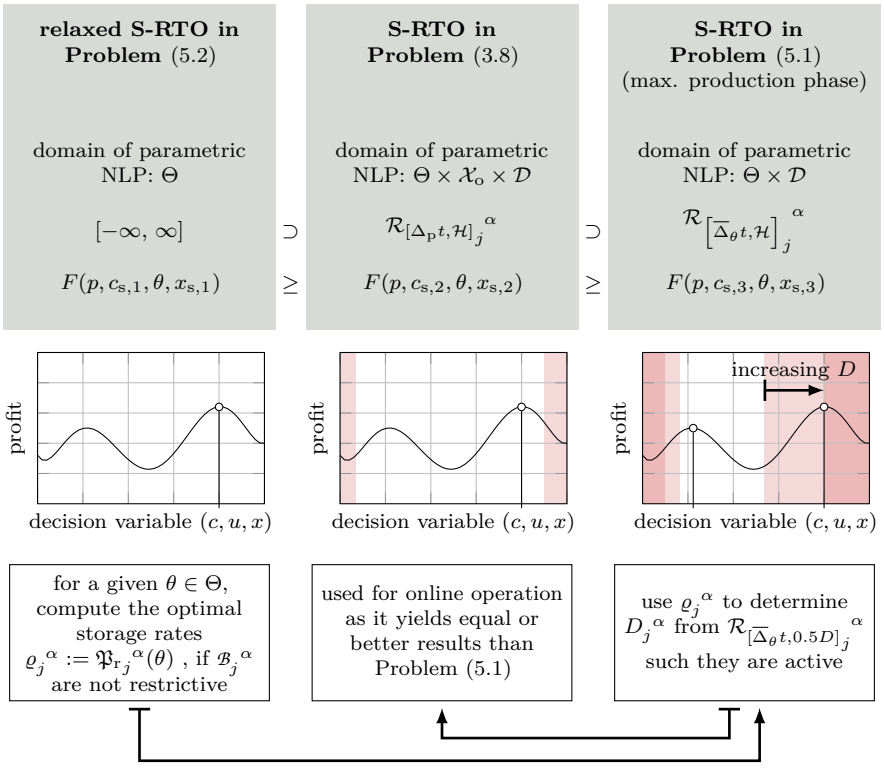

Figure 5.2: Roadmap of the concepts introduced to estimate the storage size.

maximal production phase has the form

$$\overline{\mathcal{S}}_{\text{opl}} := \underset{c,\,u,\,x}{\arg\max} \quad F(p, c, \theta, x) \tag{5.1a}$$

$$\text{subject to} \qquad 0 = f\left(x, u\right), \tag{5.1b}$$

$$0 = c - h(x), \tag{5.1c}$$

$$0 \geq s\left(x, u\right), \tag{5.1d}$$

$$0 \geq \omega\left(x\right), \tag{5.1e}$$

$$\rho_j{}^{\alpha}\left(x, u\right) \in \mathcal{R}_{\left[\overline{\Delta}_\theta t, \mathcal{H}\right]_j}{}^{\alpha}, \tag{5.1f}$$

$$x \in \mathcal{X},\, c \in \mathcal{C}_{\text{o}},\, u \in \mathcal{U}. \tag{5.1g}$$

The solution set $\overline{\mathcal{S}}_{\text{opl}} := \left\{(c_\text{s}, u_\text{s}, x_\text{s}) \in \mathcal{C}_\text{o} \times \mathcal{U} \times \mathcal{X}_\text{o}\right\}$ of Problem (5.1) contains all operation points that maximize the profit function. Since the transition time is not required, the current state $x \in \mathcal{X}_\text{o}$ of the system is not longer needed. It follows that the optimal profit value, as well as storage charging rate are only depend on the feed parameter $\theta \in \Theta$ and storage level $\ell \in \mathcal{D}$, cf. Figure 5.2 right-hand side. Note that the storage level enters the calculation of $\mathcal{R}_{\left[\overline{\Delta}_\theta t, \mathcal{H}\right]_j}^{\ \alpha}$ as stated in (3.6).
Since the length of the maximum production phase is defined by the length $\overline{\Delta}_\theta t$ of constant feed parameters, for the storage constraints in (5.1f) it holds $\mathcal{R}_{[\Delta_\text{p} t, \mathcal{H}]_j}^{\ \alpha} \supset \mathcal{R}_{\left[\overline{\Delta}_\theta t, \mathcal{H}\right]_j}^{\ \alpha}$. Therefore, the optimal profit value of (5.1) is worse or equal than in the original Problem (3.8). This situation is indicated by the two diagrams in the center and on the right-hand side in Figure 5.2. There, the profit is shown in the dependency of the decision variables. The red areas illustrate the boundaries of the storage constraints $\mathcal{R}_{[\cdot, \mathcal{H}]_j}^{\ \alpha}$ for a given storage size D. An increase in the storage size D increases the set of admissible storage rates. Thus the domain of decision variables for optimization becomes larger. For sufficiently large storage elements, the result of the S-RTO (3.8) and Problem (5.1) coincides, cf. Figure 5.2.

When we go a step further and neglect the storage constraints completely, one obtains the relaxed S-RTO problem of the form

$$\begin{aligned}
\mathcal{S}_{\text{opl}}^{\infty} := \ & \underset{c,\, u,\, x}{\arg\max} && F(p, c, \theta, x) && \text{(5.2a)}\\
& \text{subject to} && 0 = f\left(x, u\right), && \text{(5.2b)}\\
& && 0 = c - h(x), && \text{(5.2c)}\\
& && 0 \geq s\left(x, u\right), && \text{(5.2d)}\\
& && 0 \geq \omega\left(x\right), && \text{(5.2e)}\\
& && x \in \mathcal{X},\, c \in \mathcal{C}_\text{o},\, u \in \mathcal{U}. && \text{(5.2f)}
\end{aligned}$$

The solution set $\mathcal{S}_{\text{opl}}^{\infty} := \left\{(c_\text{s}, u_\text{s}, x_\text{s}) \in \mathcal{C}_\text{o} \times \mathcal{U} \times \mathcal{X}_\text{o}\right\}$ of this problem is equal to Problem (3.8) if the storage elements are infinitely large and sufficiently filled. Consequently, it yields the best possible solution if the storage system is not a limiting factor. On the left-side in Figure 5.2, this relaxed S-RTO is classified according to the cases described above. This problem can be interpreted as S-RTO, where the box constrains for the storage rates are given by $[-\infty, \infty]$. The diagram on the left-hand side in Figure 5.2 shows the profit over its decision variables.

To solve Problem (5.2), only the feed parameter $\theta \in \Theta$ must be known. The profit at the optimal operating point might be greater than in the other two cases since no restrictions apply to the storage rate.
By comparing the optimal profit value, as obtained by solving Problem (5.2) and (5.1), we can define for a fixed selling price $p \in \mathbb{R}^+$ the map

$$\begin{aligned} &\mathfrak{F} : \Theta \times \mathcal{D} \to \mathbb{R}_0^+,\ (\theta, \ell) \mapsto \mathfrak{F}(\theta, \ell), \\ &\quad \mathfrak{F}(\theta, \ell) := F\big(p, \mathrm{pr}_1(\mathfrak{o}_1), \theta, \mathrm{pr}_3(\mathfrak{o}_1)\big) - F\big(p, \mathrm{pr}_1(\mathfrak{o}_2), \theta, \mathrm{pr}_3(\mathfrak{o}_2)\big), \end{aligned} \tag{5.3}$$

where $\mathfrak{o}_1 \in \mathcal{S}_{\mathrm{opl}}^{\infty}$ and $\mathfrak{o}_2 \in \overline{\mathcal{S}}_{\mathrm{opl}}$ are the operating points that can be reached in minimal time. This map describes the gap between the relaxed Problem (5.2) and the original Problem (5.1) with a production phase of length $\overline{\Delta}_\theta t$. The map is used to evaluate the storage size, as shown in the next section.
For later discussions about the storage size and classification of the set Θ we define functions that yield the optimal storage rates. These functions are derived from the solution of (5.2) and are given by

$$\mathfrak{P}_{\mathrm{r}_j}{}^{\alpha} : \Theta \to \mathbb{R},\ (\theta) \mapsto \mathfrak{P}_{\mathrm{r}_j}{}^{\alpha}(\theta) := \rho_j{}^{\alpha}\big(\mathrm{pr}_3(\mathfrak{o}), \mathrm{pr}_2(\mathfrak{o})\big), \tag{5.4}$$

where $\mathfrak{o} \in \mathcal{S}_{\mathrm{opl}}^{\infty}$. For a given feed parameter, it is possible to determine the changes in the storage levels from the optimal rates resulting from $\mathfrak{P}_{\mathrm{r}_j}{}^{\alpha}$.
Considering the admissible intervals (3.6), one can determine the size $D_j{}^{\alpha}$ so that the optimal rate $\mathfrak{P}_{\mathrm{r}_j}{}^{\alpha}(\theta)$ is just in $\mathcal{R}_{[\Delta_{\mathrm{p}} t, \mathcal{H}]_j}{}^{\alpha}$. For this purpose, we use the interval as it occurs in Problem (5.1), which forms a conservative approximation compared to the original Problem (3.8). However, the storage levels are also relevant to calculate the boundaries, so we assume they are half-filled. This means a maximum distance from the boundaries for the size is assumed. Thus, it ensures that the design of the storage system and the subsequent setup are independent of the $\theta \in \Theta$ that initially acts on the system. This procedure is shown in the bottom section of Figure 5.2. For a given θ, the optimal rate $\mathfrak{P}_{\mathrm{r}_j}{}^{\alpha}(\theta)$ can be deployed for the upper bound in (3.5) which yields the storage size

$$D_j{}^{\alpha} = 2\overline{\Delta}_\theta t \left| \mathfrak{P}_{\mathrm{r}_j}{}^{\alpha}(\theta) \right|. \tag{5.5}$$

Here, the maximum production phase is set to be $\Delta_{\mathrm{p}} t = \overline{\Delta}_\theta t$ since the transition time is zero. The main idea is to start by finding the best operating point for a given θ, thus determining the corresponding storage rate (5.4) through the relaxed S-RTO Problem (5.2). Subsequently, the storage size is calculated to ensure that the interval of storage constraints is large enough to make the previously determined operating point for Problem (5.1) feasible. In other words, the size calculated in this way makes the storage restrictions active. Since this problem represents a conservative estimate of the original problem, it

is guaranteed that the optimal operating point also belongs to the solution set of Problem (3.8), cf. Figure 5.2.

Remark 5.1. *Similar to Assumption 3.2, it is assumed that the solution of the two NLPs exists for corresponding parameters. Furthermore, if there is more than one solution, the operating point that can be reached in the shortest time has to be selected.*

Remark 5.2. *In the following and w.l.o.g., the safety boundary ${\zeta_j}^{\alpha}$ of the element ${\mathcal{B}_i}^{\alpha}$ is set to be zero. After the storage size estimation, the corresponding values can be added again.*

5.3 Minimum Storage Size

The goal of this section is to derive the minimum storage size based on the feed parameter space Θ. For this purpose, we use the map $\mathfrak{F}$ to classify the state space $\mathcal{D}$ of the storage level ℓ and thus define what is meant by the minimum storage size. Following this classification structure, we can determine the storage sizes ${D_j}^{\alpha}$. First of all, independent of a given scenario $\theta \in \Theta$ only by Θ. The resulting storage size is the minimum size required to ensure the best economical operation for a particular level, according to the relaxed S-RTO in (5.2). In the next section, we extend the storage size to guarantee the best economic operation for a random evolution of the feed parameter.

For the production system $\mathcal{P}$, the space $\mathcal{D}$ has the dimension $n_{\mathcal{B}} := n_1 + n_2$, which corresponds to the number of all storage elements. A point $\ell \in \mathcal{D}$ represents the storage level of all storage elements. Using $\mathfrak{F}$, we define a subset $\mathcal{A}_{\mathfrak{F}}$ of $\mathcal{D}$ given by

$$\mathcal{A}_{\mathfrak{F}} := \{\xi \in \mathcal{D} \mid \mathfrak{F}(\theta, \xi) = 0, \quad \forall \theta \in \Theta\} \subset \mathcal{D}.$$

This subset $\mathcal{A}_{\mathfrak{F}}$ is denoted as attractive region for the storage level ℓ. Whenever $\mathfrak{F}$ is zero, the storage constraints do not lead to performance deterioration of the original Problem (3.8) compared to the relaxed S-RTO. From this, we can derive that the storage systems $\mathcal{B}_j$ are well-designed if $\mathcal{A}_{\mathfrak{F}} \neq \emptyset$ otherwise, at least one storage element is too small. In the latter case, all initial levels $\ell \in \mathcal{D}$ the storage constraints are active within Problem (3.8). In other words, the production level to be set for the next production phase always deviates from the optimal level if $\mathcal{B}_j$ would be larger.

Next, we address the minimum size, which the smallest size D for which $\mathcal{A}_{\mathfrak{F}}$ is not empty. For this purpose, we choose again an initial level that has a maximum distance from the boundaries 0 and ${D_j}^{\alpha}$. In this way, we reduce the

degree of freedom and combine storage size design with the condition for the attractive region. For the minimum storage size $\underline{D}$ the requirement

$$\mathfrak{F}\left(\theta, \frac{\underline{D}}{2}\right) = 0, \quad \forall \theta \in \Theta \tag{5.6}$$

has to be fulfilled. Since $\mathfrak{F}$ implies the evaluation of two optimization problems, it is hard to solve this implicit equation directly. However, it follows from the definition of $\mathfrak{F}$ in (5.3) that the solution for the relaxed problem has to agree with Problem (5.1) for a sufficiently large D. This means that for such a D the storage constraints become active. The relationship between the optimal rates for a given $\theta \in \Theta$ and the storage size is described in (5.5). Hence the minimum storage size for ${\mathcal{B}_j}^{\alpha}$ can be calculated as follows

$${\underline{D}_j}^{\alpha} := \underset{\theta \in \Theta}{\text{maximize}} \quad 2\overline{\Delta}_\theta t \left|{\mathfrak{P}_{\mathrm{r}_j}}^{\alpha}(\theta)\right|. \tag{5.7}$$

In general, this optimization problem holds several challenges, especially if a gradient method is used. Firstly, the objective function is not twice continuously differentiable due to the absolute value of the rates. Secondly, the map ${\mathfrak{P}_{\mathrm{r}_j}}^{\alpha}$ again represents an optimization problem so that (5.7) describes a bilevel optimization.
For this reason, we will discuss how to reformulate Problem (5.7) in the next step. First, we will focus on the objective function. Although the optimal value for ${D_j}^{\alpha}$ (and thus the maximum absolute value of the storage rate) is of interest, it is initially sufficient to find θ where this occurs. The special structure of the objective function makes it possible to determine first

$${\hat{\theta}_j}^{\alpha} := \underset{\theta \in \Theta}{\arg\max} \quad \left|{\mathfrak{P}_{\mathrm{r}_j}}^{\alpha}(\theta)\right|.$$

From this, we can conclude for the storage size that

$${\underline{D}_j}^{\alpha} = 2\overline{\Delta}_\theta t \left|{\mathfrak{P}_{\mathrm{r}_j}}^{\alpha}\left({\hat{\theta}_j}^{\alpha}\right)\right|. \tag{5.8}$$

So the general idea is first to determine $\hat{\theta} \in \Theta$, which yields the highest rate, and calculate that rate afterward. Nevertheless, it is a bilevel optimization

problem of the form

$$\hat{\theta}_j^{\,\alpha} = \underset{\theta \in \Theta}{\arg\max} \quad \left|\rho_j^{\,\alpha}\left(x_\mathrm{s}, u_\mathrm{s}\right)\right| \tag{5.9a}$$

$$\text{subject to} \quad (c_\mathrm{s}, u_\mathrm{s}, x_\mathrm{s}) \in \underset{c,\,u,\,x}{\arg\max} \quad F(p, c, \theta, x), \tag{5.9b}$$

$$\text{subject to} \quad 0 = f\left(x, u\right), \tag{5.9c}$$

$$0 = c - h(x), \tag{5.9d}$$

$$0 \geq s\left(x, u\right), \tag{5.9e}$$

$$0 \geq \omega\left(x\right), \tag{5.9f}$$

$$x \in \mathcal{X},\ c \in \mathcal{C}_\mathrm{o},\ u \in \mathcal{U} \tag{5.9g}$$

where the lower-level optimization is identical with Problem (5.2). The upper-level optimization considers the storage rate of $\mathcal{B}_j^{\,\alpha}$ and is used to identify the feed quality $\hat{\theta}_j^{\,\alpha}$. A common approach to solve Problem (5.9) is to replace the lower-level optimization with its first-order optimality conditions, cf. [93]. In this way, the problem becomes a high-dimensional NLP whose decision variables are given by θ, and the variables of the relaxed problem and by the Lagrange multiplier resulting from the equation and inequality constraints. However, this approach has some drawbacks. Firstly, it is possible that the rate functions $\rho_j^{\,\alpha}$ are non-convex, which means we have to use a global solver to make a reliable prediction about the storage size. Secondly, we have to check the sufficient conditions for the solution afterward, because otherwise, it cannot be guaranteed that the solution is a profit-maximizing operating point.
For this reason, a derivative-free optimization is proposed, where the gradient of $\rho_j^{\,\alpha}$ and the constraints are not necessary, cf. [137]. In particular, we use a stochastic heuristic for a global optimizer, such as the genetic algorithm [101]. This allows us to approximate the global solution within Θ, but there is no method to measure the quality of the current optimal solution [181]. However, since we estimate the minimum storage size, the exact value is not crucial. This has practical reasons, e.g., a safety margin ζ is added to the storage size, or the size of the installed storage elements is only available in discrete steps.
As the bounded space Θ of the decision variable is always two-dimensional, the computational effort for searching in Θ is moderate, regardless of the production system $\mathcal{P}$. Furthermore, Problem (5.9) is solved offline before the system is started up so that the computational time is not a limiting factor.

The following algorithm describes the determination of the minimum storage size by means of a genetic algorithm, adapted from Ferentinos et al. [61]. For a

more detailed description of genetic algorithms, we refer to [234].

Algorithm 5.1: Determine the Minimum Storage Size

Input: the set Θ and the functions ${\mathfrak{P}_{\mathrm{r}_j}}^{\alpha}$

initialize a population $P_0 := \{\xi \in \Theta\}$ 1
for $j = 1, 2$ **do** 2
  for $\alpha = 1, \ldots, n_j$ **do** 3
    set generation index $i_{\mathrm{g}} = 0$ 4
    while $i_{\mathrm{g}} < \bar{i}_{\mathrm{g}}$ **do** 5
      evaluate fitness of all θ within population $P_{i_{\mathrm{g}}}$ using $\left|{\mathfrak{P}_{\mathrm{r}_j}}^{\alpha}(\theta)\right|$ 6
      choose the best elements according to their fitness 7
      perform crossover and mutation 8
      determine $P_{i_{\mathrm{g}}+1}$ using elements after crossover and mutation 9
      set the index $i_{\mathrm{g}} \leftarrow i_{\mathrm{g}} + 1$ 10
    end 11
    determine optimal ${\hat{\theta}_j}^{\alpha}$ using a genetic algorithm 12
    compute the storage size ${\underline{D}_j}^{\alpha}$ by (5.8) 13
  end 14
end 15

Result: the minimum storage size $\underline{D}$

To obtain the minimum size $\underline{D}$, each storage element of $\mathcal{B}_j$ has to be analyzed separately since each element has its maximum rate ${\mathfrak{P}_{\mathrm{r}_j}}^{\alpha}(\theta)$ at a different point in Θ. Note that the condition (5.6) must be fulfilled for a size $\underline{D}$, so the attractive region $\mathcal{A}_{\mathfrak{F}}$ contains at least one point. Figure 5.3 (a) illustrates the space $\mathcal{D}$ with minimum size $\underline{D}$ for a system with two storage elements resulting from Algorithm 5.1. For half-filled storage elements, the S-RTO yields the economically best possible operating point independent of the value θ affecting the system.

So far we have discussed the minimum size of $\mathcal{B}_j$. However, for $\ell \neq 0.5\underline{D}$, there might be values for θ, so that the optimal production level differs from that of the relaxed S-RTO since the storage constraints become active. The question arises of how the sizes ${D_j}^{\alpha} = {\underline{D}_j}^{\alpha} + {\hat{D}_j}^{\alpha}$ can be effectively increased by ${\hat{D}_j}^{\alpha} \in \mathbb{R}^+$ without oversizing $\mathcal{B}_j$. In this way, $\mathcal{A}_{\mathfrak{F}}$ is enlarged, as illustrated in Figure 5.3 (b). If ℓ is changed during unsteady operation, it is desirable that afterward, $\ell \in \mathcal{A}_{\mathfrak{F}}$ applies.
Assuming a symmetrical region and by using the minimum size ${\underline{D}_j}^{\alpha}$, the

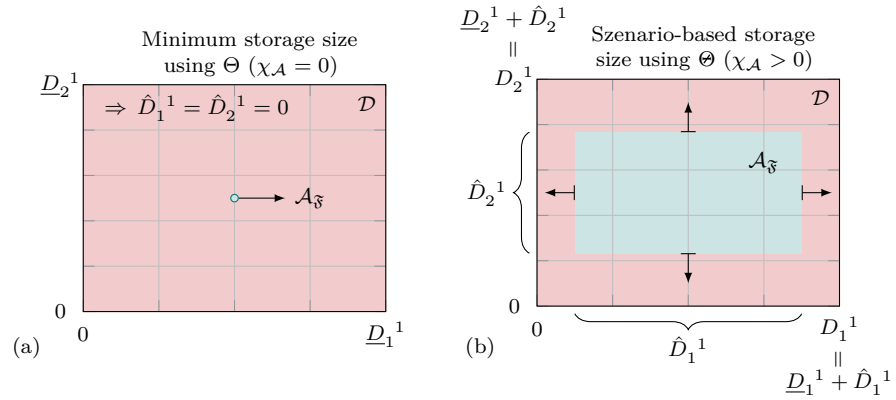

Figure 5.3: Illustration of the storage size design for a system of two storage elements.

attractive region region can also be described by

$$\mathcal{A}_{\mathfrak{F}} = \prod_{\alpha=1}^{n_1} \left[\underline{D}_1{}^{\alpha} - \frac{\hat{D}_1{}^{\alpha}}{2}, \underline{D}_1{}^{\alpha} + \frac{\hat{D}_1{}^{\alpha}}{2} \right] \times \prod_{\alpha=1}^{n_2} \left[\underline{D}_2{}^{\alpha} - \frac{\hat{D}_2{}^{\alpha}}{2}, \underline{D}_2{}^{\alpha} + \frac{\hat{D}_2{}^{\alpha}}{2} \right] \subset \mathcal{D}.$$

Furthermore, we define the attractive ratio $\chi_{\mathcal{A}}$ of entire storage system as follows

$$\chi_{\mathcal{A}} := \frac{\prod_{\alpha=1}^{n_1} \hat{D}_1{}^{\alpha} \prod_{\alpha=1}^{n_2} \hat{D}_2{}^{\alpha}}{\prod_{\alpha=1}^{n_1} D_1{}^{\alpha} \prod_{\alpha=1}^{n_2} D_2{}^{\alpha}} \in [0,\, 1)\,.$$

For the minimum size, we have an attractive ratio of $\chi_{\mathcal{A}} = 0$ because $\hat{D}_j{}^{\alpha} = 0$ holds, see Figure 5.3 (a). An enlargement of $\mathcal{A}_{\mathfrak{F}}$, and thus, an increase of $\chi_{\mathcal{A}}$, is associated with identifying a suitable $\hat{D}_j{}^{\alpha} \in \mathbb{R}^+$. This identification is achieved according to the $\emptyset \in \Theta$ scenarios that may occur. In the next section, we propose a technique for identifying $\hat{D}_j{}^{\alpha}$ using a stochatic description of the scenarios.

Example 5.1 (Minimum storage size for a coupled AD- and RSR-process (4.4 continued))**.** *So far, we have discussed the identification of new setpoints for the production based on feed parameters (see Example 3.1) and the transition to these setpoints (see Example 4.3). For this operational strategy, we will determine the minimum storage size using the space* Θ *and not any scenarios (e.g., as introduced in Example 2.5).*

As described above, we determine the minimum storage size based on the relaxed S-RTO, which was already discussed in Example 3.1 by the case (ii). It means, we have to determine the storage capacity such that for all $\theta \in \Theta$ and certain production time, no storage-based restrictions have to be considered when determining the optimal operating point. The length of this time horizon is assumed to be 1800 min *as given in Example 2.5.*
This example allows for the reformulation of the internal Problem in (5.9) *by the necessary conditions for the optimality of the NLP. Thus the bilevel optimization problem became a one-layer problem. Moreover, in the objective function, we also reformulate the absolute value by the square of the rate, which has no effect on the position of the optimal point but leads to a differentiable cost function. Thus, the resulting optimization problem to identify the feed parameter that yields the highest storage rate can be solved with gradient-based methods. Note, Algorithm 5.1 is more robust because it only requires the calculation of the objective function, but it is also more time consuming since many points must be evaluated.*
Similar to the other examples before, we use CasADi/ipopt with the Matlab frontend to solve the estimation problem. The estimation of storage capacity has to be done for each element individually, which means that two optimization problems have to be solved.

We start with the element ${\mathcal{B}_1}^1$, which holds the component C*, a byproduct of $\mathcal{S}_1$. Figure 5.4 shows the storage rate (in (a)) and the negative objective function over Θ (in (b)). The span for the storage rate ${\varrho_1}^1$ that applies at optimal production levels is given by $[-0.903, 1.312]$ and is encoded by the color gradient in Figure 5.4 (a). It can be concluded that for low substrate qualities θ^1 and*

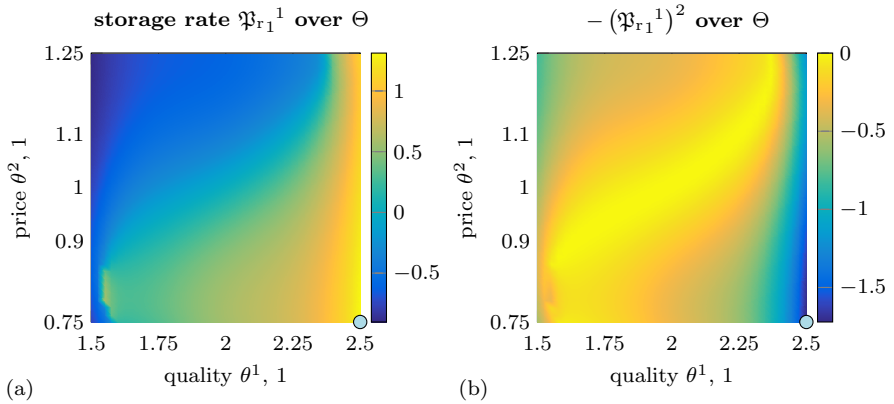

Figure 5.4: Storage rate for ${\mathcal{B}_1}^1$ and its negative square over Θ.

high prices θ^2, the storage ${\mathcal{B}_1}^1$ is preferably discharged. Indeed, under these conditions, $\mathcal{S}_2$ consumes less C *because the process is slowed down, but $\mathcal{S}_1$ also produces less* C *as it operates below nominal production. Conversely, both processes achieve a higher output at high substrate qualities and low prices, which yields an increased production and consumption of* C*. However, the effect of $\mathcal{S}_1$ is larger, so that the storage ${\mathcal{B}_1}^1$ is charged in the bottom right area of Θ, cf. Figure 5.4 (a). In Figure 5.4 (a) and (b), the value θ resulting in the highest rate during the production phase is marked by a blue dot at the bottom right corner of the graphs.*
For $\theta = (2.5, 0.75)$, the storage rate is ${\varrho_1}^1 = 1.312$, which implies that ${\mathcal{B}_1}^1$ is charged at this point. Using the maximum possible time period for which this feed parameter value is maintained, it follows that the storage level is changed by ${\ell_1}^1 = 2361.6\,\mathrm{mol}$. It follows that the minimum storage capacity, where the subset $\mathcal{A}_{\mathfrak{F}}$ exist is ${\underline{D}_1}^1 = 4.7232\,\mathrm{kmol}$.

Next, we analyze the element ${\mathcal{B}_2}^1$, which temporarily stores heat energy generated during the exothermic reaction in $\mathcal{S}_2$. Again, Figure 5.5 illustrates the storage rate (in (a)) and the negative objective for the estimation of the capacity over Θ (in (b)). For this element, the span of the storage rate ${\varrho_2}^1$ occurring at optimal production levels is given by $[-1.438, 0.953]$, as shown by the color gradient in Figure 5.5 (a). As for ${\mathcal{B}_1}^1$, the range of storage rates covers negative to positive values. Thus, at low substrate qualities and high prices, the element ${\mathcal{B}_2}^1$ is charged, and the storage level rises. This is because $\mathcal{S}_1$ requires less energy since it is economically more efficient to reduce production. The lower energy consumption is dominant, which can be observed from the fact that the storage is always charged independent of the price and thus of the production of $\mathcal{S}_2$.

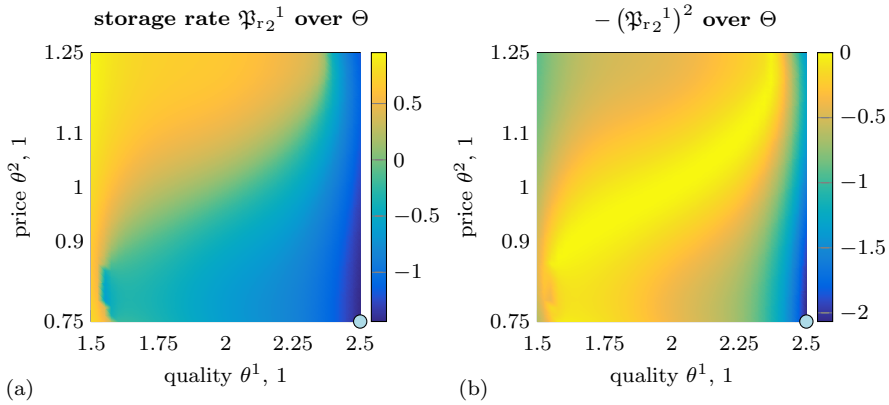

Figure 5.5: Storage rate for ${\mathcal{B}_2}^1$ and its negative square over Θ.

This result coincides with the behavior of the storage ${\mathcal{B}_1}^1$*. For high substrate qualities and low prices, the stored energy is reduced as both processes have a higher production output.*
The heat map also shows that this correlation is directly obvious. For instance, one could assume that the lowest rate would occur if the substrate quality and price were high. At this point, $\mathcal{S}_1$ *would probably need the most energy, and* $\mathcal{S}_2$ *would supply the least, as it is slowed down to a lower level. Nevertheless, additional factors (e.g., downstream process constraints) ensure that the production levels cannot be set independently of each other, even if the storage levels can be neglected for the relaxed case.*
In Figure 5.4, the feed parameter, which yields the highest absolute value of the rate for a production phase, is marked as a blue dot. Again, this value is at $\theta = (2.5,\, 0.75)$*, where the storage rate is* ${\varrho_2}^1 = -1.438$*, and* ${\mathcal{B}_2}^1$ *is discharged at this point. Using the maximum possible time period yields a change of the storage level by* ${\ell_2}^1 = -2588.4\,\mathrm{kJ}$*. Finally, the minimum storage capacity, where the subset* $\mathcal{A}_{\mathfrak{F}}$ *exist is* ${\underline{D}_2}^1 = 5177\,\mathrm{kJ}$*.*

5.4 Scenario-Based Storage Size

In the previous section, the minimum storage size was determined for which the storage constraints do not lower the economic outcome. It guarantees that there exists one point in the feed parameter space, for which the storage constraints will not be active when starting with storage levels at half of the minimum storage size. This minimum storage size $\underline{D}$ is independent of the feed parameter changes. In this section, we take the feed parameter changes into account by considering a probabilistic formulation of the scenarios. We calculate the necessary additional storage size $\hat{D}$ by which $\underline{D}$ must be increased to guarantee the optimal operation of the overall production system with a predefined probability for a specific time span called the design horizon. In other words, the goal of this section is to design the size ${D_j}^\alpha = {\underline{D}_j}^\alpha + {\hat{D}_j}^\alpha$ of the storage elements such that the image of the trajectory $\ell : \mathbb{R}^+ \to \mathcal{D}$ lies with high probability within $\mathcal{A}_{\mathfrak{F}}$.

Considering Definition 2.14, the set Θ of possible scenarios can be characterized by means of the tuples $\hat{\theta}$ for the feed parameters and T_θ of corresponding time horizons. The main idea of the process design is described in Figure 5.6. The storage size is defined before the production system starts operation. Since the feed parameter changes during the production are, in general, not entirely known in the planning phase, we propose a stochastic description of these. For this, two options on how to proceed in the following can be posed. First, a signal of feed parameters known from the past can be analyzed, and general properties

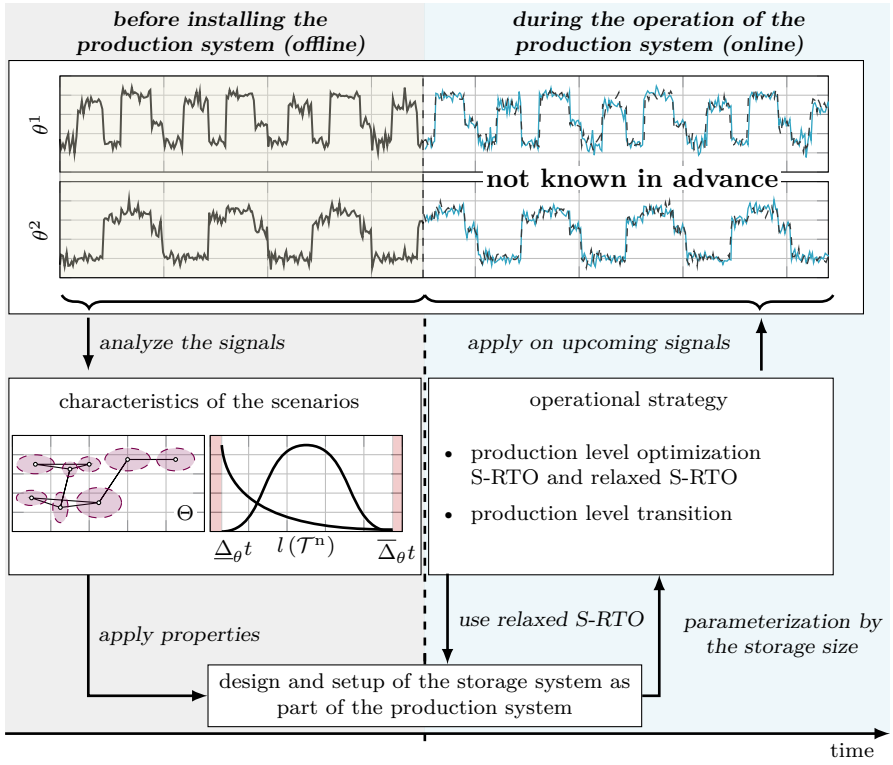

Figure 5.6: Overview of scenario-based storage size estimation.

can be derived, cf. gray box on the left side in Figure 5.6. These properties are defined by probability density functions (pdfs) for the duration of constant feed parameters and the preferred subsets in Θ at certain times. Second, assumptions can be made directly about the pdfs to describe the scenarios. In this way, we can describe the future behavior of feed parameter changes. These properties and the realxed S-RTO in Problem (5.2) are used to design the storage system, cf. Figure 5.6. The proposed storage size parametrizes the S-RTO Problem (3.8) and the transition Problem (4.9) for the online operation of the system, as indicated in Figure 5.6.

In the following, we assume that the characteristic properties describing the scenarios include a nominal trajectory within Θ, combined with a random deviation around it. Based on (2.20), we further assume that a scenario is composed by two signals given by

$$\boldsymbol{\theta}(t) = \boldsymbol{\theta}^{\mathrm{n}}(t) + \boldsymbol{\theta}^{\mathrm{r}}(t), \tag{5.10}$$

where

$$\theta^{\mathrm{n}}(t) := \sum_{k=0}^{n_\theta} \hat{\theta}^{\mathrm{n}}{}_k \, \mathbb{1}_{\mathcal{T}_\theta^{\mathrm{n}}{}_k}(t),$$

is called the nominal scenario and

$$\theta^{\mathrm{r}}(t) := \sum_{k=0}^{n_\theta} \sum_{l=0}^{m_k} \hat{\theta}^{\mathrm{r}}{}_{kl} \, \mathbb{1}_{\mathcal{T}_\theta^{\mathrm{r}}{}_{kl}}(t),$$

the random scenario. For the disjoint time spans $\mathcal{T}_\theta^{\mathrm{r}}{}_{kl}$ holds that for all $\mathcal{T}_\theta^{\mathrm{n}}{}_k$ it exists $m_k \in \mathbb{N}$ such that

$$\mathcal{T}_\theta^{\mathrm{n}}{}_k := \bigcup_{l=0}^{m_k} \mathcal{T}_\theta^{\mathrm{r}}{}_{kl}. \tag{5.11}$$

We call $\mathcal{T}_\theta^{\mathrm{n}}{}_k$ the k-th season of a scenario. It describes long time periods where the feed parameter changes around a certain mean $\hat{\theta}^{\mathrm{n}}{}_k$. As given in (2.21), the length of the time horizons is specified by a lower and upper bound. Thus, from the definition of the season $\mathcal{T}_\theta^{\mathrm{n}}{}_k$ it follows that for its length $l\left(\mathcal{T}_\theta^{\mathrm{n}}{}_k\right) \geq \underline{\Delta}_\theta t$ holds. As the feed parameter change can occur at any time, we state that the length $l\left(\mathcal{T}_\theta^{\mathrm{r}}{}_{kl}\right)$ of the time span is a continuous random variable described by an aribitary pdf $p_{\mathrm{t}} : \left[\underline{\Delta}_\theta t, \overline{\Delta}_\theta t\right] \to \mathbb{R}^+$. However, we assume that $\hat{\theta}^{\mathrm{r}}{}_{kl}$ are Gaussian distributed random variables $\hat{\theta}^{\mathrm{r}}{}_{kl} \sim \mathcal{N}\left(0, P^{\mathrm{n}}{}_k\right)$, where the covariance $P^{\mathrm{n}}{}_k \in \mathbb{R}^{2,2}$ is piecewise constant and changes with the seasons $\mathcal{T}_\theta^{\mathrm{n}}{}_k$.

Remark 5.3. *Even if the production system consists of two independent processes, it is possible that the two feed parameter correlate with each other.*

A production change – based on the operational strategy intervention – should only occurs if the subsequent production phase is maintained for at least the time $\underline{\Delta}_{\mathrm{s}} \in \mathbb{R}^+$. This condition and the fact that the scenario indicates a particular system's operation means that only those scenarios are used for which the lower bound $\underline{\Delta}_\theta t \in \mathbb{R}^+$ fulfills the condition

$$\underline{\Delta}_\theta t \geq \sup \mathfrak{T}_{\mathrm{t}}^{\mathrm{e}} + \underline{\Delta}_{\mathrm{s}}.$$

Here, $\mathfrak{T}_{\mathrm{t}}^{\mathrm{e}}$ represents the transition-time map defined in (2.23).

Considering the feed parameter changes as described through (5.10), it can be deduced that the elements $\mathcal{B}_j{}^{\alpha}$ have to be charged and discharged alternately for a feasible operation. This requirement avoids that the elements are permanently full or empty after a certain time, as there is no direct level control. The following definition specifies this aspect. A key aspect to the success of a dynamic operational strategy is a frequent change in sign of the storage rates, which has not been addressed so far and is described in the following definition.

Definition 5.1 (Feasibility for Dynamic Operation)**.** *Given are a well-designed production system $\mathcal{P}$ with a strictly positive attractive ratio $\chi_{\mathcal{A}} > 0$, the set Θ of all feed parameters and the functions ${\mathfrak{P}_{\mathrm{r}_j}}^{\alpha}$ as defined by* (5.4)*. The system $\mathcal{P}$ is said to be feasible for dynamic operation under the relaxed S-RTO, if for each element ${\mathcal{B}_j}^{\alpha}$ there exist two real numbers ${\underline{\xi}_j}^{\alpha} \in \mathbb{R}^+$ and ${\overline{\xi}_j}^{\alpha} \in \mathbb{R}^+$ such that*

$$ {\mathfrak{P}_{\mathrm{r}_j}}^{\alpha}(\Theta) = \left[-{\underline{\xi}_j}^{\alpha},\ {\overline{\xi}_j}^{\alpha} \right]. $$

The system $\mathcal{P}$ needs to be feasible for dynamic operation, otherwise the elements ${\mathcal{B}_j}^{\alpha}$ can only be charged or discharged within Θ. In other words, the operational strategy (i.e., cl S-RTO) defined in Chapters 3 and 4 causes strongly connected processes in the long term according to Definition 2.3. For instance, if only for one element applies that ${\mathfrak{P}_{\mathrm{r}_j}}^{\alpha}(\theta) > 0$ or ${\mathfrak{P}_{\mathrm{r}_j}}^{\alpha} < 0$, $\forall \theta \in \Theta$, then its initial level cannot be reset without leaving $\mathcal{A}_{\mathfrak{F}}$. We rely on the following assumptions to ensure that our proposed operational strategy is applicable.

Assumption 5.1. *The system $\mathcal{P}$ is well-designed with an attractive ratio $\chi_{\mathcal{A}} > 0$ and is feasible for dynamic operation.*

In order to determine if a system fulfills Assumption 5.1, we refer to the analysis of Θ described in Appendix B.2. There we propose a technique to classify Θ according to the signs of the storage rates.
Another aspect resulting from a given scenario is introduced in the next definition.

Definition 5.2 (Self-Regulation of the Storage System)**.** *Let $\mathcal{P}$ be a production system with a non-empty attractive region $\mathcal{A}_{\mathfrak{F}}$. Assume that the transition time to reach the optimal production level $c \in \mathcal{C}_{\mathrm{o}}$ given by the relaxed S-RTO Problem* (5.2) *is zero. For each element ${\mathcal{B}_j}^{\alpha}$ and for a given time span $[0, T_{\max}]$, the self-regulating factor with respect to a certain scenario $\boldsymbol{\theta} \in \boldsymbol{\Theta}$ is defined by the integral*

$$ {\mathfrak{s}_j}^{\alpha}(\boldsymbol{\theta}) := \int_0^{T_{\max}} \left({\mathfrak{P}_{\mathrm{r}_j}}^{\alpha} \circ \boldsymbol{\theta} \right)(t) \mathrm{d}t. \tag{5.12} $$

We call ${\mathcal{B}_j}^{\alpha}$ self-regulating with respect to the scenario $\boldsymbol{\theta}$ and $T_{\max} \in \mathbb{R}^+$, iff ${\mathfrak{s}_j}^{\alpha}(\boldsymbol{\theta}) = 0$ and otherwise not self-regulating with grade ${\mathfrak{s}_j}^{\alpha}(\boldsymbol{\theta})$.

The self-regulating factor describes the change of the storage level along a sequence of feed parameter changes and is highly dependent on the scenario $\boldsymbol{\theta}$. For instance, the storage level at time $T_{\max}$ is given by $\mathit{l}(T_{\max}) = \mathit{l}(0) + {\mathfrak{s}_j}^{\alpha}(\boldsymbol{\theta})$. The assumption within Definition 5.2 is no direct restriction for self-regulation

if the length of the production phase is much longer than the transition phase. Otherwise, the transition time and the size of the terminal region within $\mathcal{D}$ for the transition has to be included.
Since we only consider special types of scenarios given by piecewise constant functions (i.e., (5.10)), (5.12) can also be formulated as series. Deploying the nominal scenario in (5.12), the self-regulating factor reads

$$\mathfrak{s}_j{}^{\alpha}\left(\boldsymbol{\theta}^{\mathrm{n}}\right) = \sum_{k=1}^{n_\theta} l\left(\mathcal{T}_{\theta}^{\mathrm{n}}{}_k\right) \mathfrak{P}_{\mathrm{r}}{}_j{}^{\alpha}\left(\hat{\theta}^{\mathrm{n}}{}_k\right). \tag{5.13}$$

This nominal self-regulation factor (5.13) is generally not equal to that one calculated by averaging Monte Carlo simulations for different realizations of $\mathcal{T}_{\theta}^{\mathrm{r}}{}_{kl}$ and $\hat{\theta}^{\mathrm{r}}{}_{kl}$. However, we use it as an approximation to describe the following concepts. Later in this section, we show that the mean of the self-regulating factor is obtained by employing the scenario-based storage design.

The storage size needs to be designed according to a design horizon $\Delta_{\mathrm{d}} \in \mathbb{R}^+$ for which the storage level has to stay within $\mathcal{A}_{\mathfrak{F}}$ with a certain probability. For this horizon, the probability distribution around the nominal trajectory and thus about the preference of certain regions within Θ needs to be known. The design horizon Δ_{d} is characterized by the nominal scenario $\boldsymbol{\theta}^{\mathrm{n}}$ and, thus, by the upper bound $\overline{\Delta}_{\theta} t$. More precisely, the longer a given feed parameter value remains constant, the larger the storage elements need to be to avoid additional disturbance from an operational change.

Next, we focus on the nominal scenario $\boldsymbol{\theta}^{\mathrm{n}}$, which is uniquely determined by the tupels $\hat{\theta}^{\mathrm{n}}$ and $\mathcal{T}^{\mathrm{n}}$. Moreover, the tuple $\hat{\theta}^{\mathrm{n}}$ is restricted by demanding that there exists an $\bar{n}_\theta \in \mathbb{N}$, called cycle length, so that for all components $\hat{\theta}^{\mathrm{n}}{}_k$ holds $\hat{\theta}^{\mathrm{n}}{}_k = \hat{\theta}^{\mathrm{n}}{}_{k+\bar{n}_\theta}$ and $P^{\mathrm{n}}{}_k = P^{\mathrm{n}}{}_{k+\bar{n}_\theta}$. Using this cyclic property, the concept of a sequence is introduced, which describes the order of transitions. A sequence is defined by the feed parameters that occur within a longer time period starting at $\hat{\theta}^{\mathrm{n}}{}_k$. In general, we write for a sequence that starts at $\hat{\theta}^{\mathrm{n}}{}_k$ and has the length $\bar{n}_\theta$

$$\underbrace{\hat{\theta}^{\mathrm{n}}{}_k \mapsto \hat{\theta}^{\mathrm{n}}{}_{k+1} \mapsto \ldots \mapsto \hat{\theta}^{\mathrm{n}}{}_{k+\bar{n}_\theta-1}}_{=} \mapsto \hat{\theta}^{\mathrm{n}}{}_{k+\bar{n}_\theta}.$$

The resulting nominal trajectory is closed as illustrated in Figure 5.7 (a) by the red line for $\bar{n}_\theta = 3$. The trajectory in this example goes through several subsets of Θ that are elements of a partition Π. This partition describes if the storage elements are charged (+) or discharged (-). A more detailed explanation of how to obtain this partition and the separating curves (displayed in solid black line)

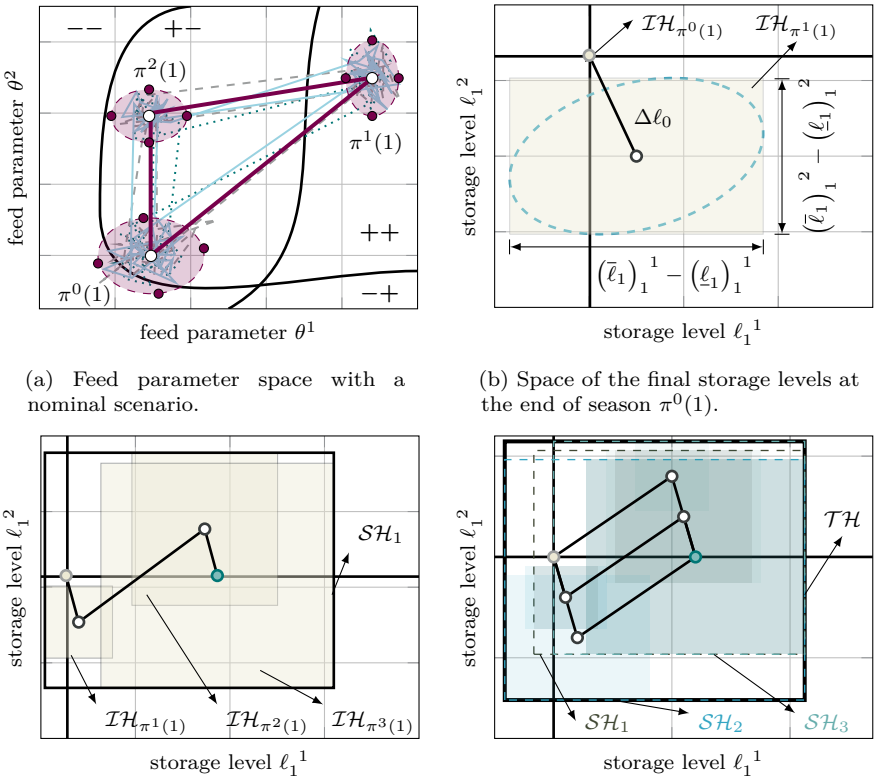

(a) Feed parameter space with a nominal scenario.

(b) Space of the final storage levels at the end of season $\pi^0(1)$.

(c) Space of the final storage levels at the end of one cycle starting with $\pi^0(1)$.

(d) Space of the final storage levels at the end of one cycle after varying all initial seasons.

Figure 5.7: Schematic representation of scenario-based storage sizing.

is given in Appendix B.2.

For the sake of simplicity, we set $k = 1$ and use the brief notation $1 \mapsto \ldots \mapsto \bar{n}_\theta \mapsto 1$ for the sequence using the indices. Based on this sequence, we define a cyclic permutation given by the $\bar{n}_\theta$-cycle $(1 \ldots \bar{n}_\theta)$, see [141]. We will need this permutation later to make the estimation method independent of the initial feed parameter. For reasons of readability, the cyclic permutation is represented in a compact fashion by the permutation map

$$\pi : \{1, \ldots, \bar{n}_\theta\} \to \{1, \ldots, \bar{n}_\theta\},$$

where $\pi := (1 \ldots \bar{n}_\theta)$. For the n-times composition of π we can write

$$\pi^n := \underbrace{\pi \circ \ldots \circ \pi}_{n\text{-times}}.$$

Furthermore, it applies that $\pi^0(i) := i$. Due to the definition of π, it is easy to see that $\pi^{\bar{n}_\theta+1} = \pi$. Using π, a new sequence can be determined by rotating the initial feed parameters. In total, there are $\bar{n}_\theta$ sequences, where the k-th element starting at i is given by $\pi^k(i)$.

Example 5.2. *Consider a scenario with three feed parameters as mean $\boldsymbol{\theta}^{\mathrm{n}}$ for $\boldsymbol{\theta}$ corresponding to the sequence $1 \mapsto 2 \mapsto 3 \mapsto 1$. This means that if we start at feed parameter 1, we go to 2 and then to 3 and finally back to 1. For the permutation map we obtain $\pi := (1\,2\,3)$ such that $\pi(1) = 2$, $\pi(2) = 3$ and $\pi(3) = 1$. A 2-times composition yiels $\pi^2(1) = 3$, $\pi^2(2) = 1$ and $\pi^2(3) = 2$. That means, if we start now with the feed parameter 3, it goes next to 1, then to 2 and finally back to 3.*

Next, we consider the tuple $\mathcal{T}^{\mathrm{n}}$, whose components are time intervals of the seasons with varying lengths. In contrary to $\hat{\theta}^{\mathrm{n}}{}_k$, the lengths of the seasons are not periodic, i.e. $l\left(\mathcal{T}^{\mathrm{n}}_k\right) \neq l\left(\mathcal{T}^{\mathrm{n}}_{k+\bar{n}_\theta}\right)$. This is due to the fact of (5.11) and that the length of each time horizon is determined by a pdf f_{T}. The season length is calculated according to (5.11) as the sum of the individual lengths of the respective time periods $\mathcal{T}^{\mathrm{r}}_{\theta\,kl}$. Considering the distributions of the lengths $l\left(\mathcal{T}^{\mathrm{r}}_{\theta\,kl}\right)$, the distribution $\boldsymbol{p}_{\mathrm{s},k}$ of the k-th season length is obtained by convolution of $\boldsymbol{p}_{\mathrm{t}}$, see [127, 128]. Since the number m_k of time subhorizons can vary with each cycle, we assume that there is an average number $\bar{m}_k \in \mathbb{N}$ of production changes for each season. In this way, the number of convolutions to derive the distribution $\boldsymbol{p}_{\mathrm{s},k}$ is determined through $\boldsymbol{p}_{\mathrm{s},k} := \underbrace{\boldsymbol{p}_{\mathrm{t}} * \ldots * \boldsymbol{p}_{\mathrm{t}}}_{\bar{m}_k\text{-times}}$.
Based on $\boldsymbol{p}_{\mathrm{s},k}$ we introduce a characteristic length $\Delta t_{\mathrm{s},k}$ of the k-th season, with $\bar{m}_k \underline{\Delta}_\theta t \leq \Delta t_{\mathrm{s},k} \leq \bar{m}_k \overline{\Delta}_\theta t$. According to the specification for the storage estimation and the information about $\boldsymbol{p}_{\mathrm{t}}$ this length can be given e.g. by the mean of $\boldsymbol{p}_{\mathrm{s},k}$ or by the upper bound of the interval. For $\bar{n}_\theta$ seasons, the design horizon can be determined by

$$\Delta_{\mathrm{d}} := z \sum_{k=1}^{\bar{n}_\theta} \Delta t_{\mathrm{s},k},$$

where $z \in \mathbb{N}$ indicates the number of repetitions of the cycles to be addressed.

Finally, we will discuss the determination of the storage capacity based on $\boldsymbol{\theta}^{\mathrm{n}}$. The basic idea is – starting from an initial storage level – to determine the box constrained region where the time evolution of the storage level ℓ

occurs with a certain probability and over a certain time period. Since we are only interested in the box size, it is assumed that the initial storage level is $\ell(0) = \ell_0 = 0$. The considered design horizon Δ_d, has a direct effect on the box size. We propose to use $z \geq 1$ to determine Δ_d, depending on the individual season lengths. In this way, it is necessary to find a trade-off between the time period in which economically optimal production levels are guaranteed and the related investment costs of the storage elements. In case the system is self-regulating ($\left(\mathfrak{s}_j{}^{\alpha}(\boldsymbol{\theta}^\mathrm{n}) = 0\right)$) or can be brought to self-regulation by varying the system parameters, the problem simplifies, such that $z = 1$.

Let us return to the design process and consider a given nominal scenario $\boldsymbol{\theta}^\mathrm{n}$. This is fully described by the individual mean values $\hat{\theta}^\mathrm{n}{}_k$, the corresponding covariances $P^\mathrm{n}{}_k$ and the average number $\bar{m}_k$ of production changes per season k. The evolution of the storage level within each season is determined by $\mathfrak{P}_{\mathrm{r}\,j}{}^{\alpha}$ and those feed parameters that live around the mean during that season. Based on the assumption of a Gaussian distribution for the feed parameters within each season, we can determine the mean rate constant within a season. Moreover, we consider the storage level only at the end of each season, i.e., at discrete time steps. Starting in the i-th season, the mean values of the storage levels of each element at the end of season $\pi^k(i)$ are given by

$$\left(\ell_{k+1}\right)_j{}^{\alpha} = \ell_j{}^{\alpha}\left(\sum_{l=0}^{k} \Delta t_{\mathrm{s},\pi^l(i)}\right) = \left(\ell_k\right)_j{}^{\alpha} + \left(\Delta\ell_k\right)_j{}^{\alpha}, \tag{5.14}$$

where the means of the level change are calculated by

$$\left(\Delta\ell_k\right)_j{}^{\alpha} := \Delta t_{\mathrm{s},\pi^k(i)} M\left[\mathfrak{P}_{\mathrm{r}\,j}{}^{\alpha}\right]\left(\hat{\theta}^\mathrm{n}{}_{\pi^k(i)}, P^\mathrm{n}{}_{\pi^k(i)}\right).$$

Here, $M[\mathfrak{P}_{\mathrm{r}\,j}{}^{\alpha}]$ is the mean function of the unscented transformation applied on the storage rate $\mathfrak{P}_{\mathrm{r}\,j}{}^{\alpha}$, which is introduced in (A.7), see Appendix A.4. By Definition 5.2, a storage element is called average self-regulating, if $\left(\ell_{\bar{n}_\theta}\right)_j{}^{\alpha} = 0$.

Remark 5.4. *From the definition of the mean function follows that*

$$\Delta t_{\mathrm{s},\pi^k(i)} M\left[\mathfrak{P}_{\mathrm{r}\,j}{}^{\alpha}\right] = M\left[\Delta t_{\mathrm{s},\pi^k(i)}\, \mathfrak{P}_{\mathrm{r}\,j}{}^{\alpha}\right].$$

Therefore it is not important to determine the average rate and then the average storage change or if the latter is determined directly.

To estimate the size of $\mathcal{B}_j{}^{\alpha}$, however, not only the final storage level is of interest, but all possible intermediate levels. The function $V[\cdot]$ for the standard deviation in (A.8) of the unscented transformation offers a useful tool for estimating this region. From this, the storage size can be described by a (total) hypercube

$\mathcal{TH} \subset \mathbb{R}^{n_{\mathcal{B}}}$, which is the smallest axis-parallel outer envelope of the covariance ellipsoid around the mean value determined by $M[\cdot]$, see [23]. The dimension of $\mathcal{TH}$ is identical to the number of storage elements. In general, we require that the evolution of the storage level has to stay with a certain probability within $\mathcal{TH}$ during the time horizon $[0,\, \Delta_{\mathrm{d}}]$. In other words, the task of estimating the storage capacity is determined by the following problem.

Problem 5.1 (Estimation of the storage size)**.** *Let $\mathcal{P}$ be a production system with the profit function F and let $\boldsymbol{\theta} \in \boldsymbol{\Theta}$ be a scenario for the feed parameter. For a given probability p_{set} and design horizon $[0,\, \Delta_{\mathrm{d}}]$, find the smallest hypercube $\mathcal{TH}$ such that for the probability holds*

$$P\big(\mathcal{l}(t) \in \mathcal{TH}\big) > p_{\mathrm{set}}, \quad \forall t \in [0,\, \Delta_{\mathrm{d}}]\,,$$

where $\mathcal{l}(0) = 0 \in \mathbb{R}^{n_{\mathcal{B}}}$.

Remark 5.5. *It should be noted that Problem 5.1 is formulated for a general scenario, but in the following, we focus on the scenarios given by* (5.10)*.*

The hypercube $\mathcal{TH}$ is specified by its boundaries through

$$\mathcal{TH} := \Big[\underline{b}_{\mathrm{t}},\, \overline{b}_{\mathrm{t}}\Big],$$

where the lower and the upper bound $\underline{b}_{\mathrm{t}} \in \mathbb{R}^{n_{\mathcal{B}}}$ and $\overline{b}_{\mathrm{t}} \in \mathbb{R}^{n_{\mathcal{B}}}$ are constructed componentwise by analyzing the effect of the nominal scenario $\boldsymbol{\theta}^{\mathrm{n}}$ on the optimal storage rates. For this purpose, we consider the set of initial values from which a level change in the $\pi^k(i)$-th season starts through

$$\mathcal{IH}_{\pi^k(i)} := \big[\underline{\ell}_k,\, \overline{\ell}_k\big]\,.$$

Since the storage level is known when the storage systems $\mathcal{B}_j$ are started up, it can be stated that $\underline{\ell}_0 = \overline{\ell}_0 = 0$. To obtain the individual boundaries, we use the unscented transformation introduced in Appendix A.4. In addition to the mean function (A.7), the variance function (A.8) plays an important role, because it can be used to describe a confidence interval for each storage element containing the initial values for the next season. The boundaries of $\mathcal{IH}_{\pi^k(i)}$ at the end of season $\pi^k(i)$ are determined by the distribution of the storage level at that time. More precisely, the boundaries are obtained from the sum of the mean values and the variance up to this season. Finally, we write

$$\big(\underline{\ell}_{k+1}\big)_j^{\,\alpha} = \big(\ell_{k+1}\big)_j^{\,\alpha} - Z_{p_{\mathrm{set}}}\big(S_{k+1}\big)_j^{\,\alpha}, \tag{5.15a}$$

$$\big(\overline{\ell}_{k+1}\big)_j^{\,\alpha} = \big(\ell_{k+1}\big)_j^{\,\alpha} + Z_{p_{\mathrm{set}}}\big(S_{k+1}\big)_j^{\,\alpha}, \tag{5.15b}$$

where the mean of the storage level at the end of season $\pi^k(i)$ is given by (5.14), and its standard deviation is calculated by

$$\left(S_{k+1}\right)_j^{\ \alpha} = \sqrt{\sum_{l=0}^{k} V\left[\Delta t_{\mathrm{s},\pi^l(i)}\, \mathfrak{P}_{\mathrm{r}\,j}{}^{\alpha}\right]\left(\hat{\theta}^{\mathrm{n}}{}_{\pi^l(i)}, P^{\mathrm{n}}{}_{\pi^l(i)}\right)}. \tag{5.16}$$

Here, the parameter $Z_{p_{\mathrm{set}}} \in \mathbb{R}^+$ is used to scale the standard deviation to the desired probability level p_{set} as specified in Problem 5.1. The function we use to calculate the variance by the unscented transformation is the rate multiplied with the corresponding time, i.e., this function yields the storage level change directly.

Remark 5.6. *Using the unscented transformation, the distribution of the storage level change is approximated by a Gaussian distribution from that one of the feed parameters by determining the mean value, and the variance for each element. The sum of the individual storage level changes is again a random variable. Hence, their distribution at any discrete time is given by the convolution of the individual distributions. However, since these are Gaussian random variables, their sum is again a Gaussian distribution in which the parameters (mean and variance) result from the sum of the individual distribution parameters. Indeed, it is necessary to validate this approximation for a given system and to evaluate the error that may occur. In general, this is not systematically possible due to the nature of the functions* $\mathfrak{P}_{\mathrm{r}\,j}{}^{\alpha}$.

In Figure 5.7 (b) the evolution of the hypercube of the initial values is illustrated using a system with two storage elements. Starting from the zero level, the storage levels at the end of season $1 = \pi^0(1)$ or at the beginning of season $2 = \pi^1(1)$ are located in the ochre rectangle. The length of the edges results from the difference between the upper and lower boundaries $\mathcal{IH}_{\pi^k(i)}$.
Considering (5.15), the boundaries at the end of each season depend on the season i, from which the cycle begins, and the individual seasons (numbered by the index k), which successively contribute to the storage level change. After a certain number z of cycle repetitions has been completed, the traversed region can be determined componentwise by analyzing the minimum and maximum boundary values. In this way, the seasonal hypercubes $\mathcal{SH}_i$ can be defined, where i indicates that it was started in season i. Figure 5.7 (c) illustrates this process and also the corresponding region after one cycle ($z = 1$). The black line in Figure 5.7 (c) indicates the evolution of the mean of the storage level. The final level (green dot) for $\mathcal{B}_1{}^1$ is higher than the initial level, which means that this element is not self-regulating, and the level will increase on average. In contrast, $\mathcal{B}_1{}^2$ has reached the initial level after one cycle, making it self-regulating.

Finally we have to go through all possible seasons as initial point to make the result independent of the initial feed parameter of the path. This procedure is shown in Figure 5.7 (d). Again, the black lines indicate the evolution of the mean of the storage level starting at different seasons. The final level (green dot) is independent of the initial season. The lower and the upper bound $\underline{b}_{\mathrm{t}} \in \mathbb{R}^{n_{\mathscr{B}}}$ and $\overline{b}_{\mathrm{t}} \in \mathbb{R}^{n_{\mathscr{B}}}$ is obtained by analyzing the minimum and maximum boundary values over all seasonal hypercube $\mathcal{SH}_i$. It follows that the total hypercube $\mathcal{TH}$ is the smallest hypercube that encloses all $\mathcal{SH}_i$. The following algorithm describes the construction of the $\mathcal{SH}_i$ and $\mathcal{TH}$.

Algorithm 5.2: Obtain smallest axis-parallel hypercube

Input: the tupels $\hat{\theta}^{\mathrm{n}}$ and P^{n}, a probability p_{set} and a design horizon by a number z of repetitions

initialize the set ${B_{\mathrm{t}}}_j{}^{\alpha} := \emptyset$ of total boundaries,
determine $Z_{p_{\mathrm{set}}}$ from p_{set} by lookup tables or integration,
for $i = 1, \ldots, \bar{n}_\theta$ **do**
  initialize the set ${B_{\mathrm{l}}}_j{}^{\alpha} := \emptyset$ of local boundaries
  for $k = 1, \ldots, z\bar{n}_\theta$ **do**
    compute $\mathcal{IH}_{\pi^k(i)}$ using (5.15),
    update ${B_{\mathrm{l}}}_j{}^{\alpha} = {B_{\mathrm{l}}}_j{}^{\alpha} \cup \left\{ {(\underline{\ell}_k)}_j{}^{\alpha},\ {(\overline{\ell}_k)}_j{}^{\alpha} \right\}$
  end
  calculate ${\underline{b}_{\mathrm{l}}}_j{}^{\alpha} := \min\ \left({B_{\mathrm{l}}}_j{}^{\alpha}\right)$ and ${\overline{b}_{\mathrm{l}}}_j{}^{\alpha} := \max\ \left({B_{\mathrm{l}}}_j{}^{\alpha}\right)$ and
  define the seasonal hypercube $\mathcal{SH}_i := \left[\underline{b}_{\mathrm{l}},\ \overline{b}_{\mathrm{l}}\right]$
  update ${B_{\mathrm{t}}}_j{}^{\alpha} = {B_{\mathrm{t}}}_j{}^{\alpha} \cup \left\{ {\underline{b}_{\mathrm{l}}}_j{}^{\alpha},\ {\overline{b}_{\mathrm{l}}}_j{}^{\alpha} \right\}$
end
calculate ${\underline{b}_{\mathrm{t}}}_j{}^{\alpha} := \min\ \left({B_{\mathrm{t}}}_j{}^{\alpha}\right)$ and ${\overline{b}_{\mathrm{t}}}_j{}^{\alpha} := \max\ \left({B_{\mathrm{t}}}_j{}^{\alpha}\right)$ and
define the total hypercube $\mathcal{TH} := \left[\underline{b}_{\mathrm{t}},\ \overline{b}_{\mathrm{t}}\right]$

Result: the total hypercube $\mathcal{TH}$ with the lower and upper bound $\underline{b}_{\mathrm{t}}$ and $\overline{b}_{\mathrm{t}}$

Finally, we can update the minimum storage capacity derived in Section 5.3 by the additional space of the total hypercube $\mathcal{TH}$. However, the boundaries $\underline{b}_{\mathrm{t}}$ and $\overline{b}_{\mathrm{t}}$ do not necessarily have to be symmetrical, so our approach to calculate the additional scenario-based capacities is given by

$$ {D_{\boldsymbol{\theta}}}_j{}^{\alpha} := 2 \max\ \left(\left| {\underline{b}_{\mathrm{t}}}_j{}^{\alpha} \right|, \left| {\overline{b}_{\mathrm{t}}}_j{}^{\alpha} \right| \right). \tag{5.17} $$

This yields for the entire storage capacity

$$ {D}_j{}^{\alpha} = {\underline{D}}_j{}^{\alpha} + {D_{\boldsymbol{\theta}}}_j{}^{\alpha}. \tag{5.18} $$

The hypercube within $\mathcal{D}$, which is symmetrically located around the center and has the corner length $D_{\hat{\theta}}$, describes the subset $\mathcal{A}_{\mathfrak{F}}$.

Remark 5.7. *The additional scenario-based capacity $D_{\hat{\theta}}$ is one candidate for a suitable $\hat{D}$ introduced in Section 5.3.*

Example 5.3 (Storage size for a coupled AD- and RSR-process (B.2 continued))**.** *In the following we want to estimate the capacity of the storage and thus $\mathcal{A}_{\mathfrak{F}}$ based on certain scenario characteristics. For this purpose, we use the scenario already introduced in Example 2.5 and extend it according to the approach described in this section given in* (5.10)*. The key idea is that, even though we do not know exactly which feed parameter will be set at which time, we can describe the scenarios by probability distributions. With this additional structure for the set Θ of scenarios, we perform the estimation of the storage capacity on a subset of Θ, which still contains infinite functions.*

In this context, we describe the total scenario θ using a nominal and a random scenario. The nominal scenario θ^{n} gives us rough information about where the feed parameters to be realized are located at certain time periods called seasons. To define θ^{n} we use the tuple $\hat{\theta}$ from Example 2.5 from (2.25a)*. The elements of this tuple are interpreted as mean values, each belonging to a season and valid for that particular time period. From θ^{n} we conclude that 3 seasons are used. However, the length of these seasons depends on the distribution of the lengths of the subseasons for which the feed parameters are constant and on the average number of changes taken into account.*

For the following analysis, we considered 100 cycles of the nominal scenario, with all random variables determined by a random generator. Such an analysis can be carried out, for instance, using measurement data obtained in advance, i.e., before the storage system is designed.

We assume that the length of the subhorizons with constant feed parameter is given by a two-sided truncated exponential distribution $\mathrm{tExp}(\lambda)$

$$p_{\mathrm{T},i}(t) := \begin{cases} \dfrac{\mathrm{e}^{\frac{-(t-500)}{\lambda_i}}}{\lambda_i \left(1 - \mathrm{e}^{\frac{-(1800-500)}{\lambda_i}}\right)} & t \in [500,\, 1800]\,, \\ 0 & t \notin [500,\, 1800]\,, \end{cases} \tag{5.19}$$

where each season has its own mean parameter $\lambda_i \in \mathbb{R}^+$. The subdomain $[500,\, 1800]$ *of $f_{\mathrm{T},i}$ is chosen according to Example 2.5. On the left hand side in Figure 5.8, the distributions $\mathrm{p}_{\mathrm{T},i}$ are shown, where the data of the 100 cycles are represented by a normalized histogram in blue. In addition, the curve of the pdf from the analytical formula is shown for each season as solid black line. The mean parameters λ_i of* (5.19) *can read from Table 5.1 as well as the*

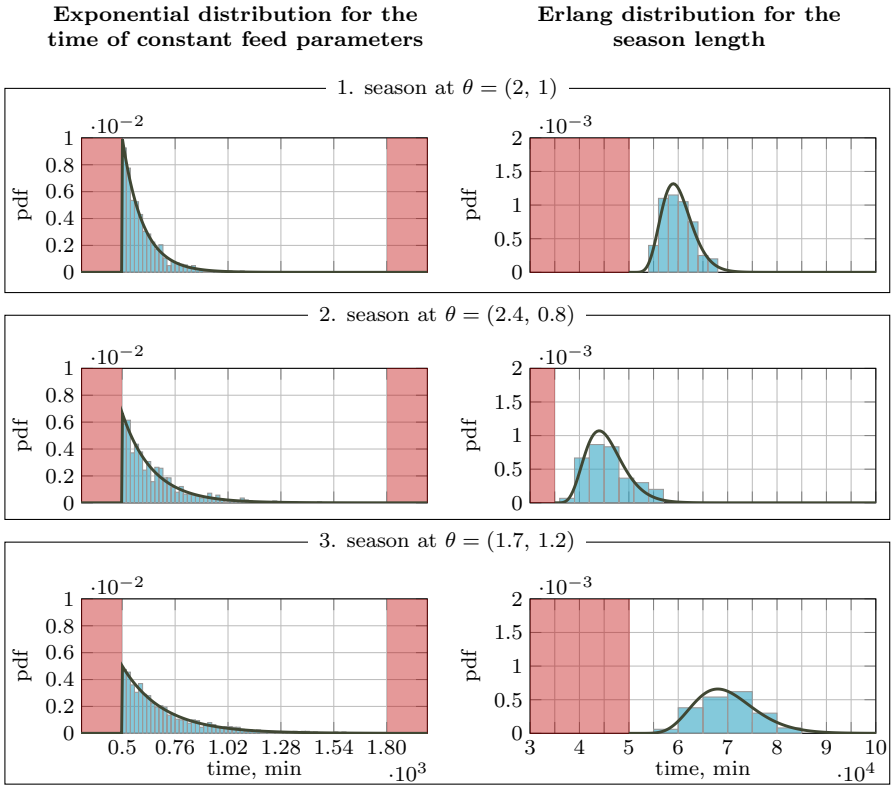

Figure 5.8: Distribution of the time length of the production phase and the seasons.

average number of production changes per season to be assumed. This table also shows the minimum and maximum lengths that have occurred during the 100 cycles with all subseasons. The higher λ*, the higher is the probability of longer periods for which the feed parameter is constant. Based on the characteristics of* $\mathrm{tExp}(\lambda)$*, the mean value of* $\mathrm{tExp}(\lambda)$ *can be determined from the mean parameter of* $\mathrm{tExp}(\lambda)$*. For a distribution only bounded by the lower bound of 500* min*, the seasonal mean value is given by 500* $\mathrm{min}+\lambda_i$*. The mean value of the two-sided truncated distribution in* (5.19) *is calculated numerically with Matlab. These values are listed in Table 5.1 together with the mean value determined from the data. It is easy to see that the values from the data differ from the true mean value, cf. in th fifth row.*

Finally, we want to use the information how long the feed parameter is in a certain subset of Θ *to determine the mean storage change.*

The pdf of the season length can be derived from that of the subseasons, since it is a finite sum of random variables. In general, the pdf of the sum of random variables is determined by convolution of the individual pdfs, which is related to high computational costs, especially if this operation is to be done several times. However, there exist analytical expressions for a large number of distributions. For this purpose, we assume for a moment that the upper bound in (5.19) *does not exist and we have a one-sided truncated pdf. The distribution resulting from the sum of n random variables with this pdf is a one-side truncated Erlang distribution* $\mathrm{tErl}(\lambda, n)$*. For the i-th season, its pdf is given by*

$$p_{\mathrm{S}}(t) := \begin{cases} \dfrac{{\lambda_i}^{-n_i}\,(t - n_i 500)^{n_i - 1}}{(n_i - 1)!} \mathrm{e}^{-\frac{(t - n_i 500)}{\lambda_i}} & t \geq t - n_i 500, \\ 0 & t < t - n_i 500, \end{cases} \tag{5.20}$$

using the lower bound from (5.19)*. We use* (5.20) *to approximate the true distribution formed from the two-sided truncated one. On the right hand side in Figure 5.8, the normalized histogram of the individual seasons based on the data of the 100 cycles is shown in blue. Besides, the one-side truncated Erlang distribution curve is shown in black to assess how accurate the approximation is. Similiar to the subseasons the minimum and the maximum length of the season for the 100 cycles is given in Table 5.1. Figure 5.8 shows that the pdf of* $\mathrm{tErl}(\lambda, n)$ *is influenced by the average number of production changes per season and the rate parameter. Thus the lower boundary naturally shifts with the average number of subseasons, whereas the rate parameter determines the width of the unimodal distribution. From* (5.20) *the mean can determined by* $n_i \lambda_i$*. Table 5.1 shows these mean values of both* $\mathrm{tErl}(\lambda, n)$ *and the data from the 100 cycles. Moreover, using Matlab, the mean value of the two-sided truncated Erlang distribution can also be determined numerically with the help of a Gamma distribution. We can see in the eighth row of Table 5.1 that the approximation of the mean via* $\mathrm{tErl}(\lambda, n)$ *is sufficient for the given parameters. It can be shown that with increasing parameter* λ *also the deviation between* t_1 *and* t_2 *is growing. Finally, the last row in Table 5.1 also gives the error between the mean determined by* $\mathrm{tErl}(\lambda, n)$ *and the data.*

After discussing the distribution of the lengths of the subseasons, we now focus on the distribution of the θ *values, which describe the dispersion around the mean values in* $\boldsymbol{\theta}^{\mathrm{n}}$ *presented in Table 5.2. We assume that the feed parameter that occurs can be described by a time-dependent Gaussian distribution. The mean value is used for the nominal scenario* $\boldsymbol{\theta}^{\mathrm{n}}$ *in* (5.10)*. The random scenario* $\boldsymbol{\theta}^{\mathrm{r}}$ *takes the information about the standard deviation to describe the variation around* $\boldsymbol{\theta}^{\mathrm{n}}$*. In Table 5.2 the standard deviations valid within each season are given. Figure 5.9 shows the total scenario* $\boldsymbol{\theta}$ *for the 100 cycles by the grey lines and the nominal scenario by the blue blue lines within* Θ*. Furthermore, the nominal values and the covariance ellipsoids are depicted. Such a scenario type*

Table 5.1: Summary of the information obtained from the distribution of time horizons for which the feed parameters are constant. The theoretical values from the one-side (t_1) and two-side (t_2) truncated distribution as well as from the given data (d) are represented. All time related data is presented in minutes.

	1. season	2. season	3. season
Double truncated exponential distribution			
Mean parameter λ_i	100	150	200
Average production change per season	10	7	10
Minimum length of the subseason	500.09	500.14	500.77
Maximum length of the subseason	1326.9	1492.4	1771.5
Mean length of the subseason (t_2/d)	600.0/ 600.4	649.8/ 656.5	698.0/702.3
Erlang distribution			
Minimum length of the season	5424.1	3795.0	5885.6
Maximum length of the season	6812.9	5818.4	8874.6
Mean length of the season (t_1/t_2)	6000/ 6000	4550/ 4550	7000/ 7000
Mean length of the season (d)	6004	4595	7023
Error (between t_1 and d)	0.06%	0.99%	0.33%

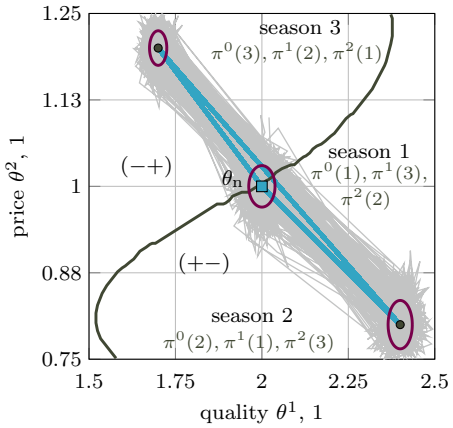

Figure 5.9: Random-based scenario (grey lines) within Θ. The nominal scenario is represented by th blue lines.

can be derived from the analysis of the electricity price on the electricity market or from more precise information on the origin of the organic substrate.
The solid black in Figure 5.9 partitions the feed parameter space Θ into a region

where the first storage is emptied, and the second one is filled (-+) and its complement (+-). Further details on this partition can be found in Example B.2 in Appendix B.2. Compared to the previously discussed scenario, the production system will now be operated over a longer time period according to the economic characteristics of the respective section. This means that the storage elements are now charged or discharged over a longer time span before they operate in the reverse direction. Hence, we can conclude that the storage capacity has to be chosen larger than in the examples before.

Table 5.2: Summary of the information obtained from the distribution of the realization of the feed parameters.

	1. season	2. season	3. season
Gaussian distribution			
Mean of the feed parameter	(2.0, 1.0)	(2.4, 0.8)	(1.7, 1.2)
Standard deviation of the feed parameter	(0.038, 0.030)	(0.035, 0.035)	(0.025, 0.025)

We use Algorithm 5.2 to estimate the smallest size so that the storage level remains within $\mathcal{A}_{\mathfrak{F}}$ with a predefined probability. For this purpose, the individual seasons are used successively as initial points to determine the seasonal hypercubes $\mathcal{SH}_i$ as shown in Figure 5.10 (a) by dark green areas. The parameters used for this analysis are presented in Table 5.3.

Table 5.3: Summary of the parameter used to estimate the storage capacity.

Probability p_{set} for confidence interval	95.45%
Design horizon by repetition number z	1
Design horizon by time Δ_{d}	$17,550\,\text{min}/\,12.18\,\text{d}$
Sigma-point parameters (α, β, κ)	(0.5, 2.0, 0.0)

If the production system is started in season 1, only small fluctuations of the storage level around the initial value would occur. Afterwards, the feed parameters, which determine the system operation in season 2, ensure that the storage levels in ${\mathcal{B}_1}^1$ increase while they decrease in ${\mathcal{B}_2}^1$. Finally, the feed parameters in season 3 will bring the level back close to the initial level. This is illustrated by the black curve in Figure 5.10, where the storage levels at the end of each season are marked by the black points. In Figure 5.10 (b), the final space $\mathcal{D}$ is shown composed by the minimum and the scenario-based size. Here the blue square and the green circle represent the initial and the final level.
Independent of the season in which the operation begins, the final storage level is reached again on average. However, the paths are different, which has an

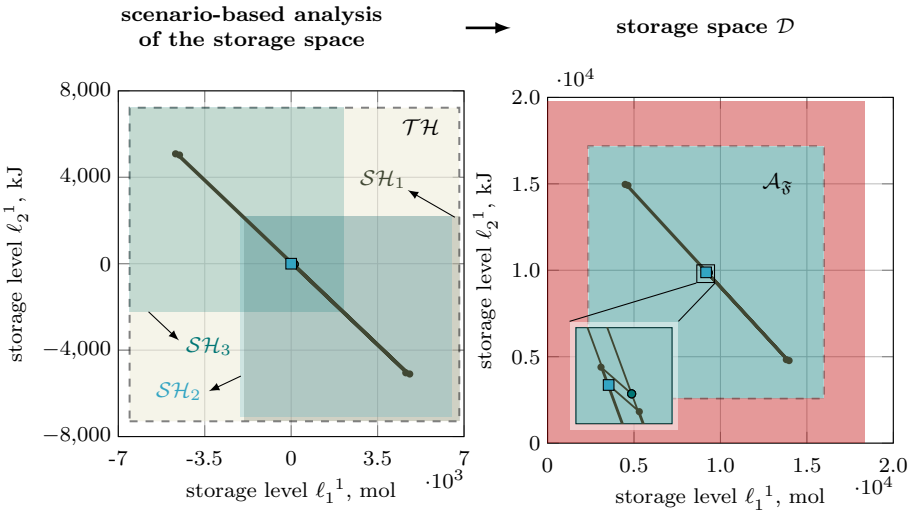

(a) Scenario-based construction of the storage level space.

(b) Total space $\mathcal{D}$ of the storage level (minimum + scenario-based)

Figure 5.10: Schematic illustration of the scenario-based construction of the storage size.

effect on the capacity. Thus, if the operation starts in season 2, the storage level moves first to the lower right corner in $\mathcal{TH}$ or in $\mathcal{D}$. Conversely, a production system that starts its operations in season 3 would initially move the level to the upper left corner in $\mathcal{TH}$ or in $\mathcal{D}$. For this reason we can see this spatial separation of the seasonal hypercubes $\mathcal{SH}_1/\mathcal{SH}_2$ and $\mathcal{SH}_3$.
The fact that the hypercube $\mathcal{SH}_1$ and $\mathcal{SH}_2$ are similarly positioned has two reasons. Firstly, the feed parameters around the nominal value cause only minor level changes, which indicates a good process design as they are well suited to each other. Secondly, the operation strategy and the distribution around θ_{n} ensures that $\mathcal{B}_1{}^1$ is preferably charged and $\mathcal{B}_2{}^1$ preferably discharged.

After the seasonal hypercube is determined, the total hypercube $\mathcal{TH}$ can be determined as the smallest outer axis-parallel envelope illustrated in Figure 5.10 (a) by the light beige area. The boundaries for $\mathcal{TH}$ are given by

$$\underline{b}_{\mathrm{t}} = (-6542.5,\, -7292.8) \;\; \textit{and} \;\; \overline{b}_{\mathrm{t}} = (6808.5,\, 7218.9)\,.$$

Due to the fact that each season was used as initial point, the lower and upper boundary has to be relatively symmetrical the closer the final level is to zero. In

our case, the deviation from the initial value is

$$\ell\left(\Delta_{\mathrm{d}}\right) = (119.8,\, -18.4)\,.$$

Thus, we can conclude that even after several cycles, the storage levels remain in $\mathcal{A}_{\mathfrak{F}}$ *with a high probability. This means that the storage restrictions do not become active when new production levels are calculated and that the storage system does not negatively influence the optimal operating point.*
Using (5.17)*, we obtain for the additional storage capacity*

$$D_{\emptyset} = (13.6169 \text{ kmol},\, 14585.7 \text{ kJ})\,.$$

Hence, the total storage capacity is given by

$$D = (18.340 \text{ kmol},\, 19761 \text{ kJ})\,,$$

where we use the result for the lower storage capacity from Example 5.1. The right hand side of Figure 5.10 (b) shows the entire storage space $\mathcal{D}$ *with the subspace* $\mathcal{A}_{\mathfrak{F}}$ *in green, where the time evolution of the storage levels occurs. As can be seen, the storage level never leave* $\mathcal{A}_{\mathfrak{F}}$*, which underlines that the designed storage has a suitable size. The attractive ratio for our system achieved by this sceanrio is given by* $\chi_{\mathcal{A}} = 0.548$*.*

Conclusion and Bibliography

Chapter 6

Conclusions and Perspectives

To face the growing challenges of our time, it is crucial not only to operate chemical process networks in an economically optimal way but also to consider fluctuating factors that affect the operational costs. For this purpose, the consideration of storage elements is decisive. Modern operational strategies must explicitly account for the storage capacities and the current storage levels to avoid emptying or overflowing the storages over desired planning horizons. Moreover, the storage capacities have to be designed not to restrict the optimal operation negatively. For this purpose, the storage design must be tailored to the operational strategy to be used.
Optimal and interconnected operation and storage design can be achieved by an optimization-based operational strategy that addresses various constraints and the process and storage dynamics. This storage design requires quantifying the fluctuating factors and analyze their effect on the production system, taking into account the operational strategy.

This thesis proposes concepts for an optimization-based operational strategy and the design of storage capacities. A generic production system consisting of two parallel processes connected via storages is considered to develop these concepts. We described and defined the production system in general mathematical form and addressed the individual components, such as storage rates, product quality, and downstream process constraints. In particular, this includes a characterization of the economic objective function, which we described using a hybrid semiparametric model. This hybrid model defines the profit of the production system, whereby the operational costs of the individual processes are described by Gaussian processes depending on the feed parameters as economic measures. In this way, the objective function can be trained using uncertain

data from a detailed economic model or experience. Furthermore, we discussed the structure of the time horizon in terms of frequency of feed parameter changes and time constants of the production system. We pointed out that the production system always changes between transition and production phases. As a result, the need for an operational strategy continuously redefines the production levels and provides a control policy to steer the system towards these new points in minimal time. We refrain from using an averaging level controller for the storages since this would couple the process operation. Instead, we considered an unsteady operation of the storages, which requires a concept for designing storage capacities.

6.1 Operational Strategy

One main contribution of this thesis is the development of an operational strategy for an unsteadily operating production system. The operational strategy proposes optimal operating points as well as the transition between those in minimal time. To do so, we proposed a closed-loop static real-time optimization (RTO) with integrated trajectory generation. The conceptual idea behind this approach is to determine the production level by a static RTO, where an underlying dynamical optimal control problem (OCP) has to be solved. The OCP provides the transition time to the new production level to predict the evolution of the storage level, thus avoiding premature emptying or overflowing. Since this bilevel optimization problem is complex and computationally demanding, we solved the layers separately. For this separation, we introduced storage constraints, which refer to the storage rates within the static RTO to restrict the slope of the storage level dynamics. Moreover, constraints on the terminal storage levels are included within the dynamic OCP to make the static RTO feasible. Furthermore, we use the transition-time map to transfer the transition time from the dynamic OCP to the static RTO. These constraints and the transition-time map enable an efficient implementation of the proposed closed-loop static RTO.
The following five items summarize the contribution to the operational strategy. Moreover, we give an outlook on possible future research directions in the individual subtasks.

1. Static RTO. We presented a static optimization to determine a new production level, which maximizes the profit of the production system. In this optimization, the storage level is predicted by considering the storage rates. The restriction of the rates guarantees a feasible operation for a particular time for unsteadily operating storages.

Outlook: The static RTO is formulated in the original coordinates of the system. In future works, the coordinates used for the controller design could be utilized for the RTO. In this way, some states are fixed to zero, which reduces the number of equality constraints and potentially the computational time.

2. Controller for transition. We develop a control law for the transition phase based on a partial system inversion and a novel setup function. This function guarantees a smooth connection of two operating points and allows a suitable adaptation of the trajectory between them to ensure different process and system constraints. The optimal parameters for the setup function are determined by solving a dynamic OCP where the transition time has to be minimized.
Outlook: For a real application, it is necessary to analyze the robustness of the transition controller. Primarily this concerns the fact whether the transition starts from the stationary state or not. Of particular interest is the sensitivity of the transition times to the initial states, which can be analyzed by future works.

3. Trajectory generation. The trajectory generation is achieved by integrating the system model employing the control law and the optimal parameter obtained by solving the dynamic OCP. The accuracy of the trajectory can be arbitrarily set and is determined by the step size of the integration. Thus, a transition in minimal time is achieved.
Outlook: This thesis did not explicitly discuss the control architecture of the supervisory layer in order to achieve a trajectory from the RTO layer. A further step of the operational strategy would be designing a control law, which applies the given reference trajectory accurately while ensuring disturbance rejection.

4. Controller for transition & production. For minimum-phase systems, we designed a control law for the transition and production phase to compensate the internal dynamics after reaching the stationary production level. This procedure ensures that the production level remains constant at its optimal setpoint.
Outlook: An extension of this control law could be derived to address non-minimum-phase systems.

5. Transition-time map. To provide transition times for the static RTO, we presented an algorithm to generate a surrogate model for the transition-time map utilizing a Gaussian process. This map enables the computation of the minimum transition time via interpolation between explicitly given data points. Consequently, the OCP does not have to be solved simultaneously with the S-RTO. We briefly touched on the concept of globally and locally valid transition-time maps.
Outlook: An essential point that must be investigated in more detail is the accuracy of the map. This involves the question of how many training points are

needed and where they have to be located. Also, the transition-time map offers a good tool to analyze the dynamic properties of a process. This enables us to identify areas with higher inertia to production changes and study the causes more precisely. Unfortunately, there is still no precise condition as to whether a globally valid transition-time map can be generated for a given production system.

The novel aspect of our operational strategy is combining the classical approach of static RTO with the closed-loop behavior of the underlying control system. In this way, the static RTO result depends on the controller implemented to reach the new operating point. This concept of a closed-loop S-RTO provides two major benefits:

1. The operating point defined by the bilevel closed-loop S-RTO is reachable. In this case, it is not necessary to consider additional techniques such as the two-stage approach at MPC layer [271, 166, 200].

2. The closed-loop S-RTO allows predicting the future behavior of unsteady states of the production system while including information from the controller. This information can not be applied in classical S-RTO approaches.

This second point allows us to consider storage levels that change over time explicitly. This, in turn, enables higher degrees of freedom in operation and results in optimal operation of the overall production. In general, the static RTO is suitable if the profit of the operational point computed without considering constraints arising from coupling is higher than that of the operational point considering a strong coupling.
An essential aspect that is not yet been integrated into the operational strategy is evaluating whether a transition is necessary. For this purpose, it is important to assess if the profit of the new production level will compensate for the transition costs. Considering a given stochastic scenario, we observed that the initial storage level is probably not precisely reached again after frequent operational changes, even if the trajectory of the feed parameter is a closed cycle in Θ. Hence, it is crucial to circumvent the original objective of static RTO after a particular time to return the storage levels to a defined initial value. This recovery mode of the RTO has not yet been addressed and designed. Likewise, we have not yet discussed when such a mode needs to be performed.

6.2 Storage Design

The second main contribution of this thesis is the design of storage capacities, which takes the proposed operational strategy into account. In particular, we use a relaxed version of the static RTO to define a function that provides the optimal storage rates depending on the feed parameter.
The controller affects the S-RTO if the storage level is nearly at the lower or upper boundary of the storage space. Only in this case, the prediction of the storage behavior within the production phase has a restrictive effect on the optimization result. For this reason, we defined a relaxed RTO without constraints for the storage rates as a reference as it describes the optimal production level to be achieved if the storage is not limiting. The following three items summarize the contribution to the storage design utilizing the relaxed RTO.

1. Structuring of the Feed Parameter Space Θ. Depending on the respective feed parameter, the relaxed RTO yields corresponding optimal storage rates. From the signs of these rates, it can be deduced whether the storages are filled or emptied under ideal conditions. Based on this distinction, we presented an algorithm to partition the feed parameter space Θ into separate parts. This partitioning allows us to analyze in advance how changes in the feed parameter will affect the storage levels using the proposed operational strategy. Hence, one can decide in advance whether this strategy is applicable in this form or, if possible, whether it is necessary to influence the scenarios for the feed parameter.
Outlook: The structuring concerns until now only Θ. Since the sales price is another economic variable that affects the production levels and, thus, the storage rates, an extension of the approach might be useful.

2. Minimum storage capacity. Using the relaxed RTO, we showed how to identify the feed parameter that yields the highest absolute value of the optimal storage rate. Combined with a given time, the highest absolute value for the change of storage levels can be calculated. We exploited this change in the storage level to define the lower bound of the storage capacity. For storages with this capacity, which are half-filled in the beginning, the static RTO is not limited by the storage constraints, at least not during the first operation.
Outlook: The sales price is not yet included in the analysis of the minimum required storage capacity. An extension of the determination of the lower bound might be relevant, as product prices can fluctuate over time.

3. Scenario-based storage capacity. We propose a design approach to measure the evolution of storage levels for a given stochastic scenario of feed

parameters. For this purpose, the definition of a scenario as a time-dependent, piecewise constant, feed-parameter value function is extended by a stochastic description. More precisely, the value of the feed parameter is described by truncated probability-density distribution. This stochastic approach allows considering uncertainties. Employing the unscented transformation, we showed how the distribution of storage rates is approximated from the distribution of feed parameters by determining mean and variance. The storage capacity is defined over the confidence interval in which the storage levels are contained with a given probability. Therefore, this design concept for dimensioning the storages does not lead to a conservative overestimation, which would lead to high investment costs.
Outlook: In further studies, the integration of the sales price by a stochastic description offers a more comprehensive description of the storage size. So far, the approach neglected the economic aspects of storage capacities, i.e., the investment costs. However, this consideration is essential to decide which storage capacity must be installed in a real application. A related issue is the design horizon, or more precisely, how many cycles are considered. For instance, the storage costs determine the design horizon that influences the storage size and should therefore be investigated in future works.

6.3 Concluding Remarks

The integrated design of efficient control strategies and production system components is a challenging task that will remain important in the future. In particular, the requirement to achieve dynamic and flexible process operations, required by the growing use of renewable energies and raw materials together with the integration of sustainable production methods, still offers broad potential for development. Storage elements are essential components here, as they buffer fluctuations and provide more flexibility in the coupling of processes that can be considered in production system operation.
This work addresses some of these challenges by introducing a new approach to an operational strategy located at the RTO layer. The RTO strategy combines the identification of economically optimal operating points and calculates a time-optimal trajectory that steers the production system to that point while considering the presence of unsteady operating storages. Furthermore, the operational strategy is used to design the storages by presenting a methodology that allows an estimation of the average minimum capacities. An application of the developed concepts promises an enhancement of the economic operation of chemical process networks facing unsteady and dynamical operation challenges.

Bibliography

[1] J. Adamy. *Nichtlineare Systeme und Regelungen*. Springer-Verlag Berlin Heidelberg, 2014.

[2] R. Amrit, J.B. Rawlings, and D. Angeli. Economic optimization using model predictive control with a terminal cost. *Annual Reviews in Control*, 35(2):178–186, 2011.

[3] A. Anastasovski. Design of Heat Storage Units for use in repeatable Time Slices. *Applied Thermal Engineering*, 112:1590 – 1600, 2017.

[4] B.D. Anderson and J.B. Moore. *Optimal control: linear quadratic methods*. Prentice-Hall, Inc., 1990.

[5] J. Andersson. *A General-purpose software framework for dynamic optimization*. PhD thesis, Faculty of Engineering, KU Leuven, 2013.

[6] J.A.E. Andersson, J. Gillis, G. Horn, J.B. Rawlings, and M. Diehl. CasADi – A software framework for nonlinear optimization and optimal control. *Mathematical Programming Computation*, 11(1):1–36, 2019.

[7] L.E. Andersson, E.C. Bradford, and L. Imsland. Distributed learning for wind farm optimization with Gaussian processes*. In *2020 American Control Conference (ACC)*, pages 4058–4064, 2020.

[8] M. Athans and P.L. Falb. *Optimal Control - An Introduction to the Theory and Its Applications*. Dover Publications Inc., 1966.

[9] E.G. Aufuldish and S.S. Melsheimer. Optimization of Surge Capacity. *Chemical Engineering Communications*, 129(1):251–275, 1994.

[10] I.V. Babich and J.A. Moulijn. Science and technology of novel processes for deep desulfurization of oil refinery streams: a review. *Fuel*, 82(6): 607–631, 2003.

[11] T. Backx, O. Bosgra, and W. Marquardt. Integration of Model Predictive Control and Optimization of Processes: Enabling Technology for Market Driven Process Operation. *IFAC Proceedings Volumes*, 33(10):249–260, 2000. IFAC Symposium on Advanced Control of Chemical Processes 2000, Pisa, Italy, 14-16 June 2000.

[12] M. Baerns, A. Behr, A. Brehm, J. Gmehling, H. Hofmann, U. Onken, A. Renken, K.-O. Hinrichsen, and R. Palkovits. *Technische Chemie*. John Wiley & Sons, 2013.

[13] B. Bank, J. Guddat, D. Klatte, B. Kummer, and K. Tammer. *Non-Linear Parametric Optimization*. Birkhäuser, Basel, 1983.

[14] L. Beckenbach, P. Osinenko, and Streif. Addressing infinite-horizon optimization in MPC via Q-learning. *IFAC-PapersOnLine*, 51(20):60 – 65, 2018. 6th IFAC Conference on Nonlinear Model Predictive Control NMPC 2018.

[15] M. Benosman and G. Le Vey. Stable inversion of SISO nonminimum phase linear systems through output planning: an experimental application to the one-link flexible manipulator. *IEEE Transactions on Control Systems Technology*, 11(4):588–597, 2003.

[16] A. Bensmann, R. Hanke-Rauschenbach, R. Heyer, F. Kohrs, D. Benndorf, U. Reichl, and Sundmacher K. Biological methanation of hydrogen within biogas plants: A model-based feasibility study. *Applied Energy*, 134: 413–425, 2014.

[17] O. Bernard, Z. Hadj-Sadok, D. Dochain, A. Genovesi, and J.P. Steyer. Dynamical model development and parameter identification for an anaerobic wastewater treatment process. *Biotechnology and bioengineering*, 75(4):424–438, 2001.

[18] N. Bhat, P. Minderman, and T. McAvoy. Use of Neural Nets for Modeling of Chemical Process Systems. *IFAC Proceedings Volumes*, 22(8):169–175, 1989.

[19] S.A. Bhat and D.N. Saraf. Steady-State Identification, Gross Error Detection, and Data Reconciliation for Industrial Process Units. *Industrial & Engineering Chemistry Research*, 43(15):4323–4336, 2004.

[20] L.T. Biegler. Solution of dynamic optimization problems by successive quadratic programming and orthogonal collocation. *Computers & Chemical Engineering*, 8(3):243–247, 1984.

[21] H.G. Bock and K.J. Plitt. A Multiple Shooting Algorithm for Direct Solution of Optimal Control Problems*. *IFAC Proceedings Volumes*, 17 (2):1603 – 1608, 1984. 9th IFAC World Congress: A Bridge Between Control Science and Technology, Budapest, Hungary, 2-6 July 1984.

[22] L. Bonfim-Rocha, A.B. Silva, S.H. Bernardo de Faria, M.F. Vieira, and M. de Souza. Production of Sodium Bicarbonate from CO_2 Reuse Processes: A Brief Review. *International Journal of Chemical Reactor Engineering*, 18(1), 2020.

[23] S. Brandt. *Statistical and Computational Methods for Scientists and Engineers*. Springer International Publishing, 2014.

[24] J. Bremer, K.H.G. Rätze, and K. Sundmacher. CO_2 methanation: Optimal start-up control of a fixed-bed reactor for power-to-gas applications. *AIChE Journal*, 63(1):23–31, 2017.

[25] M. Brunner, U. Rosolia, J. Gonzales, and F. Borrelli. Repetitive learning model predictive control: An autonomous racing example. In *2017 IEEE 56th Annual Conference on Decision and Control (CDC)*, pages 2545–2550, 2017.

[26] A. Campisano and C. Modica. Regional scale analysis for the design of storage tanks for domestic rainwater harvesting systems. *Water science and technology: a journal of the International Association on Water Pollution Research*, 66:1–8, 2012.

[27] P.J. Campo and M. Morari. Model predictive optimal averaging level control. *AIChE Journal*, 39(4):579–591, 1989.

[28] S. Cao and R.R. Rhinehart. An efficient method for on-line identification of steady state. *Journal of Process Control*, 5(6):363–374, 1995.

[29] B. Chachuat, B. Srinivasan, and Bonvin. Adaptation strategies for real-time optimization. *Computers & Chemical Engineering*, 33(10):1557–1567, 2009. Selected Papers from the 18th European Symposium on Computer Aided Process Engineering (ESCAPE-18).

[30] K.P.B. Chandra and D. Gu. *Nonlinear Filtering - Methods and Applications*. Springer International Publishing, 2019.

[31] C.Y. Chen and B. Joseph. On-line optimization using a two-phase approach: an application study. *Industrial & Engineering Chemistry Research*, 26(9):1924–1930, 1987.

[32] S.-S. Chern, W.-H. Chen, and K.S. Lam. *Lectures on Differential Geometry*. Series on University Mathematics. World Scientific, 1999.

[33] T.-F. Cheung and W.L. Luyben. Liquid-Level Control in Single Tanks and Cascades of Tanks with Proportional-Only and Proportional-Integral Feedback Controllers. *Industrial & Engineering Chemistry Fundamentals*, 18(1):15–21, 1979.

[34] Z. Chong and C.L.E. Swartz. Optimal operation of process plants under partial shutdown conditions. *AIChE Journal*, 59(11):4151–4168, 2013.

[35] Z. Chong and C.L.E. Swartz. Optimal response under partial plant shutdown with discontinuous dynamic models. *Computers & Chemical Engineering*, 86:120–135, 2016.

[36] L. Consolini and A. Piazzi. Minimum-time feedforward control with input and output constraints. In *2006 IEEE Conference on Computer Aided Control System Design, 2006 IEEE International Conference on Control Applications, 2006 IEEE International Symposium on Intelligent Control*, pages 1538–1543, 2006.

[37] A. Costalunga and Piazzi. A behavioral approach to inversion-based control. *Automatica*, 95:433 – 445, 2018.

[38] J.R. Couper, W.R. Penney, J.R. Fair, and S.M. Walas. *Chemical Process Equipment: Selection and Design*. Butterworth-Heinemann, 3 edition, 2012. ISBN 012396959X,9780123969590.

[39] J.E. Cuthrell and L.T. Biegler. Simultaneous optimization and solution methods for batch reactor control profiles. *Computers & Chemical Engineering*, 13(1):49–62, 1989. Computer Applications to Batch Chemical Processing.

[40] M. L. Darby and M. Nikolaou. MPC: Current practice and challenges. *Control Engineering Practice*, 20(4):328–342, 2012. Special Section: IFAC Symposium on Advanced Control of Chemical Processes - ADCHEM 2009.

[41] M.L. Darby, M. Nikolaou, J. Jones, and D. Nicholson. RTO: An overview and assessment of current practice. *Journal of Process Control*, 21(6): 874–884, 2011.

[42] M.T. de Gouvêa and Odloak. One-layer real time optimization of LPG production in the FCC unit: procedure, advantages and disadvantages. *Computers & Chemical Engineering*, 22:191–198, 1998. European Symposium on Computer Aided Process Engineering-8.

[43] S. Devasia. Nonlinear minimum-time control with pre- and post-actuation. *Automatica*, 47(7):1379–1387, 2011.

[44] S. Devasia. Time-Optimal Control With Pre/Post Actuation for Dual-Stage Systems. *IEEE Transactions on Control Systems Technology*, 20 (2):323–334, 2012.

[45] S. Devasia, D. Chen, and B. Paden. Nonlinear inversion-based output tracking. *IEEE Transactions on Automatic Control*, 41(7):930–942, 1996.

[46] N. Devore, H. Yip, and J. Rhee. Domestic Hot Water Storage Tank: Design and Analysis for Improving Thermal Stratification. *Journal of Solar Energy Engineering*, 135(4), 10 2013.

[47] M. Diehl, A. Schäfer, H.G. Bock, J.P. Schlöder, and D.B. Leineweber. Optimization of multiple-fraction batch distillation with recycled waste cuts. *AIChE Journal*, 48(12):2869–2874, 2002.

[48] J.J. Downs and S. Skogestad. An industrial and academic perspective on plantwide control. *Annual Reviews in Control*, 35(1):99–110, 2011.

[49] T. Eggeman. *Sodium Carbonate*, pages 1–11. American Cancer Society, 2011.

[50] A.A. Elbaset. Design, modeling and control strategy of PV/FC hybrid power system. *Journal of Electrical Systems*, 7(2):270–286, 2011.

[51] M. Ellis, H. Durand, and P.D. Christofides. A tutorial review of economic model predictive control methods. *Journal of Process Control*, 24(8): 1156–1178, 2014. Economic nonlinear model predictive control.

[52] S. Engell. Feedback control for optimal process operation. *Journal of Process Control*, 17(3):203–219, 2007.

[53] A. Faanes and Skogestad. A systematic approach to the design of buffer tanks. *Computers & Chemical Engineering*, 24(2):1395–1401, 2000.

[54] A. Faanes and S. Skogestad. Buffer tank design for acceptable control performance. *Industrial and Engineering Chemistry Research*, 42(10): 2198–2208, 2003.

[55] N. Faiz, S.K. Agrawal, and R.M. Murray. Trajectory Planning of Differentially Flat Systems with Dynamics and Inequalities. *Journal of Guidance, Control, and Dynamics*, 24(2):219–227, 2001.

[56] T. Faulwasser. *Optimization-based solutions to constrained trajectory-tracking and path-following problems*. Shaker Verlag, 2013.

[57] T. Faulwasser, V. Hagenmeyer, and R. Findeisen. Optimal exact path-following for constrained differentially flat systems. In *IFAC Proceedings Volumes (IFAC-PapersOnline)*, volume 44, pages 9875–9880, 2011.

[58] T. Faulwasser, V. Hagenmeyer, and R. Findeisen. Constrained reachability and trajectory generation for flat systems. *Automatica*, 50(4):1151–1159, 2014.

[59] T. Faulwasser, M. Korda, C.N. Jones, and D. Bonvin. Turnpike and dissipativity properties in dynamic real-time optimization and economic MPC. In *53rd IEEE Conference on Decision and Control*, pages 2734–2739, 2014.

[60] T. Faulwasser, L. Grüne, and M. Müller. Economic Nonlinear Model Predictive Control. *Foundations and Trends in Systems and Control*, 5: 1–98, 2018.

[61] K.P. Ferentinos, K.G. Arvanitis, and N. Sigrimis. Heuristic optimization methods for motion planning of autonomous agricultural vehicles. *Journal of Global Optimization*, 23(2):155–170, 2002.

[62] A. Ferramosca, D. Limon, I. Alvarado, T. Alamo, and E.F. Camacho. MPC for tracking of constrained nonlinear systems. In *Proceedings of the 48h IEEE Conference on Decision and Control (CDC) held jointly with 2009 28th Chinese Control Conference*, pages 7978–7983, 2009.

[63] A. Ferramosca, D. Limon, I. Alvarado, and E.F. Camacho. Cooperative distributed MPC for tracking. *Automatica*, 49(4):906–914, 2013.

[64] T.d.A. Ferreira, G. François, A.G. Marchetti, and D Bonvin. Use of Transient Measurements for Static Real-Time Optimization. *IFAC-PapersOnLine*, 50(1):5737–5742, 2017. 20th IFAC World Congress.

[65] T.d.A. Ferreira, H.A. Shukla, T. Faulwasser, C.N. Jones, and D. Bonvin. Real-Time optimization of Uncertain Process Systems via Modifier Adaptation and Gaussian Processes. In *2018 European Control Conference (ECC)*, pages 465–470, 2018.

[66] D.A. Fetisov. A Method for Solving a Point-to-Point Steering Problem for a Class of Nonlinear Control Systems *. In *2020 European Control Conference (ECC)*, pages 1153–1158, 2020.

[67] R. Findeisen and F. Allgöwer. Computational Delay in Nonlinear Model Predictive Control. *IFAC Proceedings Volumes*, 37(1):427–432, 2004. 7th International Symposium on Advanced Control of Chemical Processes (ADCHEM 2003), Hong-Kong, 11-14 January 2004.

[68] W. Findeisen, F.N. Bailey, Brdys. M., K. Malinowski, P. Tatjewski, and A. Wozniak. *Control and Coordination in Hierarchical Systems*. International Series on Applied Systems Analysis. John Wiley & Sons, 1980.

[69] R.J. Flassig and K. Sundmacher. Optimal design of stimulus experiments for robust discrimination of biochemical reaction networks. *Bioinformatics*, 28(23):3089–3096, 2012.

[70] M. Fliess, J. Lévine, P. Martin, and P. Rouchon. Flatness and defect of non-linear systems: introductory theory and examples. *International Journal of Control*, 61(6):1327–1361, 1995.

[71] M. Fliess, H. Mounier, P. Rouchon, and J. Rudolph. A distributed parameter approach to the control of a tubular reactor: a multivariable case. In *Proceedings of the 37th IEEE Conference on Decision and Control*, volume 1, pages 439–442, 1998.

[72] T. Frankel. *The Geometry of Physics: An Introduction*. Cambridge University Press, 3 edition, 2011.

[73] J. Frasch. Parallel Algorithms for Optimization of Dynamic Systems in Real-Time, 2014.

[74] K. Gadkar, F. Doyle, T. Crowley, and J. Varner. Cybernetic Model Predictive Control of a Continuous Bioreactor with Cell Recycle. *Biotechnology Progress*, 19(5):1487–1497, 2003.

[75] E. Gail, S. Gos, R. Kulzer, J. Lorösch, A. Rubo, M. Sauer, R. Kellens, J. Reddy, N. Steier, and W. Hasenpusch. *Cyano Compounds, Inorganic*. American Cancer Society, 2011.

[76] A. Galkina. *Combination of Flatness and Model Predictive Control for Mechatronical Applications*. 08 2018. ISBN 978-3-8440-6109-3.

[77] W. Gao and Engell. Using Transient Measurements in Iterative Steady-State Optimizing Control. In Zdravko Kravanja and Miloš Bogataj, editors, *26th European Symposium on Computer Aided Process Engineering*, volume 38 of *Computer Aided Chemical Engineering*, pages 511–516. Elsevier, 2016.

[78] R.S. Garcia and Weisser. A wind–diesel system with hydrogen storage: Joint optimisation of design and dispatch. *Renewable Energy*, 31(14):2296 – 2320, 2006.

[79] F. Goodridge and K. Scott. *Cost Estimation, Profit Appraisal, Process Modeling, and Optimization*, pages 245–293. Springer US, 1995.

[80] A. Gopalakrishnan and L.T Biegler. Economic Nonlinear Model Predictive Control for periodic optimal operation of gas pipeline networks. *Computers & Chemical Engineering*, 52:90–99, 2013.

[81] K. Graichen. *Feedforward Control Design for Finite-Time Transition Problems of Nonlinear Systems with Input and Output Constraints*. Berichte aus dem Institut für Systemdynamik, Universität Stuttgart. Shaker, 2006.

[82] K. Graichen and M. Zeitz. Feedforward control design for finite-time transition problems of nonlinear systems with input and output constraints. *IEEE Transactions on Automatic Control*, 53(5):1273–1278, 2008.

[83] K. Graichen, V. Hagenmeyer, and M. Zeitz. A new approach to inversion-based feedforward control design for nonlinear systems. *Automatica*, 41 (12):2033–2041, 2005.

[84] A. Grancharova, J. Kocijan, and T.A. Johansen. Explicit stochastic predictive control of combustion plants based on Gaussian process models. *Automatica*, 44(6):1621–1631, 2008. Stochastic Modelling, Control, and Robust Optimization at the Crossroads of Engineering, Environmental Economics, and Finance.

[85] S. Gros, B. Srinivasan, B. Chachuat, and Bonvin. Neighbouring-extremal control for singular dynamic optimisation problems. Part I: single-input systems. *International Journal of Control*, 82(6):1099–1112, 2009.

[86] S. Grossberg. Nonlinear neural networks: Principles, mechanisms, and architectures. *Neural Networks*, 1(1):17–61, 1988.

[87] L. Grüne and J. Pannek. *Nonlinear Model Predictive Control: Theory and Algorithms*. Springer Publishing Company, Incorporated, 2013.

[88] F. Gustafsson and G. Hendeby. On nonlinear transformations of stochastic variables and its application to nonlinear filtering. In *2008 IEEE International Conference on Acoustics, Speech and Signal Processing*, pages 3617–3620, 2008.

[89] P. Haessig, B. Multon, H.B. Ahmed, S. Lascaud, and P. Bondon. Energy storage sizing for wind power: impact of the autocorrelation of day-ahead forecast errors. *Wind Energy*, 18(1):43–57, 2015.

[90] V. Hagenmeyer and E. Delaleau. Exact feedforward linearization based on differential flatness. *International Journal of Control*, 76(6):537–556, 2003.

[91] S.M. Hall. *Rules of Thumb for Chemical Engineers*. Elsevier, 2018.

[92] G. Hämmerlin and K.-H. Hoffmann. *Numerische Mathematik*. Springer-Verlag Berlin Heidelberg, 1994.

[93] K. Hatz. *Efficient numerical methods for hierarchical dynamic optimization with application to cerebral palsy gait modeling.* PhD thesis, Ruprecht-Karls-University Heidelberg, 2014.

[94] J. Hauser and R. Hindman. Maneuver Regulation from Trajectory Tracking: Feedback Linearizable Systems*. *IFAC Proceedings Volumes*, 28(14):595–600, 1995.

[95] M. Heidarinejad, J. Liu, and P.D. Christofides. Economic model predictive control of nonlinear process systems using Lyapunov techniques. *AIChE Journal*, 58(3):855–870, 2012.

[96] T. Heine, M. Kawohl, and R. King. Robust model predictive control using the unscented transformation. In *2006 IEEE Conference on Computer Aided Control System Design, 2006 IEEE International Conference on Control Applications, 2006 IEEE International Symposium on Intelligent Control*, pages 224–230, 2006.

[97] A. Helbig, O. Abel, and W. Marquardt. Structural Concepts for Optimization Based Control of Transient Processes. In *Nonlinear Model Predictive Control*, pages 295–311, 2000.

[98] D. Henrion and J. . Lasserre. LMIs for constrained polynomial interpolation with application in trajectory planning. In *2004 IEEE International Conference on Robotics and Automation (IEEE Cat. No.04CH37508)*, pages 220–224, 2004.

[99] A Hiester, S. Melsheimer, and E. Vogel. Optimum size and location of surge capacity in continuous chemical processes. *AIChe Annual Meeting*, 1987.

[100] A. Himmel, S. Sager, and K. Sundmacher. Time-minimal set point transition for nonlinear SISO systems under different constraints. *Automatica*, 114:108806, 2020.

[101] J.H. Holland. Genetic Algorithms and the Optimal Allocation of Trials. *SIAM Journal on Computing*, 2(2):88–105, 1973.

[102] B. Hu and S. Mishra. Time-Optimal Trajectory Generation for Landing a Quadrotor Onto a Moving Platform. *IEEE/ASME Transactions on Mechatronics*, 24(2):585–596, 2019.

[103] B. Hu, L. Lu, and S. Mishra. A Control Architecture for Time-Optimal Landing of a Quadrotor Onto a Moving Platform. *Asian Journal of Control*, 20(5):1701–1712, 2018.

[104] A. Isidori. *Nonlinear Control Systems*. Springer-Verlag London, 3rd edition, 1995.

[105] A. Isidori. The zero dynamics of a nonlinear system: From the origin to the latest progresses of a long successful story. *European Journal of Control*, 19(5):369–378, 2013.

[106] M.Z. Jamaludin and C.L.E. Swartz. Dynamic real-time optimization with closed-loop prediction. *AIChE Journal*, 63(9):3896–3911, 2017.

[107] M.Z. Jamaludin and C.L.E. Swartz. Approximation of closed-loop prediction for dynamic real-time optimization calculations. *Computers and Chemical Engineering*, 103:23–38, 2017.

[108] S.-S. Jang, B. Joseph, and H. Mukai. Control of Constrained Multivariable Nonlinear Process Using a Two-Phase Approach. *Industrial and Engineering Chemistry Research*, 26(10):2106–2114, 1987.

[109] P. Janssens, G. Pipeleers, and J. Swevers. Model-free iterative learning of time-optimal point-to-point motions for LTI systems. In *2011 50th IEEE Conference on Decision and Control and European Control Conference*, pages 6031–6036, 2011.

[110] P. Janssens, W. Van Loock, G. Pipeleers, and J. Swevers. Efficient computation of time-optimal point-to-point motion trajectories. *IEEE Transactions on Control Systems Technology*, 23(2):679–686, 2015.

[111] A. Jess and P. Wasserscheid. *Chemical Technology: From Principles to Products*. Wiley-VCH, 2 edition, 2020.

[112] L. Jetto, V. Orsini, and R. Romagnoli. Output-transition optimization through a multi-objective least square procedure. In *53rd IEEE Conference on Decision and Control*, pages 3173–3179, 2014.

[113] H. Jiang, R. Patwardhan, and S.L. Shah. Root cause diagnosis of plant-wide oscillations using the concept of adjacency matrix. *Journal of Process Control*, 19(8):1347–1354, 2009.

[114] S. Julier and J.K. Uhlmann. A General Method for Approximating Nonlinear Transformations of Probability Distributions. Technical report, University of Oxford, 1996.

[115] S. J. Julier. The scaled unscented transformation. In *Proceedings of the 2002 American Control Conference (IEEE Cat. No.CH37301)*, volume 6, pages 4555–4559, 2002.

[116] S. J. Julier, J.K. Uhlmann, and H.F. Durrant-Whyte. A new approach for filtering nonlinear systems. In *Proceedings of 1995 American Control Conference - ACC'95*, volume 3, pages 1628–1632, 1995.

[117] S.J. Julier and J.K. Uhlmann. New extension of the Kalman filter to nonlinear systems. In *Signal Processing, Sensor Fusion, and Target Recognition VI*, volume 3068, pages 182–193, 1997.

[118] S.J. Julier and J.K. Uhlmann. Unscented filtering and nonlinear estimation. *Proceedings of the IEEE*, 92(3):401–422, 2004.

[119] S.J. Julier, J.K. Uhlmann, and H.F. Durrant-Whyte. A new method for the nonlinear transformation of means and covariances in filters and estimators. *IEEE Trans. Automat. Contr.*, 45:477–482, 2000.

[120] L. Jürgensen, E.A. Ehimen, J. Born, and Holm-Nielsen J.B. Utilization of surplus electricity from wind power for dynamic biogas upgrading: Northern germany case study. *Biomass and Bioenergy*, 66:126–132, 2014.

[121] J.V. Kadam and W. Marquardt. Sensitivity-based solution updates in closed-loop dynamic optimization. In *IFAC Proceedings Volumes (IFAC-PapersOnline)*, volume 37, pages 947–952, 2004.

[122] J.V. Kadam, M. Schlegel, W. Marquardt, Tousain. R.L., D.H. van Hessem, J. van den Berg, and O.H. Bosgra. A Two-Level Strategy of Integrated Dynamic Optimization and Control of Industrial Processes—a Case Study. In Johan Grievink and Jan van Schijndel, editors, *European Symposium on Computer Aided Process Engineering-12*, volume 10 of *Computer Aided Chemical Engineering*, pages 511–516. Elsevier, 2002.

[123] B. Käpernick and K. Graichen. Transformation of Output Constraints in Optimal Control Applied to a Double Pendulum on a Cart. *IFAC Proceedings Volumes*, 46(23):193–198, 2013. 9th IFAC Symposium on Nonlinear Control Systems.

[124] R. Kemp and S.E. Keegan. *Calcium Chloride*. American Cancer Society, 2000.

[125] H.K. Khalil. *Nonlinear systems; 3rd ed.* Prentice-Hall, 2002.

[126] E.S. Kikkinides, M.C. Georgiadis, and A.K. Stubos. On the optimization of hydrogen storage in metal hydride beds. *International Journal of Hydrogen Energy*, 31(6):737–751, 2006.

[127] A. Klenke. *Wahrscheinlichkeitstheorie*. Springer-Verlag Berlin Heidelberg, 2013.

[128] A. Klenke. *Probability Theory A Comprehensive Course*. Springer-Verlag London, 2014.

[129] J. Ko, D.J. Klein, D. Fox, and D. Haehnel. Gaussian Processes and Reinforcement Learning for Identification and Control of an Autonomous Blimp. In *Proceedings 2007 IEEE International Conference on Robotics and Automation*, pages 742–747, 2007.

[130] J. Kocijan. *Modelling and control of dynamic systems using Gaussian process models*. Springer International Publishing Switzerland, 2016.

[131] J. Kocijan and R. Murray-Smith. *Nonlinear Predictive Control with a Gaussian Process Model*, pages 185–200. Springer Berlin Heidelberg, 2005.

[132] J. Kocijan, R. Murray-Smith, C.E. Rasmussen, and A. Girard. Gaussian process model based predictive control. In *Proceedings of the 2004 American Control Conference*, volume 3, pages 2214–2219, 2004.

[133] B. Kolar. *Contributions to the Differential Geometric Analysis and Control of Flat Systems*. PhD thesis, Johannes Kepler University Linz, 2016.

[134] T. Koller, F. Berkenkamp, M. Turchetta, J. Bödecker, and A. Krause. Learning-based Model Predictive Control for Safe Exploration and Reinforcement Learning. *arXiv preprint*, 2019.

[135] D. Krishnamoorthy, B. Foss, and Skogestad. Steady-state real-time optimization using transient measurements. *Computers & Chemical Engineering*, 115:34–45, 2018.

[136] P. Kythe and P. Puri. *Computational Methods for Linear Integral Equations*. Birkhäuser Basel, 2002.

[137] J. Larson, M. Menickelly, and S. M. Wild. Derivative-free optimization methods. *Acta Numerica*, 28:287–404, 2019.

[138] J.P. Lasalle. The 'bang-bang' principle. *IFAC Proceedings Volumes*, 1(1): 503–507, 1960.

[139] A. Lederer, J. Umlauft, and S. Hirche. Uniform error bounds for Gaussian process regression with application to safe control. *Advances in Neural Information Processing Systems*, pages 659–669, 2019.

[140] E.S. Lee and G.V. Reklaitis. Intermediate storage and operation of batch processes under equipment failure. *Computers and Chemical Engineering*, 13:491–498, 1989.

[141] J. Lee. *Introduction to Smooth Manifolds*. Springer-Verlag New York, 2nd edition, 2012.

[142] J.H. Lee, J. Shin, and M.J. Realff. Machine learning: Overview of the recent progresses and implications for the process systems engineering field. *Computers & Chemical Engineering*, 114:111–121, 2018.

[143] K.-J. Lee, M.-J. Lee, and Hwang. High-temperature steam electrolysis combined with methane partial oxidation by solid oxide electrolyzer cells. *Applied Surface Science*, 473:746–749, 2019.

[144] J. Lévine. *Differentially Flat Systems*, pages 131–179. Springer Berlin Heidelberg, 2009.

[145] H. Li and C.L.E. Swartz. Dynamic real-time optimization of distributed MPC systems using rigorous closed-loop prediction. *Computers & Chemical Engineering*, 122:356–371, 2019. 2017 Edition of the European Symposium on Computer Aided Process Engineering (ESCAPE-27).

[146] J. Li, X. Li, R. Du, Y. Wang, and J. Tu. A new design concept of thermal storage tank for adaptive heat charging in solar heating system. *Applied Thermal Engineering*, 165:114617, 2020.

[147] X. Li and T.E. Marlin. Model predictive control with robust feasibility. *Journal of Process Control*, 21(3):415–435, 2011.

[148] X. Li, L. Zhang, M. Nakaya, and A. Takenaka. Application of economic MPC to a CSTR process. In *Proceedings of 2016 IEEE Advanced Information Management, Communicates, Electronic and Automation Control Conference, IMCEC 2016*, pages 685–690, 2017.

[149] G. Liesche and K. Sundmacher. Identification of Key Transport Phenomena in High-Temperature Reactors: Flow and Heat Transfer Characteristics. *Industrial & Engineering Chemistry Research*, 57(46): 15884–15897, 2018.

[150] G. Liesche, D. Schack, and K. Sundmacher. The FluxMax approach for simultaneous process synthesis and heat integration: Production of hydrogen cyanide. *AIChE Journal*, 65(7), 2019.

[151] B. Likar and Kocijan. Predictive control of a gas–liquid separation plant based on a Gaussian process model. *Computers & Chemical Engineering*, 31(3):142 – 152, 2007.

[152] D. Limon, A. Ferramosca, I. Alvarado, and T. Alamo. Nonlinear MPC for tracking piece-wise constant reference signals. *IEEE Transactions on Automatic Control*, 63(11):3735–3750, 2018.

[153] A. Lindholm. A method for improving plant availability with respect to utilities using buffer tanks. In *Proceedings of the IASTED International Conference on Modelling, Identification and Control*, pages 378–383, 2011.

[154] T. Lipp and S. Boyd. Minimum-time speed optimisation over a fixed path. *International Journal of Control*, 87(6):1297–1311, 2014.

[155] T. Liu, H. Liu, X. Zhang, L. Lei, Y. Zhang, Z. Yuan, F. Chen, and Y. Wang. A robust solid oxide electrolyzer for highly efficient electrochemical reforming of methane and steam. *J. Mater. Chem. A*, 7:13550–13558, 2019.

[156] S. Lucia, J.A.E. Andersson, H. Brandt, M. Diehl, and S. Engell. Handling uncertainty in economic nonlinear model predictive control: A comparative case study. *Journal of Process Control*, 24(8):1247–1259, 2014.

[157] W.L. Luyben. Chapter A1 - The need for simultaneous design education. In Panos Seferlis and Michael C. Georgiadis, editors, *The Integration of Process Design and Control*, volume 17 of *Computer Aided Chemical Engineering*, pages 10–41. Elsevier, 2004.

[158] L. L. Lynn, E. S. Parkin, and R. L. Zahradnik. Near-Optimal Control by Trajectory Approximation. Tubular Reactors with Axial Dispersion. *Industrial & Engineering Chemistry Fundamentals*, 9(1):58–63, 1970.

[159] L.L. Lynn and R.L. Zahradnik. The use of orthogonal polynomials in the near-optimal control of distributed systems by trajectory approximation. *International Journal of Control*, 12(6):1079–1087, 1970.

[160] J.M. Maciejowski and X. Yang. Fault tolerant control using Gaussian processes and model predictive control. In *2013 Conference on Control and Fault-Tolerant Systems (SysTol)*, pages 1–12, 2013.

[161] R.S.H. Mah. *Chemical Process Structures and Information Flow*. Butterworth-Heinemann, 1990.

[162] R.V. Mahajanam and A. Zheng. Evaluation of Cost of Dynamic Controllability and Optimal Surge Capacity without Dynamic Models. *Industrial & Engineering Chemistry Research*, 41(16):3877–3883, 2002.

[163] M. Maiworm, C. Wagner, R. Temirov, F.S. Tautz, and R. Findeisen. Two-degree-of-freedom control combining machine learning and extremum seeking for fast scanning quantum dot microscopy. In *2018 Annual American Control Conference (ACC)*, pages 4360–4366, 2018.

[164] A. Malek, M.N.A. Hawlader, and J.C. Ho. Design and economics of RO seawater desalination. *Desalination*, 105(3):245 – 261, 1996.

[165] A. Mansour, A.E. Bouaswaig, and S. Engell. Time Optimal Control of Particle Size Distribution in Emulsion Polymerization. *Computer Aided Chemical Engineering*, 29:557–561, 2011.

[166] A.G. Marchetti, A. Ferramosca, and A.H. González. Steady-state target optimization designs for integrating real-time optimization and model predictive control. *Journal of Process Control*, 24(1):129–145, 2014.

[167] A.G. Marchetti, T. De Avila Ferreira, S. Costello, and D. Bonvin. Modifier Adaptation as a Feedback Control Scheme. *Industrial and Engineering Chemistry Research*, 59(6):2261–2274, 2020.

[168] T.E. Marlin. *Process Control: Designing Processes and Control Systems for Dynamic Performance*. Mcgraw-Hill Higher Education, 2000.

[169] T.E. Marlin and A.N. Hrymak. Real-time operations optimization of continuous processes. *AIChE Symposium Series*, 93:156–164, 1997.

[170] J.O.A. Matias and G.A.C. Le Roux. Real-time Optimization with persistent parameter adaptation using online parameter estimation. *Journal of Process Control*, 68:195–204, 2018.

[171] J. Matschek, T. Bäthge, T. Faulwasser, and R. Findeisen. *Nonlinear Predictive Control for Trajectory Tracking and Path Following: An Introduction and Perspective*. Birkhäuser, 2018.

[172] J. Matschek, A. Himmel, K. Sundmacher, and R. Findeisen. Constrained Gaussian process learning for model predictive control. In *IFAC World Congress*, 2020.

[173] L.S. Maxeiner and S. Engell. Comparison of dual based optimization methods for distributed trajectory optimization of coupled semi-batch processes. *Optimization and Engineering*, 2020.

[174] D.Q. Mayne, J.B. Rawlings, C.V. Rao, and P.O.M. Scokaert. Constrained model predictive control: Stability and optimality. *Automatica*, 36(6): 789–814, 2000.

[175] K. A. McDonald, T. J. McAvoy, and A. Tits. Optimal averaging level control. *AIChE Journal*, 32(1):75–86, 1986.

[176] D. Mellinger and V. Kumar. Minimum snap trajectory generation and control for quadrotors. In *2011 IEEE International Conference on Robotics and Automation*, pages 2520–2525, 2011.

[177] C. Mihálykó and É. Orbán-Mihálykó. Sizing intermediate storages in discrete models under stochastic operational conditions. *Periodica Polytechnica Chemical Engineering*, 60(3):192–200, 2016.

[178] K.P. Murphy. *Machine Learning: A Probabilistic Perspective*. The MIT Press, 2012.

[179] V. Musolino, A. Pievatolo, and Tironi. A statistical approach to electrical storage sizing with application to the recovery of braking energy. *Energy*, 36(11):6697 – 6704, 2011.

[180] Z.K. Nagy, B. Mahn, R. Franke, and F. Allgöwer. Evaluation study of an efficient output feedback nonlinear model predictive control for temperature tracking in an industrial batch reactor. *Control Engineering Practice*, 15(7):839–850, 2007.

[181] A. Neumaier. Complete search in continuous global optimization and constraint satisfaction. *Acta Numerica*, 13:271–369, 2004.

[182] S. Ochoa, J.-U. Repke, and Wozny. Integrating real-time optimization and control for optimal operation: Application to the bio-ethanol process. *Biochemical Engineering Journal*, 53(1):18–25, 2010. Special Section: CHEMPOR2008 - Integration of Life Sciences and Engineering.

[183] T.O. Odi and I.A. Karimi. A general stochastic model for intermediate storage in noncontinuous processes. *Chemical Engineering Science*, 45 (12):3533 – 3549, 1990.

[184] J. Oldenburg and W. Marquardt. Flatness and higher order differential model representations in dynamic optimization. *Computers and Chemical Engineering*, 26(3):385–400, 2002.

[185] É. Orbán-Mihálykó and B.G. Lakatos. Intermediate storage in batch/continuous processing systems under stochastic operation conditions. *Computers and Chemical Engineering*, 28(12):2493–2508, 2004.

[186] É. Orbán-Mihálykó and C. Mihálykó. Investigation of operation of intermediate storages applying probability density functions satisfying linear differential equation. *Periodica Polytechnica Chemical Engineering*, 56(2):77–82, 2012.

[187] É. Orbán-Mihálykó and C. Mihálykó. Sizing problem of intermediate storages under stochastic operational conditions. *Periodica Polytechnica Chemical Engineering*, 59(3):236–242, 2015.

[188] J. O'Reilly. The discrete linear time invariant time-optimal control problem-an overview. *Automatica*, 17(2):363–370, 1981.

[189] C.J. Ostafew, A.P. Schoellig, and T.D. Barfoot. Learning-based nonlinear model predictive control to improve vision-based mobile robot path-tracking in challenging outdoor environments. In *2014 IEEE International Conference on Robotics and Automation (ICRA)*, pages 4029–4036, 2014.

[190] C.J. Ostafew, A.P. Schoellig, T.D. Barfoot, and J. Collier. Learning-based Nonlinear Model Predictive Control to Improve Vision-based Mobile Robot Path Tracking. *Journal of Field Robotics*, 33(1):133–152, 2016.

[191] H. Perez and S. Devasia. Optimal output-transitions for linear systems. *Automatica*, 39(2):181–192, 2003.

[192] H.J. Pesch. Real-time computation of feedback controls for constrained optimal control problems. part 1: Neighbouring extremals. *Optimal Control Applications and Methods*, 10(2):129–145, 1989.

[193] A. Piazzi and Visioli. Using stable input–output inversion for minimum-time feedforward constrained regulation of scalar systems. *Automatica*, 41 (2):305–313, 2005.

[194] A. Piazzi and A. Visioli. Optimal inversion-based control for the set-point regulation of nonminimum-phase uncertain scalar systems. *IEEE Transactions on Automatic Control*, 46(10):1654–1659, 2001.

[195] A. Piazzi and A. Visioli. Optimal noncausal set-point regulation of scalar systems. *Automatica*, 37(1):121–127, 2001.

[196] Z.N. Pintarič and Z. Kravanja. Selection of the Economic Objective Function for the Optimization of Process Flow Sheets. *Industrial & Engineering Chemistry Research*, 45(12):4222–4232, 2006.

[197] J.M. Pinto, M. Joly, and L.F.L. Moro. Planning and scheduling models for refinery operations. *Computers & Chemical Engineering*, 24(9):2259 – 2276, 2000.

[198] A Piéplu, O Saur, J.-C. Lavalley, O. Legendre, and C. Nédez. Claus Catalysis and H_2S Selective Oxidation. *Catalysis Reviews*, 40(4):409–450, 1998.

[199] L.S. Pontryagin, V.G. Boltyanski, R.V. Gamkrelidze, and E.F. Miscenko. *The Mathematical Theory of Optimal Processes*. Wiley, Chichester, 1962.

[200] L.F. Pozas and L.V.R. de Arruda. A New Approach to Integrate SSTO, MPC and RTO Using Online Identified Models: Use of Updated Models to Smooth Integration. *Journal of Control, Automation and Electrical Systems*, 29(5):566–575, 2018.

[201] J. Prüher and S. Särkkä. On the use of gradient information in Gaussian process quadratures. In *2016 IEEE 26th International Workshop on Machine Learning for Signal Processing (MLSP)*, pages 1–6, 2016.

[202] S.J. Qin and T.A. Badgwell. A survey of industrial model predictive control technology. *Control Engineering Practice*, 11(7):733–764, 2003.

[203] C.E. Rasmussen and C.K.I. Williams. *Gaussian Processes for Machine Learning*. MIT Press, 2006.

[204] J.B. Rawlings and R. Amrit. *Optimizing Process Economic Performance Using Model Predictive Control*, pages 119–138. Springer Berlin Heidelberg, 2009.

[205] J.B. Rawlings, D.Q. Mayne, and M.M. Diehl. *Model Predictive Control: Theory, Computation, and Design*. Nob Hill Publishing, LLC, 2nd edition, 2018.

[206] J.E.J. Remigio and C.L.E. Swartz. Production scheduling in dynamic real-time optimization with closed-loop prediction. *Journal of Process Control*, 89:95–107, 2020.

[207] D Rodrigues, M Amrhein, J Billeter, and D. Bonvin. Fast Estimation of Plant Steady State for Imperfectly Known Dynamic Systems, with Application to Real-Time Optimization. *Industrial & Engineering Chemistry Research*, 57(10):3699–3716, 2018.

[208] K. Roh, L.C. Brée, K. Perrey, A. Bulan, and Mitsos. Flexible operation of switchable chlor-alkali electrolysis for demand side management. *Applied Energy*, 255:113880, 2019.

[209] P. Rosander, A.J. Isaksson, J. Löfberg, and K. Forsman. Practical Control of Surge Tanks Suffering from Frequent Inlet Flow Upsets. *IFAC Proceedings Volumes*, 45(3):258–263, 2012. 2nd IFAC Conference on Advances in PID Control.

[210] U. Rosolia, A. Carvalho, and F. Borrelli. Autonomous racing using learning Model Predictive Control. In *2017 American Control Conference (ACC)*, pages 5115–5120, 2017.

[211] N. Rossner, T. Heine, and R. King. Quality-by-Design Using a Gaussian Mixture Density Approximation of Biological Uncertainties. *IFAC Proceedings Volumes*, 43(6):7–12, 2010. 11th IFAC Symposium on Computer Applications in Biotechnology.

[212] C. Rösmann, F. Hoffmann, and T. Bertram. Timed-Elastic-Bands for time-optimal point-to-point nonlinear model predictive control. In *2015 European Control Conference, ECC 2015*, pages 3352–3357, 2015.

[213] C. Rösmann, F. Hoffmann, and T. Bertram. Integrated online trajectory planning and optimization in distinctive topologies. *Robotics and Autonomous Systems*, 88:142–153, 2017.

[214] C. Santos and Taveira-Pinto. Analysis of different criteria to size rainwater storage tanks using detailed methods. *Resources, Conservation and Recycling*, 71:1 – 6, 2013.

[215] L.O. Santos, P.A.F.N.A. Afonso, J.A.A.M. Castro, N.M.C. Oliveira, and L.T. Biegler. On–line implementation of nonlinear MPC: an experimental case study. *Control Engineering Practice*, 9(8):847–857, 2001.

[216] D. Sbarbaro and Ortega. Averaging level control: An approach based on mass balance. *Journal of Process Control*, 17(7):621–629, 2007.

[217] R. Scattolini. Architectures for distributed and hierarchical Model Predictive Control – A review. *Journal of Process Control*, 19(5):723–731, 2009.

[218] P. Schäfer, A. Caspari, A. Mhamdi, and A. Mitsos. Economic nonlinear model predictive control using hybrid mechanistic data-driven models for optimal operation in real-time electricity markets: In-silico application to air separation processes. *Journal of Process Control*, 84:171–181, 2019.

[219] P. Schäfer, T.M. Daun, and A. Mitsos. Do investments in flexibility enhance sustainability? A simulative study considering the German electricity sector. *AIChE Journal*, 66(11):e17010, 2020.

[220] R. Schenkendorf, A. Kremling, and M. Mangold. Optimal experimental design with the sigma point method. *IET Systems Biology*, 3(1):10–23, 2009.

[221] K. Schlacher and M. Schöberl. CONSTRUCTION OF FLAT OUTPUTS BY REDUCTION AND ELIMINATION. *IFAC Proceedings Volumes*, 40 (12):693–698, 2007. 7th IFAC Symposium on Nonlinear Control Systems.

[222] K. Schlacher and M. Schöberl. Geometrische Darstellung nichtlinearer Systeme. *at - Automatisierungstechnik*, 62(7):452–462, 2014.

[223] K. Schlacher and K. Zehetleitner. Basic Differential Geometry for Mechanics and Control. In *Advanced Dynamics and Control of Structures and Machines*, pages 97–125. Springer-Verlag Wien, 1999.

[224] K. Schlacher, S. Fuchshumer, and Holl J. Some Applications of Differential Geometry in Control. In *Advanced Dynamics and Control of Structures and Machines*, pages 249–260. Springer-Verlag Wien, 1999.

[225] K. Schlacher, M. Schöberl, and B. Kolar. A Jet Space Approach to Derive Flat Outputs. *IFAC-PapersOnLine*, 48(11):131–136, 2015. 1st IFAC Conference onModelling, Identification andControl of Nonlinear SystemsMICNON 2015.

[226] T. Schwarzgruber, P. Colaneri, and L. Del Re. Minimum-time control of a class of nonlinear systems with partly unknown dynamics and constrained input. *IFAC Proceedings Volumes*, 46(23):211–216, 2013.

[227] M. Semaan, S.D. Day, M. Garvin, N. Ramakrishnan, and A. Pearce. Optimal sizing of rainwater harvesting systems for domestic water usages: A systematic literature review. *Resources, Conservation & Recycling: X*, 6:100033, 2020.

[228] R. Seydel. *Practical Bifurcation and Stability Analysis*. Springer, New York, NY, 2010.

[229] M.R. Shabani and R. Yekta. Chemical processes equipment cost estimation using parametric models. *Cost engineering*, 48:26–32, 2006.

[230] M. Sharifzadeh. *Integrated design and control with a focus on control structures*. PhD thesis, Imperial College London, Chemical Engineering, 2013.

[231] K. Shin and N. McKay. Minimum-time control of robotic manipulators with geometric path constraints. *IEEE Transactions on Automatic Control*, 30(6):531–541, 1985.

[232] J. Sikder, M. Roy, P. Dey, and Pal. Techno-economic analysis of a membrane-integrated bioreactor system for production of lactic acid from sugarcane juice. *Biochemical Engineering Journal*, 63:81 – 87, 2012.

[233] D. Simon. *Optimal State Estimation: Kalman, H Infinity, and Nonlinear Approaches*. John Wiley & Sons, Ltd, 2006.

[234] S.N. Sivanandam and S.N. Deepa. *Introduction to Genetic Algorithms*. Springer, Berlin, Heidelberg, 2008.

[235] S. Skogestad and I. Postlethwaite. *Multivariable Feedback Control: Analysis and Design*. John Wiley & Sons, Inc., 2005.

[236] E. Solak, R. Murray-Smith, W.E. Leithead, D.J. Leith, and C.E. Rasmussen. Derivative Observations in Gaussian Process Models of Dynamic Systems. In S. Becker, S. Thrun, and K. Obermayer, editors, *Advances in Neural Information Processing Systems 15*, pages 1057–1064. MIT Press, 2003.

[237] R. Soloperto, M.A. Müller, S. Trimpe, and F. Allgöwer. Learning-Based Robust Model Predictive Control with State-Dependent Uncertainty. *IFAC-PapersOnLine*, 51(20):442 – 447, 2018. 6th IFAC Conference on Nonlinear Model Predictive Control NMPC 2018.

[238] E.D. Sontag. *Mathematical Control Theory - Deterministic Finite Dimensional Systems*. Springer-Verlag New York, 1998.

[239] G. Steiner, D. Watzenig, C. Magele, and U. Baumgartner. Statistical robust design using the unscented transformation. *COMPEL - The International Journal for Computation and Mathematics in Electrical and Electronic Engineering*, 24(2):606–619, 2005.

[240] J. Stoer and R. Bulirsch. *Introduction to Numerical Analysis*. Springer-Verlag New York, 2002.

[241] R. Suresh, A. Sivaram, and V. Venkatasubramanian. A hierarchical approach for causal modeling of process systems. *Computers & Chemical Engineering*, 123:170–183, 2019.

[242] F. Svaricek. Nulldynamik linearer und nichtlinearer Systeme: Definitionen, Eigenschaften und Anwendungen (Zero Dynamics of Linear and Nonlinear Systems: Definitions, Properties and Applications). *at - Automatisierungstechnik*, 54(7):310–322, 2006.

[243] A. Tamar, G. Thomas, T. Zhang, S. Levine, and P. Abbeel. Learning from the hindsight plan – episodic MPC improvement. In *2017 IEEE International Conference on Robotics and Automation (ICRA)*, pages 336–343, 2017.

[244] P. Tatjewski. *Advanced Control of Industrial Processes. Structures and Algorithms*. Springer-Verlag London, 2007.

[245] P Tatjewski. Advanced control and on-line process optimization in multilayer structures. *Annual Reviews in Control*, 32(1):71–85, 2008.

[246] T. Tosukhowong, J.M. Lee, J.H. Lee, and Lu. An introduction to a dynamic plant-wide optimization strategy for an integrated plant. *Computers & Chemical Engineering*, 29(1):199–208, 2004.

[247] M. Treuer, T. Weissbach, and V. Hagenmeyer. Flatness-Based Feedforward in a Two-Degree-of-Freedom Control of a Pumped Storage Power Plant. *IEEE Transactions on Control Systems Technology*, 19(6):1540–1548, 2011.

[248] J. Umlauft, T. Beckers, and S. Hirche. Scenario-based Optimal Control for Gaussian Process State Space Models. In *2018 European Control Conference (ECC)*, pages 1386–1392, 2018.

[249] V. Uraikul, C.W. Chan, and Tontiwachwuthikul. Artificial intelligence for monitoring and supervisory control of process systems. *Engineering Applications of Artificial Intelligence*, 20(2):115–131, 2007.

[250] L. Van den Broeck. Time optimal control of mechatronic systems through embedded optimization (tijdsoptimale controle van mechatronische systemen door middel van ingebedde optimalisatie), 2011.

[251] R. Van Der Merwe. *Sigma-Point Kalman Filters for Probabilistic Inference in Dynamic State-Space Models*. PhD thesis, Oregon Health & Science University, 2004.

[252] W. Van Loock, G. Pipeleers, M. Diehl, J. De Schutter, and J. Swevers. Optimal path following for differentially flat robotic systems through a geometric problem formulation. *IEEE Transactions on Robotics*, 30(4): 980–985, 2014.

[253] W. Van Loock, G. Pipeleers, and J. Swevers. Optimal motion planning for differentially flat systems with guaranteed constraint satisfaction. In *2015 American Control Conference (ACC)*, pages 4245–4250, 2015.

[254] M.J. Van Nieuwstadt and R.M. Murray. Real-time trajectory generation for differentially flat systems. *International Journal of Robust and Nonlinear Control*, 8(11):995–1020, 1998.

[255] H.N. Verma and P.B.S. Sarma. Design of storage tanks for water harvesting in rainfed areas. *Agricultural Water Management*, 18(3):195 – 207, 1990.

[256] D. Verscheure, B. Demeulenaere, J. Swevers, J. De Schutter, and M. Diehl. Time-Optimal Path Tracking for Robots: A Convex Optimization Approach. *IEEE Transactions on Automatic Control*, 54(10):2318–2327, 2009.

[257] R. Verschueren, H.J. Ferreau, A. Zanarini, M. Mercangoz, and M. Diehl. A stabilizing nonlinear model predictive control scheme for time-optimal point-to-point motions. In *2017 IEEE 56th Annual Conference on Decision and Control (CDC)*, pages 2525–2530, 2018.

[258] S. Waldherr and M. Zeitz. Conditions for the existence of a flat input. *International Journal of Control*, 81(3):439–443, 2008.

[259] H. Wang, Q. Zou, and Xu. Inversion-based optimal output tracking–transition switching with preview for nonminimum-phase linear systems. *Automatica*, 48(7):1364–1371, 2012.

[260] H. Wang, K. Kim, and Zou. B-spline-decomposition-based output tracking with preview for nonminimum-phase linear systems. *Automatica*, 49(5): 1295–1303, 2013.

[261] Y. Wang, T. Liu, S. Fang, G. Xiao, H. Wang, and F. Chen. A novel clean and effective syngas production system based on partial oxidation of methane assisted solid oxide co-electrolysis process. *Journal of Power Sources*, 277:261–267, 2015.

[262] B. Waśkowicz. Statistical analysis and dimensioning of a wind farm energy storage system. *Archives of Electrical Engineering*, 66(2):265–277, 2017.

[263] P. Wieland, T. Meurer, K. Graichen, and M. Zeitz. Feedforward control design under input constraints for a tubular reactor model. In *Proceedings of the 45th IEEE Conference on Decision and Control*, pages 3968–3973, 2006.

[264] J. Witte, J. Settino, S.M.A. Biollaz, and Schildhauer T.J. Direct catalytic methanation of biogas – Part I: New insights into biomethane production using rate-based modelling and detailed process analysis. *Energy Conversion and Management*, 171:750–768, 2018.

[265] I.J. Wolf, D.A. Muñoz, and Marquardt. Consistent hierarchical economic NMPC for a class of hybrid systems using neighboring-extremal updates. *Journal of Process Control*, 24(2):389–398, 2014.

[266] N. Wu, M. Zhu, L. Bai, and Z. Li. Short-term scheduling of crude oil operations in refinery with high-fusion-point oil and two transportation pipelines. *Enterprise Information Systems*, 10(6):581–610, 2016.

[267] Q. Wu, Y. Xi, Z. Nagy, and D. Li. A real-time optimization framework for the time-varying economic environment. *Computers & Chemical Engineering*, 115:333–341, 2018.

[268] L. Würth, R. Hannemann, and W. Marquardt. Neighboring-extremal updates for nonlinear model-predictive control and dynamic real-time optimization. *Journal of Process Control*, 19(8):1277–1288, 2009.

[269] A. Wächter and L.T. Biegler. On the implementation of an interior-point filter line-search algorithm for large-scale nonlinear programming. *Mathematical Programming*, 106(1):25–57, 2006.

[270] L. Würth, R. Hannemann, and Marquardt. A two-layer architecture for economically optimal process control and operation. *Journal of Process Control*, 21(3):311–321, 2011.

[271] C.-M. Ying and B. Joseph. Performance and stability analysis of LP-MPC and QP-MPC cascade control systems. *AIChE Journal*, 45(7):1521–1534, 1999.

[272] W.S. Yip and T.E. Marlin. Multiple data sets for model updating in real-time operations optimization. *Computers & Chemical Engineering*, 26(10):1345 – 1362, 2002.

[273] U. Zahid, J. An, C.-J. Lee, U. Lee, and C. Han. Design and Operation Strategy of CO_2 Terminal. *Industrial & Engineering Chemistry Research*, 54(8):2353–2365, 2015.

[274] A. I. Zečević and D. D. Šiljak. Regions of Attraction. In *Control of Complex Systems: Structural Constraints and Uncertainty*. Springer US, 2010.

[275] M. Zeitz. Minimalphasigkeit – keine relevante Eigenschaft für die Regelungstechnik! *at - Automatisierungstechnik*, 62(1):3–10, 2014.

[276] Q. Zhang and S.-R. Li. Efficient computation of smooth minimum time trajectory for CNC machining. *International Journal of Advanced Manufacturing Technology*, 68(1-4):683–692, 2013.

[277] A. Zheng and R.V. Mahajanam. A Quantitative Controllability Index. *Industrial & Engineering Chemistry Research*, 38(3):999–1006, 1999.

[278] J. Zhuge and M.G. Ierapetritou. Integration of scheduling and control for batch processes using multi-parametric model predictive control. *AIChE Journal*, 60(9):3169–3183, 2014.

[279] Q. Zou. Optimal preview-based stable-inversion for output tracking of nonminimum-phase linear systems. *Automatica*, 45(1):230–237, 2009.

Part IV

Appendices

Appendix A

Mathematical Background

A.1 Mathematical Preparations: Differential Geometry

Throughout this thesis, we use concepts and notations of differential geometry. In particular, this is true for the description of the system models and the control strategy. The most important terms and concepts are briefly presented below. For a detailed introduction, see [141, 32].

Let $\mathcal{X}$, $\dim(\mathcal{X}) = n_{\mathrm{x}}$ a manifold with local coordinates $\left(x^1, \ldots, x^{n_{\mathrm{x}}}\right)$ or shortly (x^α), $\alpha = 1, \ldots, n_{\mathrm{x}}$. For a given point $p \in \mathcal{X}$, for the sake of simplicity we denote by x on the one hand a local chart $x : \mathcal{X} \to \mathbb{R}^{n_{\mathrm{x}}}$, $x(p) = \left(x^1, \ldots, x^{n_{\mathrm{x}}}\right)$ and on the other hand the local coordinates.
The tangent space at a point $p \in \mathcal{X}$ is presented by $\mathcal{T}_p\mathcal{X}$ and the cotangent space by $\mathcal{T}_p^*\mathcal{X}$. The union $\mathcal{T}\mathcal{X} := \cup_{p\in\mathcal{X}}\mathcal{T}_p\mathcal{X}$ and $\mathcal{T}^*\mathcal{X} := \cup_{p\in\mathcal{X}}\mathcal{T}_p^*\mathcal{X}$ combined with surjective maps $\tau_{\mathcal{X}} : \mathcal{T}\mathcal{X} \to \mathcal{X}$ and $\tau_{\mathcal{X}}^* : \mathcal{T}\mathcal{X} \to \mathcal{X}$ denote as the tagent and the cotagent bundle. Based on a local chart x on $\mathcal{X}$, $\mathcal{T}\mathcal{X}$ and $\mathcal{T}^*\mathcal{X}$ are equipped with induced charts $\xi_{(x)}$ and $\xi_{(x)}^*$, respectively. For the tagent bundle $\mathcal{T}\mathcal{X}$, the induced coordinates are $\left(x^1, \ldots, x^{n_{\mathrm{x}}}, \dot{x}^1, \ldots, \dot{x}^{n_{\mathrm{x}}}\right)$ and for the cotangent bundle $\mathcal{T}^*\mathcal{X}$ are $\left(x^1, \ldots, x^{n_{\mathrm{x}}}, \dot{x}_1, \ldots, \dot{x}_{n_{\mathrm{x}}}\right)$.
Let $X \in \mathcal{T}\mathcal{X}$ be a vector field and $\omega \in \mathcal{T}^*\mathcal{X}$ be a covector field or 1-form on $\mathcal{X}$. The vector field X is smooth map that assigns to each point $p \in \mathcal{X}$ an element $X_p \in \mathcal{T}_p\mathcal{X}$. A map of this type is also called section of the tangent bundle and the set of all vector fields on $\mathcal{X}$ is denoted by $\Gamma(\mathcal{T}\mathcal{X})$. In local coordinates, the field X is given by $X = X_{(x)}^\alpha(x)\frac{\partial}{\partial x^\alpha}$. Likewise, a covector field (or 1-forms) ω is

smooth map that assigns to each point $p \in \mathcal{X}$ an element $\omega_p \in \mathcal{T}_p^* \mathcal{X}$. Similarly, the set of all 1-forms on $\mathcal{X}$ is denoted by $\Gamma(\mathcal{T}\mathcal{X}^*)$. In local coordinates, the field ω is given by $\omega = \omega_{(x),\alpha}(x)\mathrm{d}x^\alpha$.
The Table A.1 summarize the most important concepts and point out the concepte of a change of coordinates.

Table A.1: Overview about the most important notations.

	Abstract Form	**Coordinate Form & Coordinate Change**
1	vector: $X_p \in \mathcal{T}_p\mathcal{X}$ vector field: $X \in \Gamma(\mathcal{T}\mathcal{X})$	general form: $X_p = X^\alpha_{(x)} \left(\frac{\partial}{\partial x^\alpha}\right)_p$ basis change: $\left(\frac{\partial}{\partial x^\alpha}\right)_p = \left(\frac{\partial z^m}{\partial x^\alpha}\right)_p \left(\frac{\partial}{\partial z^m}\right)_p$ components change: $X^\alpha_{(z)} = \left(\frac{\partial z^m}{\partial x^\alpha}\right)_p X^\alpha_{(x)}$
2	covector or 1-form: $\omega_p \in \mathcal{T}_p^* \mathcal{X}$ covector field: $\omega \in \Gamma(\mathcal{T}^*\mathcal{X})$	general form: $\omega_p = \omega_{(x),\alpha} \left(\mathrm{d}x^\alpha\right)_p$ basis change: $\left(\mathrm{d}x^\beta\right)_p = \left(\frac{\partial x^\beta}{\partial z^\alpha}\right)_p (\mathrm{d}z^\alpha)_p$ components change: $\omega_{(z),\beta} = \left(\frac{\partial x^\alpha}{\partial z^\beta}\right)_p \omega_{(x),\alpha}$
3	map $g : \mathcal{X} \to \mathcal{Y}$ $\Rightarrow\ g \in C^\infty(\mathcal{X}, \mathcal{Y})$ --- map $h : \mathcal{X} \to \mathbb{R}$ $\Rightarrow\ h \in C^\infty(\mathcal{X})$	general form: $g_{(y,x)} = y \circ g \circ x^{-1}$ change: $g_{(y,z)} = \left(y \circ g \circ x^{-1}\right) \circ \left(x \circ z^{-1}\right) = g_{(y,x)} \circ \Phi_{(xz)}$ --- general form: $h_{(x)} = h \circ x^{-1}$ change: $h_{(z)} = \left(h \circ x^{-1}\right) \circ \left(x \circ z^{-1}\right) = h_{(x)} \circ \Phi_{(xz)}$
4	exterior derivative: $\mathrm{d} : C^\infty(\mathcal{X}) \to \Gamma(\mathcal{T}^*\mathcal{X}),\ h \mapsto \mathrm{d}h$ --- $\mathrm{d}h : \Gamma(\mathcal{T}^*\mathcal{X}) \to C^\infty(\mathcal{X}),\ X \mapsto \mathrm{d}h(X) := X(h)$	general form: $\mathrm{d}h = \frac{\partial h}{\partial x^\alpha}\mathrm{d}x^\alpha$ --- $\mathrm{d}h(X) = \frac{\partial h}{\partial x^\alpha}\mathrm{d}x^\alpha \left(X^\alpha_{(x)} \frac{\partial}{\partial x^\alpha}\right) = \frac{\partial h}{\partial x^\alpha} X^\alpha_{(x)}$

	Abstract Form	**Coordinate Form & Coordinate Change**
5	flow for $X \in \Gamma(\mathcal{TX})$: $\phi^X : \mathbb{R} \times \mathcal{X} \to \mathcal{X},$ $(t,p) \mapsto \phi_t^X(p)$	———
6	Pushforward: $g_* : \mathcal{TX} \to \mathcal{TY},$ $X \mapsto g_*(X)$ $g_*(X)(h) := X(h \circ g)$	$\big(g_*(X)\big)^{\alpha}_{(y)} = Y^{\alpha}_{(y)} = \left(\frac{\partial g^{\beta}_{(yx)}}{\partial x^{\alpha}}\right)_p X^{\alpha}_{(x)}$
7	Pullback: $g^* : \mathcal{T}^*\mathcal{Y} \to \mathcal{T}^*\mathcal{X},$ $\omega \mapsto g^*(\omega)$ $g^*(\omega)(X) := \omega\big(g_*(X)\big)$	$\big(g^*(\omega)\big)_{(x),\alpha} = \psi_{(x),\alpha} = \left(\frac{\partial g^{\beta}_{(yx)}}{\partial x^{\alpha}}\right)_p \omega_{(y),\beta}$
8	Lie derivative: $L_X h := \lim_{t\to 0} \frac{\left(\phi_t^X\right)^* h - h}{t}$ $= \mathrm{d}h(X)$	$L_X h = \frac{\partial h}{\partial x^{\alpha}} X^{\alpha}_{(x)}$

Remark A.1. *For the sake of simplicity, we will abstain from explicit notation of the underlying coordinates if this is not important. For example, instead of* $h_{(x)} := h \circ x^{-1}$ *we simply write* h.

Remark A.2. *Considering* n *points* $p_1, \ldots, p_n$ *on a manifold* $\mathcal{X}$ *and a local chart* x. *The local coordinates of the individual points are read as* ${x_i}^{\alpha} := (x_i)^{\alpha} := x^{\alpha}(p_i)$.

Remark A.3. *To keep the formulas short and readable, we use tensor notation and the Einstein summation convention throughout this document. For instance, we write*

$$\sum_{\alpha=1}^{n_{\mathcal{X}}} \omega_{\alpha} X^{\alpha} = \omega_{\alpha} X^{\alpha}.$$

Throughout this thesis denote the

state trajectory: $\chi : \mathbb{R} \to \mathcal{X},\ t \mapsto x := \chi(t),$

input/manipulating trajectory: $u : \mathbb{R} \to \mathcal{U},\ t \mapsto u := u(t),$

and the controlled variable trajectory: $c : \mathbb{R} \to \mathcal{C},\ t \mapsto c := c(t)$

In general, we define $C\left(\mathcal{Y}_{[0,T]}\right) := C\left([0,T], \mathcal{Y}\right)$.
In the sense of a simple notation, we consider the simple manifold that is a open convex subset $\mathcal{X} \subset \mathbb{R}^n$. If nothing else is mentioned, we choose the standard chart map $id : \mathbb{R}^n \to \mathbb{R}^n$. To simplify the notation, we write for a point $p \in \mathcal{X}$ on the manifold its chart representation $x = x(p) \in \mathcal{X}$.

Below some further definitions are presented.

Definition A.1 (Pullback Bundle)**.** *Let $(\mathcal{E}_1, \pi_1, \mathcal{B}_1)$ be a bundle and $g : \mathcal{B}_2 \to \mathcal{B}_1$ be a map between two manifolds. The pullback bundle $(\mathcal{E}_2, \pi_2, \mathcal{B}_2)$ induced by g is defined by $\mathcal{E}_2 := \left\{(p,q) \in \mathcal{B}_2 \times \mathcal{E}_1 \mid g(p) = \pi_1(q)\right\}$ and $\pi_2(p,q) := p$.*

Definition A.2 (Open ball)**.** *Let $x \in \mathbb{R}^n$ and $\delta \in \mathbb{R}^+$. An open ball of radius δ around the point x is defined by*

$$\mathcal{B}_\delta(x) := \left\{ \xi \in \mathbb{R}^n \;\middle|\; \sum_{\alpha=1}^{n} \left(\xi^\alpha - x^\alpha\right)^2 < \delta \right\}$$

Definition A.3 (Metric on $\mathbb{R}^n$)**.** *Let $p, q, r \in \mathbb{R}^n$ be three points and let*

$$\delta_{\alpha\beta} := \begin{cases} 1 & \text{if } \alpha = \beta, \\ 0 & \text{in all other cases.} \end{cases}$$

The following two functions describe a metric on $\mathbb{R}^n$.

$$\boldsymbol{m}_2 : \mathbb{R}^n \times \mathbb{R}^n \to \mathbb{R}_0^+,$$

$$(p,q) \mapsto \boldsymbol{m}_2(p,q) := \delta_{\alpha\beta}\left(p^\alpha - q^\alpha\right)\left(p^\beta - q^\beta\right)$$

$$\boldsymbol{m}_\mathrm{d} : \mathbb{R}^n \times \mathbb{R}^n \times \mathbb{R}^n \to \mathbb{R}_0^+,$$

$$(p,q,r) \mapsto \boldsymbol{m}_\mathrm{d}(p,q,r) := \frac{\delta_{\alpha\beta}\left(p^\alpha - q^\alpha\right)\left(q^\beta - r^\beta\right)}{\sqrt{\boldsymbol{m}_2(p,q)}\sqrt{\boldsymbol{m}_2(q,r)}}.$$

A.2 Gaussian Process

A Gaussian process (GP) is a machine learning technique that allows to approximate a funcion $h \in C^\infty\left(\mathbb{R}^{n_\mathrm{x}}\right)$ by a function $\tilde{h} \in C^\infty\left(\mathbb{R}^{n_\mathrm{x}}\right)$ based

on a set

$$\mathscr{D} := \left\{ \{(x_l,\, y_l,\, z_l)\}_{l=1,\dots,n} \mid x_l \in \mathbb{R}^{n_\mathrm{x}},\, y_l = h\left(x_l\right),\, \left(z_l\right)_\alpha := \partial_\alpha h(x_l) \right\},$$

of training data, where x_l, y_l and z_l are denoted as training input, measurements and measurements of the derivatives. From a mathematical point of view, a GP is a stochastic process where $(y_1, \dots, y_n)$ are n-dimensional Gaussian distributed, see [128]. In other words, the map $\tilde{h} \in C^\infty\left(\mathbb{R}^{n_\mathrm{x}}\right)$ is Gaussian distributed $\tilde{h} \sim \mathcal{N}\left(\mu, \kappa\right)$, where $\mu \in C^\infty\left(\mathbb{R}^{n_\mathrm{x}}\right)$ and $\kappa \in C^\infty\left(\mathbb{R}^{n_\mathrm{x}} \times \mathbb{R}^{n_\mathrm{x}}\right)$ are called mean and kernel function. The latter one represents the variance or covariance. For a detailed introduction to this topic and an overview of different application areas, we refer to [203, 178, 130].
Employing the stochastic nature of GPs, several advantages can be concluded:

(i) measurement noise of y_l or z_l can be explicitly addressed in designing $\tilde{h}$.

(ii) prior knowledge from mathematical-physical models can be incorporated into the design of $\tilde{h}$.

(iii) the tendency for overfitting is reduced

(iv) besides the function value of $\tilde{h}$ at a certain point, the confidence interval and the associated uncertainty of $\tilde{h}$ can be described, which allows evaluating the approximation quality of $\tilde{h}$ compared to h

(v) the dimension of involved parameters is independent from the number n of training data

During the last decades, GPs achieved great success in modelling static [163, 172] and dynamic [132, 189, 248] systems. Furthermore they are used in the field of model predictive control [151, 131, 190], for numerical integration [201] or to estimate the system-model mismatch in context of real-time optimization [65] or modifier adaptation [7].

Before we describe the design of $\tilde{h}$ in detail, the following assumption is made.

Assumption A.1. *If there is nothing else specified, the observation* $y_l = h(x_l) + \epsilon_\mathrm{y},\ \epsilon_\mathrm{y} \sim \mathcal{N}\left(0, {\sigma_\mathrm{y}}^2\right)$ *and the partial derivative* $\left(z_l\right)_\alpha := \partial_\alpha h(x_l) + \epsilon_\mathrm{z},\ \epsilon_\mathrm{z} \sim \mathcal{N}\left(0, \sigma_\mathrm{z}^2\right)$ *are affected by noise.*

Remark A.4. *To simplify index work, we use Latin letters* $(l, m, \dots)$ *to indicate the training point and Greek letters* $(\alpha, \beta, \dots)$ *to indicate the component of a variable. For instance,* $\left(x_l\right)^\alpha$ *describes the coordinate* α *of the* l*-th input or* $\left(z_l\right)_\alpha$ *describes the derivative with respect to the* α *component of* h*, evaluated for the* l*-th input* x*.*

An essential aspect of a GP is the kernel function κ, which describes the relation of two points in $\mathbb{R}^{n_\mathrm{x}}$. Thus, the influence of the points in a neighborhood of $x \in \mathbb{R}^{n_\mathrm{x}}$ on the function value $h(x)$ can be expressed. The following gives a formal definition of this fact.

Definition A.4 (Kernel Function)**.** *Given is the product space $\mathbb{R}^{n_\mathrm{x}} \times \mathbb{R}^{n_\mathrm{x}}$. A function $\kappa : \mathbb{R}^{n_\mathrm{x}} \times \mathbb{R}^{n_\mathrm{x}} \to \mathbb{R}^+$ is called kernel function, if it satisfied for $x, y \in \mathbb{R}^{n_\mathrm{x}}$*

(i) κ is symmetrical in both entries: $\kappa(x, y) = \kappa(y, x)$,

(ii) $\kappa(x, y) \leq \kappa(x, x)$, $\forall y \in \mathbb{R}^{n_\mathrm{x}}$.

From the definition of a GP as a stochastic process, whose random variables $(y_1, \ldots, y_n)$ are normally distributed, the Bayesian formalism can be used to compute posterior probability based on the prior knowledge of the functions μ and κ. This way $\tilde{h}$ can be calculated as an element of an infinite-dimensional space $C^\infty(\mathbb{R}^{n_\mathrm{x}})$ over a finite number of training points. This update generates the posterior mean $\hat{\mu} \in C^\infty(\mathbb{R}^{n_\mathrm{x}})$ and posterior kernel $\hat{\kappa} \in C^\infty(\mathbb{R}^{n_\mathrm{x}} \times \mathbb{R}^{n_\mathrm{x}})$, where $\tilde{h} := \hat{\mu}$.
The rest of this section deals with the derivation of functions $\hat{\mu}$ and $\hat{\kappa}$. For this purpose we define the derivatives of the kernel function κ through its components as follows

$$\chi_\alpha : (x, y) \mapsto \chi_\alpha(x, y) := \big(\partial_{n_\mathrm{x}+\alpha}\, \kappa(x, \cdot)\big)(y), \quad \alpha = 1, \ldots, n_\mathrm{x}$$

$$\psi_{\alpha\beta} : (x, y) \mapsto \psi_{\alpha\beta}(x, y) := \big(\partial_\beta\, \chi_\alpha(\cdot, y)\big)(x), \quad \beta = 1, \ldots, n_\mathrm{x}.$$

We denote the predictions made by the prior μ by $\boldsymbol{M}_l := \mu(x_l)$. Likewise, the evaluation of the components of $\mathrm{d}\mu$ at x_l are given by $(\boldsymbol{D}_l)_\alpha := \partial_\alpha \mu(x_l)$. Considering the kernel function κ, we introduce the function ${\eta^{\boldsymbol{x}}}_l \in C^\infty(\mathbb{R}^{n_\mathrm{x}})$ by

$$(y) \mapsto {\eta^{\boldsymbol{x}}}_l(y) := \kappa(x_l, y), \quad x_l \in \mathscr{X} := \{x_1, \ldots, x_n\}$$

that provides a relationship of for any point $y \in \mathbb{R}^{n_\mathrm{x}}$ over a base point $x_l \in \mathscr{X}$ of the training inputs. In the same way we define componentwise a map $({\rho^{\boldsymbol{x}}}_l)_\alpha \in C^\infty(\mathbb{R}^{n_\mathrm{x}})$ by

$$(y) \mapsto ({\rho^{\boldsymbol{x}}}_l)_\alpha(y) := \chi_\alpha(x_l, y), \quad x_l \in \mathscr{X}.$$

Remark A.5. *For reasons of readability, we will not use brackets to separate the l-th point or coordinate and the α-th index in the following. For instance, instead of $(z_l)_\alpha$, we now write $z_{l\alpha}$. Due to the omission of this explicit separation, only Greek letters are used as indices.*

Based on $\eta^{\boldsymbol{x}}$ and $\rho^{\boldsymbol{x}}$, we construct the posterior mean function $\hat{\mu}$ by

$$\hat{\mu}\left(x\right) := \Big(\mu + a^{\iota}{\eta^{\boldsymbol{x}}}_{\iota} + b^{\iota\zeta}{\rho^{\boldsymbol{x}}}_{\iota\zeta}\Big)(x). \tag{A.1}$$

Here, the first term in the definition denote the prior mean function μ. In the second term the relationship of x to all input data $\mathscr{X}$ is weighted with a factor a^{ι} and in the third term the derivative of the kernel is weighted with a factor $b^{\iota\zeta}$. Both factors are evaluated from the training data $\mathscr{D}$ as follows

$$a^{\alpha} := L^{\alpha\iota}\left(y_{\iota} - \boldsymbol{M}_{\iota}\right) + M^{\alpha\iota\zeta}\left(z_{\iota\zeta} - \boldsymbol{D}_{\iota\zeta}\right),$$

$$b^{\alpha\beta} := M^{\iota\alpha\beta}\left(y_{\iota} - \boldsymbol{M}_{\iota}\right) + R^{\alpha\iota\beta\zeta}\left(z_{\iota\zeta} - \boldsymbol{D}_{\iota\zeta}\right).$$

In order to obtain these three matrices $L^{\alpha\beta}$, $M^{\alpha\beta\gamma}$ and $R^{\alpha\beta\gamma\varepsilon}$, we first have to introduce

$$\begin{aligned} K_{lm} :=& \kappa(x_l, x_m) + {\sigma_{\mathrm{y}}}^2\delta_{lm}, \\ \left(P_{lm}\right)_{\alpha} :=& \chi_{\alpha}(x_l, x_m), \\ \left(Q_{lm}\right)_{\alpha_\beta} :=& \psi_{\alpha\beta}(x_l, x_m) + {\sigma_{\mathrm{z}}}^2\left(\delta_{lm}\right)_{\alpha_\beta}, \end{aligned}$$

for each input $x_l, x_m \in \mathscr{X}$. Interpreting K, P and Q as parts of a block matrix, we define L, M and R as blockwise inverse by using the analytic formula as discussed below. For this we make use of Remark A.5 and define first the inverse $\tilde{K}$ and $\tilde{Q}$ by

$$\tilde{K}^{\alpha\iota}K_{\iota\beta} = \delta^{\alpha}_{\beta}, \quad \text{and} \quad \tilde{Q}^{\alpha\iota\beta\chi}Q_{\iota\gamma\chi\varepsilon} = \delta^{\alpha}_{\gamma}\delta^{\beta}_{\varepsilon}.$$

Finally, L, M and R are given as follows

$$L^{\alpha\iota}\Gamma_{\iota\beta} = \delta^{\alpha}_{\beta}, \text{ where } \Gamma_{\alpha\beta} := K_{\alpha\beta} - P_{\alpha\iota\zeta}\,P_{\beta\chi\psi}\,\tilde{Q}^{\iota\chi\zeta\psi},$$

$$R^{\alpha\iota\beta\chi}\Lambda_{\iota\gamma\chi\varepsilon} = \delta^{\alpha}_{\gamma}\delta^{\beta}_{\varepsilon}, \text{ where } \Lambda_{\alpha\beta\gamma\varepsilon} := Q_{\alpha\beta\gamma\varepsilon} - P_{\iota\alpha\beta}\,P_{\zeta\gamma\varepsilon}\,\tilde{K}^{\iota\zeta}$$

and

$$M^{\alpha\beta\gamma} := -L^{\alpha\iota}P_{\iota\zeta\chi}\,\tilde{Q}^{\zeta\beta\chi\gamma}.$$

Remark A.6. *Following, we use the squared exponential kernel (Gaussian kernel)*

$$\kappa(x_1, x_2) := {\sigma_{\mathrm{f}}}^2\exp\left(-\frac{1}{2}\Big(l_{\alpha}\left({x_1}^{\alpha} - {x_2}^{\alpha}\right)\Big)^2\right),$$

where $l_{\alpha} \in \mathbb{R}^{+}$ is the horizontal length scale and $\sigma_{\mathrm{f}} \in \mathbb{R}^{+}$ controls the vertiacal variation. The parameters $\mathscr{H} := (l, \sigma_{\mathrm{f}}, \sigma_{\mathrm{y}}, \sigma_{\mathrm{z}})$ are called hyperparameter.

There are two special cases that can be derived from the posterior mean function (A.1).

Zero prior mean function: If there is no previous knowledge about the process, it is possible to set the prior mean function to zero. Thus the meaningful domain of $\hat{\mu}$ is restricted to the area in which training data is available, since only interpolation is feasible. An extrapolation will lead to the prior mean value i.e. zero. For the posterior mean function, we obtain

$$\hat{\mu}\left(x\right) := \left(a^{\iota}\eta^{\boldsymbol{x}}{}_{\iota} + b^{\iota\zeta}\rho^{\boldsymbol{x}}{}_{\iota\zeta}\right)(x), \tag{A.3}$$

where

$$\begin{aligned} a^{\alpha} :=& L^{\alpha\iota}y_{\iota} + M^{\alpha\iota\zeta}z_{\iota\zeta}, \\ b^{\alpha\beta} :=& M^{\iota\alpha\beta}y_{\iota} + R^{\alpha\iota\beta\zeta}z_{\iota\zeta}. \end{aligned}$$

Zero prior mean function and no derivative information: It is often the case that no information is available regarding the partial derivatives. This is particularly true when training data are obtained from measurements or observations and not from complex white box models. The posterior mean function is given by

$$\hat{\mu}\left(x\right) := a^{\iota}\eta^{\boldsymbol{x}}{}_{\iota}(x), \tag{A.4}$$

where

$$a^{\alpha} := L^{\alpha\iota}y_{\iota}.$$

Posterior covariance: The posterior kernel function that describes the variance or covariance is given by

$$\begin{aligned} \hat{\kappa}\left(x\right) :=& \kappa(x,x) - L^{\alpha\iota}\eta^{\boldsymbol{x}}{}_{\iota}(x)\eta^{\boldsymbol{x}}{}_{\alpha}(x) - 2M^{\alpha\iota\zeta}\rho^{\boldsymbol{x}}{}_{\iota\zeta}(x)\eta^{\boldsymbol{x}}{}_{\alpha}(x) \\ & - R^{\alpha\iota\beta\zeta}\rho^{\boldsymbol{x}}{}_{\iota\zeta}(x)\rho^{\boldsymbol{x}}{}_{\alpha\beta}(x) \end{aligned} \tag{A.5}$$

A.3 Optimization – Parametric Sensitivity

Consider an objectiv function $J : \mathbb{R}^{n_{\mathrm{x}}} \times \mathbb{R}^{n_{\mathrm{p}}} \to \mathbb{R}$ where $x \in \mathbb{R}^{n_{\mathrm{x}}}$ is called optimization variable and $p \in \mathbb{R}^{n_{\mathrm{p}}}$ is a parameter. Moreover, let $g : \mathbb{R}^{n_{\mathrm{x}}} \times \mathbb{R}^{n_{\mathrm{p}}} \to \mathbb{R}^{n_{\mathrm{g}}}$ and $h : \mathbb{R}^{n_{\mathrm{x}}} \times \mathbb{R}^{n_{\mathrm{p}}} \to \mathbb{R}^{n_{\mathrm{h}}}$ be two functions. For given boundaries $\underline{x}, \overline{x} \in \mathbb{R}^{n_{\mathrm{x}}}$

and $\underline{h}, \overline{h} \in \mathbb{R}^{n_\mathrm{h}}$ a parametric NLP reads

$$\underset{x,p}{\text{minimize}} \quad J(x,p) \tag{A.6a}$$

$$\text{subject to} \qquad 0 = g(x,p), \tag{A.6b}$$

$$\underline{h} \leq h(x,p) \leq \overline{h}, \tag{A.6c}$$

$$(\underline{x}, p_\mathrm{s}) \leq (x,p) \leq (\overline{x}, p_\mathrm{s}), \tag{A.6d}$$

where $p_\mathrm{s} \in \mathbb{R}^{n_\mathrm{p}}$ is a parameter to be set. The functions g and h represents the equality and inequality constraints.

Let $\lambda_\mathrm{x} \in \mathbb{R}^{n_\mathrm{x}}$, $\lambda_\mathrm{p} \in \mathbb{R}^{n_\mathrm{p}}$, $\lambda_\mathrm{g} \in \mathbb{R}^{n_\mathrm{g}}$ and $\lambda_\mathrm{h} \in \mathbb{R}^{n_\mathrm{h}}$ be the Lagrange multiplier of the optimization variable, the parameter, the equality and the inequality constraints. From the Lagrangian

$$L\left(x,p,\lambda_\mathrm{x},\lambda_\mathrm{p},\lambda_\mathrm{g},\lambda_\mathrm{h}\right) := J(x,p) + \lambda_{\mathrm{g}_\alpha}\, g^\alpha(x,p) + \lambda_{\mathrm{h}\beta}\, h^\beta(x,p) + \lambda_{\mathrm{x}\gamma}\, x^\gamma + \lambda_{\mathrm{p}_\iota}\, p^\iota,$$

and KKT condition follows that the parametric sensitivity is given by

$$\lambda^*_{\mathrm{p}\alpha} = -\partial_{p^\alpha} J(x^*, p_\mathrm{s}) - \lambda^*_{\mathrm{g}\beta}\, \partial_{p^\alpha} g^\beta(x^*, p_\mathrm{s}) - \lambda^*_{\mathrm{h}\gamma}\, \partial_{p^\alpha} h^\gamma(x^*, p_\mathrm{s})$$

where $\left(x^*, \lambda^*_\mathrm{g}, \lambda^*_\mathrm{h}\right)$ is the primal-dual solution of (A.6), [5].

A.4 Unscented Transformation

Consider a Gaussian distributed random variable θ, with mean value $\hat{\theta} \in \mathbb{R}^n$ and covariance $P \in \mathbb{R}^{n,n}$. In order to propagate the distributed information by a nonlinear function $h : \mathbb{R}^n \to \mathbb{R}$, the unscented transformation was developed by [116]. The main idea of this method is to approximate a density function of a distribution by a finite number of sigma points. Subsequently, the image of these sigma points using the function h is recombined by weighting factors so that the mean value and the variance/covariance approximate the distribution in the codomain.
The following descriptions are already adapted to the specific application used in this work. For instance, the codomain of the function h is only 1-dimensional since the maps derived here are applied to the rate functions ${\mathfrak{P}_{\mathrm{r}_j}}^\alpha$ of the individual storage elements. For a comprehensive introduction to this topic, we refer to the works of Julier in [116, 114, 119, 115, 118] or to a book about nonlinear filtering [30]. Some of the advantages of the unscented transformation are

(i) the computational effort for the unscented transformation scales with $(2n+1)$ [116],

(ii) the calculation of the mean value and the variance is parallizable, since each sigma point can propagate independently [69],

(iii) for scalar parameter, one can show that the error of the mean and variance is up to the order of four [116, 88],

(iv) the unscented transformation utilizes the first, second and higher moments of the pdf, which makes it more accurate than a linearization [116].

In the last decades the unscented transformation has been applied in many fields, such as for state estimation [117, 251], for robust MPC [96], to compute optimal process trajectories [211], for optimal experimental design [220, 69] or for statistical robust design [239].

To describe this method we start with the generation of the sigma points by the map

$$\mathit{Sp}: \left(\hat{\theta}, P\right) \mapsto \mathit{Sp}\left(\hat{\theta}, P\right) := \left\{\tilde{\theta}_0, \ldots, \tilde{\theta}_n\right\},$$

where the sigma points are defined componentwise by

$$\begin{aligned}
\tilde{\theta}_0{}^{\alpha} &:= \hat{\theta}^{\alpha}, \\
\tilde{\theta}_i{}^{\alpha} &:= \hat{\theta}^{\alpha} + S^{\alpha}{}_{\beta}(e_i)^{\beta}, \qquad i = 1, \ldots, n, \\
\tilde{\theta}_{n+i}{}^{\alpha} &:= \hat{\theta}^{\alpha} - S^{\alpha}{}_{\beta}(e_i)^{\beta}, \qquad i = 1, \ldots, n.
\end{aligned}$$

Here, S is defined as square root following

$$\tilde{P}^{\alpha}{}_{\beta} = S^{\alpha}{}_{\iota} S^{\iota}{}_{\beta},$$

where $\tilde{P}^{\alpha}{}_{\beta} := (n+\lambda) P^{\alpha}{}_{\beta}$ is the weighted covariance using $\lambda := \alpha^2(n+\kappa) - n$, which is determined by the parameters $\alpha, \kappa \in \mathbb{R}$. The components of the object e_i are given through $(e_i)^{\alpha} := \delta_i^{\alpha}$. Using these sigma points we obtain the mean value in the codomain under the function h by the map

$$\begin{aligned}
&M[h] : \mathbb{R}^n \times \mathbb{R}^{n,n} \to \mathbb{R}^n, \\
&\left(\hat{\theta}, P\right) \mapsto M[h]\left(\hat{\theta}, P\right) := \sum_{i=0}^{2n} w^{\mathrm{m}}{}_i \, h(\theta_i), \quad \theta_i \in \mathit{Sp}\left(\hat{\theta}, P\right)
\end{aligned} \tag{A.7}$$

where the weight factors are given by

$$w^{\mathrm{m}}{}_0 := \frac{\lambda}{n+\lambda},$$

$$w^{\mathrm{m}}{}_i := \frac{1}{2\,(n+\lambda)}, \qquad i = 1, \ldots, 2n.$$

The superscript m denotes that the weight factors are used for the mean. Finally, the variance is described by

$$V[h] : \mathbb{R}^n \times \mathbb{R}^{n,n} \to \mathbb{R}^+, \ \left(\hat{\theta}, P\right) \mapsto V[h]\left(\hat{\theta}, P\right) := P_{\mathrm{h}} \tag{A.8}$$

where P_{h} using the sigma points $\theta_i \in \mathcal{Sp}\left(\hat{\theta}, P\right)$ is given by

$$P_{\mathrm{h}} := \sum_{i=0}^{2n} w^{\mathrm{c}}{}_i \left(h(\theta_i) - M[h]\left(\hat{\theta}, P\right)\right)\left(h(\theta_i) - M[h]\left(\hat{\theta}, P\right)\right).$$

The weight factors used for the covariance are determined by

$$w^{\mathrm{c}}{}_0 := \frac{\lambda}{n+\lambda} + (1 - \alpha^2 + \beta),$$

$$w^{\mathrm{c}}{}_i := w^{\mathrm{m}}{}_i, \qquad i = 1, \ldots, 2n,$$

where $\beta \in \mathbb{R}$ is another parameter. For Gaussian distributions, Julier and Uhlmann [118] proposes that $\beta = 2$. The parameter α scales the spread of the sigma points around the mean value. It is recommended that $0 \leq \alpha \leq 1$, and it needs to be chosen to minimize the scaling effects in higher order of the Taylor series expansion, since the parameter only affects this one [115]. Van Der Merwe [251] indicates that there is no global-valid optimal parameter setting or tuning rules for determineng α, β and κ.

A.5 Parameter for the Setup Function

The parameter for basic term A in Table 4.1 in Section 4.2 are determined by the relative degree of the processes model. Himmel et al. [100] presented that the coefficients for the polynomial term are given by

$$p_i = \frac{(-1)^{i-1}(2r+1)!}{(i+r)\cdot r!(i-1)!(r+1-i)!}.$$

Furthermore, the coefficients for the trigonometric series are defined using Algorithm A.1. It should be emphasized that for a high relative degree r, the matrix A can be ill-conditioned. At this point, further modifications have to be made, e.g., regularisation techniques. The convergence rate of Algorithm A.1 is similar to computing the solution of a linear equation.

Algorithm A.1: Coefficients for the trigonometric series.

$m := 2$; $v := 0$; $I := [0\ 0]$; $k := 1$ 1
for $i = 1 : 2 : r$ **do** 2
  $m \leftarrow m + 2$ $v \leftarrow v + 2$ $I \leftarrow [I\ v\ v]$ 3
end 4
$b := \text{zeros}(m, 1)$, $b(2) \leftarrow 1$ $A := \text{zeros}(m, m)$ **for** $i = 1 : numel(I)$ **do** 5
  for $ii = 1 : m$ **do** 6
    if $mod(k, 2) = 0$ **then** 7
    $h := pow\big(ii - 1, I(i)\big)$ $A(k, ii) \leftarrow h \cos\big((ii - 1)\pi\big)$ 8
    else $A(k, ii) \leftarrow pow\big(ii - 1, I(i)\big)$ 9
  end 10
  $k \leftarrow k + 1$ 11
end 12
$p \leftarrow A \backslash b$ 13

Appendix B

Example of a Production System

B.1 Production System for a Biological and Catalytic Production of a Joint Product

We consider two process $\mathcal{S}_1$ and $\mathcal{S}_2$ that produce M from different raw material feeds. The first process represents a biological way to produce M from an organic raw material by anaerobic digestion (AD). A byproduct of this decomposition is C, which is stored and then converted in the second process. In the second process, C taken from the storage system is converted with H by a classical reactor-separation-recycle (RSR) proces to M and W.

Before we explain the entire production system in detail, the individual process architecture is be discussed. For this purpose we will use reduced models in which the input/output behavior, the dynamic properties and the characteristics of certain crucial states are preserved compared to the detailed models. The parameter values used here are chosen so that the processes and thus the two models are compatible with each other. This means that the material and energy flows that both processes exchange have the same proportions. It is therefore important that the AD produces approximately the same amount of C at its nominal operational point as is required by the RSR at its nominal operational point. In addition, the dynamic properties of both processes have to be similar. This means that the time constants of both processes need to be in the same order of magnitude, resulting similar transition times for operational

changes.
In general, the parameters of the simplified models can be estimated from measurement data of real processes or more detailed models.

Brief description: In $\mathcal{S}_1$, only the reactor in which the decomposition reaction takes place is modelled since this is the time dominating process element. The RSR-process in $\mathcal{S}_2$ follows the classical recycling structure consisting of a mixer, a reactor, and a separation system. The temperature modelling in both processes is important. For instance, the decomposition in $\mathcal{S}_1$ is done by microorganisms, the temperatures should not fluctuate too much as the resulting stress would harm the yield of M. Furthermore, the death of the microorganisms would cause a complete shutdown of production. From [24] we know that production changes in the catalytic reactor can lead to the formation of a temperature hot spot because the heat cannot be dissipated quickly enough. This effect has to be included in the transition times for production changes. Since the purification of M in $\mathcal{S}_2$ cannot be fully guaranteed due to high costs, we assume that light impurities of H may be present in the product. However, these impurities should not be too high, as this would harm the selling price. Therefore, the production quality is also included in the description of the production system. As the production system is part of a process network, the product has to satisfy downstream process constraints. In this context, we consider the total material flow and the product quality of the production system, which needs to lie within the defined box-constrained area.

Classically, the feed parameter of $\mathcal{S}_1$ describes the quality of the organic substrate. In standard modeling approaches a change of θ^1 would have a direct effect on the process, e.g. in the form of changing stoichiometric parameters or intermediate products and thus also changing the quantity of M. That means a higher quality would lead to higher production of M while using the same amount of feed. To avoid this, we propose an alternative modelling approach to describe the substrate quality. The key idea is that the substrate is composed of inert materials and an active component that is decomposed to C and M. Hence, we assume that the components responsible for the production of M can be purchased and added separately. Figure B.1 illustrates this concept that a low price implies more M-producing components, which means that higher quality can be achieved. For the RSR-process, we use the electricity price to

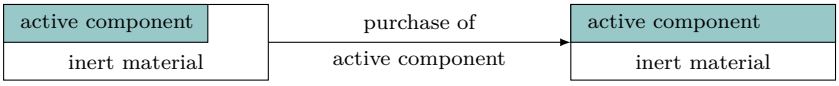

Figure B.1: Illustration of the feed quality concept.

parametrize the operating costs, since H is produced via an upstream process

element, the electricity price correlates directly with the price of input stream of H.

Process $\mathcal{S}_1$ (anaerobic digestion)

Mathematical model: The internal process topology of $\mathcal{S}_1$ is illustrated in Figure B.2. The process consists of a bioreactor and a separator. However, the latter process element will not be described by the mathematical model, since the dynamics of the process is mainly determined by the bioreactor. Within the liquid phase of the reactor an organic substrate A is deomposed by the reactions

$$k_1\mathrm{A} \xrightarrow{\mathrm{r}_1} \mathrm{X}_1 + k_2\mathrm{B} + k_4\mathrm{C},$$

$$k_3\mathrm{B} \xrightarrow{\mathrm{r}_2} \mathrm{X}_2 + k_5\mathrm{C} + k_6\mathrm{M}.$$

The feed stream of the reactor is primarily composed of an inert material for the reaction and a reactive substance A, supplied by the molar flow ${G_{\mathrm{ex}}}^{\mathrm{A}}$. Furthermore, it is assumed that

$$V_{\mathrm{m}}^{\mathrm{A}}\,{G_{\mathrm{ex}}}^{\mathrm{A}} \ll F_{\mathrm{ex}},$$

where $V_{\mathrm{m}}^{\mathrm{A}}$ is the molar volume of A and F_{ex} the volume flow of the inert material. In this way a change of ${G_{\mathrm{ex}}}^{\mathrm{A}}$ has only a marginal effect on the entire volume flow that enters the reactor. Consequently, we consider a constant volume flow and a stationary level of the liquid phase within the reactor ($F_{\mathrm{ex}} = F_{\mathrm{wast}}$). Depending on the concentration of carbon dioxide C and methane M within the liquid phase, C and M also accumulate in the gas phase above. This gas mixture is finally cleaned and separated into its components. As the decomposition reaction is strongly temperature dependent, the reactor needs heat flow Q from the element ${\mathcal{B}_2}^1$ to stay within the optimal temperature range.

In the following we will briefly discuss the mathematical model of the process based on the Bernard et al. [17]. The external input feed stream is given by the molar flow ${G_{\mathrm{ex}}}^{\mathrm{A}}$ of the component A. We describe the bioreactor by a continuous stirred tank reactor, whereby the volume of the liquid phase is constant. Using the dilution rate

$$D = \frac{F_{\mathrm{ex}}}{V_{\mathrm{r}}},$$

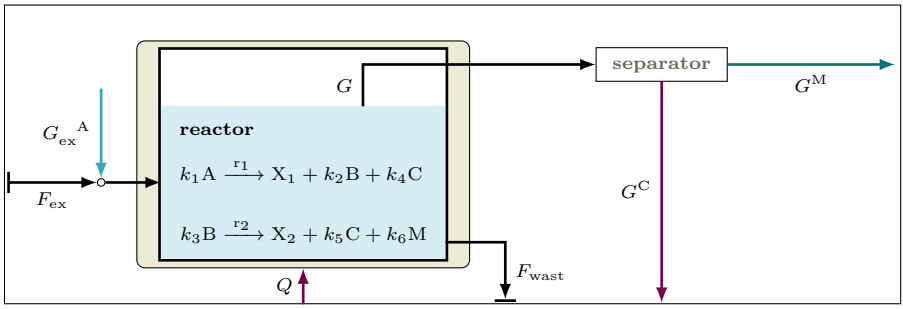

Figure B.2: Structure of Process $\mathcal{S}_1$.

the system reads

$$\dot{T}_\mathrm{j} = \kappa_2 \left[T_\mathrm{r} - T_\mathrm{j}\right] + \kappa_3 Q, \tag{B.1a}$$

$$\dot{T}_\mathrm{r} = h\left(r_1, r_2, T_\mathrm{r}\right) + \kappa_1 \left[T_\mathrm{j} - T_\mathrm{r}\right] + D\left[T_\mathrm{r}^\mathrm{i} - T_\mathrm{r}\right], \tag{B.1b}$$

$$\dot{c}^{\mathrm{X}_1} = -D\,\alpha c^{\mathrm{X}_1} + r_1, \tag{B.1c}$$

$$\dot{c}^{\mathrm{X}_2} = -D\,\alpha c^{\mathrm{X}_2} + r_2, \tag{B.1d}$$

$$\dot{c}^\mathrm{A} = -Dc^\mathrm{A} - k_1 r_1 + \frac{1}{V_\mathrm{r}} {G_\mathrm{ex}}^\mathrm{A}, \tag{B.1e}$$

$$\dot{c}^\mathrm{B} = -Dc^\mathrm{B} + k_2 r_1 - k_3 r_2, \tag{B.1f}$$

$$\dot{c}^\mathrm{C} = -Dc^\mathrm{C} + k_4 r_1 + k_5 r_2 - \frac{1}{V_\mathrm{r}} G^\mathrm{C}, \tag{B.1g}$$

$$\dot{c}^\mathrm{M} = -Dc^\mathrm{M} + k_6 r_2 - \frac{1}{V_\mathrm{r}} G^\mathrm{M}, \tag{B.1h}$$

where the reaction rates r_1 and r_2 are given by temperature dependent Monod equations. These equations are given by

$$r_1 := \sigma_1\left(T_\mathrm{r}\right) \frac{\bar{\mu}_1\, c^\mathrm{A} c^{\mathrm{X}_1}}{c^\mathrm{A} + K_1} \quad \text{and} \quad r_2 := \sigma_2\left(T_\mathrm{r}\right) \frac{\bar{\mu}_2\, c^\mathrm{B} c^{\mathrm{X}_2}}{c^\mathrm{B} + K_2},$$

where the temperature coefficient is determined through

$$\sigma_i(T_\mathrm{r}) := \exp \frac{-(T_\mathrm{r} - T_\mathrm{ref})^2}{\vartheta_\mathrm{sens}}.$$

Here, T_{ref} describes the reference temperature where the decomposition reactions are most powerful and $\vartheta_{\mathrm{sens}}$ is used to describe the temperature sensitivity. By changing the supplied heat flow Q, it has to be ensured that the temperature of the liquid phase is always around T_{ref}. If the temperature fluctuates too much, the reaction rates decrease or even stop completely. The reaction-induced change in temperatur can be described by

$$h\left(r_1, r_2\right) = -\kappa_4 V_{\mathrm{r}}\ \left(r_1 \Delta h_1 + r_2 \Delta h_2\right).$$

To describe the gas transfer between the liquid and the gas phase, we use the ansatz

$$G^{\alpha} := k_{\mathrm{L},\alpha} V_{\mathrm{r}}\, c^{\alpha}, \quad \alpha \in \{\mathrm{C}, \mathrm{M}\}$$

The individual parameter and state variabels are summarized in the table B.1.

Table B.1: Physical properties of the model parameter for $\mathcal{S}_2$.

symbol	**description**	**dimension**
V_{r}	volume of the liquid phase	m^3
D	dilution rate	1/s
G	molar flow	mol/s
r_{α}	reaction term	$\mathrm{mol/m}^3\mathrm{/s}$
α	Proportion of dilution rate for bacteria	1
κ_1	heat conductivity parameter	1/s
κ_2	heat conductivity parameter	1/s
κ_3	heat parameter	K/kJ
κ_4	heat capacity parameter	K/kJ
$\bar{\mu}_{\alpha}$	maximum bacterial growth rate	1/s
K_{α}	half-saturation constant	$\mathrm{mol/m}^3$
$\vartheta_{\mathrm{sens}}$	temperatur sensitivity of the reaction	K
T_{ref}	optimal reaction temperatur	K
$k_{\mathrm{L},\alpha}$	liquid-gas transfer coecient	1/s
$F_{\mathrm{ex}}, F_{\mathrm{wast}}$	volume flow	$\mathrm{m}^3\mathrm{/s}$
Δh_{α}	reaction enthalpy	kJ/mol
Q	heat flow	kJ/s
V_{r}	volume of the liquid phase	m^3
$T_{\mathrm{r}}, T_{\mathrm{s}}$	temperatur	K

Secondary feed: In addition to the reactive substance A, the process also consumes heat to keep the necessary temperature for the anaerobic digestion. This heat is extracted from an energy storage element ${\mathcal{B}_2}^1$, where the index number 2 indicates that the process $\mathcal{S}_2$ is the heat source. The key factor here

is the amount of heat flow in order to maintain the reference temperature in the reactor. In particular when the molar flow ${G_{\mathrm{ex}}}^{\mathrm{A}}$ changes, more or less energy is required. We use the ansatz

$$ {w_{2|1}}^{1} := \; Q = Q_{\mathrm{n}} + \beta \left(T_{\mathrm{ref}} - T_{\mathrm{r}} \right) $$

to determine the heat flow. Here, Q_{n} is the nominal heat flow at the nominal operational point and β a scaling factor.

Primary product: Since we assume that the speparator works perfectly, the production level is given by the molar flow

$$ {c}^{1} := \; G^{\mathrm{M}} = k_{\mathrm{L,M}} V_{\mathrm{r}} \, c^{\mathrm{M}}, $$

of the component M.

Byproduct: The level of the byproduct is described by the molar flow

$$ {v_{1}}^{1} := \; G^{\mathrm{C}} = k_{\mathrm{L,C}} V_{\mathrm{r}} \, c^{\mathrm{C}} $$

of the component C. This flow is send to the storage element ${\mathcal{B}_{1}}^{1}$.

Feed parameter: The approach to describe the entire feed stream (sum of inert and reactive material) discussed above results from the characterization of the feed parameter. Usually a bioreactor is fed with a feed stream consisting of different components (e.g. A). However, it is possible that the composition and hence the concentration of A might change over time, which would also cause a change in the production level. In this case the feed parameter is given by the concentration of A, which means that it would act directly on the process model as model parameter. If the concentration of A changes (and thus the quality of the feed), the volume flow also has to be modified in order to ensure a stable production level.
An alternative approach is to assume that an inert volume flow F_{ex} is enriched with substance A and that the price of A can change over time. In this way, the feed quality is expressed by a price, which can later be used to describe the operational costs.

Process $\mathcal{S}_2$ (RSR-process)

Mathematical model: The internal process topology of $\mathcal{S}_2$ is illustrated in Figure B.3. The main process elements are the reactor, the separator and the mixer that are connected to each other, including a recycle system. In process $\mathcal{S}_2$, we consider the substance set $\mathcal{S} := \{\mathrm{H}, \mathrm{C}, \mathrm{M}, \mathrm{W}\}$. Within the reactor the

substances H and C react with each other following the scheme

$$4\mathrm{H} + \mathrm{C} \underset{\mathrm{r}_{1-}}{\overset{\mathrm{r}_{1+}}{\rightleftharpoons}} \mathrm{M} + 2\mathrm{W}.$$

The external molar flow ${G_{\mathrm{ex}}}^{\mathrm{H}}$ of $\mathcal{S}_2$ contains pure H. In combination with the recycling stream $G_{\mathrm{s}}^{\mathrm{t}}$ from the first separator and the molar flow ${G_{\mathrm{s}}}^{\mathrm{C}}$ from the storage element ${\mathcal{B}_1}^1$, the individual components are mixed up. The mixer is also considered as an intermediate storage element, which supplies a feed stream to the reactor according to the stored amount of material. Within the reactor an equilibrium reaction takes place depending on the pressure and temperature level. Furthermore, the reaction is exothermic, so that the produced energy can be dissipated via cooling jacket and transferred to the energy storage element ${\mathcal{B}_2}^1$. The product of the reactor is then purified in a first separation stage so that primarily the components H and C are separated from M and W. The recycled stream $G_{\mathrm{s}}^{\mathrm{t}}$ contains mainly the components H and C, whereas the second stream $G_{\mathrm{s}}^{\mathrm{b}}$ is mainly composed of M and W. Finally, $G_{\mathrm{s}}^{\mathrm{b}}$ is further separated in a second separation stage, so that the product of $\mathcal{S}_2$ is a composition of M and a minor proportion of H.

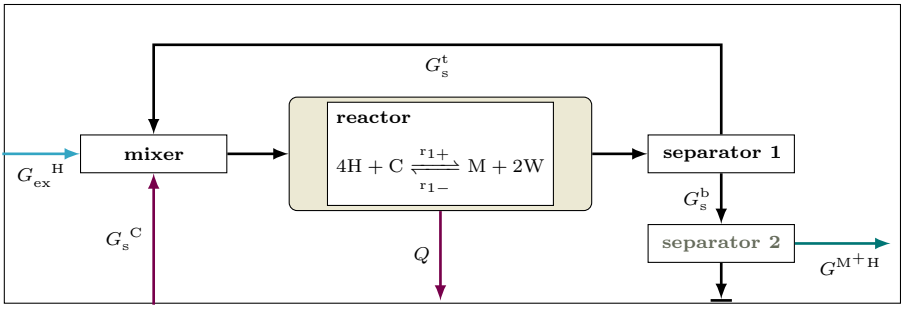

Figure B.3: Structure of Process $\mathcal{S}_2$.

In the following, we will briefly discuss the mathematical model of the process. We focus on the modelling of the mixer, the reactor and the first separator stage, as it is assumed that these elements significantly determine the dynamics. The dynamical equations of the process reads for the individual elements:

mixer:

$$\dot{N}_{\mathrm{m}}{}^{\mathrm{H}} = G_{\mathrm{ex}}{}^{\mathrm{H}} + G_{\mathrm{s}}^{\mathrm{t}\,\mathrm{H}} - G_{\mathrm{m}}{}^{\mathrm{H}}, \tag{B.2a}$$

$$\dot{N}_{\mathrm{m}}{}^{\mathrm{C}} = G_{\mathrm{s}}{}^{\mathrm{C}} + G_{\mathrm{s}}^{\mathrm{t}\,\mathrm{C}} - G_{\mathrm{m}}{}^{\mathrm{C}}, \tag{B.2b}$$

$$\dot{N}_{\mathrm{m}}{}^{\mathrm{M}} = G_{\mathrm{s}}^{\mathrm{t}\,\mathrm{M}} - G_{\mathrm{m}}{}^{\mathrm{M}}, \tag{B.2c}$$

$$\dot{N}_{\mathrm{m}}{}^{\mathrm{W}} = G_{\mathrm{s}}^{\mathrm{t}\,\mathrm{W}} - G_{\mathrm{m}}{}^{\mathrm{W}}, \tag{B.2d}$$

reactor:

$$\dot{\omega} = \kappa_3 \left(T_{\mathrm{j}} - T_{\mathrm{r}}\right) \tag{B.2e}$$

$$\dot{T}_{\mathrm{r}} = h\left(r, T_{\mathrm{r}}\right) + \omega + D\left[T_{\mathrm{r}}^{\mathrm{i}} - T_{\mathrm{r}}\right], \tag{B.2f}$$

$$\dot{N}_{\mathrm{r}}{}^{\alpha} = G_{\mathrm{m}}{}^{\alpha} - G_{\mathrm{r}}{}^{\alpha} + \Gamma^{\alpha}, \tag{B.2g}$$

separator:

$$\dot{N}_{\mathrm{s}}{}^{\alpha} = G_{\mathrm{r}}{}^{\alpha} - G_{\mathrm{s}}^{\mathrm{t}\,\alpha} - G_{\mathrm{s}}^{\mathrm{b}\,\alpha}. \tag{B.2h}$$

Frst, we consider the mixer as process element that gets raw material from external sources via the flows $G_{\mathrm{ex}}{}^{\mathrm{H}}$ and $G_{\mathrm{s}}{}^{\mathrm{C}}$. Beside these streams, the element obtains a recycled molar stream $G_{\mathrm{s}}^{\mathrm{t}}$ from the first separator. The output of the mixer is defined as follows

$$G_{\mathrm{m}}{}^{\alpha} = DN_{\mathrm{m}}{}^{\alpha},$$

where D is a velocity determining factor of the mixer. As no specific technology is addressed, it should be assumed that the factor D is constant for the considered operational area.
The molar flow G_{m} is the input for the reactor, where the output flow is given by

$$G_{\mathrm{r}}{}^{\alpha} = DN_{\mathrm{r}}{}^{\alpha}.$$

The individual reaction terms are given by

$$\Gamma^{\mathrm{H}} := -4r, \quad \Gamma^{\mathrm{C}} := -r, \quad \Gamma^{\mathrm{M}} := r, \quad \Gamma^{\mathrm{W}} := 2r,$$

where the reaction rate is defined by the the equation

$$r := \bar{k} \exp\left(\frac{-E}{T_{\mathrm{r}}}\right)\left(\left(c_{\mathrm{r}}{}^{\mathrm{H}}\right)^4 \left(c_{\mathrm{r}}{}^{\mathrm{C}}\right)^1 - \tilde{K}\left(c_{\mathrm{r}}{}^{\mathrm{M}}\right)^1 \left(c_{\mathrm{r}}{}^{\mathrm{F}}\right)^2\right).$$

Here, the equilibrium constant $\tilde{K}$ of the reaction is assumed to be constant within the operational area. The reaction-induced change of the reactor temperatur T_r can be described by

$$h\left(r\right) := -\kappa_2\, r\, \Delta H,$$

where $\Delta H \in \mathbb{R}^+$ is the enthalpy of the reaction. The reactor is surrounded by a cooling jacket, which absorbs the energy and transfers it to storage ${\mathcal{B}_2}^1$. Since the cooling jacket cannot absorb the released energy as fast as it might be generated when the production level changes, we use (B.2e) to describe this delay, cf. [24]. In this way the formation of a hot-spot can be modelled. Assuming that the temperatur T_j of the cooling jacket is constant, the heat flow is determined by the ansatz

$$Q := \kappa_1 \omega.$$

Finally, we want to describe the separation within the first separator. We use a dynamic model, since we want to use this one seaparator to represent the potential inertia of the entire purification process. The key idea here is that the separator should also be understood as a buffer. The composition of the two molar flows leaving the separator does not depend directly on the molar fractions in the input flow, but on the stored amount of the individual substances. Using the split factor ψ_s, the distribution coefficients K_α and the molar fraction

$$x_\mathrm{s}{}^\alpha := \frac{{N_\mathrm{s}}^\alpha}{\bar{N}_\mathrm{s}}, \text{ with } \bar{N}_\mathrm{s} := \sum_{\alpha\in\mathcal{S}} {N_\mathrm{s}}^\alpha,$$

of the separator, the molar output flows are given by

$$G_\mathrm{s}^{\mathrm{t}\,\alpha} := \psi_\mathrm{s} \bar{G}_\mathrm{r} \frac{K_\alpha}{1+\psi_\mathrm{s}(K_\alpha - 1)} {x_\mathrm{s}}^\alpha,$$

$$G_\mathrm{s}^{\mathrm{b}\,\alpha} := (1-\psi_\mathrm{s})\, \bar{G}_\mathrm{r} \frac{1}{1+\psi_\mathrm{s}(K_\alpha - 1)} {x_\mathrm{s}}^\alpha.$$

The split factor is defined by

$$\psi_\mathrm{s} := \frac{\bar{G}_\mathrm{s}^\mathrm{t}}{\bar{G}_\mathrm{r}},$$

where $\bar{G}_\mathrm{s}^\mathrm{t} := \sum_{\alpha\in\mathcal{S}} G_\mathrm{s}^{\mathrm{t}\,\alpha}$ and $\bar{G}_\mathrm{r} := \sum_{\alpha\in\mathcal{S}} {G_\mathrm{r}}^\alpha$ are the total molar flows. Furthermore, it is assumed that there is no accumulation of the total amount of material within the separator. The distribution coefficients K_α for each substance are determined by the temperatur and pressure level of the separator and assumed to be constant.

Table B.2: Physical properties of the model parameter for $\mathcal{S}_2$.

symbol	**description**	**dimension**
κ_1	heat conductivity parameter	$\mathrm{m^3K/kJ}$
κ_2	heat conductivity parameter	$1/\mathrm{s}$
κ_3	heat conductivity parameter	$1/\mathrm{s}$
κ_4	heat extraction parameter	$\mathrm{kJ/K/s}$
$\tilde{K}$	equilibrium factor of the reaction	$\mathrm{m^6/mol^2}$
$\bar{k}$	reaction velocity feactor	$\mathrm{m^6/mol^2/s}$
E	activation energy factor	K
ΔH	reaction enthalpy	kJ/mol
Q	heat flow	kJ/s
V_r	volume of the reactor	$\mathrm{m^3}$
$T_\mathrm{r}, T_\mathrm{j}, T_\mathrm{r}^\mathrm{i}$	temperatur	K

The individual parameter and state variabels are summarized in the Table B.2.

Secondary feed: In addition to the substance H, the process obtains the molar flow ${G_\mathrm{s}}^\mathrm{C}$ from the storage element ${\mathcal{B}_1}^1$. The amount C from ${\mathcal{B}_1}^1$ has to be adapted to the current flow ${G_\mathrm{ex}}^\mathrm{H}$ according to a stoichiometric ratio. We use the ansatz

$$ {w_{1|2}}^1 := \ {G_\mathrm{s}}^\mathrm{C} = 0.25\, {G_\mathrm{ex}}^\mathrm{H} $$

to determine the molar flow.

Primary product: The bottom stream G_s^b consists primarily of M and W. Nevertheless, there are traces of H, which cannot be completely removed. For this reason the product level of this process is given by

$$ c^2 := \ G^{\mathrm{M}^+\mathrm{H}} = G_\mathrm{s}^{\mathrm{b}\,\mathrm{M}} + \varepsilon\, G_\mathrm{s}^{\mathrm{b}\,\mathrm{H}}, $$

where ε describes the portion of H.

Byproduct: As already stated above, the level of the byproduct is given by the heat flow

$$ {v_2}^1 := \ Q = \kappa_1 \omega. $$

Feed parameter: The feed parameter for $\mathcal{S}_2$ describes directly the price of H. In this context, it is true that the more expensive the substance H is, the higher the operating costs increase, which makes it necessary to reduce the amount of H consumed. As a consequence, less M is produced and also less Q.

Production System $\mathcal{P}$

The states of the system are formed by the the dynamical states of the individual processes and the storage levels of the two storage elements, so that we obtained

$$x = \big(T_{\mathrm{j}}, T_{\mathrm{r}}, c^{\mathrm{X}_1}, c^{\mathrm{X}_2}, c^{\mathrm{A}}, c^{\mathrm{B}}, c^{\mathrm{C}}, c^{\mathrm{M}}, {N_{\mathrm{m}}}^{\mathrm{H}}, {N_{\mathrm{m}}}^{\mathrm{C}}, {N_{\mathrm{m}}}^{\mathrm{M}}, {N_{\mathrm{m}}}^{\mathrm{W}}, \omega, T_{\mathrm{r}}, \dots$$
$${N_{\mathrm{r}}}^{\mathrm{H}}, {N_{\mathrm{r}}}^{\mathrm{C}}, {N_{\mathrm{r}}}^{\mathrm{M}}, {N_{\mathrm{r}}}^{\mathrm{W}}, {N_{\mathrm{s}}}^{\mathrm{H}}, {N_{\mathrm{s}}}^{\mathrm{C}}, {N_{\mathrm{s}}}^{\mathrm{W}}, {N_{\mathrm{s}}}^{\mathrm{W}}, {\ell_1}^1, {\ell_2}^1\big).$$

Table B.3: Specifications of the production system.

	value
nominal production level	$\big(40\ \mathrm{mol\,min^{-1}}, 27\ \mathrm{mol\,min^{-1}}\big)$
nominal feed parameter	(2, 1)
nominal reactor temperatur	(300 K, 480 K)
temperatur for $\mathcal{S}_1$	[283K, 315 K]
temperatur for $\mathcal{S}_2$	[450K, 500 K]

Beside the dynamical equations of the processes in (B.1) and (B.2) and thus of the system itself, we have to formulate the dynamical equations for the storage elements by specifing the rates in (2.8) as follows:

$${\rho_1}^1(x,u) := {v_1}^1 - {w_{1|2}}^1, \tag{B.3a}$$

$${\rho_2}^1(x,u) := {v_2}^1 - {w_{2|1}}^1. \tag{B.3b}$$

Furthermore, the storage level the individual elements are the amount of the substance C ${\ell_1}^1 := N^{\mathrm{C}}$ and the stored energy level ${\ell_2}^1 := E_{\mathrm{heat}}$.

It is assumed that the system is not operated in isolation, but is part of a larger production network. Hence one has to formulate downstream process constraints. Here we determine that the total amount of both products (sum of the product streams) has to be within predefined boundaries $\underline{G}_{\mathrm{tot}}, \overline{G}_{\mathrm{tot}} \in \mathbb{R}^+$ and write

$$\omega^1(x) = G_{\mathrm{tot}}(x) - \overline{G}_{\mathrm{tot}}, \tag{B.4}$$

$$\omega^2(x) = \underline{G}_{\mathrm{tot}} - G_{\mathrm{tot}}(x), \tag{B.5}$$

where the function of the total product stream is

$$G_{\mathrm{tot}}(x) := G^{\mathrm{M}} + G^{\mathrm{M^+H}}.$$

Finally we describe the product quality by

$$q_{\mathrm{s}}(x) := -a\left(I(x) - I_{\mathrm{n}}\right)^2 + 1,$$

where $I(x)$ is denotated as impurity factor, which is defined by

$$I(x) := \frac{\varepsilon\, G_{\mathrm{s}}^{\mathrm{b}^{\mathrm{H}}}}{G_{\mathrm{tot}}}. \tag{B.6}$$

This factor quantifies the amount of impurities of H. It is clear that $Q := \{q_{\mathrm{s}}\}$ contains only one element.

B.2 Classification of the Feed Parameter Set

This section describes how the feed parameter space Θ can be classified according to the sign of the optimal storage rates obtained by the relaxed S-RTO. Based on this classification, we can analyze whether a production system is feasible for dynamic operation (see Definition 5.1) according to a scenario of feed parameter changes. For this purpose, we assume that the system is well-designed and the subset $\mathcal{A}_{\mathfrak{F}} \subset \mathcal{D}$ is sufficiently large. The set $\mathcal{A}_{\mathfrak{F}}$ contains all storage levels, for which the storage size constraints in the S-RTO are not active. Furthermore, for a given initial level $\ell \in \mathcal{A}_{\mathfrak{F}}$, it holds that the optimal storage rate can be computed by the map ${\mathfrak{P}_{\mathrm{r}}}_j^{\alpha}$.

In the following, we want to examine the set Θ for a possible partition based on the sign of the storage rates obtained by ${\mathfrak{P}_{\mathrm{r}}}_j^{\alpha}$. Therefore, we define $\mathfrak{P}_{\mathrm{s}} : \Theta \to \{-1,\, 1\}^{n_{\mathcal{B}}}$ componentwise through

$${\mathfrak{P}_{\mathrm{s}}}_j^{\alpha} : \Theta \to \{-1, 0,\ 1\}, (\theta) \mapsto {\mathfrak{P}_{\mathrm{s}}}_j^{\alpha}(\theta) := \mathrm{sgn} \circ {\mathfrak{P}_{\mathrm{r}}}_j^{\alpha}(\theta). \tag{B.7}$$

This function $\mathfrak{P}_{\mathrm{s}}$ yields $n_{\mathcal{B}}$ integers describing whether the storage elements are charged (1), discharged (-1), or the level stays constant (0). Using $\mathfrak{P}_{\mathrm{s}}$ we can introduce an equivalence relation. Two feed parameters $\theta_1, \theta_2 \in \Theta$ are said to be equivalent under the equivalence relation $\sim$, iff it holds

$$\theta_1 \sim \theta_2 \quad \Leftrightarrow \quad \mathfrak{P}_{\mathrm{s}}(\theta_1) = \mathfrak{P}_{\mathrm{s}}(\theta_2).$$

Subsequently, it is possible to define the equivalence class for $\theta \in \Theta$ by $[\theta] := \{\xi \in \Theta \mid \xi \sim \theta\}$. It can also be shown that the set $\Pi := \big\{\, [\theta] \mid \theta \in \Theta \big\}$, is a partition of Θ, which means

$$\Theta = \bigcup_{A_i \in \Pi} A_i. \tag{B.8}$$

Considering the individual sets within Π, it is easy to see that they are not only disjoint, but there might exist a complementary element $\tilde{\Theta}_i^{\mathrm{s}} \in \Pi$ for each element $\Theta_i^{\mathrm{s}} \in \Pi$, which is characterized by

$$\mathfrak{P}_{\mathrm{s}}(\theta_1) = -\mathfrak{P}_{\mathrm{s}}(\theta_2), \quad \forall (\theta_1, \theta_2) \in \Theta_i^{\mathrm{s}} \times \tilde{\Theta}_i^{\mathrm{s}}.$$

Hence, one can reformulate (B.8) by

$$\Theta = \bigcup_{i \in \mathbb{I}_1^{\mathrm{t}}} \Theta_i^{\mathrm{s}} \cup \bigcup_{i \in \mathbb{I}_2^{\mathrm{t}}} \tilde{\Theta}_i^{\mathrm{s}}.$$

where the index sets $\mathbb{I}_i^{\mathrm{t}}$ indicate the number of the particular subsets $\Theta_i^{\mathrm{s}} \in \Pi$ and $\tilde{\Theta}_i^{\mathrm{s}} \in \Pi$. It can be derived that the number of subsets is related to the number of storage elements. For instance, if the system has $n_{\mathcal{B}}$ elements, a maximum of $2^{n_{\mathcal{B}}}$ subsets can be constructed. Note that the number of elements in Π is affected by two factors. First, it depends on the system $\mathcal{P}$ itself in the form of the function $\mathfrak{P}_{\mathrm{s}}$. Second, it depends on the number of storage elements and thus the dimension of the codomain of $\mathfrak{P}_{\mathrm{s}}$, which directly affects the combinatorial complexity of the integers -1 and 1. Assumption 5.1 enables to derive that the minimum number of elements of Π is two since, for each storage element, it needs to be ensured that a switch in the sign of the rate can occur. This is necessary to ensure a switch between charging and discharging of the storage element from time to time. Furthermore, it can be stated that for each set Θ_i^{s} there can also exist a complementary set $\tilde{\Theta}_i^{\mathrm{s}}$. To characterize the partition of Θ, we use the following notion.

Definition B.1 (Completeness of the Partition)**.** *Let Θ be the set of feed parameters and $\mathfrak{P}_{\mathrm{s}}$ be a function as defined in* (B.7) *for a given system $\mathcal{P}$. The partition Π of the set Θ is called*

(i) incomplete, iff it contains for no $\Theta_i^{\mathrm{s}} \in \Pi$ its complementary set $\tilde{\Theta}_i^{\mathrm{s}}$.

(ii) partially complete, iff it contains for some $\Theta_i^{\mathrm{s}} \in \Pi$ its complementary set $\tilde{\Theta}_i^{\mathrm{s}}$.

(iii) complete, iff it contains for all $\tilde{\Theta}_i^{\mathrm{s}}$ its complementary set $\tilde{\Theta}_i^{\mathrm{s}}$.

Remark B.1. *Consider a system $\mathcal{P}$ that is feasible for dynamic operation. If $\mathcal{P}$ has only one storage element, the partition is always complete. If $\mathcal{P}$ has two storage elements, the partition is at least partially complete. Incomplete partitions require a minimum of three elements.*

Depending on the number of storage elements and also the system itself, the distribution and form of the subsets can be very complex. For this, the optimal

rate function (5.4) is decisive. In order to obtain and analyze the partition, it is necessary to look at the individual elements first.
Considering ${\mathcal{B}_j}^{\alpha}$, the boundary set ${W_j}^{\alpha} := \ker {\mathfrak{P}_{\mathrm{r}j}}^{\alpha}$ separates the regions ${}^{-}{\Theta_j}^{\alpha}$ and ${}^{+}{\Theta_j}^{\alpha}$ with negative and positive rate signs. Depending on the form of ${\mathcal{W}_j}^{\alpha}$ and the resulting intersections ${\mathcal{W}_i}^{\alpha} \cap {\mathcal{W}_j}^{\beta}$ of the individual boundary sets, it is possible that the equivalence classes are not connected with each other.

An alternative way to represent the partition Π of Θ is based on a graph using nodes and edges, where the the subsets $\Theta_i^{\mathrm{s}}, \tilde{\Theta}_i^{\mathrm{s}} \in \Pi$ are the nodes. Two nodes are connected by an edge whenever there is a boundary ${\mathcal{W}_j}^{\alpha}$ between the two sets. Moreover, if we assume that $\left|{\mathcal{W}_i}^{\alpha} \cap {\mathcal{W}_j}^{\beta}\right|$ is finite for $i \neq j$ or $\alpha \neq \beta$, the properties of Π formulated in Definition B.1 can be derived directly from the graph. This assumption implies that the transition between two adjacent nodes along the common edge changes only the sign of one storage element. Thus, the shortest path between two complementary nodes corresponds to the number $n_{\mathcal{B}}$ of elements.

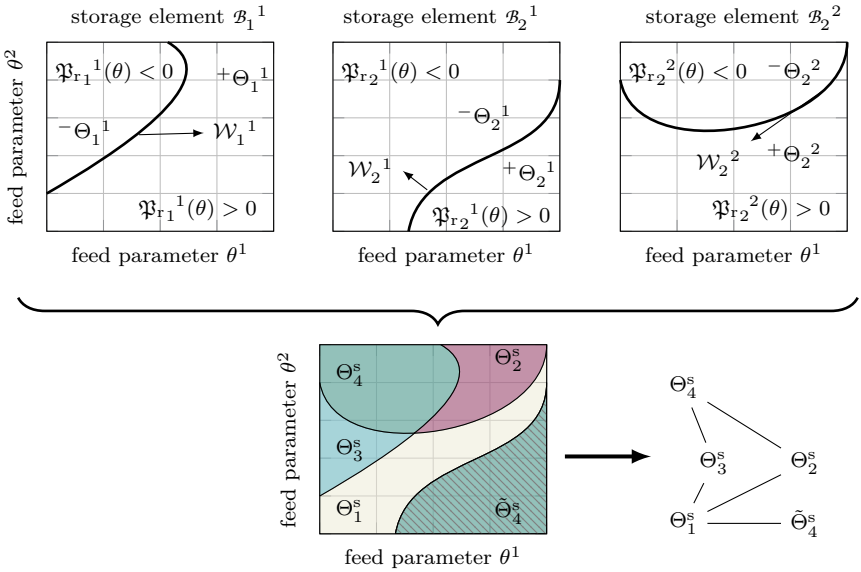

Figure B.4: Construction of the partition Π for a production system with three storage elements.

Example B.1 (Three arbitrary storage elements)**.** *We consider a production system $\mathcal{P}$ with three storage elements. Figure B.4 (bottom left) illustrates*

the structure of Θ in a set-based fashion, while Figure B.4 (bottom right) shows the graph representation of the partition of Theta. In total, the partition $\Pi = \{\Theta_1^{\mathrm{s}}, \Theta_2^{\mathrm{s}}, \Theta_3^{\mathrm{s}}, \Theta_4^{\mathrm{s}}, \tilde{\Theta}_4^{\mathrm{s}}\}$ consists of 5 subsets. The boundary sets ${\mathcal{W}_j}^{\alpha}$ which seperate the subsets ${}^{-}{\Theta_j}^{\alpha}$ and ${}^{+}{\Theta_j}^{\alpha}$ for each storage element are depicted as black thick lines in Figure B.4 (top). The partition of Θ under $\mathfrak{P}_{\mathrm{s}}$ is partially complete since only for the subset Θ_4^{s} its complement is also contained in Π. From a practical point of view, it means that if the feed parameter $\theta_k \in \Theta_4^{\mathrm{s}}$ changes to the value $\theta_{k+1} \in \tilde{\Theta}_4^{\mathrm{s}}$ in the next time step, the sign of all storage rates change completely. The elements that were previously charged or discharged are now discharged or charged, respectively.

Next, we discuss how the partition of Θ can be constructed. Formally, one has to identify and parameterize the boundary set ${\mathcal{W}_i}^{\alpha}$ for each ${\mathcal{B}_j}^{\alpha}$. In the following, we assume that ${\mathcal{W}_i}^{\alpha}$ is a one dimensional submanifold of Θ, and we call it boundary path. The identification of the path ${\mathcal{W}_i}^{\alpha}$ requires, however, that we find all the solutions $\theta_0 \in \Theta$ of the root-finding problem $0 = {\mathfrak{P}_{\mathrm{r}_j}}^{\alpha}(\theta_0)$. Note that ${\mathfrak{P}_{\mathrm{r}_j}}^{\alpha}$ is defined by solving the relaxed Problem (5.2) to determine the optimal production level. Therefore, a direct solution of the root-finding problem is typically difficult.
An alternative approach is to separate the two subsets formed by ${\mathcal{W}_i}^{\alpha}$ with a suitable method and describe them directly. Thus we avoid the parameterization of the path ${\mathcal{W}_i}^{\alpha}$. In the literature, several approaches are mentioned to solve this kind of problem, especially the field of machine learning offers many tools and methods. For instance, support vector machines [203] can be used to separate data points by hyperplanes. These points have to be calculated first using ${\mathfrak{P}_{\mathrm{s}_j}}^{\alpha}$. Afterward, the hyperplanes used to approximate ${\mathcal{W}_i}^{\alpha}$ can be calculated. The main disadvantage, however, is that new points cannot be added adaptively. If one starts with a few points, the distance between some data points might be too large, so it is useful to generate new points, which yields a better approximation of ${\mathcal{W}_i}^{\alpha}$ by the hyperplanes. Therefore, for an accurate approximation, one has to start with a highly dense grid (particularly in the neighborhood of ${\mathcal{W}_i}^{\alpha}$), which increases the computational effort.

Instead of approximating ${\mathcal{W}_i}^{\alpha}$ by hyperplanes to subsequently describe the subsets ${}^{-}{\Theta_j}^{\alpha}$ and ${}^{+}{\Theta_j}^{\alpha}$ from it, we will follow the reverse order. The first step is to describe the two subsets for each storage element by evaluating ${\mathfrak{P}_{\mathrm{r}_j}}^{\alpha}$ at corner points of rectangles within Θ. By an iterative refinement of the rectangles and evaluation of ${\mathfrak{P}_{\mathrm{r}_j}}^{\alpha}$, the boundary can be approximated arbitrarily precisely. Afterward, the boundary and the individual equivalence classes are derived from the rectangles assigned to ${}^{-}{\Theta_j}^{\alpha}$ or ${}^{+}{\Theta_j}^{\alpha}$.
This approach uses the fact that we are not only interested in the boundary but also for later developments on the surface of each field. To this end, we discretize Θ by an initially equidistant grid and evaluate ${\mathfrak{P}_{\mathrm{r}_j}}^{\alpha} a$ at the grid points. The

rectangular areas through which the boundary passes are then further refined. This procedure is repeated until a predefined tolerance is reached. Algorithm B.1 presents the individual steps in detail.

Algorithm B.1: Subdivision of Θ for a storage element ${\mathcal{B}_j}^{\alpha}$

Input: the set Θ and the functions ${\mathfrak{P}_{\mathrm{r}}}_j^{\alpha}$

choose a tolerance ε, initialize ${}^{+}\mathcal{R}, {}^{-}\mathcal{R}, {}^{0}\mathcal{R} = \emptyset$ and discretize Θ by

$\underline{\theta}^1 = {\theta_1}^1 < \ldots < {\theta_{n_{\theta,1}}}^2 = \overline{\theta}^1$ and $\underline{\theta}^2 = {\theta_1}^2 < \ldots < {\theta_{n_{\theta,2}}}^2 = \overline{\theta}^2$;

for $i = 1, \ldots, n_{\theta,1} - 1$ **do**

  for $j = 1, \ldots, n_{\theta,2} - 1$ **do**

    compute ${\mathfrak{P}_{\mathrm{s}}}_j^{\alpha}$ for all 4 corner points of the rectangle

    $\mathcal{R}_{ij} := \left\{ \left({\theta_i}^1, {\theta_j}^2\right), \left({\theta_{i+1}}^1, {\theta_j}^2\right), \left({\theta_{i+1}}^1, {\theta_{j+1}}^2\right), \left({\theta_i}^1, {\theta_{j+1}}^2\right) \right\}$

    if $\forall p \in \mathcal{R}_{ij}$, ${\mathfrak{P}_{\mathrm{s}}}_j^{\alpha}(p) > 0$ **then** update ${}^{+}\mathcal{R} \leftarrow \mathcal{R}_{ij}$

    if $\forall p \in \mathcal{R}_{ij}$, ${\mathfrak{P}_{\mathrm{s}}}_j^{\alpha}(p) < 0$ **then** update ${}^{-}\mathcal{R} \leftarrow \mathcal{R}_{ij}$

    if $\exists p_1, p_2 \in \mathcal{R}_{ij}$, ${\mathfrak{P}_{\mathrm{s}}}_j^{\alpha}(p_1) \neq {\mathfrak{P}_{\mathrm{s}}}_j^{\alpha}(p_2)$ **then** update ${}^{0}\mathcal{R} \leftarrow \mathcal{R}_{ij}$

  end

end

initialize the stack $\overline{\mathcal{R}} \leftarrow {}^{0}\mathcal{R}$ of rectangles to be refined

while $\overline{\mathcal{R}} \neq \emptyset$ **do**

  pick $\overline{\mathcal{R}}_i \in \overline{\mathcal{R}}$ and divide it into 4 sub-rectangles $\left\{\overline{\mathcal{R}}_{i,a}, \overline{\mathcal{R}}_{i,b}, \overline{\mathcal{R}}_{i,c}, \overline{\mathcal{R}}_{i,d}\right\}$

  for $l \in \{a, b, c, d\}$ **do**

    compute ${\mathfrak{P}_{\mathrm{s}}}_j^{\alpha}$ for all 4 corner points of the rectangle $\overline{\mathcal{R}}_{i,l}$

    if $\forall p \in \overline{\mathcal{R}}_{i,l}$, ${\mathfrak{P}_{\mathrm{s}}}_j^{\alpha}(p) > 0$ **then** update ${}^{+}\mathcal{R} \leftarrow \overline{\mathcal{R}}_{i,l}$

    if $\forall p \in \overline{\mathcal{R}}_{i,l}$, ${\mathfrak{P}_{\mathrm{s}}}_j^{\alpha}(p) < 0$ **then** update ${}^{-}\mathcal{R} \leftarrow \overline{\mathcal{R}}_{i,l}$

    if $\sum_{p \in \overline{\mathcal{R}}_{i,l}} \left({\mathfrak{P}_{\mathrm{r}}}_j^{\alpha}(p)\right)^2 < \varepsilon$ **then**

      update ${}^{0}\mathcal{R} \leftarrow \mathcal{R}_{ij}$

    else

      update $\overline{\mathcal{R}} \leftarrow \overline{\mathcal{R}}_{i,l}$

    end

  end

end

Result:

set ${}^{+}\mathcal{R}$ to cover ${}^{+}{\Theta_j}^{\alpha} \approx {}^{+}\hat{\Theta}_j^{\alpha} := \bigcup {}^{+}\mathcal{R}$

set ${}^{-}\mathcal{R}$ to cover ${}^{-}{\Theta_j}^{\alpha} \approx {}^{-}\hat{\Theta}_j^{\alpha} := \bigcup {}^{-}\mathcal{R}$

set ${}^{0}\mathcal{R}$ to cover the boundary ${\mathcal{W}_j}^{\alpha} \approx {}^{0}\hat{\Theta}_j^{\alpha} := \bigcup {}^{0}\mathcal{R}$

Figure B.5 illustrates the procedure for the element ${\mathcal{B}_1}^1$ from Example B.1. The blue (-) and beige (+) rectangles in Figure B.5 (a) indicate the areas in which

the sign of the storage rate is negative or positive, respectively. Red rectangles represent the initial subset in which the boundary is located. In Figure B.5 (b), the final separation of Θ is depicted, where the subset containing the boundary is more detailed (green rectangles). According to a given tolerance, we can pose that the green rectangles approximate the boundary.

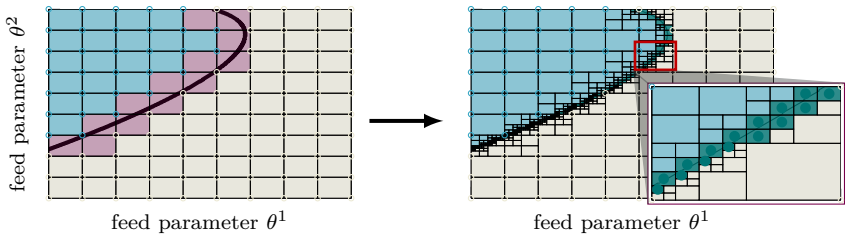

(a) Initial separation of Θ by rectangles due to the different signs of the rates.

(b) Final separation of Θ by rectangles due to the refinement of the rectangles.

Figure B.5: Illustration of splitting Θ for one storage element.

Note that Algorithm B.1 has to be executed for each storage element individually. In this way we get for each element not only the boundary path but also the two additional sets ${}^{-}\hat{\Theta}_j{}^{\alpha}$ and ${}^{+}\hat{\Theta}_j{}^{\alpha}$ consisting of elementary rectangles that can be used to approximate the two areas ${}^{-}\Theta_j{}^{\alpha}$ and ${}^{+}\Theta_j{}^{\alpha}$.

The boundary $\mathcal{W}_j{}^{\alpha}$ is described by ${}^{0}\hat{\Theta}_j{}^{\alpha}$. Based on the specified tolerance, the detection of the boundary is sufficiently accurate. To derive the boundary as one dimensional submanifold of Θ, we propose to use centers of the elementary rectangles in ${}^{0}\hat{\Theta}_j{}^{\alpha}$. However, the construction of ${}^{0}\hat{\Theta}_j{}^{\alpha}$ described in Algorithm B.1 does not follow a special order of the rectangles to be checked. Thus the boundary points are not passed through in the order as they occur in ${}^{0}\hat{\Theta}_j{}^{\alpha}$. If $\mathcal{W}_i{}^{\alpha}$ runs from one edge of Θ to another (as illustrated in Figure B.5), the boundary points can be sorted by Algorithm B.2 using the metrics m_2 and m_{d} from Definition A.3 in Appendix A.1.

The metric m_2 in Algorithm B.2 denotes the Euclidean norm of the last point in Q to the new one to be added. Contrary to this, the norm m_{d} uses the last two points of Q and evaluates how much the direction of the boundary path changes by the new point. This can also be interpreted as a measure of the local "smoothness" of $\hat{\mathcal{W}}_j{}^{\alpha}$. Indeed, the construction of Q uses initially any point. Of course, this can also be located anywhere in Θ. For this reason, the path needs to be flipped in the direction at least once. In this way, one goes from an arbitrary initial point first to one of the two boundary points and from

Algorithm B.2: Sort the boundary points for a storage element ${\mathcal{B}_j}^{\alpha}$

Input: the boundary set ${}^{0}\hat{\Theta}_j{}^{\alpha}$
choose suitable tolerances ε_1, ε_2 and initialize $l := 3$, $f := 1$, 1
choose suitable scaling factors $\gamma_1, \gamma_2 \in \mathbb{R}^+$, 2
compute for all elements in ${}^{0}\hat{\Theta}_j{}^{\alpha}$ the center and write it in B, 3
initialize $Q := B_1$, and update $B := B \setminus \{B_1\}$ 4
compute $\hat{p} := \underset{p \in B}{\operatorname{argmin}}\, \boldsymbol{m}_2(Q_1, p)$ and update $Q \leftarrow \hat{p}$ and $B := B \setminus \{\hat{p}\}$ 5
while $B \neq \emptyset \vee f = 1$ **do** 6
  compute $\hat{p} := \underset{p \in B}{\operatorname{argmin}}\, \gamma_1 \boldsymbol{m}_2(Q_{l-1}, p) - \gamma_2 \boldsymbol{m}_{\mathrm{d}}(Q_{l-2}, Q_{l-1}, p)$ 7
  if $\boldsymbol{m}_{\mathrm{d}}(Q_{l-2}, Q_{l-1}, \hat{p}) < \varepsilon_1 \vee \boldsymbol{m}_2(Q_{l-1}, \hat{p}) > \varepsilon_2$ **then** 8
    flip Q in the left-right direction and set $f := 0$ 9
  else 10
    update $Q \leftarrow \hat{p}$, $B := B \setminus \{\hat{p}\}$ and $l := l + 1$ 11
  end 12
end 13
Result: set of sorted boundary points ${\mathcal{W}_j}^{\alpha} \approx {\hat{\mathcal{W}}_j}^{\alpha} := Q$

there to the second. However, an additional flip would disturb the order again. This effect is used to filter the original center point data generated from ${}^{0}\hat{\Theta}_j{}^{\alpha}$. In general, ${\hat{\mathcal{W}}_j}^{\alpha}$ contains less elements than ${}^{0}\hat{\Theta}_j{}^{\alpha}$.

After the set Θ was divided for each ${\mathcal{B}_j}^{\alpha}$ individually into the two areas ${}^{-}\hat{\Theta}_j{}^{\alpha}$ and ${}^{+}\hat{\Theta}_j{}^{\alpha}$, the elements of Π can be identified. To this end, the various combinations of signs are used to derive the classification. The number of combinations results from the total number $n_{\mathcal{B}}$ of storage elements. It is generally difficult and impractical to describe the forms of the individual equivalence classes Θ_i^{s} and $\tilde{\Theta}_i^{\mathrm{s}}$ by their boundaries. Hence, we use the information obtained above to define an indicator function $\chi_\Theta : \Theta \to \left\{-\frac{2^{n_{\mathcal{B}}}}{2}, \ldots, \frac{2^{n_{\mathcal{B}}}}{2}\right\}$ that describes, for a given point $\theta \in \Theta$, in which class it is located. Algorithm B.1 describes how χ_Θ is obtained by the results from.

From the determination of χ_Θ by the Algorithm B.3 it can be deduced that two complementary classes differ by their sign according to

$$\chi_\Theta(\theta_1) = -\chi_\Theta(\theta_2), \quad \forall(\theta_1, \theta_2) \in \Theta_i^{\mathrm{s}} \times \tilde{\Theta}_i^{\mathrm{s}}.$$

Using χ_Θ, the partition Π is uniquely defined and can be expressed arbitrarily exactly corresponding to ${}^{-}\hat{\Theta}_j{}^{\alpha}$ and ${}^{+}\hat{\Theta}_j{}^{\alpha}$. The points $\theta \in \Theta$ for which $\chi_\Theta(\theta) = 0$ yields, describe the boundary paths between the classes.

Algorithm B.3: Construction of an indicator function for the partition Π

Input: for all storage elements the sets ${}^{-}\hat{\Theta}_j{}^{\alpha}$ and ${}^{+}\hat{\Theta}_j{}^{\alpha}$
initialize $Q := \emptyset$,
for $j = 1, 2$ **do**
  for $\alpha = 1, \ldots, n_{\theta,j}$ **do**
    generate indicator functions ${}^{-}\chi_j{}^{\alpha}$ and ${}^{+}\chi_j{}^{\alpha}$ for ${}^{-}\hat{\Theta}_j{}^{\alpha}$ and ${}^{+}\hat{\Theta}_j{}^{\alpha}$,
    which states if $\theta \in \Theta$ lies in them and update $Q \leftarrow \left({}^{-}\chi_j{}^{\alpha}, {}^{-}\chi_j{}^{\alpha}\right)$
  end
end
compute $C := \neg A \otimes [1,\, 0] + A \otimes [0,\, 1]$ where A contains all permutations with repetition of $[0,\, 1]$ if $n_{\mathcal{B}}$ elements taken, (each row $C_{l,:}$ of C contains a possible result of Q),
initialize $\psi := 0$ and $E := \left\{-\frac{2^{n_{\mathcal{B}}}}{2}, \ldots, \frac{2^{n_{\mathcal{B}}}}{2}\right\}$,
for $l = 1, \ldots, 2^{n_{\mathcal{B}}}$ **do**
  if $Q(\theta) = C_l$ **then** $\psi := E_l$ (E_l is l-th element of E)
end
define $\chi_{\Theta}(\theta) := \psi$
Result: indicator function χ_{Θ}

So far, we have analyzed the structure of Θ under a given operational strategy. In particular, we can characterize the effects on the storage level caused by changes in the feed parameter.
Keep in mind that the goal is to classify Θ to evaluate the storage level change within DD driven by the cl S-RTO under a feed parameter scenario. For this purpose, D should be chosen so that the storage constraints are active only in a neighborhood of the boundary of $\mathcal{D}$ (red area in Figure 5.3). This ensures that in most cases, the optimal operating point obtained from Problem (5.2) can be reached.

However, the previously discussed structure of Θ can be used to give an initial evaluation of the ability of the storage elements to be self-regulating (cf. Definition 5.2) under a certain $\boldsymbol{\theta}$. For this purpose, it is necessary to consider the mean positive and negative rates as well as the corresponding size of the areas. If the mean rates differ only by their sign, a periodic change of θ between the regions ${}^{-}\Theta_j{}^{\alpha}$ and ${}^{+}\Theta_j{}^{\alpha}$ can have a balancing effect on the storage levels. However, the sizes of the two regions are a measure of how frequently negative or positive rates occur. Therefore, we define

$$\mathfrak{c}_j{}^{\alpha} := \frac{\left|\int_{-\Theta_j{}^{\alpha}} \mathrm{d}\theta\, \mathfrak{P}\mathrm{r}_j{}^{\alpha}(\theta)\right|}{\int_{+\Theta_j{}^{\alpha}} \mathrm{d}\theta\, \mathfrak{P}\mathrm{r}_j{}^{\alpha}(\theta)} \approx \frac{\left|\int_{-\hat{\Theta}_j{}^{\alpha}} \mathrm{d}\theta\, \mathfrak{P}\mathrm{r}_j{}^{\alpha}(\theta)\right|}{\int_{+\hat{\Theta}_j{}^{\alpha}} \mathrm{d}\theta\, \mathfrak{P}\mathrm{r}_j{}^{\alpha}(\theta)}, \tag{B.9}$$

which describes the capacity of ${\mathcal{B}_j}^{\alpha}$ for self-regulation. The ratio ${\mathfrak{c}_j}^{\alpha}$ of integrated storage rates is a kind of static system inherent property since no scenario θ is required. If the factor is close to one, it can be seen as an indication that the system has a high potential for self-regulation for ${\mathcal{B}_j}^{\alpha}$. In other words, the set $\mathit{\Theta}$ of scenarios that lead to the self-regulation behavior of the system might be more powerful.

Example B.2 (Structure of Θ for a coupled AD- and RSR-process)**.** *In this example, we analyze the relationship between θ and the storage rates. From Example 5.1, we know the rate with the highest absolute value and the heat map of the rate over Θ. For the following considerations, the exact values of the rates are not relevant for the two storage elements, but only their signs. It means that we identify the level set with a zero rate value, which separates Θ for each element into two subspaces. Hence, we assume that, in addition to the minimum size determind in Example 5.1, the storage capacity is chosen sufficiently high so that the attractive ratio is $\chi_{\mathcal{A}} \gg 0$.*

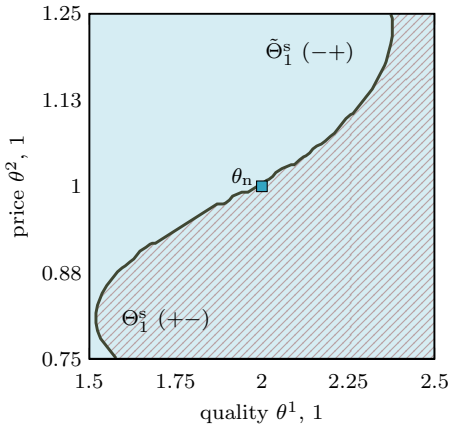

Figure B.6: Partition of Θ.

We apply Algorithm B.1 to detect the boundary, using $n_{\theta,1} = 15$ and $n_{\theta,2} = 12$ intermediate points for the initial grid. The grid should be fine enough to avoid two sign changes along the edges between two grid points, and rough enough to avoid unnecessary computational costs. Afterwards, the areas in which a change of sign occurs are refined. The tolerance we have chosen for the stopping criterion is $\varepsilon = 2 \cdot 10^{-2}$.
The level set of the zero value for both storage elements has an similar form, cf. Figure 5.4 and 5.5 Figure B.6 shows this shared boundary for both elements by a black curve. Based on this boundary, two complementary subsets of Θ can be

determined which are the two elements of the partition

$$\Pi := \left\{\Theta_1^{\mathrm{s}}, \tilde{\Theta}_1^{\mathrm{s}}\right\},$$

where

$$\Theta_1^{\mathrm{s}} := \left\{\theta \in \Theta \mid {\mathfrak{P}_{\mathrm{s}_1}}^1(\theta) = 1,\ {\mathfrak{P}_{\mathrm{s}_2}}^1(\theta) = -1\right\},\ \textit{and}$$

$$\tilde{\Theta}_1^{\mathrm{s}} := \left\{\theta \in \Theta \mid {\mathfrak{P}_{\mathrm{s}_1}}^1(\theta) = -1,\ {\mathfrak{P}_{\mathrm{s}_2}}^1(\theta) = 1\right\}.$$

Based on Definition B.1, we can also state that the partition is complete. Since Π *contains only two elements, we can conclude that a change of the feed parameter between these two subsets will always cause an opposite dynamic response of the storage levels. This contrary behavior of* ${\mathcal{B}_1}^1$ *and* ${\mathcal{B}_2}^1$ *means that a higher level in* ${\mathcal{B}_1}^1$ *corresponds with a lower level in* ${\mathcal{B}_2}^1$ *and vice versa. Of course, this only applies if the storage constraints are not active during the relaxed S-RTO, i.e., if the storage elements are not too full or too empty (i.e.,* $\ell \in \mathcal{A}_{\tilde{\mathcal{S}}}$*). Thus, if external conditions can be favoured in a way that the system is only exposed to* θ *changes between these subsets, the storage levels might regulate themselves. This would have a positive effect on the required storage capacity.*
The nominal feed parameter for which the nominal operation of the two processes of the production system is designed is shown in Figure B.6. Note that this point is close to the boundary. This is favorable for the production system and should be achieved by the design of both processes. During nominal operation, the processes should be synchronized so that the amount of produced byproducts corresponds to the amount required for the other process.

Table B.4: Analysis of the storage elements for the rates at the optimal operational point.

	storage ${\mathcal{B}_1}^1$	storage ${\mathcal{B}_2}^1$
Negative area fraction	44%	54%
Positive area fraction	54%	45%
Boundary area fraction	2%	1%
Mean negative rate	-0.46 $\mathrm{mol}\cdot\mathrm{min}^{-1}$	-0.60 $\mathrm{mol}\cdot\mathrm{kJ}^{-1}$
Standard deviation negative rate	0.05 $\mathrm{mol}\cdot\mathrm{min}^{-1}$	0.06 $\mathrm{mol}\cdot\mathrm{kJ}^{-1}$
Mean positive rate	0.56 $\mathrm{mol}\cdot\mathrm{min}^{-1}$	0.51 $\mathrm{mol}\cdot\mathrm{kJ}^{-1}$
Standard deviation positive rate	0.05 $\mathrm{mol}\cdot\mathrm{min}^{-1}$	0.05 $\mathrm{mol}\cdot\mathrm{kJ}^{-1}$
Capacity for self-regulation	0.69	1.39

After identifying the elements of Π *based on the sign of the rates, we will next analyze some characteristics, which are summarized in Table B.4. In total 54%*

of the θ values yield an increase of the storage level for ${\mathcal{B}_1}^1$ or a decrease for ${\mathcal{B}_2}^1$. So we can see that the areas with opposite signs have almost the same size for both storage elements. However, not only the size of the area is crucial to be able to predict how the storage will behave in the long term. Moreover, the absolute value of the precise rate values is also important. For this purpose, we also determined the mean and standard deviation of the rate for both subsets.

For their calculation, the numerator and denominator in (B.9) *are determined individually and related to the area. To integrate the functions ${\mathfrak{P}_{\mathrm{r}_j}}^{\alpha}$, we use an interpolation method based on a Gauss-Legendre quadrature, see [92, 240, 136]. In particular, we use a Lagrange polynomial of degree 3.*
The absolute values of the negative and positive rates for both storage elements are in similar orders of magnitude, cf. Table B.4 row 4 to 6. To compensate for the differences, it is necessary to know how long a certain feed parameter is maintained or how long it remains in the individual subsets based on a specific scenario. Thus it might be useful for ${\mathcal{B}_1}^1$ if the time span in which θ is in the upper left corner is longer than in the lower right corner. Considering the mean values of ${\mathcal{B}_2}^1$, it is obvious that the same statement applies to this element. In general, the positive rate of θ values in $\tilde{\Theta}_1^{\mathrm{s}}$ is greater than the absolute value of the negative rate in Θ_1^{s}.

This analysis shows that it can be important to carefully assess the scenarios and check whether they can be possibly modified. Otherwise, ill-conditioned scenarios would push the storage levels out of $\mathcal{A}_{\mathfrak{F}}$ for long time periods. The proposed operational strategy from Chapters 3 and 4 can still be applied, but the storage constraints would be permanently active, reducing the flexibility of the system and its economic output.

FACULTY OF PROCESS & SYSTEMS ENGINEERING
DEPARTMENT OF PROCESS SYSTEMS ENGINEERING
Universitätsplatz. 2, 39106 Magdeburg
andreas.himmel@ovgu.de
http://mpim.iwww.mpg.de/pse